AD 296 311

THE MOTIONS OF A MOORED CONSTRUCTION-TYPE BARGE IN IRREGULAR WAVES & THEIR INFLUENCE ON CONSTRUCTION OPERATION

Contract NBy - 32206

An investigation conducted by

Marine Advisers Inc.
La Jolla, California

August 1962

U. S. NAVAL CIVIL ENGINEERING LABORATORY

Port Hueneme, California

THE MOTIONS OF A MOORED CONSTRUCTION-TYPE BARGE IN IRREGULAR WAVES AND THEIR INFLUENCE ON CONSTRUCTION OPERATION

by Paul Kaplan and Robert R. Putz

The work of Dr. Paul Kaplan, of Oceanics, Inc., on the project forming the subject of this report was carried out in the capacity of Consultant to Marine Advisers, Inc.

TABLE OF CONTENTS

LIST OF FIGURES

List of Figures Continued

LIST OF SYMBOLS

A'_{ij}	Component of added mass tensor
$\bar{A}_y$	Ratio of wave amplitude to sway amplitude for lateral motion-induced wave
$\bar{A}_z$	Ratio of wave amplitude to heave amplitude for vertical motion-induced wave
a_{ij}	Matrix element for longitudinal plane motions
B^*	Local beam of ship section
C.B.	Center of bouyancy
C.G.	Center of gravity
$\lvert BG \rvert$	Vertical distance between C. B. and C. G.
$\overline{OB}$	Vertical distance from C. B. to F. S. level
$\lvert G_1M \rvert$	Perpendicular distance from C. G. to keel
$(\overline{GG_1})$	Perpendicular distance from the free surface to the C. G.
$\lvert BM \rvert$	Vertical distance between C. B. and the metacenter (metacentric radius)
$\lvert KG \rvert$	Vertical distance from keel to C. G.
L	Length of barge
H	Local section draft
B^*	Local beam of ship section
W	Displacement of barge
b_{ij}	Matrix element for lateral plane motions
C_s	Section coefficient (ratio of section area to product of section beam and draft
C_y	Three dimensional damping factor for sway motion
C_z	Three dimensional damping factor for heave motion
C_θ	Three dimensional damping factor for pitching motion
C_ψ	Three dimensional damping factor for yaw motion
c	Propagation speed of surface wave

E	Total energy (integrated area) under spectral curve
g	Acceleration due to gravity
$H_{1/3}$	Significant wave height (mean of highest third)
$\bar{h}$	Average half-draft
K	Roll moment, positive about the x-axis
k_x	Mooring spring constant for surge motion
k_y	Mooring spring constant for sway motion
k_ψ	Mooring spring constant for yawing motion
k'_y	Added mass factor for lateral motion (zero frequency)
k'_4	Frequency dependent term in lateral added mass factor
ℓ	Length of boom for lowering loads
M	Pitch moment, positive about the y-axis
m	Mass
N	Yawing moment, positive about the x-axis
N_y	Sway damping coefficient
N_z	Heave damping coefficient
N'_{yy}	Local sway damping coefficient
N'_{zz}	Local heave damping coefficient
$N_{y\psi}$	Sway-yaw coupling coefficient
$N_{z\theta}$	Heave-pitch coupling coefficient
N_θ	Pitch damping coefficient
N_ϕ	Roll damping coefficient
N_ψ	Yaw damping coefficient
$\lvert\overline{OG}\rvert$	Vertical distance from waterline to C. G.
S	Cross-sectional area

ω	Angular frequency
$\mathcal{I}m$	The imaginary part of a complex quantity
Arg	The argument or phase of a complex quantity in an Argand representation
$\mathcal{R}e$	The real part of a complex quantity
Mod	Modulus or magnitude
ζ	The phase of η when viewed as a sinusoid
δ_{bw}	Relative spectral bandwidth
σ_i^2	The r.m.s. value of a particular time history ordinate; also the second moment about the mean
M_p	Spectral moments
F	Mooring cable forces (with numbering subscripts)
I	Moment of inertia
T^{γ}	The line tension for boom-lowered loads on the boom azimuth γ.
μ_i	The first moment or mean of a distribution function; often with a subscript denoting the distribution of which it is the mean
α	The angle made by the mooring cables
P_M^-	The proportion of time relative maxima occur below the mean level in wave time history
P^-	The proportion of time the instantaneous frequency is negative
$\bar{\theta}_i(t)$	The instantaneous phase of the i^{th} time history (Chapter 5)
G(t)	The instantaneous complex gain (Chapter 5)
$e_i(t)$	The complex envelope of the i^{th} time history (Chapter 5)
L(t)	The real gain; the real part of $G(t) = \mathcal{R}e \frac{r_g(t)}{r_f(t)}$
$\xi_{gf}(t)$	The quantity: $\bar{\theta}_g(t) - \bar{\theta}_f(t)$ (Chapter 5)
R(t)	The quantity: $r_g(t)/r_f(t)$ (Chapter 5)

$s_x^{\prime}, s_y^{\prime}, s_z^{\prime}$	Net displacement of load (and lowering line) along the x, y and z axes
T	Lowering line tension
$\lvert T_{i\eta} \rvert$	Response amplitude operator
v_w	Wind speed
v_b	Effective lateral body velocity
W_ℓ	Weight of load
w_b	Effective vertical body velocity
X, Y, Z	Forces acting (positively along the x, y and z axes respectively
x, y, z	Orthogonal axis systems; x-axis horizontal positive toward the bow; y-axis horizontal, positive to port; z-axis vertical, positive upward. Also used to represent translational ship motions surge, sway and heave respectively relative to a state of rest.
α'	Elevation angle of boom in a vertical plane
α	Angle made by the mooring lines from the longitudinal axis horizontally
β_B	Heading angle of barge relative to the wind
β_w	Heading angle of an individual wave relative to the wind
β	Heading angle of waves relative to the heading of the barge ($\beta = \beta_w - \gamma_B$)
γ	Azimuth angle of boom in a horizontal plane
η	Elevation of the free surface
ϕ, θ, ψ	Angular displacements (roll, pitch and yaw) positive for rotations about the x, y and z axes, respectively.
λ	Wavelength
ξ	A dummy variable coincident with x
ρ_o	A correlation coefficient
ρ	Mass density of the fluid
$\bar{\rho}(t)$	The quantity: $e^{\ell(t)} = \frac{\cdots}{\cdots}$

$l(t)$	The quantity: $L(t) - \ln \sigma_j / \sigma_f$ (Chapter 5)
$\sigma_\beta \mid \ell = \ell_o$	The conditional standard deviation of β given the condition that $l = l_o$
$\bar{\beta}(t) =$	$[\bar{\Theta}_g(t) - \bar{\Theta}_f(t)] - A_{rf}\{e_{\beta_{rf}}(\omega)\}$; the deviation of the instantaneous phase difference from its mean value (Chapter 5)

Subscripts

bm	Due to body motions (inertial effects)
d	Due to damping
h	Due to hydrostatic effects
m	Due to moorings
w	Due to waves
o	Relative to waterline reference position
β	Relating to a particular relative heading to the waves
ω	Relating to a particular angular frequency

Superscripts

γ	Azimuthal ordering parameter for line tensions for boom-lowered loads
'	Primed quantities relate to boom lowering (cf. T', α')

ABSTRACT

Results and methods are given for a theoretical study of the behavior of a moored construction-type barge and that of a load, lowered by means of a line from the barge, in irregular seas in deep water. The mooring system considered is a conventional line-and-anchor type, with both bow and stern moorings. Load-lowering through the hull as well as by means of a boom having variable azimuth angle is considered.

Equations of motion of the system for sinusoidal waves of arbitrary length and direction are formulated for six degrees of freedom, and take into account both hydrostatic and hydrodynamic effects. Following the evaluation of the excitation functions and the coefficients in the equations (based on the particular barge under study), sinusoidal solutions of these equations are obtained for each of the six barge motions (surge, heave, pitch, sway, roll, and yaw), as well as for the three rectangular components of the load displacement vector, the vertical component of the load acceleration and the added dynamic tension in the lowering line. In addition, solutions are obtained for the forced in the mooring cables and the horizontal components of the force and the yawing moment induced by the mooring system on the barge.

The irregular sea model employed is the directional Neumann spectrum, which introduces an element of randomness into the study, in particular, the quasi-stationary Gaussian vector-stochastic-process model. Regarding the barge heading as fixed, a discrete set of seventy-two cases of such an irregular sea are considered. These consist of three wind speeds corresponding to Sea States 3, 4, and 5, together with twenty-four wind directions.

For each of the sea-state conditions, the root-mean-square (r.m.s.) values of the fluctuating barge motions and of the fluctuating load and line variables are computed, twenty-four possible boom-azimuth angles measured, from the bow, being considered. Optimum values of the boom angle, which minimize either the r.m.s. value of a component of the load displacement, the vertical load acceleration, or lowering-line tension, are identified and found to be nearly independent of the wind speed and barge heading. The resulting minimum-attainable r.m.s. values of these quantities are given for each barge heading. For the case in which the load is center-lowered through the hull, the corresponding root-mean-square values are given for each barge heading relative to the predominant wind direction. The use of the r.m.s. values for the determination of the probability of any motion exceeding any specified value is illustrated by examples.

Examples of energy spectra for the individual barge motions are presented and interpreted in terms of characteristic features visible on graphical records of the motion time histories. Examples of cross-spectra, relating pairs of barge motions, are presented and interpreted in terms of tendencies in their phase relationship and the characteristics of the barge responses to the seaway. Phase relationships between the barge motions are further investigated by means of the concepts of instantaneous phases and amplitudes; the nature of these random quantities is described by giving their probability distributions. It is shown how the expected phase difference between any two barge motions occuring in a random seaway may be determined for each of the various barge headings relative to the wind. By employing a table of random numbers and representing the individual barge motions as linear combinations of standard random variables, random samples are generated and presented as examples of typical values for the barge motions which might be expected to be seen at a randomly-selected instant.

Illustrative examples show that in a State 5 Sea, heaving and swaying attain their maximum root-mean-square values of approximately 1.7 and 1.8 feet respectively, for cross-wind barge headings, as contrasted with approximately 1.25 feet and 0.8 feet, respectively, for down-wind headings. Interpreted in terms of the Gaussian probability distribution, these r.m.s. values imply, e.g., that the instantaneous absolute value of the heaving motion for a down-wind heading in a State 5 Sea would exceed 0.6 feet approximately 62% of the time. for a center-lowered load, the r.m.s. valued (which are such that they are exceeded in absolute value approximately 32% of the time) of the vertical and the port-starboard load displacement components in a State 5 Sea reach approximately 1.9 feet for cross-wind barge headings, as contrasted with approximately 1.2 feet, for up-or down-wind barge headings. In a State 3 Sea the corresponding r.m.s. values are approximately 0.33 feet and 0.16 feet. On the other hand, the vertical load acceleration has an r.m.s. valued of approximately 1.15 feet/sec^2 for cross-wind headings in a State 5 Sea, as contrasted with 0.60 feet/sec^2 for down-wind headings. For comparison, the corresponding figures are 0.35 and 0.15 in a State 3 Sea. For the hypothetical case of a 200-ton load lowered in a State 5 Sea with a cross-wind barge heading, the downward force of impact upon the ocean floor would exceed 14.3 tons 2.3% of the time if the instant of impact were allowed to occur at random.

For a boom-lowered load, the optimum boom azimuth angle which minimizes the r.m.s. vertical load displacement corresponds to a position directly over the stern. For this boom position, the optimum barge heading is cross-wind. With this barge heading in a State 4 Sea and a boom whose projection in the barge deck is 150 feet, the r.m.s. value of the vertical load displacement is approximately 2.4 feet when the boom is in the optimum (stern) position, whereas it becomes 9.6 feet when the boom is moved to the worst position, viz. directly across the beam.

THE MOTIONS OF A MOORED CONSTRUCTION-TYPE BARGE IN IRREGULAR WAVES AND THEIR INFLUENCE ON CONSTRUCTION OPERATION

By Paul Kaplan [1] and Robert R. Putz [2]

INTRODUCTION

At present, increasing interest is being evidenced in the problems of deep-sea operations of moored vessels. This concern has been brought about by the successfully-conducted preliminary operations in drilling through the ocean bottom from a surfaced ship, the operation colloquially known as the "Mohole Project". On the other hand, from the point of view of military operations, there is need for placing instrumentation packages and possibly other military systems on the ocean floor for application to anti-submarine warfare. These operations require a definite degree of precision, safety during the course of the operation, and the capability of returning to a particular locale and retrieving information and/or the equipment itself for further study of data or for emplacement in another location.

As a result of this emphasis on deep-sea operations, it is necessary to determine the response of a representative moored construction-type barge in the open sea, and also to determine the characteristics of the important parameters associated with lowering loads from such a barge to the ocean floor and returning them to the ship. The parameters that are of interest to the construction personnel aboard the barge are the forces in the moving cables, the displacements and tensions in the lowering lines, the degree of precision in placing the loads, the accelerations acting on the loads, and the magnitudes of impact on the ocean bottom.

In order to arrive at some appropriate engineering estimates of the capabilities of carrying out such operations, a theoretical study has been carried out herein dealing with problems of this nature. The results of the present study are applied to certain representative sea states in order to determine the appropriate information under those particular conditions.

The study of motions of ships at sea is a general problem of naval concern, and has received increasing emphasis during the last ten years by virtue of the advance of statistical methods which describe the effects with greater realism than in previous studies based on simplified wave representations. Major concern has been devoted primarily to the problems of an advancing ship in head seas, with the prime variables of concern being the

(1) Oceanics, Inc.
(2) Marine Advisers, Inc.

heave and pitch motions. Recent studies, however, have been concerned with motions in oblique waves, wherein lateral motions (sway, yaw, and roll) are also important. All of these studies involved very large ships advancing in waves, and only limited theoretical studies have been developed to predict adequately the motions in all six degrees of freedom under these operating conditions. There is a large background of information related to the hydrodynamic forces for zero speed of advance, but no complete treatment of this situation for a realistic ship has been carried out, due to the lack of practical importance for this condition. A treatment of the motion of a free ship with six degrees of freedom in waves is a formidable problem that has not achieved a complete solution at the present time, and when the influences of moorings are also included, the problem is further compounded. Nevertheless, there exists a need for some means of preliminary estimation of the expected motions of a moored construction-type barge, and there appears to be enough information available on the various hydrodynamic forces to allow a study that will indicate the expected range of amplitude of motion. The present study is devoted to carrying out this task, and the results obtained will be useful as guide-lines to operating construction personnel. A required program for experimental verification of the theoretical results, together with recommendations for continued research in this field, are also presented in this study.

This work was carried out under Navy Department, Bureau of Yards and Docks Contract NBy 32206, with technical administration provided by the U. S. Naval Civil Engineering Laboratory.

1. FORMULATION OF TECHNIQUES FOR PROBLEM SOLUTION

In order to determine the motions of the moored barge in irregular waves, it is necessary to determine the motions in regular sinusoidal waves. The aim of this study is to predict these motions, and the technique to be utilized is that of spectral analysis (Reference 1) wherein the statistical definition of the seaway in the form of its energy spectrum is used as the initial data. The energy spectrum of the time history of each motion of the vessel in response to irregular waves is evaluated by the application of the ship response operators for the corresponding degrees of freedom to the energy spectrum of the seaway. These operators are obtained from the solutions for the motions in sinusoidal waves. In accordance with the basic premise of this technique of analysis, a linear theory of ships' motions is a prerequisite for this study.

The equations of motion in regular waves, for six degrees of freedom, will be formulated according to linear theory by the balance of inertial, damping, restoring, exciting, and coupling forces and moments. Both hydrodynamic and hydrostatic effects due to the body-fluid interaction will be included in the analysis, together with the influences of the mooring system. The longitudinal motions (heave, pitch, and surge) will be coupled to each other, and similarly, the lateral motions (sway, yaw, and roll) will also be coupled. There will be no coupling between the two planes of motions, in accordance with linear theory.

The hydrodynamic forces and moments such as damping, exciting effects due to waves, etc., will be determined by application and/or extension of the methods described in References 2 through 5, which represent the latest techniques available for analysis of the motion of ships in waves. Solutions of the equations will be found for regular sinusoidal seas with varying wavelength and heading relative to the barge. The response amplitude operators are found from these solutions, together with the phases of the motions relative to the system of regular waves.

Assuming a knowledge of the oncoming irregular sea conditions, (e.g. in terms of sea state, as specified by an associated surface-elevation energy spectrum from information in Reference 6), the set of energy spectra for the ship motions can be determined. Information on average values and probabilities of relatively high values of the amplitudes of oscillations in the ship-motion time histories for the different degrees of freedom can be found from the ship-motion energy spectra in accordance with the methods of Reference 1. Phase information for ship motions in a confused sea is obtained from the set of cross-spectra for the various pairs of motions. Since the spectral energy model for irregular seas does not specify individual phases for the sinusoidal components of the surface elevation, well-determined phases at a given instant cannot be calculated; however, certain tendencies can be indicated.

Cross-spectra are also used to determine the energy spectra and, hence, the various average values and the probabilities for the remaining quantities of interest in the present study (viz. load-displacement time histories and other quantities which are linear combinations of the ship motions and their time rates of change.) These energy spectra may also be obtained from the solutions of the differential equations by linear superposition, and explicit use of cross-spectra here is necessary only for obtaining phase information.

The barge will be assumed to be placed in a currentless seaway, with no wind effects being considered. This appears to be somewhat unrealistic from the practical point of view, but since concern in the present study is devoted only to the motions induced by the seaway, this neglect is reasonable. The barge is assumed to be moored with bow and stern moorings of conventional line and anchor type.

Initially, in the formulation of the program, some consideration was given to the use of a propulsion type of mooring system, using outboard motors which are controlled. The application of the outboard motors to the Mohole Project was primarily from the point of view of dynamic positioning (see Reference 7), whereby the barge was maintained in some average position, thereby overcoming the drifting effects caused by the environment. These effects are primarily due to winds and currents, and the control by means of the propulsion system was mainly concerned with these effects. If such a system were to be used for control of the motions involved in the response of the system to waves, which are oscillatory in nature, then the control effects of the motors must also be oscillatory. This imposes quite a strain on the system as originally conceived and used for dynamic positioning.

The propulsion control action is primarily proportional to the rate of the motion responses desired, i.e. it is a proportional velocity control, and hence it would be required to alter the net thrust effects of the motors in proportion to the frequencies in the waves. Aside from the strain on the system, it would be required to provide effects in surge, sway, and yaw simultaneously, which is a further complication. Representation of such action in an automatic control system applied to the construction barge would be quite complex, and there are also questions as to its actual effect on the motions of the barge. This is due to the fact that an alteration in the velocity (i.e. damping) terms for the surge, sway and yaw degrees of freedom would not have much influence on a motion phenomenon which is primarily inertial in nature, with relatively large forces occurring during the motions. In view of these various difficulties, no detailed consideration was given to the use of a propulsion system for applying the mooring restraints.

The line and anchor mooring system utilized for this study is a particular system especially suited to deep-sea operations. The effects of these moorings will be to provide restoring effects in the particular displacement of surge, sway and yaw, thereby providing "spring-like" terms in the equations for these degrees of freedom. As a result, there are certain natural frequencies associated with these

motions, which do not ordinarily occur in the case of free (unmoored) ships. The moorings are assumed to have a negligible influence on the motions of heave, pitch, and roll, which have large hydrostatic restoring effects. Since linearity is the prime assumption underlying this study, various motion effects known to occur due to the nonlinear influences will not be accounted for in this study. Effects of this nature include "induced" motions such as that of roll in regular head seas (see Reference 8), and also the nonlinear yaw tendency of ships due to nonlinear inertial effects (see Reference 9). The existence of the mooring restraints will mitigate the effects of some of these phenomena, and it is also possible that the latter may not be present to any appreciable degree when irregular waves are considered since these nonlinear effects usually depend upon long periods of continuous oscillatory wave motions for their occurrence.

Following the evaluation of the various motions of the moored barge, equations will be formulated to determine the forces in the mooring cables and the displacement of and tension in lowering line as a function of the different degrees of freedom of the oscillating barge platform moored in the seaway. The line displacement and tension, which are functions of the ship motions, will be related to the seaway and all of the resulting spectra will be determined. Operations on these quantities will provide information on expected amplitudes for particular sea states. In the course of this work, expressions for the vertical accelerations of the loads will be determined and their magnitudes will be similarly expressed. This information will be useful for study of impact of the loads on the ocean bottom.

Computations of the amplitudes and phases of the six separate motions of the moored barge for the complete range of possible headings will be carried out for wavelengths varying from 100 feet to 800 feet. This will cover the range of periods significant for ship motion in an operational environment up to sea state 5. The relatively low frequencies at larger wavelengths will allow the effects of the larger wavelengths to be determined by simple static considerations, as long as no resonance conditions occur in that range of wavelengths. These further results may be considered, if necessary to broaden the information on the response amplitude operators for application to spectral determination in the higher sea states.

The particular vessel for which computations will be carried out is the CUSS I, which was the vessel used in the preliminary Mohole drilling operation. This ship is considered representative of the class of construction-type barges which will be utilized for deep-sea construction operations. A diagram of the barge, together with its mooring and load-lowering lines, is shown in Figure 1.1. A summary of the numerical values of the parameters characterizing the moored-barge system is presented in Table 1.

In the course of the exposition, the general nature of the problem as well as its solution will be delineated using the general probabilistic model of an essentially two-parameter stochastic process, representing the seaway, exciting a rigid body representing the barge, and the related one-parameter vector stochastic process whose components are time-history functions representing the motions of the barge and the simultaneous associated mooring and load-lowering phenomena.

Table 1

Numerical Values of Moored-Barge-System

Length	$=L$	$=260$ ft.
Beam	$=B$	$=48$ ft.
Draft		$=10$ ft.
Vertical distance from CB to CG	$=\lvert BG\rvert$	$=9.8$ ft.
Vertical distance from free surface to CG	$=(\overline{OG})$	$=5.1$ ft.
Vertical distance from CG to keel	$=\lvert KG\rvert$	$=15.1$ ft.
Metacentric height	$=\lvert GM\rvert$	$=8.16$ ft.
Displacement		$=2823.2$ long tons
Weight	$=W$	$=6.324\times10^{6}$ lbs.
Mass	$=m$	$=197.624\times10^{3}$ slugs
Pitch moment of inertia [1].	$=I_{y_o}$	$=m(.25L)^2=706.7\times10^{6}$ slug-ft.^{2}
Yaw moment of inertia [1].	$=I_{z_o}$	$=m(.25L)^2=706.7\times10^{6}$ slug-ft.^{2}
Roll moment of inertia [2].	$=I_{x_o}$	$=m(B/3)^2=49\times10^{6}$ slug-ft.^{2}
Total roll moment of inertia (including added inertia due to fluid)	$=I_{x_t}$	$=78.69\times10^{6}$ slug-ft.^{2}
Surge period[3].	$=T_{surge}$	$=79$ seconds
Sway period	$=T_{sway}$	$=64.5$ seconds
Heave period	$=T_{heave}$	$=4.6$ seconds
Pitch period	$=T_{pitch}$	$=4$ seconds
Natural roll period [4].	$=T_{roll}$	$=7.75$ seconds
Effective spring constant for mooring cable [5].	$=C$	$=1250$ lbs./ft.
Effective mooring system spring constants:		
Surge	$=k_x$	$=1250$ lbs./ft.
Sway	$=k_y$	$=3750$ lbs./ft.
Yaw	$=k_\psi$	$=633.75\times10^{5}$ lb.-ft./rad.
Depth of barge	$=$	15 ft.

1. Assuming longitudinal gyradius = 0.25L
2. Without added fluid inertia; it is assumed that transverse gyradius = B/3
3. For all motions these are uncoupled periods determined in terms of effective spring constants and values of total masses or inertias. The effects of coupling will change these somewhat, but for first approximations and interpretation of critical conditions, this will suffice.
4. From Stevens Institute of Technology model tests (Reference 16, Appendix)
5. Bridge strand wire rope, of cross-section 0.595 in.^{2}

The solution to the problem will be delineated in two ways. First, it will be given in terms of the minimal information (e. g. the complete matrix -- valued cross-spectral or cross covariance functions) that is necessary in view of the assumed Gaussian nature of the input to the system, the linear nature of the system itself, and consequently, the Gaussian nature of the output of the system. Then, once the solution has been strictly characterized, it will be given in terms of examples of the available inferences and other accessible results concerning output quantities.

These inferences will include those derivable from both the descriptions of the energy spectra for individual motions, and the cross-spectra for pairs or, generally, sets of motions of time-varying quantities. In view of the knowledge concerning the energy spectra which will be obtained, the treatment will necessarily extend beyond that providable by the convenient narrow-band spectral theory. Information on the probability distributions of ordinates on the time-history curves and of instantaneous amplitudes will be supplemented by information on the distributions of the heights of the relative maxima (or peaks) on the motion curves and mean zero-crossing frequencies, together with simplified methods of obtaining it from plotted energy-spectrum curves for the motions. Information on the relative values of instantaneous amplitudes and phases of a pair of simultaneously-observed motion time histories is obtainable in the form of joint probability distributions for quantities associated with the components of the complex instantaneous gain corresponding to the motion time history pair. All available information concerned strictly with phase relationships which is contained in the probabilistic solutions is thereby obtained. Additional treatment of the general properties which include the phase-relationship concept, involving a more explicit use of the probabilistic structure of the vector stochastic process is provided by direct utilization of the cross-covariance matrix for the generation of typical sample values of the motion quantities at one fixed instant of time. The extension of this technique to the generation of sample segments of the time-history functions extending over a representative length of time would give a complete solution of the problem in graphical form. The use of this general technique yields, in addition to the sample values, the information concerning the predictability of one or more motions from a given set of motions. Examination of the spectral-coherence structure of the solutions which provides additional information related to phase relationships is obtained from the transfer functions for the generation of the time history of one motion from that of another.

Obtaining the solution to the problem of characterizing the barge, load, and mooring motions in various seaways involves a great number of cases, due to the number of possible combinations of the independent parameters, preventing that a complete presentation of these results is prohibitive. Specifically, this problem has sea state (i. e., wind speed), barge heading, relative to wind, and method of load lowering as its independent parameters; these take on, respectively, 3, 24 and 25 distinct values in this analysis, resulting in 3 x 24 x 25 = 1800 possible cases of the problem.

For each case, the solution to the problem concerns the nature of the mutual relationships among a set of 19 motions. If one restricts the nature of the solution for any one case to the determination of the minimal information necessary to specify the resulting 19-component output vector stochastic process, viz. its matrix-valued cross-spectral density function, then the formal solution is indexed by three independent parameters. These are wavelength, output time history for matrix row, and output time history for matrix column, Since the effects of each of a set of eight wavelengths were considered, the three parameters take on 8, 19 and 19 distinct values, respectively. Hence there are 8 x 19 x 19 = 2888 solution-numbers for each case, yielding a total of 1800 x 2888 = 5, 198, 400 values for the complete solution of the problem.

This comprehensive enumeration of cases may serve, in part, to clarify the structure of the problem. The results represent an overstatement of the magnitude of the task in so far as redundancies and instances of simple proportionality in the set of 19 output time histories may reduce their equivalent number to 15 or 16; likewise, the consideration of as many as 24 different barge headings relative to the wind, as well as 24 different boom angles, might be considered an extravagance -- if so, the number of different problems might be reduced by a factor of about 4. This manner of stating the task, however, is also in a sense, conservative, since it calls for no interpretation of the results, consisting solely of cross-spectral density functions; no information on total energies or root-mean-square values for the various motions, information of any kind on amplitudes of oscillation or phase relationships, or of optimum operating conditions would be included explicitly in these results.

It appears desirable to direct attention to the very real problem, encountered during the phase following the determination of the initial results (i. e., the response operators) given by the hydromechanical theory and preceding the application of the oceanographic and stochastic theory, of anticipating the most useful calculations a priori, out of the great wealth of cases possible to present. Indeed, considerable effort was directed at this time just toward determining which cases were feasible to calculate!

A change in emphasis occurring after the initial probabilistic results were obtained was primarily responsible for magnifying this problem and resulted in its reappearance after the first draft of this report had been prepared. It then appeared that the desirable form for the presentation of the solutions to the problem was substantially more comprehensive, more detailed, and more expository in nature than the form programmed.

There appears to be little doubt that the degree of completeness of the present edition of the report has been affected by the earnest attempt to increase the scope of its coverage, while at the same time satisfy the dual requirements of maintaining an adequate level of scientific style and keeping the applicable results accessible to the uninformed reader. As to the outcome, the challenge was accepted, the scope enlarged, with considerable attention being directed toward providing interpretive aid to the reader, and a resulting disproportionate amount of available effort was found to remain for preparing a totally satisfactory report to be issued

on a finally-determined date. The technical problem of presenting the results has been regarded as comprising the following requirements: to provide, (a) as much fundamental information covering as many cases as possible; (b) as much additional information having importance for applications as possible; (c) as many additional examples suggesting further results as possible; and (d) as much interpretation and insight into the manner in which the presented results arise from the given data of the problem. The reader may thus be helped to fill in gaps and extend the range of the study in directions which may not require additional digital computer time.

As a natural outcome of the results of the present study, certain specific methods of data analysis involving spectral concepts suggest themselves as a means of partial verification of these results by means of an experiment conducted with an instrumented vessel in a natural seaway in the ocean. Such methods involve either the testing of various hypothesis regarding the spectrum of the seaway and the complex response operators for the vessel or the formation of numerical estimates of these quantities.

2. APPLICATION OF PROBABILISTIC AND SPECTRAL CONCEPTS TO THE ANALYSIS OF OCEAN WAVES AND SHIP MOTIONS

Wind-generated surface waves in deep water may be regarded in the linearized theory as the result of the superposition of a continuum of elementary unidirectional sinusoidal waves, with each of which there is associated a wavelength, or frequency, and a direction of propagation. A function of frequency and direction which assigns a wave amplitude (or, equivalently, an energy) density to each elementary wave is known as a directional spectral energy-density distribution describing a given surface wave regime, or seaway. Since the wave phase remains unspecified, a seaway for which the energy spectrum alone is given, contains an element of indeterminacy. This is natural if the time and place, as well as the manner of generation, of the waves are likewise unspecified.

A precise mathematical model for the seaway which has proved useful employs the probabilistic concept of a temporally homogeneous, or stationary, vector stochastic process (Reference A). As applied to ocean surface waves, one formulation of this model associates with the unspecified set of phase angles of the elementary component surface waves a multi-dimensional probability distribution, the component random phase variables of which are independently distributed with a common uniform probability density extended over the complete 360° circle. This type of randomness for phase angles reflects a corresponding uniform randomness or indeterminacy for the variable representing the time of observation.

In general, to each set of values of the instantaneous elevation of the water surface, measured from its mean level, at a specified set of instants in time and points in space, this model ascribes a joint probability distribution of the type known as multinormal, or Gaussian. This probability distribution is unchanged if the observations are uniformly advanced or retarded in time, or if they are translated horizontally in space. Under these circumstances, the special nature of the multinormal probability distribution is such that it is uniquely determined by the specification of a set of functions, known as the cross-covariance functions, or equivalently, by the set of Fourier transforms, or spectra, of these functions. These spectra are known as the cross-spectra for the vector stochastic process corresponding to the measured time histories at the specified set of locations. The set of cross-spectra is determined by means of linear surface-wave theory by the directional spectral energy-density distributions for the surface wave regime. Equivalently, the directional spectral energy-density distribution determines the cross-covariance functions and, hence, the (joint) multinormal distribution of values for the surface elevation at specified locations.

Summarizing what has been stated above concerning the model employed for the seaway, we have (1) the seaway or surface elevation of the ocean is composed of a continuum of elementary sinusoidal waves characterized by their lengths and directions as well as their phases and amplitudes; the phases are regarded as indeterminate, but the amplitudes are specified by a directional spectral-energy

density function $|S(\omega,\beta)|^2$, (2) the phase indeterminacy results in multinormal (Gaussian) probability distributions for the values of the surface elevation at different locations; these probability distributions are completely characterized, either by a set of cross-covariance functions or by a set of cross-spectral-density functions which in turn are determined by the directional spectral energy distribution function $|S(\omega,\beta)|^2$.

It appears difficult to overemphasize the importance of the class of multinormal (Gaussian) probability distributions or to point out an excessive number of its special properties. A very general property which it possesses is that of being unaltered by the performance of linear operations. Operations of this type range from simple addition or subtraction of two components, to multidimensional linear transformations, and to mathematical transformations corresponding to passage through multi-channel systems whose net effect corresponds to the relationship between the excitation functions and the solution functions of a system of simultaneous linear integro-differential equations. These properties of linearity greatly simplify the problem of generating samples from multinormal distributions with a given set of covariances by the use of a table of random numbers.

In particular, if any subset of a set of random variables having a multinormal distribution is considered to have a given fixed set of values, the remaining complementary subset likewise has a multinormal distribution; if the first subset is deleted from the set, this result still holds. In either case, the means, variances and covariances for the remaining set of random variables are readily calculable, which is an aid to carrying out linear least-squares prediction between the random variables of the set. Each of the set of parameters necessary to specify a multinormal distribution refers to no more than two variables at a time, a reflection of the fact that all multivariable moments of order higher than the second are expressable in terms of those of second order.

The one-dimensional and the two-dimensional normal (Gaussian) or binormal distributions are extensively tabulated, including their cumulative (integral) forms. The sole parameter necessary to specify the distribution for a one-dimensional normal random variable is its r.m.s. value, or standard deviation, σ_x. The one-dimensional case will be discussed below.

The set of three parameters specifying the two-dimensional distribution for the random variable (X, Y) with zero means consists of the one covariance between X and Y and the two individual variances for X and Y. These are commonly denoted as σ_{XY}, σ_X^2, and σ_Y^2, respectively, and by definition are, respectively, the mean of the product of X and Y, the mean square of X and the mean square of Y. The square roots, σ_X and σ_Y, of the latter two are the so-called standard deviations, or root-mean-square (r.m.s.) values, of X and of Y. The ratio of the covariance between X and Y to the geometric mean of the variances of X and Y is the ordinary coefficient of correlation, $\rho_{XY} = \frac{\sigma_{XY}}{\sigma_X \sigma_Y}$.

Having described some features of the multinormal distribution, we proceed to consider the application to the moored barge and return to the consideration of the stochastic process representing the time history of the surface elevation η (0, 0, t), at the fixed point in the mean surface where coordinates are referred to the coordinate system used in Appendix A. Imagining the barge to be moored so that its center of gravity is vertically below this point, the excitation functions and equations of motion for the moored-barge system at each wave length are seen from the Appendix to be obtainable in a linear manner from η(0, 0, t). Since the system of differential equations is linear and η (0, 0, t) is random, and Gaussian, it follows that the values taken on by the seven-component vector function (X, Y, Z, ϕ, θ, ψ, η) are random, and that the vector is represented by a seven-component stochastic process. In other words, the output of the moored barge in response to the input wave regime is non-deterministic, and for no time can any definite values be assigned to the ship motions nor to the surface elevation. Only probability statements and statements about probability distributions such as average values and other moments of random variables may be obtained. The same is true of a vector function such as (X, Y, Z, ϕ, θ, ψ, η_1, η_2, ..., η_n), where the η's are surface-elevation time histories at a set of different locations. It will be seen that the effect of the general directional spectral-energy density function is to introduce a lack of coherence between the pairs of individual barge motions and surface-elevation time histories.

The complete set of cross spectral-density functions necessary to characterize this vector stochastic process may be obtained from the solutions of the differential equations, i.e. from the complex response operators and the directional spectral-energy distribution for the wave regime, as described in Appendix H, since these operators, by definition, yield the amplitudes and phases of the barge motions due to individual sinusoidal surface-elevation waves. Furthermore, the complex response operators, and hence the cross-spectral density function for any two linear combinations of barge motions and surface elevation, may be found by forming the same linear combinations of the complex response operators for the barge motions. In this way all the available information the present model of the seaway is capable of providing may be obtained in the form of the set of all possible cross spectral-density functions associated with the time histories of interest.

We next consider the interpretation and application of the information which is available, once we have computed the cross-spectral densities in the case of a random Gaussian seaway. In the first place, there are available through computation the moments of each of the cross spectral-density functions. The moment of order zero of each spectral energy-density curve, corresponding to the area under the spectrum, is also the total energy and the mean-square value of the random time history involved. Its square root is the root-mean-value for the time history.

A knowledge of the r.m.s. value for a time history, f(t), allows the fraction of the time spent by the ordinate on the time-history curve between any two specified ordinate levels to be determined. In particular, the probability that the ordinate on the curve will exceed, in absolute value, any level of interest, at an

arbitrarily-specified distance above the mean (zero) may be determined. For this purpose, tabulated values of the one-dimensional normal (Gaussian) probability integral function may be used. For convenience, the equivalent of such tables is provided by the graph shown in Figure 2.1, making use of common "normal probability" paper. Shown on the graph are representative curves, each of which corresponds to a normal distribution having a mean value of zero and the r.m.s. value, or standard deviation, σ, equal to the value labeled on the curve. The units are arbitrary and may be taken to represent linear or angular displacements, measured in feet, degrees or radians. The manner in which the curves may be used is illustrated in the following examples.

The ordinate on a time-history curve, denoted by X(t), is a random variable normally distributed about a mean value of 0 and with an r.m.s. value of 3 feet. The probability is required that X(t) will lie between +6 feet and +10 feet if the time t is selected at random. The probability expressed in percent is obtained by referring to the curve labeled $\sigma = 3$, entering the ordinate scale on the left at each of the two values +6 and +10, reading off the percentages marked on the abscissa scale at the bottom at the points at which the curve for $\sigma = 3$ intercepts the horizontal lines through +6 and +10 and subtracting. The desired probability is approximately 99.95% - 86.0% = 13.95%. As a second example, consider a case in which the two ordinates are equally distant from the mean (zero) ordinate level. Thus, the probability that X(t) will lie between $\pm$ 10 is seen to be approximately 99.95% - 0.05% = 99.90%; in this case, the symmetry in the figure may be utilized to shorten the calculation by replacing the abscissa reading which is lower in value by "50.0%" and doubling the resulting difference, yielding (99.95% - 50.0%) x 2 = 99.90%, as before. As a final example, consider a case in which the probability for the random variable to lie outside a given interval is required. Thus, if the r.m.s. value of a random variable, $\varphi(t)$, having zero mean is 5°, the probability that $|\varphi(t)| > 8°$ is given by the complement of 95.0% - 5.0%, which is 100% - 90% = 10%. The final probability obtained in this example is illustrated by the total shaded area shown under the curve appearing as an inset in Figure 2.1, if we take the values of σ and k shown there to be 5 and (1.6)5 = 8.0.

Although the limits of Figure 2.1 extend to probabilities as high as 99.98%, or as low as 0.02%, if one's interest is in extreme values, more extensive tabulations of the normal probability integral would be required to expand this range. Since confidence in the applicability of a given probability distribution is often least at its extremes, this procedure may well place an undue strain on the Gaussian seaway model.

Additional curves may be constructed for any desired values of σ by drawing the straight line of the graph in Figure 2.1 determined by the point of intersection of the curves shown and the point on the dotted vertical line through 84.1% at the height corresponding to the value of σ on the vertical scale on the left. Alternatively, the curve shown for $\sigma = 1$ may be used quite generally if one divides the ordinate levels of interest by the r.m.s. value of the random variable concerned.

In addition to the energy spectra for individual time-histories, the complete set of cross-spectral densities for the solutions determines, via the set of cross-covariance functions, the complete specification of the joint probability density for the distributions of the values of the time-history selected at any desired set of instants. The knowledge of any one of these joint distributions, together with the various marginal and conditional probability distributions arising when certain time histories are either ignored or assigned certain values, may represent a considerable amount of information.

In a meaningful sense, such information might be regarded as constituting the general solution to the problem of the present study; however, it is often desired to provide somewhat more tangible information, concerning, for example, quantities visually apparent in the geometrical structure of the trace on a graphical recording of the time histories. To obtain information regarding the probability distributions for quantities of this kind, one may augment the original set of time-history solutions by adjoining to it various closely-allied time histories such as their time rates of change and the functions in quadrature with them, i.e., their Hilbert transforms or "conjugate functions". The joint probability distributions for the enlarged set of functions are derivable from the original complete set of cross-spectral density functions. With such probability distributions available, information regarding a variety of random events and variables becomes available in principle. Among those variables for which rather complete results are known are the slope of the time-history curve, its instantaneous amplitude, its phase and frequency, and the heights of its relative maxima ("peaks", measured from its mean value). In the case of a pair of random time-history functions, information is available (see below) for the instantaneous complex-valued gain (incorporating both instantaneous phase shift and amplitude ratio).

For all of the quantities mentioned thus far, complete probability distributions have been rigorously worked out for stationary Gaussian stochastic processes, and expressions for most of them are available in the literature. In addition, expressions are available for the values of such parameters as the expected number of times per second that the time-history curve (or its slope) passes in the same direction through its mean value, the mean height of the highest one-third of the instantaneous amplitudes, and the mean height of the highest one-third of the peak heights.

The information referred to thus far, is contained entirely in a relatively small set of numbers, a few of the lower-order spectral moments. The absolute moment of the energy spectrum of order, p, if it exists, may be defined as

$$M_p = \int_{-\infty}^{\infty} d\omega\, \Phi(\omega) |\omega|^p$$

where $\Phi(\omega)$ is the bilateral spectral density function.

Figure 2.2 shows the cumulative probability distribution for the ordinate on a random time-history curve (measured from its (zero) mean ordinate) at a point which is a relative maximum on the curve. It, therefore, represents the "peak height" distribution, which is seen to depend on two parameters: viz., the r.m.s. value of the ordinate denoted by σ_i, and a dimensionless parameter denoted by ρ_o. The latter parameter has the following interpretations: (1) it is the negative of the ratio of the mean zero-crossing frequency for the ordinate to that for the slope; (2) it is the coefficient of correlation between the ordinate and the second derivative; and (3) a quantity closely related to simple ratios of moments of the energy spectrum.

The use of the curves in Figure 2.2 is illustrated by the following example. Given σ_i = 4.0 feet, ρ_o = -0.70, the probability, 99.2%, of a peak not exceeding 12 feet, i.e., three times the value of σ_i, is read in percent from the horizontal scale at the point corresponding to the intercept of the curve for -0.7 on the horizontal line through the level y = 3 on the vertical scale.

The probability distribution corresponding to the curve labelled "ρ_o = -1" in Figure 2.2 is the well-known Rayleigh distribution. This distribution is in fact the probability distribution for the ordinates on the instantaneous amplitude curve (or the real part of the complex envelope) for a given time history. It is seen here to apply to peak heights in the limiting case in which the energy spectrum for the time-history function has infinitesimal width. This distribution is often used as an approximation to the distribution of wave heights or peak heights in the absence of knowledge of the relative bandwidth of the energy spectrum.

Figure 2.3 shows the manner of variation of the mean value of the maximum wave amplitude occurring among a set of consecutive oscillations. As an example of its application, consider a case of 300 oscillations observed on a time-history record for which the r.m.s. value is 4.0 ft. Reading up from 300 on the horizontal scale, across to 3.5 on the vertical scale, and multiplying by 4.0, yields 14.0 ft. for the expected maximum amplitude during a set of 300 oscillations.

It may be seen from all three figures appearing in the present chapter, giving probability distributions or their parameters, that the r.m.s. value, σ_i, of the time-history function, or equivalently, the square root of its total energy plays a direct role. In Figure 2.1 the effect of σ_i on the percentiles of the instantaneous ordinate distributions is seen to be linear. In the remaining two figures, σ_i is the non-dimensionalizing constant used on the ordinate scales (as might also have been done on Figure 2.1). Therefore, it is clear that the values to be expected for the ordinates, or peak heights, at any given probability level, or for the average value in the case of the maximum amplitude are all directly proportional to the r.m.s. value σ_i. Of the large number of parameters available for describing an energy spectrum, its total energy, or, equivalently, the r.m.s. value of the time history, is the most important single parameter.

Leaving the subject of energy spectra, and considering briefly the subject of cross-spectra proper, it is clear that there is no less information content in this type of spectrum; on the other hand, they are considerably more numerous. However, the examples of their application given here will be relatively limited.

When a pair of time-history functions are considered, there is a single complex-valued cross spectrum or, equivalently, two real-valued co- and quadrature spectra involved. When a set of n time-history functions are considered, there are n^2 complex-valued cross spectra which include the n autospectra. The moments of these (complex-valued) cross spectra play the same role as they do in the case of energy spectra. Although there is more information present in the case of a set of time histories, relatively few interpretations or other results have appeared in the literature. One set of results is given below concerning the moment of order zero of a complex-valued cross spectrum in connection with the problem of describing the phase relationships between pairs of time histories. In this case, consideration is given to the random difference between the instantaneous phases for the two time histories, as well as the ratio of their instantaneous amplitudes. Further, the above two quantities may be paired together into the concept of instantaneous complex gain.

Further matters of interest when more than one time-history function is under consideration include questions of synchronism, coherence, and the degree of interpredictability between the time histories. Spectral coherence, or coherency has been adopted as a technical term used in the analysis of multiple time-history functions (time series). Prediction of the value of one time history at a specified time from a knowledge of the values of others at other specified times may be carried out in a predetermined optimum manner, minimizing the mean square error of predictions, if the cross-spectral densities are available. In such prediction, the values of the cross-covariance functions for appropriate values of their arguments may be used when finite predictions are employed, or the cross-spectral densities may be used more directly if optimum transfer functions are desired for use on the entire extent of the time histories. In the latter case, the phase-shift characteristics of the transfer function are of interest in describing the tendency of the phase relations between the time histories. Use of the spectral coherence function here enables the magnitude of the error of prediction to be calculated.

The information contained in the complete set of cross-spectra for a set of random time-history functions also will yield information regarding their nature by making it possible to generate simultaneous random samples from these time histories. This way of looking at typical results may be carried out by calculating the cross-covariance functions and determining coefficients to be applied to the entries in a random-number table.

Finally, cross-spectral information furnishes a means of developing test criteria and methods of estimating the true response operators of a vessel from ship-motion data taken in an actual seaway. Simultaneous recordings made of

the flow field in the water associated with the surface waves will increase the efficiency of such procedures. Analogous techniques can be used for inquiring into the nature of the directional spectral-energy distribution of the surface elevation. In this way, some of the results and assumptions of the present study can be subjected to examination.

To determine definite numerical results from a study based upon the methods and general assumptions we have described, requires that a particular, numerically specified, seaway be given. For this purpose, a convenient model is furnished by the so-called directional Neumann spectrum. As we have noted, the application of the concept of a Gaussian stationary stochastic process to the local seaway yields a number of results describing features of "individual waves" in an irregular sea such as mean wave height, significant wave height ($H_{1/3}$), etc. The theory of Neumann and Pierson has resulted from the attempt to correlate such parameters with the wind velocity, v_w, in the wave-generating area in the case of the "fully arisen sea", which results when the time duration and spatial extent of the wind field are sufficient to cause wave-equilibrium conditions. The chart appearing on the following page serves to define a "sea-state" scale for the case of a unidirectional wave spectrum analogous to the Beaufort wind scale.

For computational purposes in the present study, the Neumann-Pierson spectral-energy description of the seaway has been adopted, and calculations made for three particular sea states, corresponding to three particular wind speeds. The following table illustrates the conditions.

TABLE I

Sea State Number	Wind Speed v_w (knots)	Significant Wave Height $H_{1/3}$ (feet)	Surface Elevation (Time History and Energy Spectrum)		
			r.m.s. value, σ, (feet)	Total energy, σ^2, (feet)^2	$2\sigma^2=E$
3	14	3.3	0.81	0.66	1.32
4	19	6.9	1.75	3.05	6.10
5	22	10.0	2.50	6.23	12.46

It will be noted that in each case the variance or the square of the r.m.s. surface elevation time history, denoted by σ^2, is taken as the total spectral energy which is, in turn, one-half of the quantity often designated by "E". For clarity, we state here that the variance and the total energy are regarded in the present report as the area, over its entire range of definition, under the curve

WIND AND SEA SCALE FOR FULLY ARISEN SEA

SEA STATE [1]	SEA-GENERAL: DESCRIPTION [2]	WIND [3]: BEAUFORT WIND FORCE	WIND [3]: DESCRIPTION	WIND [3]: RANGE (KNOTS)	WIND [3]: WIND VELOCITY (KNOTS) AVERAGE	SEA [3]: WAVE HEIGHT FEET: AVERAGE	SEA [3]: WAVE HEIGHT FEET: SIGNIFICANT	SEA [3]: WAVE HEIGHT FEET: AVERAGE 1/10 HIGHEST	SEA [3]: SIGNIFICANT RANGE OF PERIODS (SECONDS)	SEA [3]: PERIOD OF MAXIMUM ENERGY OF SPECTRUM (T_{max})	SEA [3]: $\bar{T}$ (AVERAGE PERIOD)	SEA [3]: $\bar{L}$ (AVERAGE WAVE LENGTH)	SEA [3]: MINIMUM FETCH (NAUTICAL MILES)	SEA [3]: MINIMUM DURATION (HOURS)
0	Sea like a mirror.	0	Calm	Less than 1	[a] 0	0	0	0	–	–	–	–	–	–
	Ripples with the appearance of scales are formed, but without foam crests.	1	Light Airs	1 - 3	2	0.05	0.08	0.10	up to 1.2 sec	0.7	0.5	10 in.	5	38 min
1	Small wavelets, still short but more pronounced; crests have a glassy appearance, but do not break.	2	Light Breeze	4 - 6	5	0.18	0.29	0.37	0.4-2.8	2.0	1.4	6.7 ft	8	39 min
	Large wavelets, crests begin to break. Foam of glassy appearance. Perhaps scattered white horses.	3	Gentle Breeze	7 -10	8.5	0.6	1.0	1.2	0.8-5.0	3.4	2.4	20	9.8	1.7 hrs
2					10	0.88	1.4	1.8	1.0-6.0	4	2.9	27	10	2.4
	Small waves, becoming larger; fairly frequent white horses.	4	Moderate Breeze	11-16	12	1.4	2.2	2.8	1.0-7.0	4.8	3.4	40	18	3.8
3					13.5	1.8	2.9	3.7	1.4-7.6	5.4	3.9	52	24	4.8
					14	2.0	3.3	4.2	1.5-7.8	5.6	4.0	59	28	5.2
					16	2.9	4.6	5.8	2.0-8.8	6.5	4.6	71	40	6.6
4	Moderate waves, taking a more pronounced long form; many white horses are formed. (Chance of some spray).	5	Fresh Breeze	17-21	18	3.8	6.1	7.8	2.5-10.0	7.2	5.1	98	55	8.3
					19	4.3	6.9	8.7	2.8-10.6	7.7	5.4	99	65	9.2
5					20	5.0	8.0	10	3.0-11.1	8.1	5.7	111	75	10
	Large waves begin to form; the white foam crests are more extensive everywhere. (Probably some spray).	6	Strong Breeze	22-27	22	6.4	10	13	3.4-12.2	8.9	6.3	134	100	12
					24	7.9	12	16	3.7-13.5	9.7	6.8	160	130	14
6					24.5	8.2	13	17	3.8-13.6	9.9	7.0	164	140	15
					26	9.6	15	20	4.0-14.5	10.5	7.4	188	180	17
	Sea heaps up and white foam from breaking waves begins to be blown in streaks along the direction of the wind. (Spindrift begins to be seen).	7	Moderate Gale	28-33	28	11	18	23	4.5-15.5	11.3	7.9	212	230	20
					30	14	22	28	4.7-16.7	12.1	8.6	250	280	23
					30.5	14	23	29	4.8-17.0	12.4	8.7	258	290	24
					32	16	26	33	5.0-17.5	12.9	9.1	285	340	27
					34	19	30	38	5.5-18.5	13.6	9.7	322	420	30
					36	21	35	44	5.8-19.7	14.5	10.3	363	500	34

*For hurricane winds (and often whole gale and storm winds) required durations and fetches are rarely attained. Seas are therefore not fully arisen.

a)A heavy box around this value means that the values tabulated are at the center of the Beaufort range.

b)For such high winds, the seas are confused. The wave crests blow off, and the water and the air mix.

1)Encyclopedia of Nautical Knowledge, W.A. McEwen and A.H. Lewis, Cornell Maritime Press, Cambridge, Maryland, 1953, p. 483

2)Manual of Seamanship, Volume II, Admiralty, London, H.M. Stationery Office, 1952, pp. 717-718

3)Practical Methods for observing and forecasting Ocean Waves, Pierson, Neumann, James, N.Y. Univ, College of Engin, 1953.

3					16	2.9	4.6	5.8	2.0-8.8	6.5	4.6	71	40	6.6
4	Moderate waves, taking a more pronounced long form; many white horses are formed. (Chance of some spray).	5	Fresh Breeze	17-21	18	3.8	6.1	7.8	2.5-10.0	7.2	5.1	98	55	8.3
					19	4.3	6.9	8.7	2.8-10.6	7.7	5.4	99	65	9.2
5					20	5.0	8.0	10	3.0-11.1	8.1	5.7	111	75	10
	Large waves begin to form; the white foam crests are more extensive everywhere. (Probably some spray).	6	Strong Breeze	22-27	22	6.4	10	13	3.4-12.2	8.9	6.3	134	100	12
					24	7.9	12	16	3.7-13.5	9.7	6.8	160	130	14
6					24.5	8.2	13	17	3.8-13.6	9.9	7.0	164	140	15
					26	9.6	15	20	4.0-14.5	10.5	7.4	188	180	17
	Sea heaps up and white foam from breaking waves begins to be blown in streaks along the direction of the wind. (Spindrift begins to be seen).	7	Moderate Gale	28-33	28	11	18	23	4.5-15.5	11.3	7.9	212	230	20
					30	14	22	28	4.7-16.7	12.1	8.6	250	280	23
7					30.5	14	23	29	4.8-17.0	12.4	8.7	258	290	24
					32	16	26	33	5.0-17.5	12.9	9.1	285	340	27
	Moderately high waves of greater length; edges of crests break into spindrift. The foam is blown in well marked streaks along the direction of the wind. Spray effects visibility.	8	Fresh Gale	34-40	34	19	30	38	5.5-18.5	13.6	9.7	322	420	30
					36	21	35	44	5.8-19.7	14.5	10.3	363	500	34
					37	23	37	46.7	6-20.5	14.9	10.5	376	530	37
					38	25	40	50	6.2-20.8	15.4	10.7	392	600	38
8					40	28	45	58	6.5-21.7	16.1	11.4	444	710	42
	High waves. Dense streaks of foam along the direction of the wind. Sea begins to roll. Visibility affected.	9	Strong Gale	41-47	42	31	50	64	7-23	17.0	12.0	492	830	47
					44	36	58	73	7-24.2	17.7	12.5	534	960	52
9					46	40	64	81	7-25	18.6	13.1	590	1110	57
	Very high waves with long overhanging crests. The resulting foam is in great patches and is blown in dense white streaks along the direction of the wind. On the whole the surface of the sea takes a white appearance. The rolling of the sea becomes heavy and shocklike. Visibility is affected.	10	Whole Gale*	48-55	48	44	71	90	7.5-26	19.4	13.8	650	1250	63
					50	49	78	99	7.5-27	20.2	14.3	700	1420	69
					51.5	52	83	106	8-28.2	20.8	14.7	736	1560	73
					52	54	87	110	8-28.5	21.0	14.8	750	1610	75
					54	59	95	121	8-29.5	21.8	15.4	810	1800	81
	Exceptionally high waves (Small and medium-sized ships might for a long time be lost to view behind the waves.) The sea is completely covered with long white patches of foam lying along the direction of the wind. Everywhere the edges of the wave crests are blown into froth. Visibility affected.	11	Storm*	56-63	56	64	103	130	8.5-31	22.6	16.3	918	2100	88
					59.5	73	116	148	10-32	24	17.0	985	2500	101
	Air filled with foam and spray. Sea completely white with driving spray; visibility very seriously affected.	12	Hurricane*	64-71	> 64	> 80[b]	> 128[b]	> 164[b]	18-(35)	(26)	(18)	~	~	~

By or over high winds, the seas are confused. The wave crests blow off, and the water and the air mix.

1) Encyclopedia of Nautical Knowledge, W.A. McEwen and A.H. Lewis, Cornell Maritime Press, Cambridge, Maryland, 1953, p. 483

2) Manual of Seamanship, Volume II, Admiralty, London, H.M. Stationery Office, 1952, pp. 717-718

3) Practical Methods for observing and forecasting Ocean Waves, Pierson, Neumann, James, N.Y. Univ, College of Engin, 1953.

This table was compiled by Wilbur Marks D T M B

representing the spectral energy density of the surface elevation time history. It is often convenient, for formal purposes, to consider the range of frequency over which the energy-density spectrum is defined to extend from 0 to $+\infty$, or from $-\infty$ to $+\infty$ according to the context. Whichever interval of definition is used, the energy-density spectrum used with it will be adjusted by the omission or insertion of a factor of one-half in order to yield exactly equivalent results in either case.

The directional Neumann spectrum model has a number of features which result in both convenience in treatment and some degree, perhaps, of artificiality. The manner of dependence of the distribution of spectral energy over direction specified by this model is independent of wave length, which results in a considerable simplification of computations. The specific manner of energy dependence upon wave length, and also upon direction, both contribute to computational convenience, as well. Often these features are useful in simplifying and reducing the number of individual cases which must be treated.

3. RESULTS OF COMPUTATIONS FOR INDIVIDUAL BARGE MOTIONS IN VARIOUS SEA STATES

The results obtained for the barge motions, individually considered, is presented in this chapter in two parts: (1) solutions of the differential equations for the various cases of regular waves, and (2) results for the various cases of irregular waves obtained by applying the Neumann surface-elevation energy spectrum to the amplitude information implicit in these solutions. The results obtained when the simultaneously-occurring barge motions are considered together, such as the nature of the mutual covariances (or coefficients of correlation) and phase relationships among the various barge motions, are discussed in a later section.

The motions of the barge, considered as a rigid body having six degrees of freedom, and referred to a right-handed rectangular Cartesian coordinate system with origin at its center of gravity (CG), consist of three translational and three rotational motions. The former three, viz. surge (x), sway (y) and heave (z), are each defined as a rectilinear displacement whose positive sense is in the direction of one of the coordinate axes. In particular, surge displacement is in the fore-aft direction, being positive when toward the bow; sway displacement is in the port-starboard direction, being positive when toward the port side; and heave displacement is in the vertical direction, being positive when upward. The three rotational motions, viz. roll (ϕ), pitch (θ), yaw (ψ), are each defined as the angular displacement corresponding to a rotation about one of the coordinate axes, and whose positive sense is in the right-handed sense for rotation about a directed axis. In particular, roll displacement takes place about the fore-aft axis, being positive when the port side rises; pitch displacement takes place about a horizontal axis parallel to the beam, being positive when the stern rises; and yaw displacement takes place about a vertical axis amidships, being positive when the bow rotates portward.

When, as described in the Appendix, the barge is in sinusoidal surface waves, the six motions of the barge are governed by a system of six simultaneous ordinary second-order linear differential equations, with time as the independent variable. For any sinusoidal wave propagating in a direction making an angle, β, with the direction of heading of the barge (measured as positive in the counterclockwise direction when viewed from above) the excitation functions (right-hand members of the differential equations in standard form) are found to depend upon the angle β for the wave direction, as well as its wavelength, λ, whereas the coefficients of the remaining terms are independent of β.

For the deep-water conditions assumed in the present study, the length of a sinusoidal wave is determined by the relations, $c = (g\lambda/2\pi)^2$ and $T = (2\pi\lambda/g)^{1/2}$, the phase propagation speed, c, of the wave as well as the wave period, T (or, equivalently, its frequency, given by $f = 1/T$, in cycles per second, or $\omega = 2\pi/T$,

in radians per second). Vertically above the point with coordinates (x, y, z) referred to the center of gravity, CG, of the barge, the sinusoidal time history, η (x, y, t), of the elevation of the surface of the water, measured from its mean level, is given by

$$\eta(x,y;t) = a \sin \frac{2\pi}{\lambda}(x\cos\beta + y\sin\beta - ct + \delta)$$

where a is the (non-negative) amplitude of the sinusoidal wave, and δ specifies an arbitrary phase. It may be pointed out that in practice λ and β, as well as a and δ may be chosen independently of one another in order to specify a particular surface wave. The concept of a wave regime defined by an amplitude and phase spectrum corresponds to the assignment of an amplitude, a, and a phase δ to each possible pair composed of a wavelength, λ, and a wave direction, β.

The differential equations for the barge motions, used in the present study, have been formulated and solved for convenience for the case of an exciting wave for which a = 1 and δ = 0, as described in the Appendix. The time history of the surface elevation above the location of the center of gravity of the barge (in the latter's absence) is thus assumed to be given by η (0, 0, t) = a sin $\frac{2\pi}{\lambda}(-ct)$ = a cos $(\omega t + \delta_r) = Re\{a_r \exp[i(\omega t + \delta_r)]\}$ where $\omega = 2\pi/T = 2\pi(c/\lambda)$ is the angular frequency of the wave, i is the imaginary unit, and $Re\{z\}$ denotes the real part of the complex number z.

Solutions to the equations were obtained for the time history of the r-th ship motion in the form $f^{(r)}(t) = a_r \cos(\omega t + \delta_r) = Re\{a_r e^{i(\omega t + \delta_r)}\}$. Comparing with the surface elevation, η (0, 0, t) = cos $(\omega t + \pi/2)$ it is seen that the resulting ship motion is sinusoidal, with amplitude a_r times that, and phase $\theta_r = \delta_r - \pi/2$ greater than that, of the sinusoidal surface. If we set $T_{r\eta} = a_r \exp\{i\theta_r\}$, thereby choosing Mod $T_{r\eta} = |T_{r\eta}| = a_r$ and $Arg\{T_{r\eta}\} = \measuredangle T_{r\eta} = \theta_r$, we obtain the so-called complex response operator for generating the r-th ship-motion time history from a sinusoidal surface elevation time history at the location directly above the CG of the barge. Thus, if the latter is given by $\eta(t) = a\cos(\omega t + \theta_\eta) = Re\{ae^{i(\omega t + \theta_\eta)}\}$, the ship motion will be given by $f^{(r)}(t) = Re\{T_{r\eta}\, a \exp[i(\omega t + \theta_\eta)]\} =$

$$= |T_{r\eta}a|\cos(\omega t + \theta_\eta + \theta_r) = a_r a \cos(\omega t + \theta_\eta + \theta_r).$$

It may be noted that there is one such complex response operator $T_{r\eta}(\omega,\beta)$ for each wave frequency and wave-direction pair. Its modulus, or magnitude, Mod $T_{r\eta} = |T_{r\eta}|$, is the amplitude amplification factor or response-amplitude operator and its argument, Arg $T_{r\eta} = \measuredangle T_{r\eta} = \theta_\eta - \theta_r$, is the phase-shift difference or response-phase operator to be applied to the surface elevation.

In the present study, solutions to the equations were obtained for the complex response-operators $T_{r\eta}(\omega,\beta)$ for the values of ω corresponding to the eight wavelengths λ = 100, 200, ..., 800 feet, and the values of wave heading relative to that of the barge, β = 0°, ±30°, ±60°, ..., ±150°, 180°. Subsequent uses of

the response operators indicated the advisability of interpolating between these solutions to obtain values for $\beta = \pm 15°, \pm 45°, \ldots, \pm 165°$ as well. This interpolation was done graphically.

The resulting values of the two-argument, complex-valued functions $T_{r\eta}(\omega,\beta)$, may be presented in a number of ways. The real part and the imaginary part of the complex numbers may be plotted separately, as may also the modulus (amplitude ratio) and the argument (phase shift). Alternatively, the complex number plane may be utilized to display directly the complex-number values of the response operator. In any case, it is convenient to represent the variation of the response operators when one or the other of the independent variables is held fixed and the remaining one allowed to vary.

A. Solution for Regular Waves

The six response amplitude operators, $T_{r\eta}(\omega,\beta)$, are shown plotted against the wave heading, β, in Figures 3.1 through 3.16. These figures show the amplitude of the sinusoidal time history of each of the six motions of the barge as a function of wave heading relative to the barge when the latter is in simple unit-amplitude sinusoidal surface waves having one of the wavelengths, λ = 100, 200, ..., or 800 feet. The complete 360° range of directions of wave propagation relative to the barge heading (based upon the values obtained at wave headings of 0°, $\pm 15°$, $\pm 30°$, ..., $\pm 180°$) is covered. As is to be expected, the variation of the amplitude of each of the barge responses shows considerably more regularity for wavelengths substantially exceeding the barge length than for the shorter wavelengths.

The figures for the longitudinal motions (Figures 3.1 through 3.8) show that the surge and heave amplitude responses increases uniformly for all wave headings, as the wavelength increases. The pitch amplitude response exhibits a similar uniform behavior with regard to wave headings, increasing with wavelength up to wavelengths between 300 and 400 feet but decreasing thereafter. It may be seen that surge amplitude response is smallest for beam seas and largest for head and following seas rising to 0.8 for λ = 800 feet. Heave amplitude response is smallest for head and following seas and is at its maximum for beam seas, virtually attaining the value 1.0 for $\lambda \geq$ 400 feet; the variation of the amplitude of response with wave direction is relatively small for wavelengths exceeding 500 feet. Pitch amplitude response is smallest for beam seas and largest for head or following seas, provided the wavelength is at least 400 feet; it reaches a maximum of 0.022 radians (1.3°) for wavelengths in the neighborhood of 380 feet and is always least for beam seas.

The figures for the lateral motions (Figures 3.9 - 3.16) show a corresponding uniformity with respect to wave heading as regards the variation of the response amplitudes with wavelength. In addition to showing all responses to be zero for following or head seas, these figures indicate the following: (1) Sway amplitude response is at its maximum for beam seas, virtually reaching 1.0 for $\lambda \geq$ 300 feet.

(2) Roll amplitude response is maximal for beam seas, reaching a maximum of approximately 0.75 radians (4.3°) for λ near 320 feet. (3) Yaw amplitude response is virtually zero for beam seas and has its maximum values for quartering seas, on either bow or stern, reaching a maximum of 0.01 radians (0.6°) at $\pm 45°$, for λ in the neighborhood of 250 feet.

Figures 3.17 through 3.22 show the squares of the six response amplitude operators, for each of the three fixed relative wave heading angles, $\beta = 0°$, 45°, and 90°, as a function of the angular wave frequency, $\omega = (2\pi g/\lambda)^{1/2}$, in radians per second, rather than against the wavelength, λ, in feet. The above figures indicate the existence of resonance phenomena for the three rotational motions (yaw, pitch and roll) responses (in order of increasing sharpness of resonance), for quartering, following and beam seas, respectively. For heave and sway with beam seas, the squared responses rise to unity before $\lambda = 800$ feet is reached, as noted previously. As shown in Figure 3.17 the square of the surge amplitude response reaches approximately 0.64 for a following wave of length 800 feet (for which the angular frequency is approximately 0.5 radians per second).

Figures 3.23 through 3.28 show the phase lead, $\text{Arg}\{T_{r\eta}(\omega,\beta)\} = \Theta_r - \Theta_\eta$ of the sinusoidal time history, $f^{(r)}(t)$, of each of the six motions of the barge in simple sinusoidal waves, plotted against the wave heading, β, for each of the eight wavelengths considered. The possible ambiguity of an additive multiple of 360° (2π radians) in the numerical value assigned to an individual phase shift angle, requires the adoption of certain conventions when describing the variation of the values of the continuous series of phase shift angles. The intention in preparing these figures was to reproduce faithfully the variation of the quantity, $\text{Arg}\{T_{r\eta}(\omega,\beta)\}$ as β varied while ω (or, equivalently, λ) was held fixed. This meant avoiding introducing any extraneous discontinuities into the curves, and led, in some cases, to the ordinates on individual curves having a range greater than 360°.

It may be seen that the rapid change of phase shift with wave heading shown would make explicit calculations necessary in some instances at a spacing smaller than 15° for the values of β, if more accurate phase-shift information were desired at all wavelengths and wave headings. The curves shown would appear reasonably smooth in this sense except at the shorter wavelengths. In all cases, portions of the curves lying between computed ordinates and considered to be of doubtful validity, are shown as dashed lines (cf. the graphs for the 800-foot wavelength in Figures 3.25 and 3.28).

Since both the real and imaginary parts of the complex response operator, considered as a function of the wave heading, β, are even functions for all longitudinal motions and odd functions for all lateral motions, the graphs of the phase-shift responses for the former motions exhibit symmetry about $\beta = 0$, while those for the latter motions exhibit a constant difference of $\pm 180°$ between the ordinates for pairs of values of β equidistant from $\beta = 0$.

It is seen once more that the curves for wavelengths of 300-400 feet and below are less regular in appearance than those for the longer wavelengths. It is to be expected that for wavelengths which are short relative to the barge length (260 feet), the actual phase-shift responses of the barge are by nature more complex, while, on the other hand, the suitability of the slender-body theory upon which the computed phases depend is necessarily more open to question here.

For the longitudinal motions, it is seen that the phase shift exhibits generally smooth behavior for the longer wavelengths, with the exception of the rapid, but continuous, transition which occurs, as expected, for waves coming nearly on the beam ($\pm 90°$). For these wavelengths, heave response exhibits virtually zero phase shift for all wave headings, while surge and pitch response show phase shifts near $\pm 90°$, the ordinates on the latter two curves exchanging places as they pass near the wave headings, $\pm 90°$.

For the lateral motions, a prominent feature in the graphs is the $\pm 180°$ discontinuity for direct following ($0°$) or head ($\pm 180°$) waves. Aside from this, for the longer wavelengths, the phase-shift response for sway motion shows little variation, remaining near $\pm 90°$ at all headings. Similarly, the phase-shift response for roll shows, for the longer wavelengths, a variation which is smooth in the region between following and head seas; the amount of phase shift approaching $90°$ in absolute value for following seas and a somewhat smaller absolute value for head seas, but which increases with the wavelength. The phase shift of the yaw response exhibits a relatively rapid change of $180°$ as the wave heading passes through $\pm 90°$, varying rather slowly around $0°$ and $\pm 180°$, which values it approaches, for following or head seas.

B. Results for Irregular Seas

1.) Energy Spectra and Their Interpretation

The remainder of this chapter describes the results of the applications of the response amplitude operators to the case of irregular seas as described by the Neumann spectrum. As mentioned in Chapter 2, the surface elevation at any instant will be considered to consist of the linear superposition of sinusoidal waves whose amplitudes and phases vary with a frequency continuum as well as direction. Linearity and superposition of solutions being assumed properties of the moored barge system, the motions of the barge resulting from exposure to such a seaway are found by summing up (for each degree of freedom) the responses to each component wave present, taking into account its length and heading by use of the corresponding response operator and weighting each with the appropriate factor to account for the amplitude and phase of the wave (cf. Appendix and Chapter 2). This, however, not being possible, unless both amplitude and phase of each component wave are specifiable and known, such a procedure cannot be carried out for the case of a vessel in wind-generated waves. As a consequence of the lack of phase specification, only quantities which are independent of the phases of the

individual components of the seaway can be calculated. These include the probabilities of the occurrence of various events and average values derived from such probabilistic considerations. It may be noted that it is the surface elevation which is attributed a random nature in this model. The response operators for the vessel nonetheless specify the amplitude ratio and the phase shift between each sinusoidal surface component and the corresponding component of the same frequency in the ship-motion time histories. However, if the phase of one is random, that of the other will likewise be random, though the amplitudes of both may be certain and known. Thus, an individual ship-motion time history is characterized by randomness -- though its phase differences from those of single sinusoidal components of the surface elevation and possibly from those of other ship-motion time histories may be known.

The assumption of the Gaussian model for the surface elevation and by linearity, for the barge motions as well, allows a very large number of inferences to be drawn. One, mentioned in Chapter 2, is that if the ordinates on any one time-history curve, say the i-th, $f_i(t)$, have a one-dimensional Gaussian distribution, and if measured from their mean, the totality of information available for describing them individually is contained in a single parameter, their root-mean-square value, σ_i. With knowledge of this value and the Gaussian cumulative probability distribution function (Figure 2.1), the probability of the instantaneous ordinate lying within any specified interval of interest may be determined. In particular, the probability occurrence of values relatively far (high or low) from the mean may be found. Further properties of the multidimensional Gaussian distribution combined with the linearity of the system, allow the determination of the distribution of instantaneous amplitudes on the time-history curve. Whereas the r.m.s. value is determined solely by the area under the spectral energy density curve -- i.e., its moment of order zero; moments of higher order, if they exist, yield additional information about the time history, including the complete probability distribution of the heights of the peaks on the time-history curve (cf. Figure 2.2). The latter is approximated, and with increasing accuracy, by the distribution of the instantaneous amplitude (which is the absolute value of the instantaneous complex-value envelope* to the curve (cf. Appendix) as the relative bandwidth of the spectral energy distribution tends to zero. In any case, the average value of the amplitudes of the oscillations on the time-history curve for a quantity of interest or that of a specified fraction of the largest of such amplitude (such as the so-called significant wave height), may be found (cf. Appendix), though, if not sufficiently narrow band**, the knowledge of one additional moment is required. Finally, the expected value of the maximum such amplitude occurring among a given number of such oscillations may be estimated (cf. Figure 2.3). Examples of the information contained in the energy spectrum (and in its moments, specifically) have been given in Chapter 2.

*See Chapt. 5 (B) for definition and discussion.
**See Table 2 (γ_ω)

As pointed out earlier, the energy spectrum for the surface elevation, a spectrum depending both upon wavelength and wave direction, will determine, for a given vessel, the distribution of the spectral energy of each of its motions. The directional Neumann spectral energy density function, $A^2(\omega,\beta_w)$, for the surface elevation, η (t), is specified by the following expression:

$$A^2(\omega,\beta_w) = \begin{cases} c\,\frac{2}{\pi}\,\omega^{-6}\exp\left\{-\frac{2g^2}{V_w^2\omega^2}\right\}\cos^2(\beta_w-\beta_o) & , \text{ for } |\beta_w-\beta_o| \le \frac{\pi}{2} \\ 0 & , \text{ otherwise} \end{cases}$$

where $c = 51.5$ ft.^{2}/sec.^{2}, v_w is the wind speed in ft./sec., and β_o is the predominant wind direction. It is understood that the spectral energy density is zero except for wave directions confined to a half-circle symmetrically situated about the predominant wind direction. The integration,

$$\int_0^\infty d\omega \int_{-\frac{\pi}{2}}^{+\frac{\pi}{2}} d\beta\, A^2(\omega,\beta) = c\int_0^\infty d\omega\ \omega^{-6}\exp\left\{-\frac{2g^2}{V_w^2\omega^2}\right\}\frac{2}{\pi}\int_{-\frac{\pi}{2}}^{+\frac{\pi}{2}} d\beta\,\cos^2(\beta_w-\beta_o)$$

yields twice the square of the r.m.s. value of the surface elevation at any point, i.e. $E_\eta = 2\sigma_\eta^2$, where σ_η^2 is variance of the surface elevation time history.

In particular, the spectral energy density function, $A^2(\omega)$, of η (t) may be seen to be,

$$A^2(\omega) = c\int_{-\frac{\pi}{2}}^{+\frac{\pi}{2}} d\beta\,\omega^{-6}\exp\left\{-\frac{2g^2}{V_w^2\omega^2}\right\}\frac{2}{\pi}\cos^2(\beta_w-\beta_o) = c\omega^{-6}\exp\left\{-\frac{2g^2}{V_w^2\omega^2}\right\}$$

since, by definition of the energy-density spectrum, $A^2(\omega)$, we must have:

$$2\sigma_\eta^2 = E_\eta = \int_0^\infty d\omega\, A^2(\omega) = \int_0^\infty d\omega\, c\omega^{-6}\exp\left\{-\frac{2g^2}{V_w^2\omega^2}\right\}.$$

For convenience, we shall refer to the quantity, $\sigma_i^2 = \frac{1}{2}E_i$, as the total spectral energy (though strictly its analog is power) for the time history $f_i(t)$, and in practice we shall replace $A^2(\omega)$ and $A^2(\omega,\beta)$ by $A^2(\omega)/2$, and $A^2(\omega,\beta)/2$, respectively, in order to obtain variances and covariances directly from integration over the interval (0, + 00).

In the present study the angle for the predominant wind direction was taken to be $\beta_o = 0$, and a variable barge heading angle, β_B, introduced to allow for the relative heading of barge to wind. The relationships of the wind direction, the wave heading, and the barge heading are shown in the sketch below, together with the difference angle $\beta_w - \beta_B$ representing the wave heading relative to the barge heading. Also shown in this sketch are the conventions made use of later for the designation of the forces in the mooring cables and the azimuth angle for the boom used to lower loads from the barge.

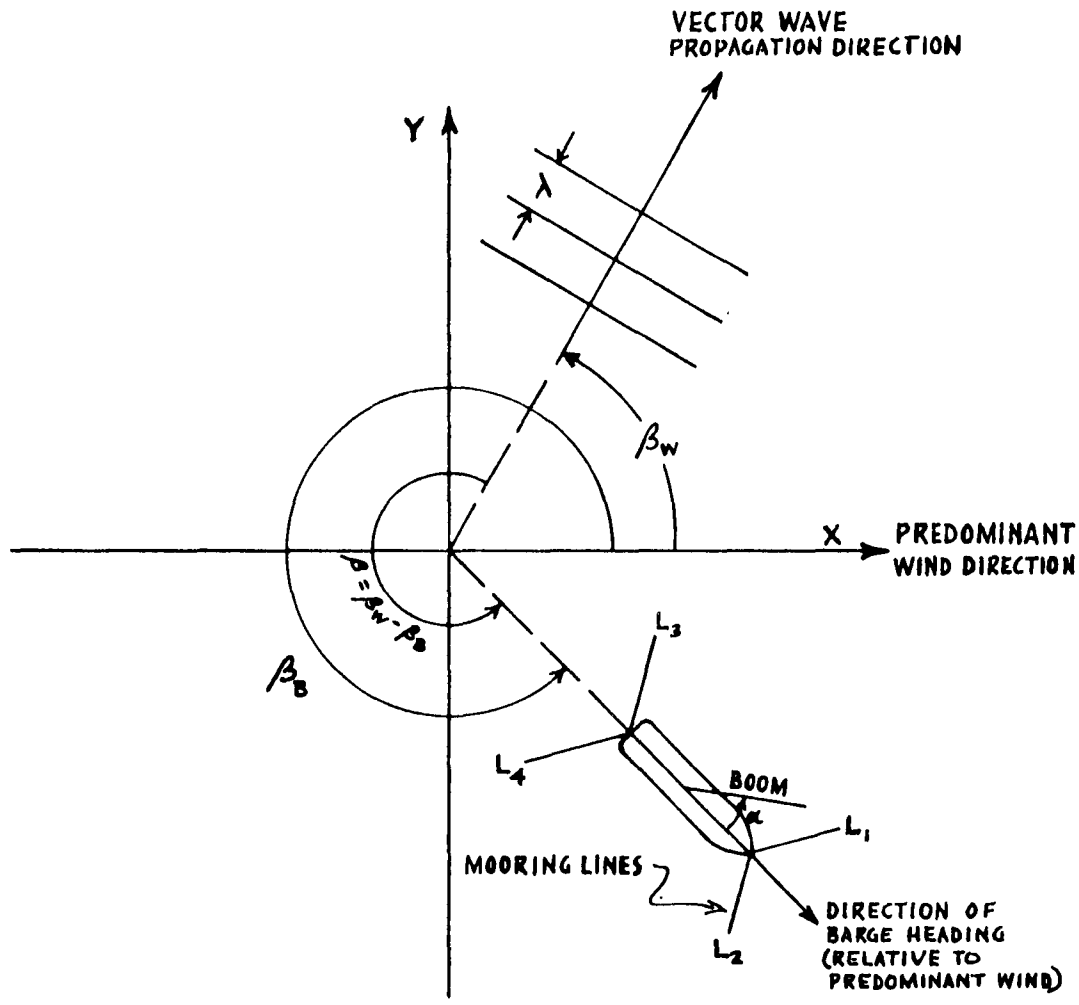

The energy spectrum for η (t) was used in the form of a spectral energy density with respect to wave length, rather than frequency, since the barge-motion response operators were evaluated at equally-spaced values of $\lambda = 2\pi g/\omega^2$.

The resulting spectral energy density becomes proportional to $\lambda^{3/2} e^{-a\lambda}$, where $a = g/\pi V_w^2$, and for a given barge heading, β_B, the spectral density (λ-density) for the i-th barge motion becomes proportional to

$$\int_{-\pi/2}^{+\pi/2} d\beta_w \lambda^{3/2} e^{-a\lambda} \cos^2(\beta_w) |T_{r\eta}(\lambda, \beta_w - \beta_B)|^2$$

where the angle β used as the second argument of the response operator must now be expressed in terms of the wave heading β_w. After evaluating this integral, to convert it back to an ω- density, it is necessary only to multiply it by the absolute value of the rate of change of λ, with respect to ω, namely $|d\lambda/d\omega| = 4\pi g/\omega^3$.

The members of the family of Neumann spectral energy density functions, $A^2(\omega)$, with respect to ω, for the surface elevation η(t), are shown in Figure 3.29 for the three wind speeds used in the present study. (For a graphical representation

Table 2

Tabulation of various parameters obtainable from low-order moments of spectral energy density function $\Phi(\omega)$ (Example for two cases in Sea State 5* (1) Barge heave motion (for cross-wind heading) and (2) surface elevation

*underlined dimensionless values are valid for all sea states

Parameter	Symbol	Formula	Numerical value for time history of: Heave, z,	Surface elevation, η,
Spectral energy density moment of order p	M_p	$\int_{-\infty}^{+\infty} d\omega\, \Phi(\omega) \lvert\omega\rvert^p$		
Total energy	$\sigma_0^2 = E/2$	M_0	3.29 (ft^2)	6.23
R. m. s. value of instantaneous ordinate (ordinate dispersion)	σ_0	$M_0^{\frac{1}{2}}$	1.81 (ft.)	2.50
Mean value of instantaneous frequency	$\bar{\theta} = \mu_\omega$	M_1/M_0	0.738 (rad/sec)	0.920
Spectral bandwidth dispersion; a scale factor for instantaneous frequency	σ_ω	$[M_2/M_0 - (M_1/M_0)^2]^{\frac{1}{2}}$	0.166 (rad/sec)	0.388
Relative spectral bandwidth	$\delta_\omega = \sigma_\omega/\mu_\omega$	$[M_0 M_2/M_1^2 - 1]^{\frac{1}{2}}$	0.224 (--)	<u>0.422</u>
Mean angular directed zero-crossing frequency for ordinate of curve	ω_0	$(M_2/M_0)^{\frac{1}{2}}$	0.756 (rad/sec)	1.00
Mean angular directed zero-crossing frequency for slope of curve	ω_+	$(M_4/M_2)^{\frac{1}{2}}$	0.834 (rad/sec)	1.73
Ordinate-second derivative correlation coefficient	$\rho_0 = -\omega_0/\omega_+$	$-M_2/(M_0 M_4)^{\frac{1}{2}}$	-0.907 (--)	<u>-0.577</u>
Slope-conjugate function correlation coefficient	$\rho_c^{*\prime} = (1+\bar{c}_\omega^2)^{-\frac{1}{2}}$	$M_1/(M_0 M_2)^{\frac{1}{2}}$	0.976 (--)	<u>0.920</u>
Mean value of peak-height distribution	$\bar{M} = \sqrt{\frac{\pi}{2}}\sigma_0(-\rho_0)$	$\sqrt{\frac{\pi}{2}} M_2/M_4^{\frac{1}{2}}$	2.06 (ft)	1.80
Mean value of instantaneous amplitude (narrow-band mean peak height)	$\bar{R} = \sqrt{\frac{\pi}{2}}\sigma_0$	$\sqrt{\frac{\pi}{2}} M_0^{\frac{1}{2}}$	2.27 (ft)	3.12
"Significant" instantaneous-amplitude height (narrow band significant peak height)	$R_{1/3} = 2\sigma_0$	$2M_0^{\frac{1}{2}}$	3.63 (ft)	5.00
Fraction of peaks below mean ordinate level (peaks which are negative)	$P_m^- = \frac{1}{2}(1+\rho_0)$	$\frac{1}{2}[1 - M_2/(M_0 M_4)^{\frac{1}{2}}]$	0.0464 (--)	<u>0.212</u>
Fraction of time instantaneous frequency is negative	$P_\theta^- = \frac{1}{2}(1+\rho_0^{*\prime})$	$\frac{1}{2}[1 - M_1^2/(M_0 M_2)^{\frac{1}{2}}]$	0.0121 (--)	<u>0.0400</u>

of the corresponding energy density with respect to λ and the reciprocal of the derivative $d\omega/d\lambda$,cf. Fig. 5.2) It is seen that for the higher sea states which correspond to higher wind speeds, a larger fraction of the energy appears at the lower frequencies (longer wave lengths), the spectral density curve, plotted versus ω, being relatively flat for the lowest of the three sea states considered. Generally speaking, the directional Neumann spectrum, $A^2(\omega,\beta)$, though somewhat special in form, as will be seen later, furnishes a useful concrete example for studies of the effect of confused seas, in which numerical results are required.

Figures 3.30 and 3.31 show the distribution of the spectral energy plotted against the angular frequency ω, for a selected set of barge headings, for each of the six barge motions in a sea state 5. (Note that $\beta_B = 0°$ corresponds to a downwind barge heading.) The relatively close agreement between the left-hand portion of the surface-elevation spectral energy density curve for the State 5 sea, and the corresponding portion of the curves for the translational motions, (particularly heave and sway - cf. Figures 3.17, 3.18 and 3.20) is a reflection of the fact that the values of the response amplitude operators for these motions are close to unity for long waves for these barge headings.

The spectral energy density curves for the rotational motions in Sea State 5, considered in the order yaw, roll and pitch, are characterized by increasingly narrow band widths. This might be expected in view of the relative locations of the maxima on the response curves for these three motions, and the fact that in the State 5 sea the maximum spectral energy density occurs near the 400-foot wave length, which is closer to the location of the peak for pitch than that for roll.

It may be pointed out that the information generated in the present study would enable the presentation of a set of 6 x 72 = 432 spectral energy curves (not discounting redundancies) for individual ship motions, including those shown in Figures 3.30 and 3.31. For any one of the set of 72 windspeed, barge heading combinations used in the computations, an intuitive idea of the composition of any one of the six corresponding energy spectra for the barge motions may be obtained by visualizing for each wave length the formation of the corresponding definite integral, taken over the angle π.

To accomplish this, one imagines replacing the curve for the relevant response amplitude operator (taken from Figures 3.1 through 3.16) by the curve for the square of this operator, sliding along it the curve plotted for the Neumann directional function $\cos^2\beta = 1/2 + 1/2 \cos 2\beta$, multiplying together the ordinates of the two curves, and estimating the area under the portion of the resulting product curve corresponding to the interval of values of β centered at $(-\beta_B)$ and of length 180°. It is apparent that the effect of any other appropriate hypothetical directional function may be examined in the same manner, by its employment in the place of the $\cos^2\beta$ function.

As an illustration of the information obtainable from the spectral energy density function, for an arbitrary time history function, an example based upon the heave motion spectrum (Sea State 5, cross-wind barge heading) in Figure 3.30 has been prepared, and the results shown in Table 2.

The information selected for presentation here includes the specification of all those parameters necessary to determine completely the probability distributions of the following time-varying quantities associated with the heave time-history curve: ordinate, instantaneous amplitude, instantaneous frequency and phase, peak heights

above (or equivalently, depths below) the mean ordinate. Also given are the mean values for the number of zero crossings of the curve itself or of its slope. It is to be noted that the parameters required, for the information being presented consist solely of four moments of the heaving motion energy spectrum. Two of these were routinely computed during the present study. The spectral moments involved are given by the expression, $M_p = \int_0^{+\infty} d\omega\, \Phi^{(z,z)}(\omega)\omega^p$, $p = 0,1,2,4$, where $\Phi^{(z,z)}(\omega)$ is the spectral energy density for heave under those conditions. In terms of the wave length, λ, we have

$$M_p = (\text{const.}) \int_0^{\infty} d\lambda\, \lambda^{+3/2} (2\pi g/\lambda)^{p/2} e^{-d\lambda} \int_{-\pi/2}^{+\pi/2} d\beta_w \cos^2\beta_w \left| T_{z\eta}(\lambda, \beta_w - \beta_B) \right|^2, \text{ with } \beta_B = +90^\circ$$

For comparison with the results calculated for the heave record in Sea State 5, the corresponding results for the surface-elevation time history, $\eta(t)$, itself are given in Table 2 on the following page for the same sea state.

It has been seen earlier (Figure 3.18) that the heave response operator for the moored barge system corresponds to a filter acting on the surface elevation time history, discriminating against the high frequencies and which thus appear considerably reduced in value in the heaving motion time history. From Table 2, the total energy, σ^2, in the surface elevation time history is seen to be reduced, in the process of being converted into heaving motion, by a factor of nearly two. The change effected in the shape of the energy spectrum is illustrated by comparing the values of each of two dimensionless parameters, δ_ω, (relative spectral bandwidth) and $|\rho_0|$ (coefficient of correlation between ordinate and second derivative). These are significantly modified - - from +0.422 to +0.224 and from +0.577 to +0.907 respectively. The corresponding marked change in the appearance of the time-history record is reflected by the reduction in the proportion of negative maxima (peaks) (P_M^-) by a factor of more than four and by the reduction in the proportion of the time the instantaneous frequency is negative (P_θ^-) by a factor of more than three.

It will be noted that the total spectral energy affects the mean value of the instantaneous amplitude, in direct proportion to its square root. However, it may also be seen that the mean peak height, $\bar{M} = (\pi/2)^{1/2}(-\rho_0)\sigma_0$ for the heaving motion, despite the reduction by a factor of nearly two in the total spectral energy, exceeds the mean peak height for the surface elevation by over 15%. This is due to the compensating effect of the change in the value of $|\rho_0|$ between the two time histories, which more than offsets the change in the value of the r.m.s. ordinate, σ_0.

The effect of the value of ρ_0 on the form of the distribution of peak heights may be seen from Figure 2.2. Three of these distributions of particular interest here are those for the values, $\rho_0 = -1.000$, -0.577 and -0.907. The first of these corresponds to the frequently-employed narrow-band spectral model (for which the relative spectral bandwidth, $\delta_\omega = 0$), while the last two follow from actual conditions assumed in the present study, for the spectral distribution of sea-surface elevation and barge heaving motion, respectively.

As an example, the percentage of peak heights between 1.5 feet and 2.5 feet is found in the real two cases to be 61% - 46% = 15% for surface elevation, and 67% - 38% = 29% for heaving (by entering with ρ_0 = -0.577 and with the ordinates $\frac{2.5}{\sigma_\eta} = \frac{2.5}{2.5}$ = 1.0 and $\frac{1.5}{\sigma_\eta} = \frac{1.5}{2.5}$ = 0.6 and with ρ_0 = -0.907 and the ordinates $2.5 / \sigma_z$ = $2.5 / 1.813$ = 1.38 and $1.5 / \sigma_z$ = $1.5 / 1.813$ = 0.828). Had both surface elevation and heave been assumed to have narrow band spectra (i.e. ρ_0 = -1.0) the corresponding ideal fractions of peak heights between 1.5 feet and 2.5 feet would have been 0.24 and 0.30 respectively. It is clear that, except in the region of the larger peak heights, the three distributions show significant differences. This reflects the fact that the average values of envelope (instantaneous amplitudes or wave heights), often given must be interpreted with care for time histories associated with the Neumann spectrum model, since the value of the parameter, ρ_0, is often far from -1.0. As the present example for the barge heaving motion shows, one time history having considerably less total spectral energy than a second time history, may, due to the different manner in which this energy is distributed, have a peak-height distribution agreeing more closely with that commonly attributed to the second than the latter's own peak height distribution.

2) Root-mean-square Values and Total Energy

Figures 3.32 and 3.33 show, for each of the six barge motions, the variation of total spectral energy with barge heading, for each of the three sea states considered. The ordinate plotted for each of the curves is the r.m.s., value, σ_i, for the time history of the barge motion represented. Again, it will be convenient to refer to the variance of the time history function, $F_i(t)$, namely σ_i^2 as the total energy for the time-history function. The r.m.s. value of any time-history function is therefore the square root of its total energy (assuming, here, as always, the mean value of the time-history function to be zero).

In these two figures, the actual r.m.s. values of the motions have significance in themselves, indicating the total energy present; the indicated range between the minimum r.m.s. value attainable and the maximum r.m.s. value encountered as the barge heading is varied is of perhaps more interest for practical operations. Examination of the figures reveals that the energy in certain sets of barge motions may be considerable and, simultaneously, reduced to their minimum values by the proper selection of the barge heading relative to the wind. For example, for each sea state the r.m.s. values of heave, sway, and roll reach, their maximum and minimum values for crosswind (±90°) and either downwind (0°) or upwind (±180°) barge headings respectively. In the case of roll, the minimum energy

occurring for the downwind heading appears to be somewhat smaller than that for the upwind heading. The ratio of the maximum to the minimum value for the higher sea states is approximately 1.5 for heave, 2.0 for sway, and somewhat larger for roll. Since these ratios also describe the relative size of the instantaneous values of each of these ship motions which are located at any given percentage point on the normal cumulative probability distribution curve (Figure 2.1), as well as the relative size of the average instantaneous amplitudes and the approximate value of the expected maximum amplitude occurring among a given number of oscillations, the significance of the r.m.s. value is apparent.

Thus in the case of sway, for example, the change is heading of 90° in a State 5 Sea results in a change in r.m.s. value of the sway motion from approximately $\sigma_Y = 1.65$ to $\sigma_Y = 0.8$. Referring to Figure 2.1, it is seen that the value of the instantaneous sway corresponding to the 99th percentile in its probability distribution (i.e., exceeded only 1% of the time) changes from 4.0 feet to 2.0 feet. Similarly, reference to Figure 2.2 shows that the 99th percentile in the distribution of the instantaneous amplitude changes from (3.0) (1.65) = 4.95 feet to (3.0) (0.8) = 2.40 feet, while the mean instantaneous amplitude changes from 1.25 (1.65) = 2.06 feet to 1.25 (0.8) = 1.00 feet. Finally, reference to Figure 1.3 shows that over a duration of time during which 200 oscillation occur, the expected (average) value of the maximum oscillation amplitude will change from 3.42 (1.65) = 5.64 feet to 3.42 (0.8) = 2.74 feet (for 100 oscillations, these expected maximum values are 3.22 (1.65) = 5.31 feet and 3.22 (0.8) = 2.58 feet).

The results for the three remaining barge motions shown in Figures 3.32 and 3.33, show less relative change in total energy with barge heading. Surge and pitch show maximum r.m.s. values for upwind and downwind headings, and minimum values for crosswind ($\pm$90°) headings. Total yaw energy is least variable, showing minima for upwind and downwind headings and somewhat broad and low maxima in the vicinity of headings of $\pm$ 75° to the wind.

4. LOWERING-LINE DISPLACEMENTS, LINE TENSION AND LOAD ACCELERATIONS AND MOORING EFFECTS

1. Theoretical considerations

The lowering line displacements are related kinematically to the body motions, and hence they are relatively simple to determine once the different methods of lowering loads are specified in this study, viz. center-lowered loads and boom-lowered loads. Center-lowered loads, as the name indicates, are lowered through some sort of opening through the ship's keel, and it is assumed that this is done at just about amidships. The instantaneous displacement vector components of the load and lowering line are s_x, s_y and s_z and are then given by simple geometry as

$$\begin{aligned} s_x &= x \\ s_y &= y + |KG|\phi \\ s_z &= z \end{aligned} \tag{4.1}$$

where x, y, z, and ϕ are the instantaneous ship motions, surge, sway, heave, and roll, respectively, and KG = 15.1 feet is the vertical distance between the center of gravity and the keel (see the sketch below.

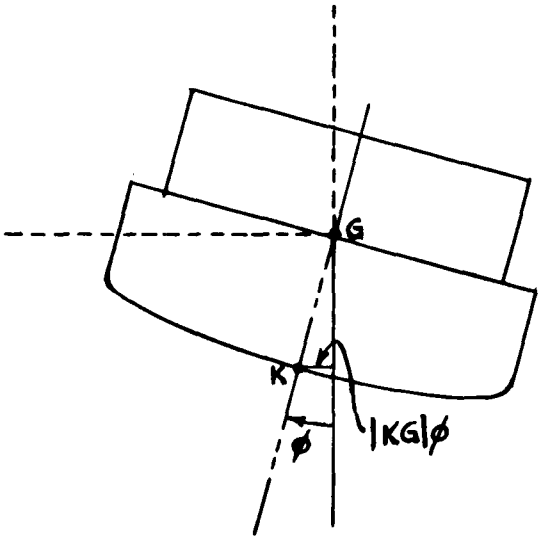

The tension, T, in the lowering line is given by the relation

$$T - W_\ell = \frac{W_\ell}{g} \times \ddot{s}_z = \frac{W_\ell}{g} \times \ddot{z} \quad ,$$

where the dots denote time rate of change, W_ℓ is the weight of the load, g is the acceleration due to gravity, and only vertical effects are considered to effect the tension. At rest,

$$T = T_o = W_\ell \quad ,$$

so that upon representing the tension as

$$T = T_o + T' = W_\ell + T',$$

where T' is the tension change due to dynamical effects, one obtains

$$\frac{T'}{W_\ell} = \frac{\ddot{z}}{g} \tag{4.2}$$

Thus, the tension variation due to the dynamics of the ship motion is directly related to the vertical acceleration of the load, and it is also proportional to the weight of the load, or equivalently, to its mass, measured in slugs.

In the derivation of the formulas given above, it is assumed that the trajectory of the load attached to the line is such that at each instant it is on the vertical line through the point of attachment of the lowering line to the barge. It is also assumed that the elastic effects of the lowering lines may be neglected, the only dynamic influences considered being those due to the ship motions. As for lateral forces, other than those directly induced by the barge, it is known that there are resisting forces acting on the line (length arbitrary here) and also on the load (shape and size arbitrary). However, the neglect of these forces (necessitated by the inability to calculate them precisely for all possible combinations) results in the displacements given in Equation (4.1) being conservative estimates (upper limits) of the expected load motions. The neglect of elastic effects in the lowering line appears to be a fairly safe assumption, since the major influence would occur only if the wave frequencies excited the natural frequency of wave propagation in the lowering line. In view of the lack of specification of the line's physical characteristics, as well as the expectation of wave-propagation frequencies out of the range of interest in the present problem, it is believed that the tensions and accelerations are adequately represented by Equation (4.2).

For boom-lowered loads, the situation may be visualized by reference to the accompanying sketch,

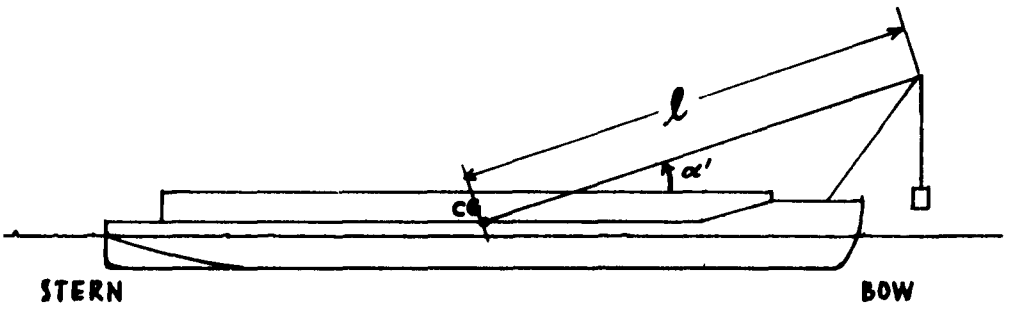

where the boom of length ℓ is elevated at an angle α'. An appropriate value for the relevant horizontal projection of the boom length ($\ell \cos\alpha'$) is considered, for computational purposes in the present case of a 260 ft. length barge, to be 150 ft. As shown below, the boom is also oriented horizontally at an azimuth angle γ, measured from the bow, positive in the counterclockwise sense, viewed from above.

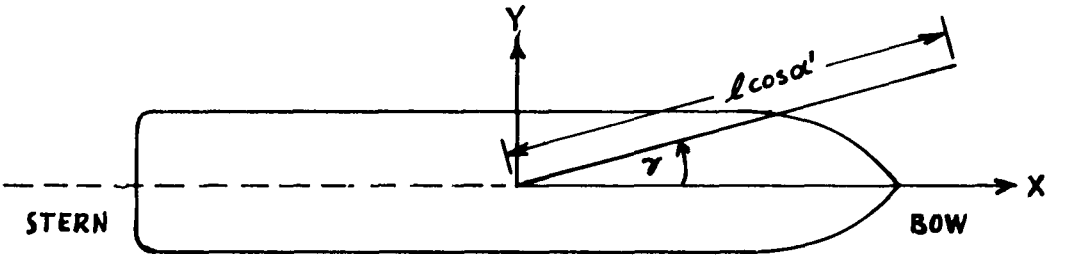

The load and lowering-line displacements about their respective equilibrium positions are given by

$$
\begin{aligned}
s_x^{\gamma} &= x - (\ell\cos\alpha')\sin\gamma\cdot\psi \\
s_y^{\gamma} &= y + (\ell\cos\alpha')\cos\gamma\cdot\psi \qquad (4.3) \\
s_z^{\gamma} &= z - (\ell\cos\alpha')\cos\gamma\cdot\theta + (\ell\cos\alpha')\sin\gamma\cdot\phi
\end{aligned}
$$

and the line tension (fluctuating part), T'^{γ}, and vertical acceleration are represented by

$$\frac{T'^{\gamma}}{W_l} = \frac{\ddot{S}_z^{\gamma}}{g} = \frac{1}{g}\left[\ddot{z} + l\cos\alpha'\left(\sin\gamma\cdot\ddot{\phi} - \cos\gamma\cdot\ddot{\theta}\right)\right] \quad (4.4)$$

where ϕ, θ, and ψ are the rotational barge motions, roll, pitch and yaw, respectively. The superscript γ denotes the boom azimuth angle.

These quantities are derived on the same basis as those for center-lowered loads, it being assumed that the boom pivots about the ship CG. The instantaneous magnitudes of these quantities thus appear as linear combinations of the instantaneous ship-motion solutions.

For the mooring system, the fluctuating parts of each of the four mooring cable tension forces * (each taken to be positive when directed toward the barge) are given by (see Appendix and Figure 4.8 for nomenclature):

$$\begin{aligned} F_1 &= -C\left\{x\cos\alpha' + \left[y + \left(\tfrac{L}{2}\right)\psi\right]\sin\alpha'\right\} \\ F_2 &= -C\left\{x\cos\alpha' - \left[y + \left(\tfrac{L}{2}\right)\psi\right]\sin\alpha'\right\} \\ F_3 &= +C\left\{x\cos\alpha' - \left[y - \left(\tfrac{L}{2}\right)\psi\right]\sin\alpha'\right\} \\ F_4 &= +C\left\{x\cos\alpha' + \left[y - \left(\tfrac{L}{2}\right)\psi\right]\sin\alpha'\right\} \end{aligned} \quad (4.5)$$

where C = 1250 lb./ft., α' = 60°, L = 260 ft., and x, y, and ψ are the ship motions of surge, sway and yaw. The effect of the mooring system on the barge, already taken into account (see Appendix) by the presence of the terms representing the net induced forces on the vessel in the direction of the x (fore-aft) and y (port-starboard) coordinate axes and the term representing the net induced yawing moment may be seen by displaying these three terms, viz.,

$$\begin{aligned} X_m &= -k_x \cdot x \\ Y_m &= -k_y \cdot y \\ N_m &= -k_\psi \cdot \psi \end{aligned} \quad (4.6)$$

where

$$\begin{aligned} k_x &= 1250 \text{ lb./ft.} \\ k_y &= 3750.16 \text{ lb./ft.} \\ k_\psi &= 633.75 \times 10^5 \text{ lb-ft./rad.} \end{aligned}$$

*It should be noted that the constraints that can be offered by the mooring lines through their elasticity to those ship motions having large hydrostatic restoring forces (heave, pitch and roll) is negligibly small in comparison with these forces. Thus, the moorings are taken into account only for those motions of the ship in which they can make a significant change. The expressions for the mooring cable tensions appearing in the text above have this viewpoint since there the effect on the motion of the barge is of primary interest. Consequently, should one be concerned instead with the effect that the ship can exert on its moorings, forces due to heave, pitch and roll would be considered in addition to the forces F_1, F_2, F_3 and F_4 considered above.

It is seen that both sets of quantities associated with the mooring system are simple linear combinations of the barge motions themselves. In fact, the r.m.s. values of the effects induced on the barge, given above in Equation (4.6) may be obtained from the corresponding quantities for the barge motions by a mere change in scale in the graphs shown in Figures 3.32 and 3.33.

2. Results for Individual Time Histories for Load and Mooring Quantities

A. Energy Spectra and Their Interpretation

Presented here, as in the preceding chapter, are the results obtained which describe individually the time histories under consideration. Discussion of the simultaneous relationships between the various time histories will appear in the following chapter.

Representative examples of calculated spectra-energy density functions for the case of the center-lowered load are presented in this report for two sea states (i.e., wind speeds) and two barge headings relative to the predominant wind direction. The presentation of the results of calculations comprehending the entire set of energy spectra of possible interest for the load and mooring variables was not deemed feasible in view of the large number of such spectra involved, although any particular one of interest may be readily obtained from the available computed results. The space required for their presentation, alone, would have been a deciding factor here as may be seen when it is recalled that for each of 3 x 24 = 72 environmental conditions for the mooring system and the center-lowered load, there are under consideration in this study seven time histories (viz. F_1, F_2, F_3, F_4, X_m, Y_m, N_m) for the mooring systems and five for the load (viz. s_x, s_y, s_z, $\ddot{s}_z$, T'). For the boom-lowered load, the consideration of twenty-four boom azimuth angles leads to a set of 3 x 24 x 24 = 1728 environmental conditions under each of which there are five quantities to be considered (viz. s_x, s_y, s_z, $\ddot{s}_z$, T'). To be sure, out of this set there exist some instances of redundancy or simple proportionality, but the number of discrete cases is still prohibitively large to exhibit in full.

The spectral-energy density functions shown for the load were calculated from those of the fundamental set of cross-spectral energy-density functions, namely, those of the six barge motions. Since the time histories of the load and mooring quantities are linear combinations of those for the motions of the barge and their second-order time derivatives,* response amplitude operators for the former may be obtained by forming appropriate linear combinations of the complex response operators, $T_{i\eta}$, for the barge motions, and calculating their

*Note that if the complex response operator for a ship motion is $T_{i\eta}(\omega,\beta)$ then the complex response operator for its time derivative of order p is $(i\omega)^p \; T_{i\eta}(\omega,\beta)$ and the squared response amplitude operator then becomes $\omega^4 T_{i\eta}(\omega,\beta)^2$.

squared absolute values. However, to avoid the inefficiency of performing an unnecessarily large number of numerical integrations, a general theorem in the theory of vector stochastic processes, providing an expression for the cross-covariance matrix for sets of random time histories which are linear combinations of a given set of random time histories was employed. In this way, certain spectral-energy density functions for the time-history functions associated with the load were obtained by hand calculation and all of the relevant r.m.s. values for the load and mooring systems were obtained by use of a high-speed computer.

A set of spectral-energy density functions for the case of a center-lowered load is illustrated in Figure 4.1. These consist of energy spectra for (1) the added-dynamic tension in the load-lowering line (or, equivalently, the vertical acceleration of the load) in Sea States 3 and 5, for one cross-wind barge heading ($\beta_B = +90°$) and (2) the port-starboard component of the displacement vector for the load in a State 5 sea for the barge headings, $\beta_B = 0°$ (downwind) and $\beta_B = \pm 90°$. (In the latter case, either cross-wind heading yields the same energy spectrum.) These examples encompass a rather wide range of spectral types, from the point of view of total spectral energy, location of the mean frequency of the spectra-energy distribution, absolute and relative spectral bandwidth, and general spectral shape.

For the case of a cross-wind barge heading, it is apparent that the port-starboard load-displacement energy spectrum shown in Figure 4.1 corresponds to a load-displacement time history which is relatively regular in appearance, exhibiting oscillations of relatively constant amplitude and duration, lasting in the neighborhood of $2\pi / 0.75 = 8.4$ seconds each; the peaks on the curve would be expected to lie on the envelope to the curve relatively often, while the heights of the peaks would be expected to follow the Rayleigh distribution ($\rho_0 = -1.0$) relatively closely. For example, from the estimates made immediately below, one will be led to expect that 99.9% of the peaks will not exceed approximately twice 3.7 ft., or 7.4 feet in height. The area representing the total spectral energy may be visually estimated to be slightly more than $1/2(0.5)(16) = 4$ ft.^{2} yielding an r.m.s. value for the load motion of approximately two feet (in Figure 4.2, below, from which this r.m.s. value for s_y at $\gamma = 90°$, may be read directly from the graph, it is seen to be between 2.10 and 2.15 feet). Thus, without calculating any moments of this spectrum, it may be inferred with some confidence that the mean value of the amplitudes of the oscillations of the lateral load displacement component, s_y, will be close to $\sqrt{\frac{\pi}{2}}\sigma_{s_y} = 2\sqrt{\frac{\pi}{2}} = 2.5$ feet while the average of the highest one-third, $H_{1/3}$, will be approximately $2.0\sigma_{sy} = 1.41\ E_{s_y} = 2(2.0) = 4.0$ ft. On this basis, the expected value of the maximum amplitude of oscillation to be encountered during an operation lasting 70 minutes (corresponding to approximately $70 \times 60/8.4 = 500$ waves of average period 8.4 seconds) would be, from Figure 2.3, approximately $3.67(2.0) = 7.3$ feet. During a shorter operation of seven minutes (=420 seconds) duration, the same graph indicates an expected value for the maximum amplitude of oscillation of approximately $3.00(2.0) = 6.00$ feet.

As far as instantaneous values of the port-starboard load displacement time history are concerned, from Figure 2.1 it is seen that since $\sigma_{s_y} = 2.0$, the displacement toward port will exceed 6.0 feet only $(100.00\% - 99.90\%) = 0.10\% = 1/1000$ of the time, while the absolute value of the displacement will exceed 6.0 feet twice as often, namely, about 1/500 of the time.

A similar discussion for the other three time histories whose energy spectra, shown in Figure 4.1, are visibly much further from having a small relative bandwidth, could be given provided one or two additional parameters were calculated directly from the spectral curves, as was illustrated in the discussion of the heaving motion in the preceding chapter. In the example shown for the added-dynamic line tension or vertical load acceleration, one may arrive at the estimates $\mu_\omega = 0.9$ rad./sec., $\sigma_\omega = 0.2$ rad./sec. and the relative bandwidth, $\delta_\omega = \sigma_\omega/\mu_\omega = 0.22$ with $\rho_o = -0.9$. Similarly, for the highly peaked narrow spectrum in the lower half of Figure 4.1, we might reasonably assume $\mu_\omega = 0.75$ rad./sec., $\sigma_\omega = 0.1$, and $\rho_o = -0.95$. On the other hand, for the broad, low spectrum in the upper half of the figure, reasonable values might be $\mu_\omega = 1.1$ rad./sec., $\sigma_\omega = 1.0$ rad./sec., and $\rho_o = -0.2$, but in this case the values should not be considered to be very accurate, since the value of $\delta_\omega = 0.91$ here is so large. However, in any case, a certain amount of insight is obtained as to the appearance of the time-history curve when δ_ω (whose estimate here would seem likely not to be too much in error) is large. For example, if it is recalled that $1/2(1 + \rho_o)$ is the fraction of peaks occurring below the mean ordinate level, it is not difficult to see that since a situation in which $\rho_o = -0.2$ corresponds to 40% of the peaks being of this kind, it is very likely that a graph of the time history for the added-dynamic line-tension in a Sea State 3 with $\beta_a = +90°$ would be rather irregular in appearance, and the heights of the peaks would fall considerably below those for a Rayleigh-distributed quantity.

B. Root-mean-square values and total energy for lowered loads

This section presents the r.m.s. values, or, equivalently, the total energy, for each sea state and barge heading, for each of the quantities of interest relating to the load-lowering operation and the mooring system. In general, as mentioned earlier, these quantities were computed in the form of linear combinations of the cross-covariance functions for the six ship-motion time histories, and (for accelerations) for their second-order time derivatives. Some insight into the manner of variation with barge heading of any one of these r.m.s. values may be obtained by considering the fact that its variation depends not only upon how the r.m.s. values of the component ship motions vary, but also, upon how the covariances between them vary. The results which show the variation of the r.m.s. values have been presented rather completely for barge headings at 15° increments in the preceding chapter. The results showing how the covariances vary with barge heading are presented in somewhat less detail in the following chapter.

For example, the lateral displacement of the center-lowered load, s_y, is the weighted sum, $y + |KG|\phi$, of two component ship motions, where $|KG| = 15.1$ feet. At any barge heading, its r. m. s. value, σ_{s_y}, is given by $\sigma_{s_y}^2 = \sigma_y^2 + 2|KG|\rho_{y\phi}\sigma_y\sigma_\phi + \sigma_\phi^2$, where σ_y, σ_ϕ and $\rho_{y\phi}$ are the r. m. s. values of the sway and roll time histories and the coefficient of correlation between them, respectively. Since the extreme values of $\rho_{y\phi}$ are -1 and +1, the value of σ_{s_y} will be seen to be confined between $|\sigma_y - 15.1\sigma_\phi|$ and $|\sigma_y + 15.1\sigma_\phi|$. For the intermediate case, $\rho_{y\phi} = 0$, the r. m. s. value for the lateral displacement is given by $\sigma_{s_y} = (\sigma_y^2 + |KG|^2\sigma_\phi^2)^{1/2}$. The general expression for $\sigma_{s_y} = \sigma_y + |KG|\phi = \sigma_y^2 + |KG|^2\sigma_\phi^2 + 2|KG|\sigma_y\sigma_\phi\rho_{y\phi}$ may be interpreted in terms of the law of cosines for plane triangles as illustrated by the sketch below, showing the effect of coefficient of correlation, $\rho_{y\phi}$.

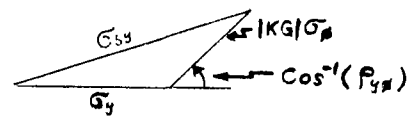

Of the curves in Figure 4.2, which show, for a center-lowered load, the r. m. s. values of s_x, s_y, s_z -- those for s_y exhibit the highest values. The r. m. s. value for s_y attains its maximum value for $\beta_B = \pm 90°$, as do the r. m. s. values of y and ϕ individually (cf. Figures 3.32 and 3.33). However, the minimum r. m. s. values for both s_y and y occur at $\beta_B = 180°$ (upwind heading), whereas the minimum r. m. s. value for ϕ occurs at $\beta_B = 0$ (downwind heading). The shift in the location of the minimum r. m. s. value here is explainable by examining the manner in which the correlation coefficient between the two motions vary with the barge heading. Thus, it may be confirmed from the information shown below in Figure 5.9 that the latter coefficient is positive for $\beta_B = 0$ and negative for $\beta_B = 180°$, the effect of the latter negative value on the r. m. s. value of s_y being to decrease it by more than enough to compensate for the effect of the larger value of the r. m. s. value of ϕ for $\beta_B = 180°$. The prediction of such effects for all the motions of interest is not entirely simple. However, the figures shown in the present chapter indicate the barge headings for which minimum and maximum r. m. s. values occur for the time histories relating to the center-lowered load.

The curves for center-lowered loads in Figure 4.2 are seen to increase in height, as expected, with sea state. It may be noted that the curves shown for s_x and s_z are, in view of Equations 4.1, exact replications of those given in Figure 3.32 for x and z, which have been replotted here for convenience. The curve for the vertical load displacement, s_z, is similar to that for s_y, showing equal maxima for cross-wind headings and unequal minima for downwind and upwind barge headings; the minima for s_z are more nearly equal to each other than are those for s_y. The ordinates on the curves for the fore-aft load displacement, s_x, are uniformly lower than those for s_y and s_z, showing equal minima for the two cross-wind headings and nearly equal minima for upwind and downwind headings, except in the lowest of the sea states considered, in which case the ordinates are relatively low and the amount of variation with barge heading is quite small.

The r. m. s. values of the vertical component of the acceleration, $\ddot{s}_z$ (in ft/sec^2) of the center-lowered load and the added dynamic tension, T' (in pounds of force per unit load mass, measured in slugs) in the lowering line are shown as a function of barge heading in Figure 4.3 for each of the three sea states. These curves are similar in appearance to the curves for the r. m. s. value of s_z (and hence of the heave, z, itself), exhibiting equal maxima for cross-wind barge headings and unequal minima for up- and down-wind barge headings. The value of the ordinate for a given barge heading on any one curve for $\ddot{s}_z$ (or T') is the same as the moment of the spectral energy density function for the corresponding heaving-motion time-history. In forming the fourth moment, all ordinates are first multiplied by ω^4 before finding the area under the curve. Thus, it is apparent that as the sea state increases and hence (in the Neumann model) the frequency at which the mean spectral energy appears decreases, the curves for $\ddot{s}_z$ become progressively lower relative to those for z. The curves for $\ddot{s}_z$ for the three sea states considered are more closely spaced than are those for z. The r. m. s. value of the vertical acceleration of the load for the range of sea states represented here is less sensitive to sea state than that of the vertical displacement, itself, of the load.

C. EFFECTS OF BOOM AZIMUTH AND BARGE HEADING ON A BOOM-LOWERED LOAD IN A SEAWAY

The results in this section show the effect on the load-lowering operation of using various combinations of boom angles and barge headings. For boom-lowered loads, Figures 4.4 through 4.7 below show the r. m. s. values for the three rectangular components of the load displacement vector, for the vertical component of the acceleration of the load as well as the added-dynamic tension in the lowering line. The r. m. s. values were obtained as before, by operating upon the set of covariance functions (evaluated for zero time lag) for the six ship motions themselves, including the variable boom azimuth angle, γ , in the computations in accordance with equations (4.3) and (4.4).

In Figure 4.4 is shown for each sea state an example of varying the boom azimuth angle, γ , on the r. m. s. value of the vertical load displacement component, s_z^{γ} , for two particular fixed barge headings. The two barge headings were selected as those 15° on either side of the downwind barge heading, for there s_z^{γ} has a relatively large r. m. s. value, no matter what the boom azimuth angle may be. It will be noted that the effect is relatively small for Sea State 3, while for Sea States 4 and 5 there is a considerable increase in the r. m. s. values themselves as well as in their variation with the angular position of the boom. For example, in a State 5 sea, the r. m. s. value of the vertical load displacement may be as large as 7.0 feet (for a boom azimuth angle of $\pm$ 105°) or as small as 4.6 feet (for a boom angle of $\pm$ 165°). From Figure 2.1, it is seen that instantaneous vertical displacements of over 17.0 feet from its mean position would be expected to occur approximately 2(100.0 - 99.5) = 1.0% of the time in the former case, compared to approximately 2 (100.0 - 99.9) = 0.2 % of the time in the latter case.

The high-speed computer was programmed to calculate in each case the r.m.s. values for the time-histories of each of the quantities of interest (viz. s_x^{γ} , s_y^{γ} , s_z^{γ} , $\dot{s}_z^{\gamma}$ or T'^{γ}) for each of a set of boom angles covering the complete azimuth circle, using an increment of 15° in the latter. From these computed results, the boom azimuth angle yielding the minimum r.m.s. value for each of the four essential quantities could be estimated, as well as the r.m.s. value resulting from the use of this boom angle, in each sea-state and barge-heading. The results showed that the optimum boom azimuth angle, γ , (measured relative to the barge, counter-clockwise from the direction of the bow) which minimized the r.m.s. values of any given one of the time histories of interest, was in general nearly independent of both barge heading and sea state.

The values found for the optimizing value of the boom azimuth angle, γ , are shown for each time history and in each case, together with the resulting minimum r.m.s. value for the time history concerned, in Figures 4.5 and 4.6. The exceptional cases in which the optimum boom angle varies with the barge heading are noted on the graphs in these figures and occur only for the vertical components of the load displacement and load acceleration (or added line tension) for the two higher sea states. Specifically, the optimum boom azimuth angle was found to be 0° or 180° for s_x , $\pm$ 90° for s_y , and 180° for both s_z and T' , uniformly for all barge headings relative to the wind, for Sea State 3. In the case of Sea States 4 and 5, the only modification which becomes necessary is that for s_z and T' the optimum boom angle varies away from 180° by amounts up to approximately 15° or 20° when the barge heading angle, β_B , is within $\pm$ 90° of the downwind direction.

In summary, it may be seen that in the lowest sea state considered, the minimum attainable r.m.s. values (i.e. those resulting from use of the optimum boom angle) do not vary greatly with the barge heading. However, with increasing sea state, the barge heading significantly affects the magnitude of the minimum-attainable r.m.s. values to an increasing degree.

In general, for each of the quantities being considered, the size of the minimum r.m.s. value attainable by proper boom orientation depends on barge heading as follows. It is smallest around $\beta_B = \pm 90°$ for both the fore-aft and the vertical load displacement components, as well as for the vertical load acceleration component (or added-dynamic line tension). It is largest for these same three quantities for $\beta_B = 0°$ and $\beta_B = 180°$. For the port-starboard load displacement component, it is smallest for $\beta_B = 0°$ and 180° and largest around $\beta_B = \pm 90°$. The minimum attainable r.m.s. values for the other three load quantities are largest for $\beta_B = 0°$.

In Sea State 5, the actual minimum-attainable r.m.s. values vary from 0.5 feet to 0.8 feet for the fore-aft load-displacement component, from 0.8 feet to 1.7 feet for the port-starboard load-displacement component, from 3.8 feet to 6.0 feet for the vertical load-displacement component, and from 2.28 feet/sec^2 (or lb/slug) to 2.98 ft/sec^2 (or lb/slug) for the vertical load acceleration component (or the added dynamic tension in the lowering line). In Sea State 4, the minimum attainable r.m.s. values vary from 0.5 feet to 1.1 feet for the

port-starboard load displacement component, from 2.4 to 3.2 for the vertical load displacement component, and from 1.63 to 2.02 ft/sec^2 (or lb/slug) for the vertical load acceleration component and added dynamic line tension.

As an example of the interpretation of some of these numerical results for the r.m.s. values attainable, reference to Figure 2.3 indicates that by proper orientations of the barge and boom, the expected maximum oscillation amplitude over a span of 500 oscillations in the port-starboard load displacement component in a State 5 sea would be reducible from the maximum attainable value at $\beta_B = \pm 90°$ of 3.67 (1.7) = 6.24 feet to the minimum attainable value at $\beta_B = 0°$ of 3.67 (0.8) = 2.94 feet. (Here in each case the optimum boom position is that corresponding to $\gamma = \pm 90°$, i.e. directly across the beam of the vessel.)

As an additional illustration of the effect of the boom azimuth angle on the r.m.s. values associated with the load-lowering operation one may contrast the results shown in Figures 4.6 and 4.7. One sees in the latter figure, for each sea state and barge heading, the r.m.s. values which would result were the boom azimuth chosen so as to maximize the vertical load displacements and added dynamic line tensions. It is seen that this "worst" boom angle changes from +90° (port side) to -90° (starboard side) as the direction of the barge heading moves across that of the predominant wind. The attainment of r.m.s. values of nearly 10 ft/sec^2 for the vertical load acceleration is seen to be possible in a Sea State 5.

D. SUPPLEMENTAL DISCUSSION ON THE OPTIMUM BOOM ANGLE

Some discussion of the optimum values for the boom azimuth angle will next be presented in view of the special nature of the results found concerning them. In the case of the fore and aft (s_x^γ) and the port-starboard (s_y^γ) load displacements, formal explanation is rather easily given. For these time histories, the expressions for which are given by Equation (4.3), we have for a given barge heading and arbitrary boom angle the following formulae for the squares of the two corresponding r.m.s. values ($\sigma_{s_x^\gamma}$ and $\sigma_{s_y^\gamma}$):

$$\begin{aligned}(\sigma_{s_x^\gamma})^2 &= \sigma_x^2 - 2(150)\sigma_x\sigma_\psi\rho_{x\psi}\sin\gamma + (150)^2\sigma_\psi^2\sin^2\gamma \\ &= \sigma_x^2(1-\rho_{x\psi}^2) + (\rho_{x\psi}\sigma_x - 150\sigma_\psi\sin\gamma)^2 \\ &\le \sigma_x^2(1-\rho_{x\psi}^2) \quad , \text{ with equality just if } \sin\gamma = +\frac{\rho_{x\psi}\sigma_x}{150\sigma_\psi}\end{aligned}$$

and

$$\begin{aligned}(\sigma_{s_y^\gamma})^2 &= \sigma_y^2 + 2(150)\sigma_y\sigma_\psi\rho_{y\psi}\cos\gamma + (150)^2\sigma_\psi^2\cos^2\gamma \\ &= \sigma_y^2(1-\rho_{y\psi}^2) + (\rho_{y\psi}\sigma_y + 150\sigma_\psi\cos\gamma)^2 \\ &\le \sigma_y^2(1-\rho_{y\psi}^2) \quad , \text{ with equality just if } \cos\gamma = -\frac{\rho_{y\psi}\sigma_y}{150\sigma_\psi}\end{aligned}$$

These results are obtained, as seen, by completing the square in each case and noting the condition on the azimuth angle, γ , which makes the square vanish. The determination of the optimizing value of γ is seen in each case to require a knowledge of two r. m. s. values and one coefficient of correlation. These vary with sea state and barge heading. An a priori guess as to the magnitudes of the above quantities might result in some confidence that the expressions for the sine and cosine of the optimum angle were close to zero in each case. Nevertheless, the high-speed computer program was allowed to generate all of the r. m. s. values resulting from the use of 15° increments in the boom angle, for each sea-state and barge-heading combination. These were then available for inspection and the minimum r. m. s. values as well as the corresponding boom angle could be immediately picked out to within 15°. In addition, the formulas above for the optimum boom angles were employed by substituting in the r. m. s. values and the covariances for Sea State 5, appearing in the computer output, and it was found that the optimizing value of γ was somewhat less in absolute value than 3° from 0° or 180° for s_x^γ , and even closer to +90° for s_y^γ . Thus, the optimum values for γ appearing on the curves in Figures 4. 5 and 4. 6 would appear to be given with more accuracy than that nominally assignable to them, the nearest 15°.

In the case of the vertical load displacement, s_z^γ , in Sea State 5, the minimizing value of γ was found to shift gradually from $\pm$ 180° at barge heading $\mp$ 180° to a value of approximately $\pm$ 159° at barge heading $\mp$ 15° (cf. Figure 4. 4) and to return abruptly to 180° (by symmetry) at barge heading 0°. The situation regarding the vertical load displacement appeared to be similar in Sea State 4.

A similar behavior was found for the boom azimuth angle minimizing the r. m. s. value of the vertical load acceleration (or added line tensions) in the two higher sea states. However, in Sea State 3, the minimizing boom azimuth angle was consistently 180° (boom over the stern) for both the vertical load displacement and acceleration.

As an example of results obtained for a 200-ton load lowered in a State 5 sea with a crosswind barge heading and with the optimum boom azimuth angle (here of 180°, -- boom over the stern), the r. m. s. value of the added-dynamic line tension given by Figure 4. 6 is (2. 38) (200) / 32. 2 = 14. 8 tons. From Figure 2. 1 it is seen that the downwind force of impact on the bottom would exceed 25. 0 tons approximately 2. 3% of the time, if the instant of impact were allowed to occur at random. For a center-lowered load under the same conditions, the r. m. s. value of its acceleration is 1. 17 (200) /32. 2 = 7. 27 tons, and the downward impact force on the bottom would exceed 14. 3 tons approximately 2. 3% of the time.

E. MOORING SYSTEM QUANTITIES

The r. m. s. values of the horizontal mooring forces and the yawing moment induced on the barge are obtainable directly from Figures 3. 30 and 3. 31 in view of equations 4. 6, since the factor of proportionality in these equations need only be applied in each case to the r. m. s. value given in these figures. Thus, the r. m. s. value of X_m , Y_m or N_m (in lbs., lbs. and ft. -lbs. respectively) for any

given barge heading and wind speed is, respectively, 1250 lbs./ft, 3750 lbs./ft. or 6.675×10^7 ft. lbs times the r. m. s. value of surge, sway or yaw under the same conditions. For example, in a Sea State 5, the induced force, X_m, on the barge will have r. m. s. value of 1250 (0. 8) = 1000 lb. with a downwind barge heading, while that for Y_m with a crosswind barge heading will be 3750 (2. 2) = 8250 lb.

The r. m. s. value of the fluctuating component of the force in each of the four mooring cables is shown in Figure 4. 8 as a function of barge heading for each sea state. The four are seen to have nearly the same r. m. s. value for any particular barge heading in a Sea State 3, the actual values varying between 300 and 600 lb. For a Sea State 4 the range is from 1100 to 1750 lb., the difference between r. m. s. values for the four fluctuating cable forces being as much as 150 lb. For Sea State 5, the range is from 1800 to 2700 lb. with differences in r. m. s. values between cables of 250 lb. In all cases the cable force r. m. s. values are greatest near crosswind, and least for upwind and downwind, barge headings.

5. CROSS-SPECTRA, PHASE DIFFERENCES AND RELATED RESULTS

The present chapter treats the phenomena of interest when more than one time history is considered at a time. In contrast to situations for the earlier-presented material on individual time histories characterizable by energy spectra, relatively little is readily available in the literature treating in detail the information contained in the cross-spectra of a stationary Gaussian vector stochastic process. The notion of the degree of synchronism between the various ship motions has occasionally been employed in discussions of theoretical aspects of the behavior of a ship in an irregular seaway. Some of the relevant problems involved here are often phrased as questions in terms of phase relations, synchronism, coherence, coupling, or the degree of correlation or predictability existing among the motions.

The information derivable from the individual energy spectra and the cross spectrum when these are given for two time-history functions, includes the complete specification of the joint probability distributions for the ordinates, measured from their mean values, on the corresponding time-history curves; this specification is provided by the set of three numbers consisting of two auto-covariances for the individual time-history functions (obtainable from their energy spectra) and the (single) cross covariance for the time-history pair (obtainable from their cross spectrum). From tabulated values of the two-dimensional Gaussian probability integral, the probability of the joint occurrence of the ordinates on the two curves below any two given ordinate levels for the two curves may be found.

In addition to this quite fundamental information, the cross-spectrum contains the complete specification of the parameters for the distribution of the instantaneous phase difference and amplitude ratio, as well as the difference in instantaneous frequencies for the two time histories.

Specifically, such information is contained in the moments of the complex-valued cross-spectral energy density function. The following discussion begins with the consideration of the latter function which is associated with any pair of time histories.

A. Cross-Spectra and Cross-Covariances

Consider any pair of ship motions r and s whose complex response operators to the waves, η , are $T_{r\eta}(\omega,\beta)$ and $T_{s\eta}(\omega,\beta)$. The complex-valued cross-spectral energy distribution for that pair is an immediate generalization of the (auto) spectral energy density function for a single time-history and is given at any frequency, ω , by

$$\Phi^{(r,s)}(\omega) = \int_{-\pi}^{+\pi} d\beta_w \left| S(\omega,\beta_w) \right|^2 T_{r\eta}^{*}(\omega,\beta)\, T_{s\eta}(\omega,\beta)$$

where $|S(\omega,\beta_w)|^2$ is the energy spectrum of the surface elevation, η, (suitably normalized so that its integral over-all wave directions, β_w, and frequencies, ω, is the variance, σ_η^2 of the surface elevation time history) and such that the "narrow band" significant wave is $2\sigma_\eta = \sqrt{2E_\eta}$. Here also, $\beta = \beta_w - \beta_B$ is the heading of a component wave relative to the barge heading, and the asterisk denotes the operation of taking the complex conjugate. When r = s, this expression is seen to reduce to the spectral energy density function $\Phi^{(r,r)}(\omega)$ the latter being a special case to which everything to be discussed below applies (though often in a trivial way).

In the present study the introduction of the Neumann spectrum for the seaway leads to the following special form for the cross-spectral energy density:

$$\Phi^{(r,s)}(\omega) = c\,\frac{2}{\pi}\,\omega^{-6} e^{-\frac{2g^2}{V_w^2\omega^2}} \int_{-\pi/2}^{+\pi/2} d\beta_w \cos^2\beta_w\, T^*_{r\eta}(\omega, \beta_w - \beta_B)\, T_{s\eta}(\omega, \beta_w - \beta_B).$$

In terms of the wave length, $\lambda = 2\pi g/\omega^2$, the density with respect to λ is given by

$$\Phi^{(r,s)}(\lambda) = c'\,\frac{2}{\pi}\,\lambda^{3/2} e^{-a\lambda} \int_{-\pi/2}^{+\pi/2} d\beta_w \cos^2\beta_w\, T^*_{r\eta}(\lambda, \beta_w - \beta_B)\, T_{s\eta}(\lambda, \beta_w - \beta_B).$$

In the expressions above, it will be noted that the symbols "Φ" and "T" used to denote the cross-spectral density and the complex response operator functions are used indiscriminantly regardless of the arguments of the functions. However, the intended meaning should be clear, so long as the arguments which undergo replacement are limited to ω and λ, it being understood that expressions containing λ are to be integrated with respect to λ while expressions denoted by $\Phi^{(r,s)}(\omega)$ are to be integrated with respect to ω. Such an integration over all λ, say, yields complex valued the cross-covariance function $\varphi^{(r,s)}(0)$ given by

$$\varphi^{(r,s)}(0) = \int_0^\infty d\lambda\, c'\frac{\pi}{2}\,\lambda^{3/2} e^{-a\lambda} \int_{-\pi/2}^{+\pi/2} d\beta_w \cos^2\beta_w\, T^*_{r\eta}(\lambda, \beta_w - \beta_B)\, T_{s\eta}(\lambda, \beta_w - \beta_B)$$

the real part of which is the ordinary coefficient of correlation $\rho^{(r,s)}(0)$ (evaluated for the time lag value of zero) between the rth and the sth ship motion time-histories when suitably normalized. Thus,

$$\rho^{(r,s)}(0) = Re\left\{\varphi^{(r,s)}(0)\right\} \Big/ \left\{\varphi^{r,r}(0)\;\varphi^{s,s}(0)\right\}^{1/2}.$$

In the present study, arguments other than $\tau = 0$ for the cross-covariance function $\varphi^{(r,s)}(\tau)$ were not employed, and in this sense this is a study of the behavior of the moored barge at isolated instants. Extension of the scope of the study to include the relationships between time histories at non-simultaneous instants would naturally lead to the evaluation of $\varphi^{(r,s)}(\tau)$ for non-zero values of τ in certain cases. One such extension would be the synthesis of examples of sufficient duration to include several oscillations of the surface elevation and the six simultaneous barge motions.

It is apparent that considering the 3x24 = 72 combinations of sea states ($V_{..}$) and barge headings ($\beta_{..}$) use for the present study, there are a large number of complex cross spectral density functions which are of potential interest. If one considers the ship motions alone, it is seen that in addition to the 432 pure spectral energy density functions enumerated in Chapter 3, there are an additional fifteen essentially different proper cross-spectral energy density functions for each of the 72 environmental conditions. The set of 30 possible required functions may be halved, since no new information is obtained by interchanging the order in which the letters r and s appear; it may be seen that such an interchange results in a function $\Phi^{(s,r)}(\lambda)$ whose value for a given λ is the complex conjugate of that of $\Phi^{(r,s)}(\lambda)$.

In addition to this set of 15x72=1080 possible cross-spectral energy density functions for the barge motions themselves under all environmental conditions, there is the possibility of considering those involving the surface elevation as well as the load-lowering and mooring systems. Fortunately, each of these is obtainable by forming linear combinations of the complete set of cross spectra for the seven fundamental time-history functions (or their time rates of change) which consists of the six ship motions and the surface elevation. However, the magnitude of the resulting overall number of cross spectra of possible interest, together with their general unfamiliarity to the general reader, suggests that routine calculation of even any sizable fraction of them would be inappropriate. Should the need for any particular set of a large number of them become apparent, a minor modification of the existing high-speed computer program will make them readily available. Those presented in the present report were obtained by hand calculation, which is a feasible method,provided a large number of cases are not required.

While it is obvious that a rather large number of the set of possible cross spectra referred to above, e. g. those involving two boom angles or barge headings which are distinct, would be of no interest in a problem concerned with but one boom and one barge, it may be suggested that certain of these would be relevant in cases where two loads were lowered from one barge or two barges were to cooperate in lowering a single load (by means of two lowering lines). In the latter case the spatial separation of the barges would introduce additional phase shifts and incoherance between the motions, but in a manner capable of analytical treatment.

Having already treated the energy spectrum case, these spectra may be considered as available for use in certain kinds of reduction or standardization of the cross-spectra and to aid in visualizing their structure and the manner in which they are formed. The latter serves to provide some insight into their meaning and interpretation, as well as to effect a saving in space required for their presentation by a condensation of the information contained in these functions. In addition, the graphs of the reduced cross-spectral densities which may be plotted present a somewhat more systematic appearance than those which would have otherwise resulted.

The analogue of the process described in the Chapter 3 for visualizing the formation of the definite integral defining the spectral energy density function,

$\Phi^{(r,r)}(\lambda)$, (viz, sliding the curve $\cos^2\beta_w = (1/2 + 1/2 \cos 2\beta_w)$ along the curve for the square of the appropriate response amplitude operator) now involves applying a set of weights proportional to $\cos^2\beta_w$ to a set of points in the complete number plane representing the plot for a fixed λ of the curve representing the Hermitian product, $H_{rs}(\lambda,\beta) = T^*_{r\eta}(\lambda, \beta_w-\beta_B)\cdot T_{s\eta}(\lambda,\beta_w-\beta_B)$, of the complex response operators, with the angle $\beta = \beta_w-\beta_B$ as parameter for the curve. For this purpose the plots in the complex plane, referred to in Chapter 3, of the complex response operators $T_{r\eta}(\lambda,\beta)$ and their Hermitian products, when taken in pairs, are convenient for vizualization purposes; the effect of the directional symmetry of the wave spectrum and the effect of the barge heading angle may be seen graphically.

Considering for any V_w and β_B, the value of the ratio,

$$\Phi^{rs}_{V_w\beta_B}(\lambda) = \frac{\Phi^{(r,s)}_{V_w\beta_B}(\lambda)}{\Phi^{\eta\eta}_{V_w}(\lambda)} = \int_{-\pi/2}^{+\pi/2} \frac{\cos^2\beta_w}{\pi/2}\, T^*_{r\eta}(\lambda,\beta_w-\beta_B)\cdot T_{s\eta}(\lambda,\beta_w-\beta_B)$$

where $\Phi^{\eta\eta}_{V_w}(\lambda) = C'\lambda^{5/2}e^{-\frac{5}{4}\frac{g^2}{V_w^2\lambda^2}}$ is the surface elevation spectral density over λ, is seen to be independent of V_w. The following interpretation for this ratio is apparent. Since $\int_{-\pi/2}^{+\pi/2} \frac{\cos^2\beta_w}{\pi/2}\, d\beta_w/\beta_w = 1$, this ratio, or relative cross spectral density for the r-th and s-th ship motions -- relative to the surface elevation -- is seen to be a weighted sum or integral average of the function of $\beta = \beta_w - \beta_B$ represented by the Hermitian product of the complex response operators, $H^{(r,s)}(\lambda,\beta) = T^*_{r\eta}(\lambda,\beta)\cdot T_{s\eta}(\lambda,\beta)$. Furthermore, the function $\cos^2\beta_w/(\pi/2)$, is non-negative and has total weight of unity. Consequently, the value of the ratio must lie within the curve representing $H^{(r,s)}(\lambda,\beta)$ if the latter is everywhere convex (i.e. contains the internal points of each of its chords) or within the smallest convex point set containing the curve. As a consequence, the direction from the origin of the point representing the complex number $\Phi^{(r,s)}_{V_w\beta_B}/\Phi^{\eta\eta}_{V_w}(\lambda)$ must lie within the angle subtended by the figure representing the plot of $H^{(r,s)}(\lambda,\beta)$. Hence we see that $\mathrm{Arg}\{\Phi^{(r,s)}(\lambda)\} = \mathrm{Arg}\{\Phi^{(r,s)}(\lambda)/\Phi^{\eta\eta}(\lambda)\}$ is a weighted average with non-negative, unit total weights of $H^{(r,s)}(\lambda,\beta) = T^*_{r\eta}(\lambda,\beta)\cdot T_{s\eta}(\lambda,\beta)$ between min Arg $\{H^{(r,s)}(\lambda,\beta)\}$ and max Arg $\{H^{(r,s)}(\lambda,\beta)\}$ and since

$$\mathrm{Arg}\{H^{(r,s)}(\lambda,\beta)\} = \mathrm{Arg}\{T^*_{r\eta}(\lambda,\beta)\cdot T_{s\eta}(\lambda,\beta)\} = \mathrm{Arg}\left\{|T_{r\eta}(\lambda,\beta)\cdot T_{s\eta}(\lambda,\beta)|\, e^{i[\mathrm{Arg}\{T_{s\eta}\}-\mathrm{Arg}\{T_{r\eta}\}]}\right\}$$

$$= \mathrm{Arg}\left\{\quad e^{i[\mathrm{Arg}\{T_{s\eta}(\lambda,\beta)\}-\mathrm{Arg}\{T_{r\eta}(\lambda,\beta)\}]}\right\}$$

Likewise $\mathrm{Arg}\{\Phi^{\eta\eta}(\lambda)\} = \mathrm{Arg}\{\Phi^{\eta\eta}(\lambda)/\Phi^{\eta\eta}(\lambda)\}$ = Arg {weighted average of $T_{s\eta}(\lambda,\beta)$} w.r.t. $\cos^2\beta_w/(\pi/2)$. Further, if we consider

$$\psi^{(r,s)}_{V_w\beta_B}(\zeta) = \psi^{(r,s)}_{\eta V_w\beta_B}(\zeta) = \int_c d\lambda\, \Phi^{\eta\eta}(\lambda)\frac{1}{\pi}\int_{-\pi/2}^{+\pi/2} d\beta_w \cos^2\beta_w\, T^*_{r\eta}(\lambda,\beta_w-\beta_B)\cdot T_{s\eta}(\lambda,\beta_w-\beta_B)$$

and if we set

$$\bar{\psi}^{(r,s)}_{\eta V_w\beta_B}(\zeta) = \frac{\psi^{(r,s)}_{\eta V_w\beta_B}(0)}{\psi^{\eta\eta}_{V_w}(\zeta)} = \frac{\int_c d\lambda\, \Phi^{\eta\eta}_{V_w}(\lambda)\, \bar{\Phi}^{(r,s)}_{\eta\beta_B}(\lambda)}{\int_c d\lambda\, \Phi^{\eta\eta}_{V_w}(\lambda)}$$

the right hand side is the weighted average of

$$\Phi^{(r,s)}_{\eta\beta_B}(\lambda)$$

and hence $\mathrm{Arg}\left\{\bar{\varphi}^{(r,s)}_{V_w,\beta_B}(0)\right\} = \mathrm{Arg}\left\{\bar{\varphi}^{(r,s)}_{\eta V_w,\beta_B}(0)\right\} = \mathrm{Arg}\left\{\text{(weighted sum of } \bar{\Phi}^{r,s}_{\eta\beta_B}(\lambda)\right\}$

Thus, the quantity being averaged over λ, is itself a weighted average over β_w of $T^*_{r\eta} \cdot T_{s\eta}$.

Next, consider:

$$\varphi^{(\eta,\zeta)}_{V_w,\beta_B}(0) = \int_0^\infty d\lambda\ \Phi^{\eta\eta}(\lambda)\frac{2}{\pi}\int_{-\pi/2}^{+\pi/2} d\beta_w \cos^2\beta_w\ T^*_{\eta\eta}(\omega,\beta_w-\beta_B)\,T_{s\eta}(\omega,\beta_w-\beta_B)$$

$$\bar{\varphi}^{(\eta,s)}_{\eta V_w,\beta_B}(0) = \frac{\varphi^{(\eta,s)}_{V_w,\beta}(0)}{\varphi^{\eta\eta}_{V_w}(0)} = \frac{1}{\varphi^{\eta\eta}_{V_w}(0)}\int_0^\infty d\lambda\ \Phi^{\eta\eta}_{V_w}(\lambda)\,\Phi^{(\eta,s)}_{\eta\beta_B}(\lambda)$$

$$= \text{weighted average of } \bar{\Phi}^{(\eta,s)}_{\eta\beta_B}(\lambda) \quad \text{w.r.t} \quad \Phi^{\eta\eta}_{V_w}(\lambda)\Big/\varphi^{\eta\eta}_{V_w}(0)$$

(non-neg., unit total weight)

Hence we have the results (1) the quantity $\bar{\Phi}^{(\eta,s)}_{\eta}(\lambda) = \bar{\Phi}^{(r,s)}_{V_w,\beta_B}(\lambda)\Big/\bar{\Phi}^{\eta\eta}_{V_w}(\lambda)$ lies in the convex hull of the curve for $\Phi^{(r,s)}(\lambda,\beta)$ in the complex plane; it is independent of V_w and may be converted into $\bar{\Phi}^{(r,s)}(\lambda)$ by multiplying by $\bar{\Phi}^{\eta\eta}_{V_w}(\lambda)$ and into $\bar{\Phi}^{(r,s)}_{V_w,\beta}(\omega)$ by multiplying by the additional factor $\left|\frac{d\lambda}{d\omega}\right| = \sqrt{2}\,\lambda^{3/2}/\sqrt{\pi g}$; (2) the quantity $\bar{\varphi}^{(r,s)}_{\eta V_w,\beta_B}(\lambda) = \varphi^{(r,s)}_{V_w,\beta_B}(0)\Big/\varphi^{\eta\eta}_{V_w}(0)$ lies in the convex hull of the curve for $\bar{\Phi}^{(r,s)}_{\eta V_w,\beta_B}(\lambda)$ in the complex plane, depends upon V_w, and may be converted into $\varphi^{(r,s)}_{V_w,\beta_B}(0)$ by multiplying by $\varphi^{(\eta\eta)}_{V_w}(0)$ which is the total energy in surface-elevation time-history spectrum for wind speed V_w. In Figure 5.1 is shown a set of cross-spectral energy-density functions for the three sea states considered and for barge heading zero for the barge motions of surge and heave, i.e. $\Phi^{(x,z)}_{V_w,\beta}(\lambda)$. plotted as a curve in the complex number plane with λ as a parameter. The increase in the size of the curves with increasing sea state is apparent; these are absolute (i.e., are not relative) cross spectra. Plotting on logarithmic scales would have been required to show on the same graph the variation of the cross-spectral energy density for Sea State 3. As noted on the plot shown, the curve appears to be located entirely at the origin. Interpolation between the points, computed for values of λ which are multiples of 100 ft., is not justified in most cases, as is indicated by the dashed portions of the curves. The points for the longer wave lengths indicate that the weighted mean of the Hermitian product, $T^*_{x\eta}(\lambda,\beta) \cdot T_{z\eta}(\lambda,\beta)$, has an angle which is near +90° for the long wave lengths falling off to approximately +45° at 300 feet, and for the estimated wave lengths rising again to the vicinity of +90°. These variations of the angle by which heave leads surge is reflected

in the graphs of Figures 3.23, 3.25 and 3.25, where heave for wave headings between $\pm$ 90° relative to the barge ($\beta_2 = 0°$ for the graphs in Figure 5.1) is seen to lead surge by nearly 90° at the long wave lengths, the amount decreasing quite appreciably at 400' and very much so at 300' as the two phase shift curves both dip toward one another. By the time 200' is reached the two curves appear to have crossed each other to the extent that for 0°, surge is leading, once more, by +270°, or heave by +90°, while between 200' and 100' a further transition seems to have taken place, with the result that at 100' heave leads once more by +450° or +90°, when β is near 0°.

It may be pointed out that the direction of each point from the origin is determined entirely by the variation of wave energy with wave direction together with the nature of the complex response operators for surge and heave. The modulus of the latter (i.e. the response amplitude operator) plays a lesser role than the argument (phase shift operator) in this example. Finally, it may be pointed out that the directions of any two points lying in different curves but associated with the same wave length are identical from one sea state to another, the only difference between the two curves being that the distances of points for corresponding wave lengths are determined by the relative energies in the two sea states. In fact, if the distance for each point were divided by the value of the surface elevation the energy density given in Figure 5.2 for the sea state and wave length to which it corresponds, then all points for the same wave length would coincide at a point whose distance from the origin is determined by the complex response operators, the directional distribution of the energy in the Neumann spectrum, and the barge heading.

Figures 5.3 through 5.5 show the values (with respect to surface elevation) of the relative complex cross spectral energy density functions and the relative complex covariance functions evaluated at time lag zero, for a selected set of ship-motions or load motion time histories and barge headings. As previously noted, multiplication of the coordinates of any point representing a relative cross spectral density in these two figures may be converted into the coordinates for an absolute cross-energy spectral density for any given sea state by multiplying by the value given in Figure 5.2 for the wave length concerned and sea state desired. Similarly, the coordinates for points corresponding to the relative cross covariance need only be multiplied by the total energy (shown in Figure 5.2) for the sea state desired to obtain the absolute cross covariance.

A common feature of all eight of the relative cross-spectral curves shown is their tendency toward forming closed convex curves always containing the point corresponding to the associated relative covariance functions.

An example of some of the information contained in a particular pair of cross spectra is illustrated by Figure 5.3 which shows the relative cross spectra for the sway-roll pair of motions as well as for the lateral load (center-lowered) displacement -- roll pair of motions, for barge headings of both 90° and 180° in one case, and 90° and 0° in the other. For the sway-roll pair, the cross-spectrum values for long wave lengths for both barge headings lie in the fourth quadrant of the complex plane, starting out with direction near zero and becoming more negative as the wave length decreases. This behavior reflects the fact that in Figures 3.27 - 3.28 roll loads sway by a small negative angle throughout the entire range of wave headings, β, relative to the barge, this angle becoming more negative, on the average, as wave length decreases, particularly for the range of wave headings that are centered, at barge heading 180°, and for which $\beta = 180° \pm \pi/2$. For the 200 - foot wave lengths, roll is leading on the average over the range

$-180° \leq \beta \leq 0°$ by a second quadrant angle and by a first quadrant angle for 100'.

The lateral load displacement vs. roll cross spectra at the bottom of the page are quite similar to those at the top, for the larger wave lengths, since each of the complex response operators for the two components of s_y, and $|KG|\phi$, has nearly the same phase-shift characteristics as the other. Thus, the resultant of the two behaves in this regard similarly to the sway response operator itself. As the wave length decreases, the difference between the complex response operator for y and s_y becomes greater and the difference between cross-spectral curves is more.

Figures 5.4 and 5.5 further illustrate average phase shift characteristics, for barge heading $\beta_R = 180°$. The mean phase lead of yaw over roll is seen to undergo a 180° change from the longest to the shortest wave length considered. Sway is seen to lag behind surge by a small positive angle for the long wave lengths, this positive angle increasing in magnitude as the wave lengths become shorter. Yaw is seen to be nearly 180° out of phase on the average with the surface elevations until the short wave lengths of 300' and below are reached. On the average, for long waves, heave is seen to lead the surface elevation by a small positive acute angle.

The significance of the relative complex cross-covariance point which has been plotted in each case will be seen later when phase relationships are discussed more fully in the next section. For the present it may be pointed out that the direction of this point from the origin in these selected graphs is again shown in the comprehensive set of graphs shown in Figure 5.9 for the time histories and barge headings in question.

It may be seen that at a given wave length the cross spectra reflect the average phase shift between the responses of each of the two motions involved to the surface elevation and hence, the average of the phase difference between the two motions themselves in unidirectional sinusoidal waves. Here the phase shift averaging is done in a weighted manner with weights corresponding to the energy in the Neumann spectral energy distribution over direction at a given frequency (wave length). The cross covariance represents a further averaging of the averages already obtained, the second averaging being a weighted average over wave length with weights corresponding to the total energy in the Neumann spectral energy at each wave length. It is clear that the values of the cross spectra obtained at each frequency from actual time-history records of ship motions in an actual seaway will depend upon, or reflect, both the variation of the ship's behavior in unidirectional sine waves (as the direction is varied) and the distribution of surface elevation spectral energy over direction at that frequency, while the cross covariance will reflect the further effect of the spectral distribution of total energy over the entire set of wave lengths. In the present problem both ship responses and surface elevation spectral energy distribution have been assumed to be given, or calculable. With an actual vessel in an actual seaway, the former need not be the case while the latter may or may not be the case. At least two types of problems are of importance here: First, without knowing the

seaway surface-elevation spectrum, how can the ship's responses to individual sine waves be estimated (or, if already calculated, to be tested) from observation of the time histories of its motions? Second, assuming the ship's response to unidirectional sine waves is known, how can the surface elevation spectrum be estimated? The two problems are related, although the second is of course the simpler. A third problem corresponds to the case in which the ship responses to unidirectional sinusoidal waves are to be estimated from their time-histories in a seaway whose surface elevation spectrum is known (e. g. when using well-calibrated directional wave making equipment in a task of known characteristics).

Instantaneous phase and amplitude

The preceding section contained examples of cross-spectra for ship and load motions and, in individual cases, pointed out their relation to the corresponding phase differences in the responses of the ship to unidirectional sinusoidal waves through a generalized averaging process with respect to the distribution, over direction, of the energy in the seaway. The relation of the complex cross-covariance to the phase differences of the complex response operator and to the directional wave spectrum by way of the cross-spectra and the spectral energy density function for the surface elevation was also mentioned.

The concept of the instantaneous phase difference between two components of a stationary Gaussian vector stochastic processes is now introduced as a means of dealing directly with the question: What are the phase relations between each pair of motions connected with the barge or its load or its mooring system at any given instant? Accompanying the concept of difference between instantaneous phases, is the concept of the ratio between the instantaneous amplitudes of the two time-histories. Both concepts are derived from that of the instantaneous complex valued envelope, $\zeta(t)$, already referred to (Chap. 3), whose modulus is the instantaneous amplitude, $r(t)$, the commonly-employed "real envelope" and whose argument is the instantaneous phase $\bar{\theta}(t)$. For an isolated single time history, the instantaneous amplitude is a random variable whose values follow the Rayleigh distribution, whereas the instantaneous phase is a random variable following the uniform distribution (i. e. having the constant probability density 1/360 per degree over the interval $(0, 360^\circ)$ or $1/2\pi$ per radian over the interval $(-\pi, +\pi)$. We shall adopt the latter interval as the interval of definition as a matter of course in the discussion to follow. The instantaneous phase for a single time-history record has therefore, by convention, the mean value zero and a standard deviation of $[(2\pi)^2/12]^{1/2} = 2\pi/\sqrt{12} = \pi/\sqrt{3}$ =1.81 radians (as compared to its range of 2π =6.28 radians.)

By expressing the random variables representing real and imaginary parts of the complex-valued envelopes of each of the time histories of sway and roll as linear combinations of conventional zero-mean, unit-standard-deviation, independently-distributed Gaussian random variables, it is possible to perform a sampling experiment using a table of random numbers to illustrate a typical set of values taken at independently-selected random times for this pair of complex-valued envelopes. This has been done for the case of a barge heading

of 90° in a State Five Sea, and the results of a sample of size ten are shown graphically in Figure 5.6. In preparing this figure, the values of the complex numbers representing the simultaneous observation at a randomly selected time, t, of the two complex envelopes $\epsilon_y(t)$ and $\epsilon_\phi(t)$ were first plotted as open circles and squares, respectively, using the individual separate scales for z, and z_2, as shown on the figures. Next, the radial line from the origin was drawn out to each of the pairs of plotted points and the association of these radii indicated graphically by joining them with a directed arc showing the phase lead of ϕ over y. The arcs are numbered in the order in which the corresponding points were obtained during the sampling procedure. The points represented by the solid circles and squares correspond to the normalized radii resulting from dividing those for y by $\sigma_y = 1.674$ and those for ϕ by $\sigma_\phi = 0.08874$. Thus, the lengths of the two arms of the difference angle are in the ratio $\rho = \frac{e_\phi}{\sigma_\phi} \Big/ \frac{e_y}{\sigma_y}$. The salient features of Figure 5.6 are two: first, the individual arms of any particular angle are not confined to any particular quadrant or quadrants; second, all indicated angular differences have the same sense, which is in the clockwise (negative) direction, and have a range of magnitudes lying between 35° and 140°, approximately. The evidence from the sample is that, although there is considerable dispersion shown by the phase difference, on the average the instantaneous phase for roll leads that for sway by a negative angular amount (approximately equal to -90°), i.e. $\bar{\theta}_\phi$ lags $\bar{\theta}_y$ by the positive angle. The numerical magnitudes of the different angles in this case are taken so as to not exceed 180°. It may be noted at this point for later reference that the three parameters characterizing the joint distribution of $\epsilon_y(t)$ and $e_\phi(t)$ are: (1) $\sigma_\phi/\sigma_y = 0.08874/1.674 = 0.0530$; (2) $\measuredangle \epsilon_{\rho_{y\phi}}(0) = -1.599$ radians (-91.6°); (3), $|\epsilon_{\rho_{y\phi}}(\tau)| = 0.614$.

Denoting by $e_f(t)$ and $e_g(t)$ the complex-valued envelopes of the time history functions f(t) and g(t), it is convenient to consider their ratio, the instantaneously varying quantity $\epsilon_g(t)/\epsilon_f(t) = \left[r_g(t)/r_f(t)\right] \exp i\left[\bar{\theta}_g(t) - \bar{\theta}_f(t)\right]$ whose argument is $Arg\left[\epsilon_g(t)/\epsilon_f(t)\right] = \bar{\theta}_g(t) - \bar{\theta}_f(t)$ and whose modulus is Mod $\epsilon_g(t)/\epsilon_f(t) = r_g(t)/r_f(t)$. Alternatively it is useful to consider the complex-valued instantaneous gain G(t) defined by $G(t) = \ln\left[\epsilon_g(t)/\epsilon_f(t)\right] = \ln\left[r_g(t)/r_f(t)\right] + i\left[\bar{\theta}_g(t) - \bar{\theta}_f(t)\right]$, whose real part is the real instantaneous gain (in the usual sense of the logarithm of an amplitude ratio) and whose imaginary part is the instantaneous phase shift or difference.

The motivation and naturalness of the definitions of instantaneous phase and amplitude having been accepted, it is reasonable to regard these concepts as natural and useful also, when two time histories are considered simultaneously. The answers to such questions as where the tip of the boom is likely to be when the barge's bow is up (e.g. when the pitch angle is at its largest value in the negative sense) can be approached by determining the probability distribution for the instantaneous phase difference $\bar{\theta}_{boom}(t) - \bar{\theta}_{pitch}(t)$; if it is found that in the environmental conditions considered (consisting of a given sea state, a given barge heading relative to the predominant wind, and a given boom azimuth angle) the probability distribution of the instantaneous phase difference is relatively highly concentrated around a specifiable mean value, then it will

be possible to predict with relatively high accuracy the instantaneous phase angle for the boom from that of the pitch motion. On the other hand, there is more likelihood that except for certain boom azimuth - barge heading angle combinations, the probability distribution of the instantaneous phase difference will not be highly concentrated around its mean, in which case, given the instantaneous phase of one, that of the other can only be said to fall within certain limits with certain probabilities. It is the purpose of what follows to show how to determine what those probabilities are for given limits for each set of environmental conditions, though lack of space will preclude the presentation of all the necessary results for dealing with all cases. In anticipation of the results (for which the data are to be found in Figures 5.9 and 5.9 (a)) it may be mentioned that, generally speaking, instantaneous phase differences for ship and load motions do not exhibit hightly concentrated probability distributions except in certain cases; among those are, for example, in a State 5 sea, pitch and heave with barge headings 0°, 180°, ±90°, pitch and yaw with barge headings of ± 90° , pitch and surface elevation for barge headings of 0° and 180°, pitch and vertical load displacement with boom azimuth angle +90°, for barge headings ±90°, pitch and vertical load displacement with boom azimuth angle 180° for all barge headings. Thus, for example, when the bow is at the maximum height of its pitching motion so that $\dot{\theta} = 0$ and $\bar{\theta}_\theta(t) = 180°$, we can expect the heaving motion to be going through zero ($\bar{\theta}_z = +90°$) or nearly so ($\bar{\theta}_z = 180 - 105° = 75°$).

It is found that the pair of quantities $R(t) = r_g(t)/r_f(t)$ and $\xi_{gf}(t) = \bar{\theta}_g(t) - \bar{\theta}_f(t)$ or alternatively, the pair of quantities $L = \ln(r_g(t)/r_f(t))$ and $\xi_{gf}(t) = \bar{\theta}_g(t) - \bar{\theta}_f(t)$, have a joint two-dimensional probability distribution which is completely characterized by a set of three parameters. These three parameters are σ_g/σ_f, and the modulus and argument of the envelope of the normalized correlation function evaluated for time lag zero: $e_{\rho_{fg}}(0) = |e_{\rho_{fg}}(0)| e^{i \operatorname{Arg} e_{\rho_{fg}}(0)}$. In fact, the mean value of $L(t)$ is $\ln(\sigma_g/\sigma_f)$ and the mean value of $\bar{\theta}_g(t) - \bar{\theta}_f(t)$ is $\operatorname{Arg}\{e_{\rho_{fg}}(0)\}$, provided that in the case of the latter phase difference, its range is defined to be $\operatorname{Arg}\{e_{\rho_{fg}}(0)\} - \pi < \bar{\theta}_g(t) - \bar{\theta}_f(t) \leq \operatorname{Arg}\{e_{\rho_{fg}}(0)\} + \pi$. It is convenient to "center" the random variables $L(t)$ and $\xi_{gf}(t)$ by subtracting off their mean values and defining the reduced random variables $l(t) = L(t) - \ln \sigma_g/\sigma_f = \ln \frac{r_g(t)/\sigma_g}{r_f(t)/\sigma_f}$ and $\beta(t) = [\bar{\theta}_g(t) - \bar{\theta}_f(t)] - \operatorname{Arg}\{e_{\rho_{fg}}(0)\}$, it being understood that $-\pi < \beta \leq +\pi$, so that we have zero for the means of both $l(t)$ and $\beta(t)$. For an arbitrary, but now fixed pair of time histories g and f, the notation $e_{\rho_{fg}}$ will be shortened in the subsequent parts to only e_ρ .

We insert here an abreviated listing of some additional properties that are useful quite generally in extensions of this discussion.

The two-dimensional probability density function for the joint probability distribution of $l(t)$ and $\beta(t)$ has a relatively simple form, being given by:

$$\frac{1 - |e_\rho(0)|^2}{4\pi} \cdot \frac{dl\, d\beta}{[\cosh l - |e_\rho(0)| \cos\beta]^2}$$

If we set $\bar{\rho}(t) = \exp[\ell(t)] = \frac{\rho_f(t)/\sqrt{\tau}}{\rho_g(t)/\sqrt{\tau}}$ we have for the two-dimensional distribution of $\bar{\rho}(t)$ and $\bar{\beta}(t)$ the expression

$$\frac{1-|\epsilon_f(0)|^2}{\pi} \cdot \frac{\bar{\rho}\, d\bar{\rho}\, d\bar{\beta}}{\left[1-|\epsilon_f(0)|\bar{\rho}\cos\bar{\beta}+\bar{\rho}^2\right]^2}$$

The marginal distribution of $\ell(t)$ is particularly simple, being an even function of $\ell(t)$, given by,

$$\frac{1-|\epsilon_f(0)|^2}{2} \cdot \frac{\cosh\ell\, d\ell}{\left[\cosh^2\ell - |\epsilon_f(0)|^2\right]^{3/2}}$$

Given the condition that $\ell(t) = \ell_0$, the conditional probability distribution of $\beta(t)$ given that $\ell = \ell_0$ (i.e., as given above, the joint probability for $\beta(t)$ and $\ell(t)$ evaluated at $\ell = \ell_0$ divided by the marginal probability for $\ell(t)$ alone evaluated at $\ell = \ell_0$) is:

$$\frac{d\beta}{2\pi} \quad \frac{\left[1-(|\epsilon_f(0)|\operatorname{sech}\ell_0)^2\right]^{3/2}}{\left[1-(|\epsilon_f(0)|\operatorname{sech}\ell_0)\cos\beta\right]^2}$$

which depends only on $\epsilon_f(0)\operatorname{sech}\ell_0$ and is an even function of ℓ_0 so that $\sigma_\beta|_{\ell=\ell_0} = \sigma_\beta|_{-\ell}$. The conditional variance of $\bar{\beta}(t)$ is a minimum when $\ell = 0$ or when $\bar{\rho} = +1.0$.

The marginal distribution of $\bar{\rho}(t)$ is given by

$$\frac{2\bar{\rho}\, d\bar{\rho}\left[1-|\epsilon_f(0)|^2\right]\left[1+(\bar{\rho})^2\right]}{\left[(1-\bar{\rho})^2+(2\bar{\rho})(1-|\epsilon_f(0)|^2)\right]^{3/2}}$$

and its reciprocal, $1/\bar{\rho}$, has the same marginal probability density, while that of $\bar{\beta}(t)$ is:

$$\frac{d\beta}{2\pi}\,\frac{\left[1-|\epsilon_f(0)|^2\right]}{\left[1-|\epsilon_f(0)|\cos\beta\right]^2}\left\{1+\frac{|\epsilon_f(0)|\cos\beta}{\sqrt{1-[|\epsilon_f(0)|\cos\beta]^2}}\left[\frac{\pi}{2}+\arctan\frac{|\epsilon_f(0)|\cos\beta}{\sqrt{1+[|\epsilon_f(0)|\cos\beta]^2}}\right]\right\}$$

where arctan denotes the principal value of the angle lying between $-\pi/2$ and $+\pi/2$.

The probability distribution for the angle,

$$\bar{\Xi}(t) = \bar{\Theta}_g(t) - \bar{\Theta}_f(t) = \arg\{\epsilon_f(0)\}$$

which is of primary interest here is characterized by a symmetric probability density around $\beta(t) = 0$ so that $\arg\{\epsilon_f(0)\}$ is the median (50% point) as well as the modal value. The larger the value of $\operatorname{Mod}\{\epsilon_f(0)\} = |\epsilon_f(0)|$, the more concentrated near zero is the probability density of $\bar{\beta}(t)$; if $|\epsilon_f(0)| = 1.0$ the probability density is entirely concentrated there, while if $|\epsilon_f(0)| = 0$,

$\overline{\beta}(t)$ is equally likely to be found anywhere in the interval $-\pi$ to $+\pi$. The probability that $|\overline{\beta}(t)|$ is less than $\pi/2$ is always:

$$\frac{[1+|\rho_{fg}(0)|]}{2}$$

while the probability that $\overline{\beta}(t)$ is in either of the intervals $(0, \pm\pi/2)$ is

$$\frac{[1+|\rho_{fg}(0)|]}{4}.$$

These features of the dependence of distribution of the instantaneous phase difference upon the value of $\rho_{fg}(0)$ are illustrated in Figure 5.7, where the curves give the cumulative probability, Prob $\{\beta \le \delta\} = \text{Prob}\{\theta_g(t) - \theta_f(t) - \angle\rho_{fg}(0) \le \delta\}$ as a function of δ for various values of $|\rho_{fg}(0)|$. For positive δ, the scale on the left is to be used in conjunction with the lower scale, while for negative δ, the scale at the right is to be read against the upper scale. The curves may also be conveniently used to obtain Prob $\{|\beta| \le \delta\}$ for $\delta \ge 0$ by reading δ from the lower scale and subtracting the corresponding value on the right-hand scale from the corresponding value on the left-hand scale. It may be seen that a deviation of more than 15° from the mean will occur more than one-half of the time unless $|\rho_{fg}(0)|$ is at least approximately 0.9, while a deviation exceeding 3° from the mean will occur one-half the time when $|\rho_{fg}(0)| = 0.9981$. From the complex values of $\rho_{fg}(0)$ given later (Figure 5.9, the approximate probability of finding the instantaneous phase in any given interval between $-\pi + \text{Arg}\{\rho_{fg}(0)\}$ and $+\pi + \text{Arg}\{\rho_{fg}(0)\}$ may be ascertained from the curves in Figure 5.7 by interpolation for those ship and load motion pairs and environmental conditions treated in Figure 5.9, a.

A more graphic interpretation of the manner in which the instantaneous phase difference and the instantaneous amplitude are jointly distributed is the basis for Figure 5.8, which is also directly useful for interpreting the information presented in Figure 5.9. The former figure is based upon the representation of the standardized complex envelope ratio $\frac{e_g/\sqrt{\sigma_g}}{e_f/\sqrt{\sigma_f}}$ as the sum of two additive components, one of which is non-random and the other of which is proportional to the ratio of two complex-valued, zero mean, unit standard deviation, independently-distributed Gaussian random variables. The representation in question is

$$\frac{e_g/\sqrt{\sigma_g}}{e_f/\sqrt{\sigma_f}} = \rho_{fg}(0) + \left\{1 - |\rho_{fg}(0)|^2\right\}^{1/2} \frac{\eta_2}{\eta_1}$$

where $\eta_1 = \epsilon_{11} + i\epsilon_{12}$, $\eta_2 = \epsilon_{21} + i\epsilon_{22}$, and the four real-valued random variables ϵ_{11}, ϵ_{12}, ϵ_{21}, ϵ_{22} have zero means, unit standard deviations, and are independently distributed with Gaussian distributions. Setting $\Delta = \left\{1 - |\rho_{fg}(0)|^2\right\}^{1/2} \eta_2/\eta_1 = |\Delta| \exp\{i \text{Arg}\,\Delta\}$ it readily shown that Mod $\Delta = |\Delta|$ and Arg Δ are independently distributed. Moreover, Arg Δ has a uniform distribution with probability density $1/2\pi$ over the interval from $-\pi$ To $+\pi$, while the quantity $\Delta' = \frac{|\Delta|}{\left[1 - |\rho_{fg}(0)|^2\right]^{1/2}}$ has the probability density $\frac{2\Delta}{(1+\Delta^2)^2}$ for $\Delta' \ge 0$, and 0 otherwise. Thus Prob $\left\{\frac{|\Delta|}{\left[1-|\rho_{fg}(0)|^2\right]^{1/2}} \le \Delta_0\right\} = \frac{\Delta_0^2}{1+\Delta_0^2}$. It may be seen that the modal (most likely) value of β is $1/2\left\{1 - |\rho_{fg}(0)|^2\right\}^{1/2}$, its

median value is $\{1-|e_{\rho_{fg}}(0)|^2\}^{1/2}$, while the 25% and 75% points in its distribution are $\sqrt{1/3}\{1-|e_{\rho_{fg}}(0)|^2\}^{1/2}$ and $\sqrt{3}\{1-|e_{\rho_{fg}}(0)|^2\}^{1/2}$ respectively, the p-th percentile point being $\{p/(1-p)\}^{1/2}\{1-|e_{\rho_{fg}}(0)|^2\}^{1/2}$, the random variable Δ has no second moment and hence no standard deviation; the probability distribution of $\frac{|\Delta|}{\{1-|e_{\rho_{fg}}(0)|^2\}^{1/2}}$ and that of its reciprocal are identical.

Putting all of the facts above together gives the resulting synthesis shown in Figure 5.8, which shows a set of 30 sample values of $(e_f/\sigma_f)+(e_y/\sigma_y)$ for the same conditions as, and including, the ten samples shown in Figure 5.6. In the complex plane draw the unit circle centered at the origin with unit radius. Locate the point e_ρ in the complex plane. Draw the chord of the unit circle passing through e_ρ and perpendicular to the line joining e_ρ to the origin: the half length of this chord is $\{1-|e_\rho|^2\}^{1/2}$. About e_ρ as center describe circles whose radii are $\sqrt{1/3}$, 1, and $\sqrt{3}$ times $\{1-|e_\rho|^2\}^{1/2}$. These circles contain, respectively, 1/4, 1/2, and 3/4, of the probability density for the (two-dimensional) distribution of the random complex number $\Delta = (e_g/\sigma_g)+(e_f/\sigma_f)-e_\rho$. In general, within any circle of radius $\sqrt{p/(1-p)}$ times the length $\{1-|e_\rho|^2\}^{1/2}$ there will be the fraction, p, of the points constituting a large sample of values of Δ; the density of such points within such a circle and in a given direction from the point e_ρ is independent of the direction. From the distribution of Δ the distribution of $(e_g/\sigma_g)+(e_f/\sigma_f)$ is visualizable by the addition of the complex numbers Δ and e_ρ. Thus, one fourth of the probability density lies in any of the four quadrants defined by two mutually perpendicular lines through e_ρ, etc.

The most immediate inference from this set of facts describing the probability density for ρ and β is that the larger $|e_\rho|$, the smaller $\{1-|e_\rho|^2\}^{1/2}$ and hence the more confined the value of Δ to a small circle around e_ρ and the more confined the angle β to a small sector around Arg e_ρ. Moreover, since the rate of change of $\{1-|e_\rho|^2\}^{1/2}$ with $1-|e_\rho|$ is $|e_\rho|/\sqrt{1-|e_\rho|^2} = \sin\gamma$, where γ is the angle between the chord and the line segment joining the end of the chord to the nearest end point of the diameter of the unit circle passing through e_ρ. Consequently, since this angle becomes small as soon as $1-|e_\rho|$ becomes small, the increase in concentration of the probability distribution of β around Arg e_ρ becomes slower and slower as $|e_\rho|$ approaches unity. This fact reflects the choice of values of $|e_\rho|$ for the curves shown in Figure 5.7.

The matrix of small graphs making up Figures 5.9 and 5.9 (a) present the value of the complex number e_ρ, for all pairs from a selected set of thirteen essentially different time histories, including those of all the ship motions ($x, y, z, \phi, \theta, \psi$), the surface elevation (η), all center-lowered load displacement components (s_x, s_y, s_z), (recalling that $s_x = x$, $s_z = z$) and at least two cases for each of the three boom-lowered load displacement components (including those boom angles yielding minimum and maximum r.m.s. values). Note that $s_x^{0°,180°} = s_x = x$ and $s_y^{\pm 90°} = y$. The environmental conditions are those of Sea State Five and β = $\pm$180°, $\pm$135°, $\pm$90°, $\pm$45°, and 0°, making eight points per graph, each point having attached to it a finite-length ray extending, from the point, in the direction of the barge heading. For

example, for the pair (y, ϕ) and the barge heading $\beta_B = +90°$, the value shown for $e_{\rho_{y\phi}}$ is $-0.01748 + i(-0.6138) = 0.6140\, e^{-i(1.599)}$, so that $|e_{\rho_{y\phi}}| = 0.6140$ and Arg $e_{\rho_{y\phi}} = -1.599$. The expanded-scale example at the lower left shows the origin and scales for both coordinate axes, with two representative hypothetical plotted points, for one of these the appropriate chord is drawn together, with the 50% circle shown in Figure 5.8, having the chord as diameter.

An example of an application of Figures 5.9 (a) and 5.7 is shown in Figure 5.10, in which various percentile points and other information are presented for the distribution of the phase difference, $\theta_\phi - \theta_y$, as a function of the barge heading, β_B, relative to the predominant wind direction, for a State 5 sea. The mean-phase-shift curve has been plotted from values computed for Arg e_ρ at 15° increments. In addition to the mean (which is also the median, or 50% level, in the probability distribution), there are shown the 25% and 75% levels, as obtained from interpolation in Figure 5.7, using the values of Mod $e_\rho = |e_\rho|$ from Figure 5.9 (a) every 45°. The extreme (0% and 100%) limits of the distribution are also shown in order to make clear the range of definition of the random variable, $\theta_\phi - \theta_y$, viz. Arg e_ρ $\pm 180°$.

In addition to the percentile (quartile) points already noted, the angular interval between the two levels, Arg e_ρ $\pm 90°$, has been indicated for each of the nine barge headings by means of a pair of arrows, and the corresponding probability that the phase difference, $\theta_\phi - \theta_y$, falls therein, is shown as a number appearing below each such interval. The values of these probabilities lie between 0.766 and 0.839, a relatively narrow range, reflecting little change with barge heading in the dispersion of the distribution of instantaneous phase difference. It will be noted that the barge heading has relatively little effect upon the mean or the dispersion of the distribution of the instantaneous phase difference between roll and sway. The former varies only between approximately -65° (for the downwind barge heading) and -100° (for the upwind barge heading), while the inter-quartile range varies between the extreme values, 65° and 87°, approximately, for these same headings. These small ranges of variation in mean and dispersion over the entire range of barge headings are reflected in the cluster-type of plot for the values of e_ρ in Figure 5.9 (a) all points having relatively constant direction (Arg e_ρ) and distance ($|e_\rho|$) from the origin.

6. SUMMARY OF FINDINGS

The very nature of this study renders the results mathematically abstract and complex in form and, hence in the large, rather insusceptible to any concise verbal presentation -- especially in concrete physical terms. However, the figures at the end of this report comprise a very suitable vehicle for presenting such information and a perusal of them gives highly succinct knowledge of these results once the meaning of the quantities shown there is understood. This chapter , then, instead of relegating itself to a necessarily sparse and qualitative coverage of the obvious content of those figures -- a task already done in the three preceding chapters -- simply and most profitably refers the reader to the figures, and if necessary, to the definitions of the displayed quantities, thus freeing itself to categorize the results and provide at least a mention of some of their salient features.

The results can be thought of as falling into three main classes: 1) the response characteristics (viz. response operators) of the various motions of the barge system to the seaway, as contrasted with 2) the motions themselves (viz. the time-histories of their amplitudes and phases) in various conditions of the seaway, and finally 3) the inter-relationships between those motions. As before, the term "motion" is used to mean any of the following parameters: the six barge motions (e.g. surge), the load-lowering line tensions, load displacements and accelerations, and the restoring forces in the mooring cables. The results in the first class are deterministic, while those in the second are probabalistic, and thus have necessitated the use of the probability terminolgy defined earlier in this report.

A. Response Characteristics

The complex response operators (for each of the six ship motions) when considered as a function of barge heading relative to wind were found to be increasingly regular as wave length increases. At the longer wave lengths, both the amplitude and phase-shift curves assumed distinctive shapes for each of the ship motions, the phase curves having been particularly irregular at 100-foot and 200-foot wave lengths. As was expected, a singularity occurred at $\pm$ 90° headings for surge, pitch and yaw response, and at 0 and $\pm$ 180° headings for sway, roll and yaw, that singularity being a cusp of the curve at the zero response level. Maximum responses were found near the 0° heading for surge and pitch, near 90° for heave, sway and roll, and near 45° for yaw.

B. The Motions

The one single parameter best suited to convey the findings in this section is the root-mean-square (r. m. s.) value of a particular motion as a function of both sea state and barge heading. Except where indicated otherwise, sea state affects only the numerical values of various quantities and not their qualitative relationships or even relative magnitudes. Hence, what follows is true for all sea states considered in this study. The ship motions and consequently other motions considered, have their respective spectral energy densities as the fundamental quantity from which their r. m. s. values arise. Hence, a note on these densities is in order before we proceed to give the findings in r. m. s. terms for all the motions.

The spectral energy densities when plotted against the wave frequency were found to have two features worthy of mention here. First, the shapes of the curves were of a rather great variety, and second, the curves for the rotational ship motions, though reflecting the first feature, were consistently more "peaked" than the translational ones, indicating that the great part of the rotational motions was due to waves in a relatively narrow frequency interval. The heave spectrum, though it is not any narrower than its translational homologues was nonetheless more peaked than might be expected in view of heave's uniformly high response to the seaway for all barge headings.

i) Ship motions

The r. m. s. value of all six ship motions, when plotted against barge heading, proved highly regular and, in the main, consistent with physical intuition. Thus, sway, heave, roll and yaw have relative maxima for beam headings and minima for head or following seas, while the opposite holds true for surge and pitch. As expected, heave and sway, in that order, had considerably higher r. m. s. values than surge, particularly so at their maxima. Among the rotational motions, roll showed outstandingly higher values than pitch or yaw, the latter being very low for all headings.

ii) Load displacements and line tensions

For the simple case of a center-lowered load, it was found that the y and z components of load displacement are very alike in their r. m. s. values as a function of barge heading. Both of the components are much higher than the remaining one for x, and have maxima at beam-sea headings. Thus, the corresponding added-dynamic line tension has its maxima, also, in beam seas.

For the case of a boom-lowered load, such a profusion of numerical results is available, due to the quite numerous individual boom orientations considered, that rather than discuss all of them in their individual aspects, only the maximizing and minimizing conditions are considered here.

It was found that the boom azimuth angle which minimized the r.m.s. values of any given displacement component or the line tension was, in general, quite independent of barge heading and sea state, and thus unique to the motion, rather than to the conditions in the seaway. Specifically, this optimum boom angle is 0° or 180° for the x-component, ± 90° for the y, and 180° for both the z-component and the tension (or equivalently, the vertical load acceleration), these two motions being quite similarly affected by boom orientation. An exception to this independence phenomenon occurs for the z-component and the load acceleration. For these two motions, the optimum boom angle shifts by 15° or 20° for barge headings near 0° in Sea States 4 and 5.

The "worst" (i.e. maximizing rather than minimizing) boom angle has similar independence. In one case, however, its sign reverses as the barge heading goes through 0°. A noteworthy feature of worst boom angles is that in combination with imprudent headings they can induce load accelerations as large as 10 ft./sec^2 in a State 5 sea.

iii) Mooring Forces

The total horizontal mooring forces and yawing moment induced on the barge have r.m.s. values which are directly proportional to their counterparts for surge, sway and yaw. The forces in each of the four mooring cables, on the other hand, are not so simply related to these horizontal ship motions. The plots of their r.m.s. values indicate small, but definite, differences from cable to cable, though all four have maxima near crosswind and minima near up- or downwind barge headings.

C. Motion Inter-Relationships

Whereas, to this point, consideration has been given only to results characterizing single motions, this section treats the quantities which describe the inter-relationships between given pairs of motions. These inter-relationships find their most useful and complete expression in the cross-spectral functions. Despite their less frequent employment and less obvious interpretation, these cross-spectra show many relatively close, but unfamiliar, analogies with the energy spectra. Their calculation provides a convenient and direct means of obtaining the relatively simple statistical parameters of interest here and may be considered basic to all. The comprehensive application of cross-spectra to the present problem and the consequent developments and interpretations represent the possible original theoretical work in this phase of study. Therefore, the discussion here is more oriented toward analytical developments than toward the summary of the results of their subsequent application.

With any specified pair of motions there is associated a cross-spectrum whose normalized zero-order moment may be interpreted as a complex cross-correlation coefficient for that pair. This coefficient completely specifies the probability distribution for the complex instantaneous gain, which is comprised of the phase-difference and the amplitude-ratio. Of these, the phase-difference is of primary interest here.

Notably, the mean value of the instantaneous phase difference is simply the argument of the cross-correlation coefficient, whereas the modulus of that coefficient determines the "shape" of the distribution. This coefficient was calculated as a function of barge heading for each pair possible from a set of thirteen particularly significant motions, and the results for a high sea state are shown among the final figures. In general, these distributions show relatively little tendency to concentrate about their means. A geometrical construction yielding certain parameters of the phase distribution was employed as an aid to the interpretation of these quantities. Also, random samples of pairs of motions, showing both instantaneous phase and amplitude at a particular time, were calculated on the basis of the complex cross correlation coefficient, by employing a set of random numbers. The resulting sample was shown graphically.

7. CONCLUSIONS

From the results and examples concerning the load-lowering operation, two conclusions are evident. First, motions having amplitudes of oscillation or giving rise to forces and accelerations sufficiently high to influence construction operations may occur under certain of the environmental conditions considered in this study -- particularly when loads are lowered by means of a boom in a high sea state. Second, the violence of these motions, forces, or accelerations may be significantly reduced by the proper choice of barge heading relative to the wind and boom azimuth angle. The latter, regardless of the sea state, has considerably the greater effect in minimizing the energy of fluctuation in the tension of the lowering line, the vertical acceleration of the load, and its three displacement components. These facts appear to provide useful information for the conducting of operations from a moored barge platform.

More specific results furnishing information useful as a guide to the operator of a construction barge during its lowering operations are available for various situations of interest and can be summarized in graphical form.

The theory employed in this study appears adequate in the sense that the results obtained here agree, in general, with what would be expected of such a vessel under such conditions. The present study supplements what may be known qualitatively in these cases by furnishing quantitative estimates for the motions and their interrelationships. The validity of these results is subject to test, although in a natural seaway the interpretation of experimental data will require sufficiently adequate techniques of analysis.

Finally, it proves feasible to treat all six degrees of freedom of a moored barge in a realistic seaway and obtain results in addition to the solutions for response characteristics, namely the amplitude and phase information for various motions of the barge and the associated load.

8. RECOMMENDATIONS

As a result of the performance of the present study, certain recommendations appear to be in order. The discussion here will treat these in categories corresponding to the following considerations concerning the results obtained: their usefulness, their extensiveness, their validity. These questions lead to recommendations for making applications, the conduct of further studies of similiar nature, and the performance of tests.

The present study resulted in such a profusion of numerical results, that more extensive work in examining them and finding interpretations suitablefor engineering use is recommended if fairly complete answers to the questions of concern are to be given. Questions which require answering here are those of identifying those characteristics and parameters implicit in the presently-available numerical results which are of maximum interest and immediate concern. Such answers would be of value in meeting the problem of selecting and supplying directly-useful information from the basic computed results.

It is felt that both theoretical and experimental programs will be needed for verification of prediction techniques for extension to other situations. The experimental programs involve both model tests and full-scale studies of data analysis. Since the theoretical phase is the most logical continuation of the present theoretical study, and since there is primarily only one aspect of theoretical studies contemplated, while the experimental phase is of much larger scope, the theoretical program recommendation is included first in this listing.

A recommended program will be further theoretical analysis with other types of mooring restraints, wherein nonlinear effects will be considered to be present in the mooring representation. Similarly, certain nonlinearities of hydrodynamic nature may also be included, depending upon the expected degree of importance. The appropriate data on the nonlinear characteristics of the moorings are considered to be supplied (from data) for different situations as functions of initial tension.

Studies have been made in the past, such as that of Abramson and Wilson, of motions in one degree of freedom with a simple nonlinear mooring characteristic, and responses to regular waves were obtained. These results show the influences of different degrees of nonlinearity, assuming that regular waves were present. However, the important information one needs will be spectral information for the case of random waves which are more representative of actual sea conditions. This can be achieve by an extension of the techniques of equivalent linearization to random functions; and hence, a generalization of the results of Abramson and Wilson, for example, for application to prediction of behavior in realistic sea

conditions, will then be available.

This type of analysis should be made for the coupled motion of the ship with six degrees of freedom and can be carried out without the use of analog computer simulations as a basic tool. Checks on the responses of the system to irregular forcing functions, by use of the analog computer, can be made at the conclusion of the analytical study. Such a program is a natural extension of the linear techniques of St. Denis and Pierson, and would be of interest in pointing out the relative influence of nonlinearities on motions of moored ships (and hence, on the variables associated with raising and lowering loads from such a ship).

Future experimental studies would include as the first possible test of the results of the present study a study involving model tests of the motions of a particular ship, such as CUSS I, which is restrained by moorings. An attempt should be made to have the mooring restraints scaled dynamically as best possible, in order to simulate the actual system behavior. The tests should be made in oblique waves, both regular and irregular, under all headings of interest, so that characteristics are obtained under controlled conditions. Analysis of the data in this program allows direct comparison with the results of the linear theory of the present study.

Full-scale measurements should be made at sea which include accelerometers and gyros for recording the motions, pressure transducers, and devices such as "Splashniks" for obtaining the wave records. It is essential that the sea conditions be known for the environmental basis of the recorded motions, thereby allowing direct correlation with analytical results. During these tests, it will also be necessary to measure the tensions in the mooring cables, in order to check the restraining effect, and the danger of breaking, etc., since the system is under an initial tension that is fairly high. Nonlinear effects may occur and the measurements of the mooring restraints are a better indication of the limits that are experienced as compared to the linear predictions.

From the measurements of the tensions in the mooring cables, some information can also be obtained on the cable fatigue loading and possible limitations in useful life under the strains imposed by different sea states. Appropriate analysis of the irregular records obtained in this study should be made on the basis of spectral theory in order to assess the fatigue characteristics. Similar studies have been made for airplane wings under gust loadings and also for the fatigue history due to jet engine effects, so that similar extensions to the present problem are definitely feasible.

At the same time, measurements should be made of the tension in the lowering lines for the different sea conditions, and these results can be compared and correlated with the motion information since the tension in the lines is related to the effective vertical accelerations. Similarly , it is necessary to

measure the load accelerations by placing accelerometers on the load and transmitting back the information along thin electric leads along the lines. This information will also be related to the body motions since the accelerations are related kinematically to the body motions in the analysis. The lowering-line displacements are related kinematically to the motions, and thus are directly correlated. In all of the general predictions of the tension and accelerations, the elastic effects of the lowering lines are neglected and only dynamic influences due to motions are directly considered. Some measure of the influences of the elasticity can possibly be obtained from such comparisons.

The above program is considered a logical continuation of the present study, and should serve to provide direct data for correlating the analytical results obtained from the present study with actual data obtained at sea. The direct results of this correlation will serve to verify the degree of precision in predicting such motions by use of the theory developed in the present study.

Further applications of the results of this study would include the utilization of the theoretical concepts and techniques developed and computer-programmed for the calculation of additional parameters supplementing these obtained for the CUSS I, for the calculation of similar numerical results for other vessels of interest, and for the numerical investigation of the effect of altering the values of the parameters used in the present study, e.g., those for the mooring system, the length of the boom, and the state of the sea. The effect of less restrictive assumptions on the functional form of the directional wave spectrum may be investigated by means of minor modifications of the present computer program, with a small number of machine runs. If well enough known, the intraction between the wave spectrum and vessel response operators, would yield information about seaways containing narrow-ban swells arising from distant areas of wave generation.

The validity of the present results must be examined in the light of the adequacy of the theory chosen to represent the response of the vessel to sinusoidal waves, the validity of the assumptions regarding the environments, and the adequacy of the numerical analysis employed for the solutions. Regarding the latter, it appears appropriate only to recommend that the determination of the vessel response operators be made for a set of wave lengths sufficiently comprehensive to provide adequate accuracy for the required numerical integrations.

In regard to the environmental conditions, the linearity of the flow field surrounding the vessel and its stationary nature in the probabilitistic sense appears to be a crucial point for obtaining and interpreting numerical results. The assumptions of the closely-related Gaussian character of the seaway is fundamental for the type of interpretation presently being given these results. Comprehensive tests would not appear to be feasible for these assumptions.

As for the determinations of the response operators for the vessel, the use of slender-body theory employed, the consequences of the linearization of the differential equation for individual sinusoidal waves, and the use of the assumption of superposition of effects over waves of differing frequencies have already been pointed out.

Suggested steps toward experimental verification of the theoretical results presented here consist of the following: (1) Model tests in unidirectional sinusoidal waves and in unidirectional non-sinusoidal waves of known characteristics, with a subsequent comparison of the results of a cross-spectrum analysis of surface elevation and motion time histories obtained in the latter case with the response operators obtained in the former. (2) Model or full-scale tests in non-unidirectional waves, of known characteristics, if possible. The results of cross-spectral analysis of the data will then provide the basis for inferences regarding the response operators for the vessel; two techniques are available for use here. One leads to the construction of numerical estimates of the response operators, the accuracy of the estimates depending upon the number and the placement of auxiliary recorders in the flow field. The other allows certain sets of hypotheses specifying the response operators to be tested for consistency with the data.

REFERENCES
(in order of first appearance of subject matter)

Chapter 1

1. St. Denis, M. and Pierson, W. J.: "On the Motions of Ships in Confused Seas", Trans. SNAME, 1953.

2. Korvin-Kroukovsky, B. V. and Jacobs, W. R.: "Pitching and Heaving Motions of a Ship in Regular Waves", Trans. SNAME, 1957.

3. Vossers, G.: "Fundamentals of the Behavior of Ships in Waves", Int. Shipbuilding Prog., 1959, 1960.

4. Kaplan, P.: "Application of Slender Body Theory to the Forces Acting on Submerged Bodies and Surface Ships in Regular Waves", Journal of Ship Research, November 1957.

5. Kaplan, P. and Hu, P. N.: "Virtual Mass and Slender Body Theory for Bodies in Waves", Proc. of Sixth Midwestern Conf. on Fluid and Solid Mechanics, Univ. of Texas, September 1959.

6. Pierson, W. J., Neumann, G. and James, R. W.: "Practical Methods for Observing and Forecasting Ocean Waves by Means of Wave Spectra and Statistics", U.S. Navy Hydrographic Office Pub. No. 603, 1954.

7. Taggart, R.: "Positioning the Drilling Ship Over the MOHO", paper presented before Chesapeake Section SNAME, Washington, D. C., February 2, 1961.

8. Grim, O.: "Rollschwingungen, Stabilitat und Sicherkeit im Seegang", Schiffstechnik, 1952.

9. Suyehiro, K.: "Yawing of Ships Caused by Oscillation Among Waves", Trans. INA, vol. 62, 1920.

10. Wold, Herman and Jureen, Lars: "Demand Analysis", John Wiley & Sons, 1953.

11. Lee, Y. W.: "Statistical Theory of Communication", John Wiley & Sons, 1960.

12. Putz, Robert R.: "Three Techniques for Measuring Flow Velocity in the Ocean Compared by the Convolution Method", Marine Advisers, Inc. Technical Report prepared for Westinghouse Electric Corporation, September 1961.

13. Cote, Louis J.: "Short Time Prediction of Sea Surface Height: Prediction of a Degenerate Stochastic Process", Proc. of First Conf. on Ships and Waves, 1955, pp. 73-77.

14. Rosenblatt, Murray: "Estimation of the Cross Spectra of Stationary Vector Processes", New York University Engineering Statistics Group, Tech. Rpt. 2, Nonr 285(17), January 1955.

15. Goodman, N. R.: "On the Joint Estimation of the Spectra, Cospectrum and Quadrature Spectrum of a Two-Dimensional Stationary Gaussian Process", New York University Engineering Statistics Laboratory, Tech. Rpt. 8, Nonr 285(17), March 1957.

16. Doob, J. L.: "Stochastic Processes", John Wiley & Sons, 1953.

17. Bartlett, M. S.: "An Introduction to Stochastic Processes", Cambridge University Press, 1960.

18. Grenander, Ulf and Rosenblatt, Murray: "Statistical Analysis of Stationary Time Series", John Wiley & Sons, 1957.

19. Kendall, Maurice G.: "The Advanced Theory of Statistics", vols. I and II, Charles Griffin & Co., 1945.

20. Grenander, Ulf and Szego, Gabor: "Toeplitz Forms and Their Applications", California Monographs in Mathematical Sciences, 1958.

21. Tick, Leo J.: "Certain Probabilities Associated with Bow Submergence and Ship Slamming in Irregular Seas", New York University Engineering Statistics Group Tech. Rpt. 1, Nonr 285(17), December 1954.

22. "Symposium on Applications of Autocorrelation Analysis to Physical Problems", Selected papers from symposium at Woods Hole, Mass., 13-14 June 1949, Office of Naval Research Publication.

23. James H. M., Nichols, N. B. and Phillips, R. S.: "Theory of Servomechanisms", McGraw-Hill, 1947.

24. Lawson, James L. and Uhlenbeck, George E.: "Threshold Signals", McGraw-Hill, 1950.

25. Davenport, Wilbur B., Jr. and Root, William L.: "An Introduction to the Theory of Random Signals and Noise", McGraw-Hill, 1958.

26. Bendat, Julius S.: "Principles and Applications of Random Noise Theory", John Wiley & Sons, 1958.

27. Goldman, Stanford: "Information Theory", Prentice-Hall, 1953.

28. Rice, S. O.: "Mathematical Analysis of Random Noise", Selected papers on Noise and Stochastic Processes (ed. Nelson Wax), Dover Publications, 1954.

29. Neumann, Gerhard and Pierson, Willard J., Jr.: "A Detailed Comparison of Theoretical Wave Spectra and Wave Forecasting Methods", Reprint from Deutschen Hydrographischen Zeitschrift, vol. 10, No. 3, 1957.

30. Munk, W. H., Snodgrass, F. E. and Tucker, M. J.: "Spectra of Low-Frequency Ocean Waves", Bulletin of the Scripps Institution of Oceanography, vol. 7, No. 4, October 1959, pp. 283-362.

31. Longuet-Higgins, M.S.: "On the Statistical Distribution of the Heights of Sea Waves", Sears Foundation: Journal of Marine Research, vol. XI, No. 3, December 31, 1952, pp. 245-266.

32. Rudnick, Philip: "Correlograms for Pacific Ocean Waves", Proc. of Second Berkeley Symp. on Math. Statistics and Probability, 1951, pp. 627-638.

33. Cartwright, D. E. and Longuet-Higgins, M. S.: "The Statistical Distribution of the Maxima of a Random Function", Proc. Royal Society, vol. 237, 1956, pp. 212-232.

34. Snodgrass, F. E. and Putz, R. R.: "Direct Reading Wave Meter", University of California Institute of Engineering Research Tech. Rpt. Ser. 3, No. 371, June 1954.

35. Wold, Herman: "Random Normal Deviates", Tracts for Computers No. XXV, Cambridge University Press, 1948.

36. Blackman, R. B. and Tukey, J. W.: "The Measurement of Power Spectra", Dover Publications, 1958.

Chapter 2

1. Pierson, W. J., Jr.: "A Unified Mathematical Theory for the Analysis, Propagation, and Refraction of Storm-Generated Ocean Surface Waves", New York University, 1952.

2. Hald, A.: "Statistical Theory with Engineering Applications", John Wiley & Sons, 1952.

3. Arley, Niels and Buch, K. Rander: "Introduction to the Theory of Probability and Statistics", John Wiley & Sons, 1950.

4. Cramer, H.: "Mathematical Methods of Statistics", Princeton University Press, 1946.

5. Munroe, M. E.: "Theory of Probability", McGraw-Hill, 1951.

6. Mood, Alexander McFarlane: "Introduction to the Theory of Statistics", McGraw-Hill, 1950.

7. Weatherburn, C. E.: "A First Course in Mathematical Statistics", Cambridge University Press, 1946.

8. Hoel, Paul G.: "Introduction to Mathematical Statistics", John Wiley & Sons, 1947.

9. Kenney, J. F. and Keeping, E. S.: "Mathematics of Statistics", parts I and II, D. Van Nostrand, 1951 (2nd ed.)

10. Snodgrass, Frank E. and Putz, Robert R.: "A Wave Height and Frequency Meter", Proc. of Sixth Conf. on Coastal Engineering, 1958, pp. 209-224.

11. Gullemin, Ernst A.: "The Mathematics of Circuit Analysis", John Wiley & Sons, 1949.

12. Lamb, Sir Horace: "Hydrodynamics", Dover Publications, 1945.

13. Milne-Thompson, L. M.: "Theoretical Hydrodynamics", Macmillan, 1949.

14. Coulson, C. A.: "Waves", Oliver & Boyd, 1947.

15. Wooding, R. A.: "An Approximate Joint Probability Distribution for Wave Amplitude and Frequency in Random Noise", New Zealand Journal of Science and Technology, vol. 36, No. 6, May 1955, pp. 537-544.

16. Titchmarsh, E. C.; "Introduction to the Theory of Fourier Integrals", Oxford University Press, 1948 (2nd ed.).

17. Putz, Robert R.: "Measurement and Analysis of Ocean Waves", Proc. of First Conf. on Ships and Waves, 1955, pp. 63-72.

18. Putz, Robert R.: "Prediction of Wave Motion", Proc. of First Conf. on Ships and Waves, 1955, pp. 33-54.

19. Goldman, Stanford: "Frequency Analysis, Modulation and Noise", McGraw-Hill, 1948.

20. Putz, Robert R.: "Comparison of the Performance of Two Flowmeters in Ocean Waves", Marine Advisers, Inc. Technical Report prepared for Westinghouse Ordnance Department, November 1961.

21. Putz, Robert R.: "Statistical Analysis of Wave Records", Proc. of Fourth Conf. on Coastal Engineering, 1954, pp. 13-24.

22. Korvin-Kroukovsky, B. V.: "Ship Motions in Irregular Sea", Second Draft for Sect. 2 of Chap. III Ships at Sea, Stevens Institute of Technology Experimental Towing Tank, July 1958.

23. Putz, Robert R.: "A Relay-Operated Device for the Measurement of Distribution and Correlation Functions", University of California Institute of Engineering Research Tech. Rpt. Ser. 61, No. 12, June 1957.

24. Putz, Robert R.: "A Method for the Measurement of the Correlation Function and Ordinate Distributions for Two Time-History Functions", University of California Institute of Engineering Research Tech. Rpt. Ser. 61, No. 11, January 1957.

25. Putz, Robert R.: "Ocean Wave Record Analysis -- Ordinate Distribution and Wave Heights", University of California Institute of Engineering Research Tech. Rpt. Ser. 3, No. 351, May 1953.

26. Putz, Robert R.: "Statistical Analysis of Ocean Waves", University of California Institute of Engineering Research Tech. Rpt. Ser. 3, No. 360, January 1954.

Chapter 3

1. Wooding, R. A.: "An Approximate Joint Probability Distribution for Wave Amplitude and Frequency in Random Noise", New Zealand Journal of Science and Technology, vol. 36, No. 6, May 1955, pp. 537-544.

Chapter 4

1. Putz, Robert R.: "Three Techniques for Measuring Flow Velocity in the Ocean Compared by the Convolution Method", Marine Advisers, Inc. Technical Report prepared for Westinghouse Electric Corporation, September 1961.

APPENDIX

A. Derivation of Equations of Motion

The equations of motion of the moored barge are derived on the basis of linear theory, with the body allowed to have six degrees of freedom. A right-hand cartesian coordinate system is chosen with the axes fixed in the body, and with the origin at the center of gravity of the body. The x-axis is chosen positive toward the bow, the y-axis is positive to port, and the z-axis is positive upward. These axes are defined to have a fixed orientation, i.e. they do not rotate with the body, but they can translate with the body. The body angular motions can be considered to be small oscillations about a mean position given by the axes. This system of axes is considered most suitable for studies of ship motion in waves (see Reference 1), and has been used in many of the studies of that subject (i.e. see Reference 2). The dynamic variables are the linear displacements x, y, and z along the respective axes, and the angular displacements ϕ , θ and ψ which are defined as positive in a direction of positive rotation about the x, y, and z axes, respectively, (i.e. port upward, bow downward and bow portward). The positive directions of the forces and moments acting on the body are similarly defined.

The equations are formulated by the balance of inertial, damping, restoring, exciting and coupling forces and moments. Both hydrodynamic and hydrostatic fluid effects, together with body inertia and mooring influences, are included in the analysis. The barge is assumed to be moored in a currentless, windless ocean, with both bow and stern moorings of conventional line and anchor type. By definition, there is no forward speed of the system, and all motions result from disturbances imposed by the sea. Since linear theory is used, there will be no coupling between the variables in the two planes of motion (longitudinal, i.e. heave, pitch and surge, and lateral, i.e. sway, yaw and roll). The longitudinal motions will be coupled to each other, and similarly the lateral equations will also be coupled. The nature of the couplings will be determined in the course of the analysis.

The fundamental analytical tool in carrying out the theoretical studies herein is slender-body theory. Essentially, this theory makes the assumption that, for an elongated body where a transverse dimension is small compared to its length, the flow at any cross-section is independent of the flow at any other section and, hence, the flow problem is reduced to a two-dimensional problem in the transverse plane. The forces at each section are found by this method, and the total force is found by integrating over the length of the body. A description of the application of slender-body theory to calculate the forces acting on submerged bodies and surface ships in waves is presented in Reference 3, where simplified interpretations of

force evaluation in terms of fluid momentum are also given. Extensive use of these results will be made in the following sections, where detailed derivations of the different components of force will be presented.

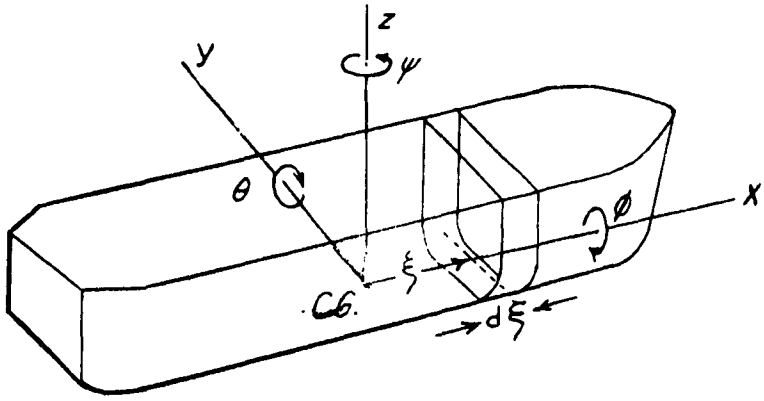

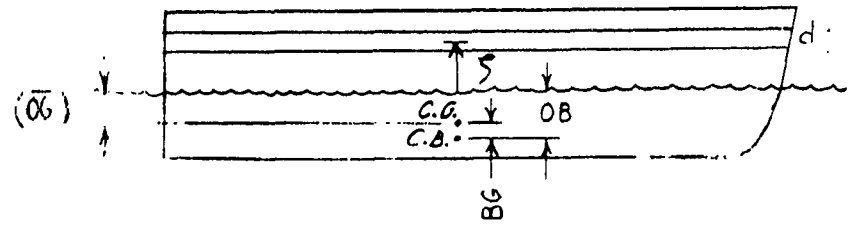

For the presentations of the following sections, the force (or moment) acting on the body is composed of the force due to dynamic body motions (denoted as F_{bm}), the force due to damping (denoted as F_d), the force due to hydrostatic restoring action (denoted as F_h), the force due to the moorings (denoted as F_m), and the force due to waves (denoted as F_w). The equations of motion are then established as

$$m\ddot{s} = F = F_{bm} + F_d + F_h + F_m + F_w \qquad (A-1)$$

for rectilinear motions (with s representing any rectilinear displacement, and m the mass of the barge), with similar representations for the angular motions.

B. Dynamic Forces and Moments Due to Motions

The hydrodynamic forces and moments considered in this section are of inertial nature, and do not contain any terms of dissipative nature. The effect of the free surface is accounted for by different frequency-dependent factors that modify the added masses of each section. All couplings of inertial nature are exhibited in the results of the analysis. In

the case of dynamic body motions, the simplified result of slender-body theory states that the local force on any section is equal to the negative time rate of change of fluid momentum (Reference 3). For the vertical force (z-force), this is expressed by

$$\frac{dZ_{bm}}{d\xi} = -\frac{D}{Dt}\left[A'_{33}\, w_b\right] , \qquad \text{(B-1)}$$

where A'_{33} is the added mass of the cross-section and w_b is the body vertical velocity, given by

$$w_b = \frac{D}{Dt}(z - \xi\theta) = \dot{z} - \xi\dot{\theta} . \qquad \text{(B-2)}$$

In the above equations, the coordinate ξ is a "dummy" variable along the longitudinal coordinate x (and coincident with it), and the time derivative $\frac{D}{Dt}$ is just the partial derivative $\frac{\partial}{\partial t}$, since there is no forward speed. The quantity A'_{33} is the added mass of the cross-section, including free-surface effects. Recent work by Grim (Reference 4) resulted in charts of the coefficient C, which is related to A'_{33} by

$$A'_{33} = C\,\frac{\rho\pi B^{*2}}{8} \qquad \text{(B-3)}$$

for the class of sections known as Lewis forms (Reference 5), where B* is the local section beam. The values of C are presented as a function of the dimensionless frequency parameter $\frac{\omega^2 B^*}{2g} = \frac{\pi B^*}{\lambda}$ (for the present case of zero forward speed), for different values of beam-draft ratio and section coefficient. Carrying out the operations specified in Equation (B-1), the local vertical force is expressed as

$$\frac{dZ_{bm}}{d\xi} = -A'_{33}\left(\ddot{z} - \xi\ddot{\theta}\right) . \qquad \text{(B-4)}$$

In a similar manner, the lateral force (along y-direction) may also be expressed by use of this same procedure, but certain additional factors enter in that case. These factors are the necessity of including roll effects which influence the lateral velocity, and also the fact that the representation of the lateral force is based upon added mass terms that are evaluated for motions relative to the free surface level, rather than the body center of gravity position. Corrections to refer the final forces to the center of gravity position are made after finding the forces referred to the free-surface position.

For the case of lateral motions, the total displacement is $(y+\xi\psi-\zeta\phi)$, where ζ is a "dummy" variable parallel to the z-axis, with its origin at the free surface level and measured positively upward (in the present case of a ship section lying below the free surface, the values of ζ are negative). The lateral body velocity is then

$$v_b = \frac{D}{Dt}(y+\xi\psi-\zeta\phi) = \dot{y}+\xi\dot{\psi}-\zeta\dot{\phi} \quad , \tag{B-5}$$

and the lateral force (referred to in the free surface level) is given by

$$\begin{aligned}\frac{dY_{obm}}{d\xi} &= -\frac{D}{Dt}\left[A'_{22}(\dot{y}+\xi\dot{\psi}-\zeta\dot{\phi}\right] \\ &= -A'_{22}(\ddot{y}+\xi\ddot{\psi})+A_{22}\zeta\ddot{\phi} \quad ,\end{aligned} \tag{B-6}$$

where A'_{22} is the section added mass for lateral motion. From previous work on submerged bodies (Reference 6), together with knowledge of the structure of the general added-mass tensor, it is known that the roll term in Equation (B-6) should be represented differently. This other representation is the replacement of $A'_{22}\zeta$ by $-A'_{42}$, which is a proper accounting for the influence of roll on lateral force (from inertial considerations) from basic principles, and thus eliminates the requirement of determining an average value of ζ in the total force evaluation by such intuitive "strip" methods. The lateral force is then given by

$$\frac{dY_{obm}}{d\xi} = -A'_{22}(\ddot{y}+\xi\ddot{\psi})-A'_{42}\ddot{\phi} \quad . \tag{B-7}$$

The added-mass coefficient A'_{22} for lateral motion is determined by a composite method, making use of values appropriate for zero frequency (added mass for lateral motion is equal to one-half of the total added mass of the reflected body, about the free surface, for zero frequency) and then modifying by a frequency-dependent function. The value of A'_{22} is represented by

$$A'_{22} = \rho Sk_y k'_4 \quad , \tag{B-8}$$

where ρSk_y is the added mass for zero frequency, and k'_4 is a frequency correction factor. The value of Sk_y is defined by

$$Sk_y = C'_z \frac{\pi H^2}{2} \quad , \tag{B-9}$$

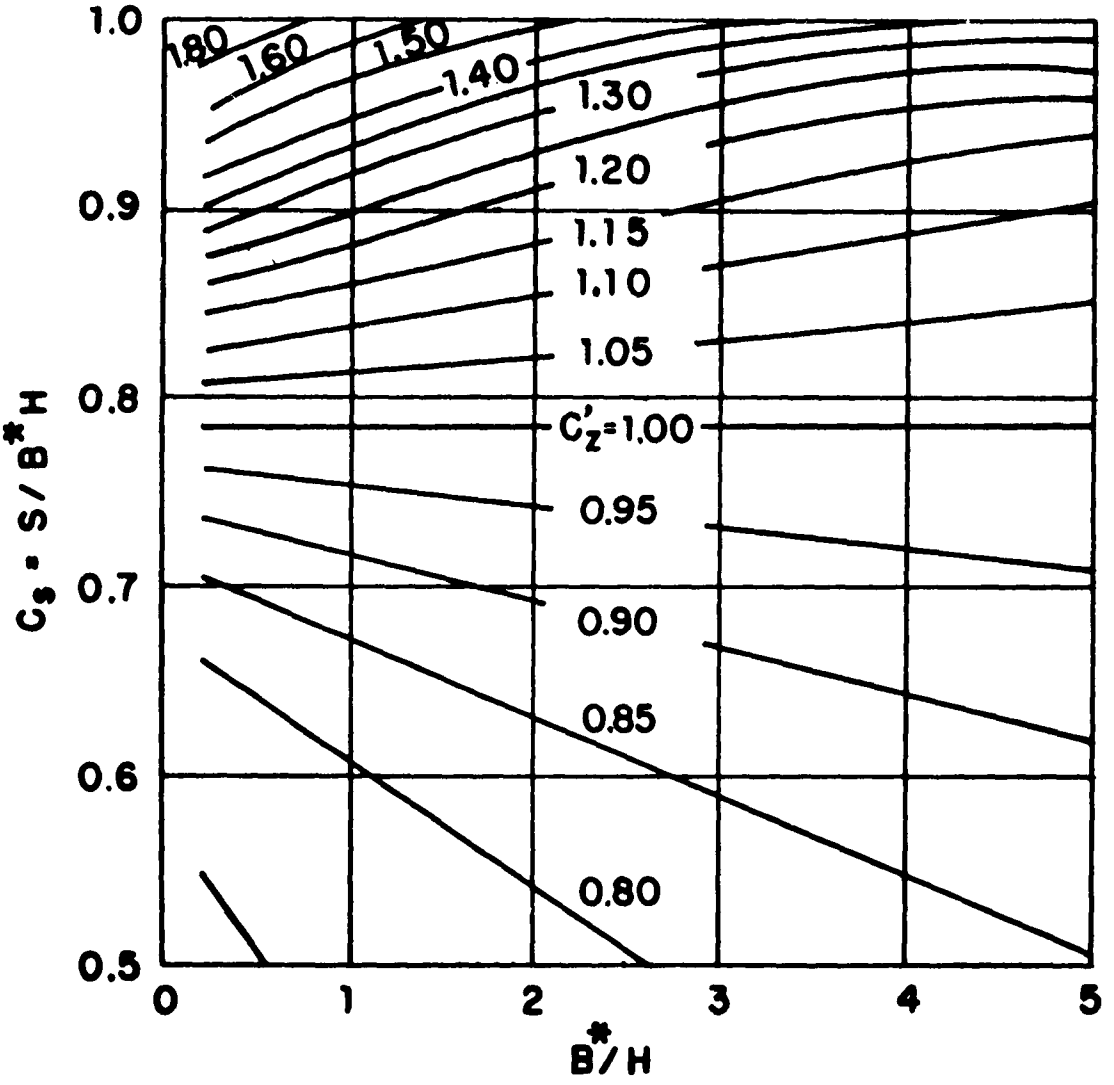

Sectional inertia coefficients C'_z as functions of the B/H ratio and section coefficient C_s. From Prohaska.

where H is the local section draft and C'_z is a factor taken from Prohaska's charts (Reference 7). The value of C'_z is found for an effective beam-draft ratio appropriate for lateral motion, which is obtained by "turning" the picture of the ship section by 90°, interpreting the effective beam-draft ratio as $\frac{4H}{B}$ for use on these charts. For given section coefficient and effective beam-draft ratio, the value of C'_z (originally derived for vertical motions at infinite frequency) is found on the chart and used in Equation (B-9). The frequency correction factor k_4 was derived in previous work as an approximation based on energy considerations, and was used in analysis of lateral bending moments in waves (Reference 8). While the form of this correction may not be precisely applicable to many different ship sections, and its frequency variation also may not be correct over the entire frequency range of interest, its use is recommended on the basis of lack of further precise information and its successful application in the previous study in Reference 8. This factor is given by

$$k'_4 = 1 - \frac{2}{\pi}\frac{w^2 H}{g} = 1 - \frac{4H}{\lambda} \qquad \text{(B-10)}$$

The value of the added mass term A'_{42} is derived in Reference 9 for the Lewis-form sections, and a graph as a function of the parameters, beam-draft ratio and section coefficient, is presented therein. Further computations were necessary in order to enlarge the range of parameters covered in that graph, because of the larger values of beam-draft ratio for the present barge. These values of A'_{42} were evaluated relative to the free surface level, and they are appropriate to the case of zero frequency. No frequency correction was used for that case, although a first order term in $\frac{w^2 H}{g} = \frac{2\pi H}{\lambda}$ was presented there. This was done for reasons of simplicity and ease of calculation, as well as an expectation of small influence for such frequency dependence.

The roll moment, relative to the free surface level, is represented in a similar manner by slender-body theory, using the added mass term A'_{42}, which is the "off-diagonal" term in the added-mass tensor which accounts for roll effects due to lateral motions. The form of this roll moment is

$$\frac{dK_{obm}}{d\xi} = -\frac{D}{Dt}\left[A'_{42}(\dot{y} + \dot{\psi} - \xi\dot{\phi}\right] \qquad \text{(B-11)}$$
$$= -A'_{42}(\ddot{y} + \xi\ddot{\psi}) + A'_{42}\xi\ddot{\phi} \ ,$$

and this is further modified to

$$\frac{dK_{o_{bm}}}{d\xi} = -A'_{42}(\ddot{y} + \xi\ddot{\psi}) - A_{44}\ddot{\phi} \quad , \tag{B-12}$$

where A'_{44} is the added moment of inertia in roll, in view of the known inertial reaction in roll, as well as a correction of the oversimplification arising from the strip method (as in the case leading to Equation (B-7). No discussion of theoretical means of evaluating the added inertia in roll is given here, since this term will be combined with the body roll moment of inertia to give the total effective roll moment of inertia. The value of that quantity will be determined from information on the natural roll period, metacentric height, etc. at a later stage in the study.

The values of the pitch moment and yaw moment easily follow from the representations of vertical and lateral forces, and they are given by

$$\frac{dM_{bm}}{d\xi} = -\xi\frac{dZ_{bm}}{d\xi} \tag{B-13}$$

and

$$\frac{dN_{o_{bm}}}{d\xi} = \xi\frac{dY_{o_{bm}}}{d\xi} \quad . \tag{B-14}$$

The total forces and moments acting on the body due to the dynamic body motions are obtained by integrating over the body length, leading to

$$Z_{bm} = -\int_{\xi_s}^{\xi_b} A'_{33}\,d\xi \cdot \ddot{z} + \int_{\xi_s}^{\xi_b} A'_{33}\,\xi\,d\xi \cdot \ddot{\theta} \quad , \tag{B-15}$$

$$Y_{o_{bm}} = -\int_{\xi_s}^{\xi_b} A'_{22}\,d\xi \cdot \ddot{y} - \int_{\xi_s}^{\xi_b} A'_{22}\,\xi\,d\xi \cdot \ddot{\psi} - \int_{\xi_s}^{\xi_b} A'_{42}\,d\xi \cdot \ddot{\phi}, \tag{B-16}$$

$$K_{o_{bm}} = -\int_{\xi_s}^{\xi_b} A'_{42}\,d\xi \cdot \ddot{y} - \int_{\xi_s}^{\xi_b} A'_{42}\,\xi\,d\xi \cdot \ddot{\psi} - \int_{\xi_s}^{\xi_b} A'_{44}\,d\xi \cdot \ddot{\phi} \quad , \tag{B-17}$$

$$M_{bm} = \int_{\xi_s}^{\xi_b} A'_{33}\,\xi\,d\xi \cdot \ddot{z} - \int_{\xi_s}^{\xi_b} A'_{33}\,\xi^2\,d\xi \cdot \ddot{\theta} \quad , \tag{B-18}$$

$$N_{o_{bm}} = -\int_{\xi_s}^{\xi_b} A'_{22}\,\xi\,d\xi \cdot \ddot{y} - \int_{\xi_s}^{\xi_b} A'_{22}\,\xi^2\,d\xi \cdot \ddot{\psi} - \int_{\xi_s}^{\xi_b} A'_{42}\,\xi\,d\xi \cdot \ddot{\phi} \quad , \tag{B-19}$$

where ξ_b and ξ_s are the bow and stern ξ -coordinates, respectively.

Referring motions and forces to the center of gravity of the barge, the roll moment is given by

$$K_{bm} = K_{o_{bm}} + |\overline{OG}|\,Y_{o_{bm}} \quad , \tag{B-20}$$

where $|\overline{OG}|$ is the vertical distance between the free surface level and the barge center of gravity (positive in the present case.) The roll moment representation to be used in the equations of motion is then

$$K_{Lm} = -\int_{\xi_s}^{\xi_b} [A'_{42} + (\overline{OG})A'_{22}]\,d\xi \cdot \ddot{y} - \int_{\xi_s}^{\xi_b} [A'_{42} + (\overline{OG})A'_{22}]\,\xi\,d\xi \cdot \ddot{\psi} - I_{xa}\,\ddot{\phi}, \tag{B-21}$$

where I_{x_a} is the final added moment of inertia in roll. Similarly, by considering the equivalence of the diagonal terms of the inertia-tensor representation of hydrodynamic forces, or by geometric decomposition of the rolling motion about the center of gravity into an equivalent linear velocity and a roll motion about the level of the free surface, the lateral force and yawing moment due to dynamic body motions are given by

$$Y_{bm} = -\int_{\xi_s}^{\xi_b} A'_{22}\,d\xi \cdot \ddot{y} - \int_{\xi_s}^{\xi_b} A'_{22}\,\xi\,d\xi \cdot \ddot{\psi} - \int_{\xi_s}^{\xi_b} [A'_{42} + (\overline{OG})A'_{22}]\,d\xi \cdot \ddot{\phi} \quad , \tag{B-22}$$

and

$$N_{bm} = -\int_{\xi_s}^{\xi_b} A'_{22}\,\xi\,d\xi \cdot \ddot{y} - \int_{\xi_s}^{\xi_b} A'_{22}\,\xi^2\,d\xi \cdot \ddot{\psi} - \int_{\xi_s}^{\xi_b} [A'_{42} + (\overline{OG})A'_{22}]\,\xi\,d\xi \cdot \ddot{\phi}. \tag{B-23}$$

All of the dynamic body motions considered above were amenable to treatment by slender-body theory, since they involved crossflows normal to the ship longitudinal axis. The only motion not considered is surge, and similarly no consideration is given to longitudinal dynamic forces. When the ship has a longitudinal acceleration, there is a hydrodynamic force proportional to the acceleration, the proportionality factor being the longitudinal added mass. Numerical estimates were made of this added mass on the basis of the geometrical parameters (ratios of major dimensions) of the barge, and it was the order of 6-7% of the actual body mass. Since slender-body theory will be used for determining the longitudinal wave force, for which there is no simple means of including such added mass effects, and since the added mass correction is so small, such a term was deleted from consideration in the equations of motion. However, one effect of the surge acceleration is an influence on the pitch moment, since the longitudinal force $m\ddot{x}$ acts through the CB of the ship, leading to a pitch moment,

$$\Delta M_{bm} = m|BG|\ddot{x} \quad , \tag{B-24}$$

where $\overline{BG}$ is the vertical distance between the CB and the CG. By similar reasoning, as in previous parts of the analysis of dynamic forces and moments, there is a longitudinal force due to pitch acceleration given by

$$X_{bm} = m|BG|\ddot{\theta} \quad , \tag{B-25}$$

from the equivalence of off-diagonal terms of the added-mass tensor representation of inertial forces.

C. Damping Forces and Moments

The damping forces and moments are dissipative in nature, and are primarily due to the generation of waves by the ship motions on the surface, which continually transfer energy by propagating outward to infinity. In accordance with the two-dimensional treatment used for the analysis of forces due to body motions, the same concept is used in evaluating the local forces at a section of the ship due to wave generation. With the ratio of the amplitude of the heave-generated, two-dimensional waves to the amplitude of heaving motion of the ship section denoted by $\overline{A}_z$, the vertical damping force per unit vertical velocity of the ship section is expressed as

$$N'_{zz} = \frac{\rho g^2 \overline{A}_z^2}{\omega^3} = \rho\omega\left(\frac{\lambda}{2\pi}\right)^2 \overline{A}_z^2 \tag{C-1}$$

(see Reference 10). Values of $\bar{A}_z$ were derived for the Lewis-form sections (Reference 11) and are available as a function of $\frac{\omega^2 B^*}{2g} = \frac{\pi^2 B^*}{\lambda}$, for different beam-draft ratios and section coefficients. Most of the data needed was available from the published results, but values of $\bar{A}_z$ were necessary for large beam-draft ratios, which are appropriate to the stern region of the barge. These values are found by replotting some curves of $\bar{A}_z$ in the form of $\bar{A}_z\left(\frac{H}{B^*}\right)$ vs. $\frac{2\pi H}{\lambda}$, which should yield (in approximate fashion) a single curve for all values of $\frac{B^*}{H}$, for particular values of section coefficient. From this "uniform" curve, the value of $\bar{A}_z$ for particular desired values of the pertinent parameters is found.

For the case of lateral motion, a similar relation holds, viz.

$$N'_{yy} = \frac{\rho g^2 \bar{A}_y^2}{\omega^3} \quad , \tag{C-2}$$

and the problem is to find $\bar{A}_y$ for the ship sections of interest. For small values of frequency, an asymptotic analysis (Reference 12) yields the expression

$$\bar{A}_y = d_y \left(\frac{\omega^2 B^*}{2g}\right)^2 = d_y \left(\frac{\pi B^*}{\lambda}\right)^2 \quad , \tag{C-3}$$

where values of the quantity d_y for Lewis forms are presented in a chart in Reference 13. Further study of the original derivation of this result allows the analytic representation as

$$d_y = \frac{4C_s}{(B^*/H)} \left(1 + K_y\right) \quad , \tag{C-4}$$

where C_s is the section coefficient. While this result is valid only for low frequencies, it is used for determining the lateral damping for all frequencies of interest. At higher frequencies, where it gives an overestimate of the damping, the lateral motions are expected to be small and, hence, the practical effect of this use will not be important. Thus the final value of N'_{yy}, the lateral damping force per unit lateral velocity of the ship section, is

$$N'_{yy} = \frac{\rho \omega B^{*2}}{4} d_y^2 \left(\frac{\pi B^*}{\lambda}\right)^2 \tag{C-5}$$

The vertical damping force at each section is

$$\frac{dZ_d}{d\xi} = -N'_{zz}\left(\dot{z} - \xi\dot{\theta}\right) \quad , \tag{C-6}$$

which includes a coupling term due to pitch velocity, and this is integrated over the ship length to determine the total vertical damping force. Since the determination of damping is two-dimensional, and three-dimensional wave generation and propagation differs from the presently-assumed method of evaluation, some allowance for three-dimensional effects should be included in the final representation of damping forces and moments. Ratios of three-dimensional to two-dimensional damping, for both heave and pitch, were determined by Havelock (Reference 14) for a submerged spheroid (at zero forward speed), and the results are generally applicable to representative surface-ship forms. Since different factors occur for heave and pitch, due to the relative degree of wave interference for the two motions, the correction factors should be applied only to the pure heave and pitch damping, and not to any associated coupling terms. Thus, with the three-dimensional damping factor for pure heave motion denoted as C_z, the total vertical damping force is

$$Z_d = - C_z N_z \dot{z} + N_{z\theta} \dot{\theta} \quad , \tag{C-7}$$

where

$$N_z = \rho \omega \left(\frac{\lambda}{2\pi}\right)^2 \int_{\xi_s}^{\xi_b} \bar{A}_z^2 \, d\xi \quad , \tag{C-8}$$

and

$$N_{z\theta} = \rho \omega \left(\frac{\lambda}{2\pi}\right)^2 \int_{\xi_s}^{\xi_b} \bar{A}_z^2 \, \xi \, d\xi \quad . \tag{C-9}$$

Since the local pitch moment due to damping is defined by

$$\frac{dM_d}{d\xi} = - \xi \frac{dZ_d}{d\xi} \quad , \tag{C-10}$$

the total pitch moment is

$$M_d = N_{z\theta} \dot{z} - C_\theta N_\theta \dot{\theta} \, , \tag{C-11}$$

where

$$N_\theta = \rho \omega \left(\frac{\lambda}{2\pi}\right)^2 \int_{\xi_s}^{\xi_b} \bar{A}_z^2 \, \xi^2 \, d\xi \, , \tag{C-12}$$

and C_θ is the three-dimensional damping factor for pure pitching motion.

For lateral motion, the damping force at each section is

$$\frac{dY_d}{d\xi} = -N'_{YY}\left(\dot{y} + \xi\dot{\psi} - \zeta\dot{\phi}\right), \tag{C-13}$$

where ζ is understood now to be measured from the CG. Three-dimensional factors for lateral damping are also required, as in the case of vertical plane motions, and values appropriate to a submerged spheroid in lateral motion were used. These three-dimensional factors were determined from the results of an analysis of lateral damping of submerged bodies (Reference 15), and are appropriate to pure swaying and yawing motion. Since the roll motion is somewhat similar to swaying, in the manner represented in Equation (C-13), i.e. as an effective geometric motion component, the sway damping three-dimensional factor is also applied to the lateral damping contribution from rolling motion. Another point in the evaluation of the total damping for the ship is that the resultant "weighting" of the value of ζ after carrying out the integrations is approximated by replacing ζ by $-|\overline{BG}|$, based on assuming an effective center of pressure for such forces to be located at the CB. On the basis of the foregoing,

$$Y_d = -C_y N_y \dot{y} - N_{y\psi}\dot{\psi} - C_y |BG| N_y \dot{\phi} \tag{C-14}$$

and

$$N_d = -N_{y\psi}\dot{Y} - C_\psi N_\psi \dot{\psi} - |BG| N_{y\psi}\dot{\phi}, \tag{C-15}$$

where

$$N_y = \frac{\rho\omega\pi^2}{4\lambda^2}\int_{\xi_s}^{\xi_b} \xi B^4 dy^2 d\xi, \tag{C-16}$$

$$N_{y\psi} = \frac{\rho\omega\pi^2}{4\lambda^2}\int_{\xi_s}^{\xi_b} B^4 dy^2 d\xi \tag{C-17}$$

$$N_\psi = \frac{\rho \omega \pi^2}{4\lambda^2} \int_{\xi_s}^{\xi_b} B^4 dy^2 \xi^2 d\xi \quad , \qquad \text{(C-18)}$$

and C_y and C_ψ are the three-dimensional factors for pure sway and yaw damping, respectively. Values of the different three-dimensional factors used for heave, pitch, sway and yaw are tabulated in Table C-I for the different wave-lengths considered in this study.

The roll moment arising from damping due to lateral motions is approximated by the relation

$$K_d = |BG| Y_d \quad , \qquad \text{(C-19)}$$

where it is tacitly assumed that the center of action of the lateral force is located approximately at the CB. (Actually, the local lateral force is assumed to act at the center of every section, and the integrated effect is approximated by the relation in Equation (C-19).) The only exception noted in the evaluation of the roll moment due to damping is in the pure roll damping term alone. The value of that quantity is determined from data obtained in a roll-decay model experiment (see Reference 16), which will be discussed following the present analytical derivations. The roll moment is thus represented by

$$K_d = -C_y |BG| N_y \dot{y} - |BG| N_\psi \dot{\psi} - N_\phi \dot{\phi} \quad , \qquad \text{(C-20)}$$

where N_ϕ is the pure roll-damping term whose value is obtained from experimental data.

In the intitial discussion of damping, emphasis was placed upon energy dissipation due to wave generation. Actually, viscous effects also manifest themselves and contribute to damping. The contribution of the viscous damping term is quite negligible for most motions, with the possible exception of roll. Roll damping due to wave generation is often small for most normal ships (however, it may be fairly appreciable for the present case of a barge of large beam-draft ratio, with a relatively flat bottom), and viscous effects (or other drag mechanisms, such as eddy-making) assume greater importance, especially if the ship is fitted with bilge keels. In that case, the roll damping is often of non-linear form, and an approximation is used to determine some equivalent linear representation. Examination of the roll decay curve from the model experiments showed only small nonlinear effects in the damping when bilge keels

were added, although there was an appreciable increase in total damping due to the presence of the bilge keels. The decay characteristics indicated that the roll damping with bilge keels was 0.10 of initial damping, and from the value of total roll moment of inertia and natural roll frequency, the value of the roll damping coefficient for the barge was found to be

$$N_\phi = 12.858 \times 10^6 \text{ lb-ft-sec.} \qquad \text{(C-21)}$$

Although the value of roll damping is known to be frequency-dependent, the value given in Equation (C-21), which is approximate to the roll natural frequency, can be used for computations at other frequencies, since roll is a highly tuned motion and the damping value is only important near the roll natural frequency.

For surging motion, the surge damping is quite small since the ship is slender and does not produce appreciable waves during such motions. Since viscous effects are small, the total surge damping is not affected much by that consideration. There has accordingly not been much concern with surge damping, and there is not much available information for computation purposes. A recent theoretical study on three-dimensional damping (due to wave generation) of submerged ellipsoids (Reference 17) has shown that, at zero forward speed, the general behavior of surge and heave damping as functions of frequency is quite similar. On that basis, and because of the relatively small influence anticipated for surge damping in the range of wavelengths of interest in this study, the surge damping coefficient is approximated by

$$N_x = \frac{1}{28} C_z N_z \quad , \qquad \text{(C-22)}$$

where the fractional factor is chosen from the ratios obtained from the results of Reference 17.

TABLE C-I

Three-Dimensional Damping Factors

λ (ft.)	C_z	C_θ	C_y	C_ψ
100	.95	.95	.94	.79
200	1.03	1.26	.86	.56
300	1.08	.90	.78	.30
400	1.08	.55	.69	.16
500	1.02	.32	.59	.09
600	.90	.22	.51	.05
700	.78	.12	.45	.035
800	.70	.10	.40	.02

D. Hydrostatic Restoring Forces and Moments

The hydrostatic restoring forces and moments are, as the name implies, due to buoyancy effects arising from static displacements. The only displacements that will result in hydrostatic restoring effects are heave, pitch and roll. On the basis of linear theory, the local hydrostatic vertical force change due to vertical displacements is

$$\frac{dZ_h}{d\xi} = \rho g B^*(z - \xi\theta) \quad , \tag{D-1}$$

where the ship is assumed to be almost wall-sided near the intersection with the free surface, and the effective buoyancy change comes from the total immersion. Similarly, the hydrostatic restoring pitch moment is

$$\frac{dM_h}{d\xi} = -\xi \frac{dZ_h}{ds} \quad , \tag{D-2}$$

leading to total hydrostatic restoring vertical force and pitch moment given by

$$Z_h = -\rho g \int_{\xi_s}^{\xi_b} B^* d\xi \cdot z + \rho g \int_{\xi_s}^{\xi_b} B^* \xi d\xi \cdot \theta \tag{D-3}$$

and

$$M_h = \rho g \int_{\xi_s}^{\xi_b} B^* \xi d\xi \cdot z - \rho g \int_{\xi_s}^{\xi_b} B^* \xi^2 d\xi \cdot \theta \tag{D-4}$$

In the case of roll motion, the hydrostatic restoring effect is a classical result known in all naval architectural work. Its derivation will not be presented precisely herein, but only the final result will be given. The necessary steps in the derivation are rather long, become complicated by geometry, and are readily available (see, for example, Reference 2). The result is

$$K_h = -\rho g \nabla |GM| \phi = -W|GM|\phi \quad , \tag{D-5}$$

where ∇ is the displaced volume, $|\underline{GM}|$ is the metacentric height (distance between the CG and the metacenter, which is a point on the ship vertical axis of symmetry where the line of action of the buoyant force intersects when small roll displacements occur), and $W = \rho g \nabla$ is the ship displacement.

E. Mooring Forces and Moments

The barge is assumed to be moored by a conventional line and anchor system, with both bow and stern moorings. However, for application to deep-sea conditions with depths of the order of 1000 fathoms, a certain particular mooring scheme is utilized. This scheme utilizes a long-wire rope for each mooring leg assembly (12,000 ft. in length), which is supported in the water by a series of submerged spherical buoys. The buoyancy of these buoys keeps the rope taut along its entire length, thereby not allowing it to assume the usual catenary shape. With this arrangement, an initial tension is applied along each mooring leg, and any changes in mooring forces on the ship (and therefore also in the cables) occur as a result of elastic forces resulting from ship displacements. A layout drawing of such a system is shown in Reference 18, which has direct applicability to ships of the same general displacement as the construction barge presently studied.

The displacements having greatest influence on the moorings are in the horizontal plane, and these are surge, sway and yaw. Very small influence results from displacements in heave, pitch and roll. These latter motions have large restoring effects of hydrostatic nature, and the mooring forces would be small relative to those hydrostatic effects. This assumption is consistent with results of other studies of moored ships in waves (see Reference 19). Since the mooring lines are fairly taut and are under an initial tension, the elastic restoring effects may be taken to be fairly linear, i.e. the restoring force is proportional to the displacement. The proportionality factor for an effective displacement along a single mooring cable is found from a knowledge of the modulus of elasticity of the cable material. For the present case of 1-inch diameter bridge strand wire rope, which is 12,000 ft. long, has a cross-section area of 0.595 $in.^2$, and an assumed modulus of 25×10^6 lb./$in.^2$, the effective spring constant for a single wire rope is found to be

$$C = 1250 \text{ lb./ft.} \qquad \text{(E-1)}$$

This linear result only holds below the yield point of 60,000 lb of static force (in a single cable), but it is anticipated that the maximum deflection necessary for attaining this force (viz. 48 ft) will not be experienced or even approached closely in the present study.

For purposes of analysis, the barge is assumed to be moored in an arrangement similar to that shown in the following sketch of the mooring plan.

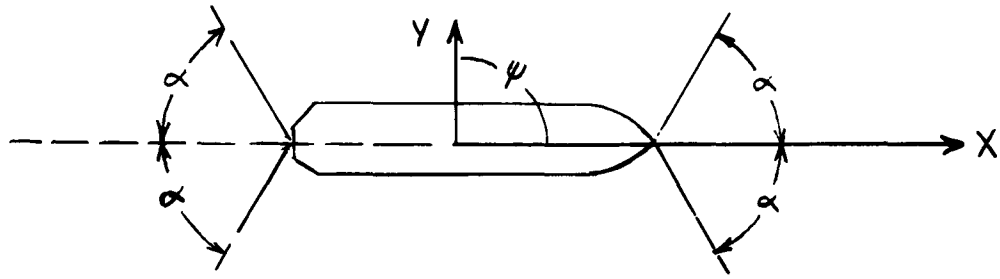

A longitudinal displacement of the barge along x, denoted as Δx, leads to an effective displacement along a single cable given by $\Delta x \cos\alpha$, where α is defined in the sketch above. The force in a single cable is then $C\Delta x \cos\alpha$. The longitudinal force component at one end of the ship is represented by

$$(C\Delta x \cos\alpha)\cos\alpha + (C\Delta x \cos\alpha)\cos\alpha = 2C\Delta x \cos^2\alpha ,$$

and since an extension of the cable at one end of the ship requires a contraction at the other end, a similar force occurs. These forces are restoring forces and the net result is a longitudinal force on the barge due to the moorings, given by

$$X_m = -4C\cos^2\alpha \cdot x = -k_x x , \qquad \text{(E-2)}$$

where x is the surge displacement variable.

In the case of sway displacement, the effective displacement along the cable is $y \sin\alpha$, and combining components for net Y-force on the barge, accounting for all the cables, leads to a net mooring lateral force given by

$$Y_m = -4C\sin^2\alpha \cdot y = -k_y y . \qquad \text{(E-3)}$$

For yaw displacements, $Y \approx \frac{L}{2}\psi$ where L is the ship length. The lateral force at one end of the ship is then

$$2C\sin^2\alpha \cdot \frac{L}{2}\psi = CL\sin^2\alpha \cdot \psi , \qquad \text{(E-4)}$$

and the contribution to the yaw moment is

$$CL\sin^2\alpha \cdot \psi\left(\frac{L}{2}\right) = \frac{1}{2}CL^2\sin^2\alpha \cdot \psi \qquad \text{(E-5)}$$

at each end. Since the forces at each end are equal and opposite (approximately, since the origin is not exactly at the ship center), the net contribution is to the yawing moment acting on the barge, given by

$$N_m = -CL^2\sin^2\alpha \cdot \psi = -k_\psi \psi . \qquad \text{(E-6)}$$

The variations in the force in the mooring cables due to the motions of the barge can easily be found, since they are related kinematically to the motions. It is seen that the longitudinal displacement, x, and the net lateral displacements, $(y + \frac{L}{2}\psi)$ at the bow and $(y - \frac{L}{2}\psi)$ at the stern, can be combined to determine the net variation in elongation of each mooring cable. The cable displacements due to surging motion of the barge are $x \cos\alpha$, while the cable displacement due to the motions of sway and yaw are $(y \pm \frac{L}{2}\psi) \sin\alpha$, according as the cable is at the bow or the stern. Here α is the angle between the mooring line and the longitudinal axis of the barge. Different effects as to cable displacement directions occur for the cables, at either the bow or the stern, for the influence of the lateral motions, while the same direction of displacement (at either bow or stern) occurs for the surge motion. The general expression for the fluctuating cable force may be written as

$$F_c = C[x\cos\alpha \pm (y \pm \tfrac{L}{2}\psi)\sin\alpha] \quad ,$$

where C is the effective spring constant for a single wire rope, and particular values for each of the four cables are given in the following, where a positive cable force is defined as that which pulls on the restraining anchor support on the ocean floor.

The expressions for the individual cable forces (c.f. sketch of mooring-line system) are listed below:

Bow

$$F_1 = -C[x\cos\alpha + (y + \tfrac{L}{2}\psi)\sin\alpha] \quad \text{port}$$

$$F_2 = -C[x\cos\alpha - (y + \tfrac{L}{2}\psi)\sin\alpha] \quad \text{starb'd}$$

(E-6.1)

Stern

$$F_3 = C[x\cos\alpha - (y - \tfrac{L}{2}\psi)\sin\alpha] \quad \text{port}$$

$$F_4 = C[x\cos\alpha + (y - \tfrac{L}{2}\psi)\sin\alpha] \quad \text{starb'd}$$

For the present case where the barge is moored with $\alpha = 60°$, L = 260 ft., the mooring system restoring constants are

$$\begin{aligned} k_x &= 1250 \text{ lb/ft} \\ k_y &= 3750 \text{ lb/ft} \\ k_\psi &= 633.75 \times 10^5 \text{ lb-ft/rad.} \end{aligned} \qquad \text{(E-7)}$$

These values are the effective spring constants for surge, sway and yaw, and as a result there also exist natural periods for these motions in the case of moored ships. There still exist natural periods of heave, pitch and roll, as in the case of free ships, and these natural periods are relatively unaffected in the present case. The introduction of the existence of natural periods in surge, sway and yaw (with possible large motions associated with resonances in these degrees of freedom) is the main characteristic of moorings applied to ships that distinguishes the resulting motions from those of free ships in waves.

F. Wave Exciting Forces and Moments

The hydrodynamic forces and moments due to waves are obtained by application of slender-body theory. A number of papers have been written on this subject (e.g. References 3 and 20), but they have been applied only to submerged bodies. However, as proposed in Reference 3, proven in Reference 9, and applied in References 8 and 21, the wave forces on a surface ship can be represented in the same manner as for a submerged body, but with the frequency dependence of the added mass terms included in the final representation. On this basis, the inertial contribution to the wave exciting forces for the present case of zero speed is represented by

$$\frac{dF_W^{(i)}}{d\xi} = \left(\rho S + A_{ii}\right) \frac{DV_{oi}}{Dt} \quad , \qquad \text{(F-1)}$$

where A_{ii} is a particular added mass term and V_{oi} is a component of the orbital velocity evaluated at some reference point on the ship hull (along the vertical centerline, because of symmetry). In order to allow for further influence of the exponential decay of waves, this point is chosen to be at the mean half-draft of the vessel, rather than at the surface, and hence a further approximation has been made. Furthermore, since the present study concerns a surface ship, certain buoyant terms due to periodic buoyancy alterations as the waves progress past the ship hull must also be included. The buoyancy effect only adds to the vertical force and it is represented by

$$\rho g B^* \eta(\xi, t) \qquad \text{(F-2)}$$

at each section.

The waves are assumed to be propagating in a direction defined by the angle β, where β is defined as the angle between the x-axis and the normal to the wave crests, with β lying in the range $-\pi \leq \beta \leq \pi$. The wave propagation speed c is always taken positive along the radial line defining the wave propagation direction, as illustrated in the sketch below.

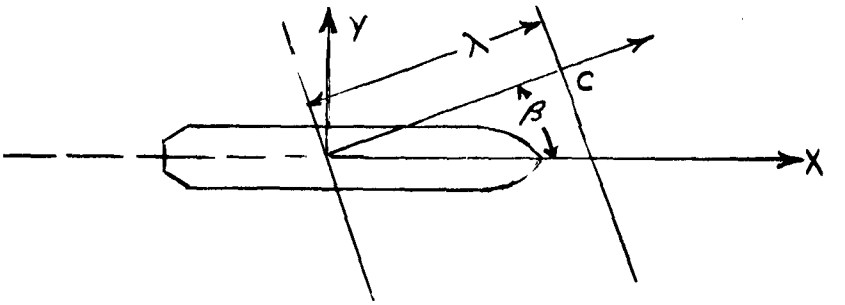

This definition differs only slightly from that used in Reference 20, but the forms of the velocity potential and other mathematical functions remain the same. This wave potential is (referred to axes on the free surface)

$$\phi_w = ace^{\frac{2\pi z}{\lambda}} \cos \frac{2\pi}{\lambda}(x\cos\beta + y\sin\beta - ct), \qquad \text{(F-3)}$$

and the surface wave elevation associated with it is

$$\eta = \frac{1}{g}\frac{\partial \phi_w}{\partial t}\bigg|_{z=0}, \text{ i.e.}$$

$$\eta = a\sin\frac{2\pi}{\lambda}(x\cos\beta + y\sin\beta - ct), \qquad \text{(F-4)}$$

where a is the wave amplitude, and $\frac{2\pi}{\lambda} = \frac{\omega^2}{g} = \frac{g}{c^2}$. See sketch below:

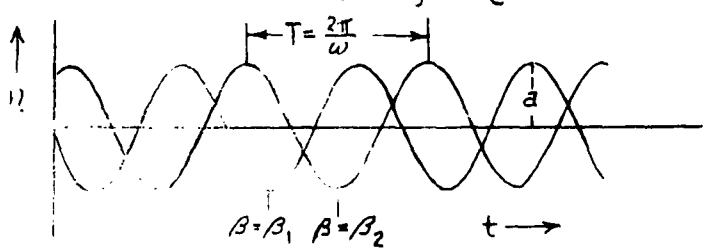

The orbital velocities along the x, y and z axes are easily obtained from Equation (F-3) and from this the wave force expressions can be shown to result according to Equations (F-1)and (F-2) in the form

$$X_w^{(1)} = -\rho g \frac{2\pi a}{\lambda} e^{-\frac{2\pi \bar{h}}{\lambda}} \cos\beta \left\{ \cos\omega t \int_{\xi_s}^{\xi_b} S \cos\left(\frac{2\pi\xi}{\lambda}\cos\beta\right) d\xi \right.$$
$$\left. + \sin\omega t \int_{\xi_s}^{\xi_b} S \sin\left(\frac{2\pi\xi}{\lambda}\cos\beta\right) d\xi \right\} , \qquad \text{(F-5)}$$

$$Y_w^{(1)} = -\rho g \frac{2\pi a}{\lambda} e^{-\frac{2\pi \bar{h}}{\lambda}} \sin\beta \left\{ \cos\omega t \int_{\xi_s}^{\xi_b} \left(S + \frac{A'_{22}}{\rho}\right) \cos\left(\frac{2\pi\xi}{\lambda}\cos\beta\right) d\xi \right.$$
$$\left. + \sin\omega t \int_{\xi_s}^{\xi_b} \left(S + \frac{A'_{22}}{\rho}\right) \sin\left(\frac{2\pi\xi}{\lambda}\cos\beta\right) d\xi \right\} , \qquad \text{(F-6)}$$

$$Z_w^{(1)} = \rho g a \left\{ \cos\omega t \int_{\xi_s}^{\xi_b} B^* \sin\left(\frac{2\pi\xi}{\lambda}\cos\beta\right) d\xi \right.$$
$$\left. - \sin\omega t \int_{\xi_s}^{\xi_b} B^* \cos\left(\frac{2\pi\xi}{\lambda}\cos\beta\right) d\xi \right\}$$
$$- \rho g \frac{2\pi a}{\lambda} e^{-\frac{2\pi \bar{h}}{\lambda}} \left\{ \cos\omega t \int_{\xi_s}^{\xi_b} \left(S + \frac{A'_{33}}{\rho}\right) \sin\left(\frac{2\pi\xi}{\lambda}\cos\beta\right) d\xi \right.$$
$$\left. - \sin\omega t \int_{\xi_s}^{\xi_b} \left(S + \frac{A'_{33}}{\rho}\right) \cos\left(\frac{2\pi\xi}{\lambda}\cos\beta\right) d\xi \right\} . \qquad \text{(F-7)}$$

The pitch and yaw moments due to waves readily follow as

$$M_w^{(1)} = -\rho g a \left\{ \cos \omega t \int_{\xi_s}^{\xi_b} B^* \xi \sin\left(\frac{2\pi \xi}{\lambda} \cos\beta\right) d\xi \right.$$
$$\left. - \sin \omega t \int_{\xi_s}^{\xi_b} B^* \xi \cos\left(\frac{2\pi \xi}{\lambda} \cos\beta\right) d\xi \right\}$$
$$+ \rho g \frac{2\pi a}{\lambda} e^{-\frac{2\pi \bar{h}}{\lambda}} \left\{ \cos \omega t \int_{\xi_s}^{\xi_b} \xi \left(S + \frac{A'_{33}}{\rho}\right) \sin\left(\frac{2\pi \xi}{\lambda} \cos\beta\right) d\xi \right. \qquad \text{(F-8)}$$
$$\left. - \sin \omega t \int_{\xi_s}^{\xi_b} \xi \left(S + \frac{A'_{33}}{\rho}\right) \cos\left(\frac{2\pi \xi}{\lambda} \cos\beta\right) d\xi \right.$$

and

$$N_w^{(1)} = -\rho g \frac{2\pi a}{\lambda} e^{-\frac{2\pi \bar{h}}{\lambda}} \sin\beta \left\{ \cos \omega t \int_{\xi_s}^{\xi_b} \xi \left(S + \frac{A'_{22}}{\rho}\right) \cos\left(\frac{2\pi \xi}{\lambda} \cos\beta\right) d\xi \right.$$
$$\left. + \sin \omega t \int_{\xi_s}^{\xi_b} \xi \left(S + \frac{A'_{22}}{\rho}\right) \sin\left(\frac{2\pi \xi}{\lambda} \cos\beta\right) d\xi \right\} . \qquad \text{(F-9)}$$

These values in Equations (F-5) to (F-9) are determined from values of the wave orbital velocities evaluated by y = o, z = $-\bar{h}$ (the average half-draft).

The roll moment is found by application of slender-body theory (in Reference 9) to be given by

$$\frac{dK_{o_w}^{(1)}}{d\xi} = \left[A'_{42} - \rho S \bar{z}_{c_b} - \frac{\rho}{12} B^{*3}\right] \frac{D v_o}{Dt} , \qquad \text{(F-10)}$$

where $\bar{z}_{c_b}$ is the location of the local c. b. of each section ($\bar{z}_{c_b} < 0$ in the present notaion, and is measured from the free surface level). Applying the same effective exponential term to this result, the roll moment (relative to the free surface position) due to waves is then

$$K_{o_w}^{(1)} = -\rho g \frac{2\pi a}{\lambda} e^{-\frac{2\pi \bar{h}}{\lambda}} \sin\beta \left\{ \cos \int_{\xi_s}^{\xi_b} \left[\frac{A'_{42}}{\rho} - S\bar{z}_{c_b} - \frac{B^{*3}}{12} \right] \cos\left(\frac{2\pi\xi}{\lambda}\cos\beta\right) d\xi \right.$$

$$\left. + \sin\omega t \int_{\xi_s}^{\xi_b} \left[\frac{A'_{42}}{\rho} - S\bar{z}_{c_b} - \frac{B^{*3}}{12} \right] \sin\left(\frac{2\pi\xi}{\lambda}\cos\beta\right) d\xi \right\} \qquad \text{(F-11)}$$

In addition to these terms of inertial nature, an effect due to damping also manifests itself. This influence is due to the relative motion between body velocities and the wave orbital velocities, i. e. the damping coefficient is applied to that difference, resulting in additional terms in the wave excitation. The basis for including such a representation in the wave-induced effects for slender bodies is in the recent thesis by Vossers (Reference 22), while it has been used in other studies purely in the basis of empirical reasoning. The added mass terms are also to be included, over and above the simple effects of the Froude-Kriloff hydrostatic hypotheses terms, according to this latter study, but they are already included in the inertial terms. Since surge and roll damping (due to wave generation) are usually quite small, the contribution of damping to the excitation in those modes of motion is neglected. On the basis of the foregoing, and using the orbital velocities referred to the location y = 0, z = $-\bar{h}$, the additional wave-excitation terms due to damping are then

$$Z_w^{(2)} = -C_z a\omega e^{-\frac{2\pi\bar{h}}{\lambda}} \left\{ \cos\omega t \int_{\xi_s}^{\xi_b} N'_{zz} \cos\left(\frac{2\pi\xi}{\lambda}\cos\beta\right) d\xi \right.$$

$$\left. + \sin\omega t \int_{\xi_s}^{\xi_b} N'_{zz} \sin\left(\frac{2\pi\xi}{\lambda}\cos\beta\right) d\xi \right\} , \qquad \text{(F-12)}$$

$$Y_w^{(2)} = C_y a\omega e^{-\frac{2\pi\bar{h}}{\lambda}} \sin\beta \left\{ \cos\omega t \int_{\xi_s}^{\xi_b} N'_{yy} \sin\left(\frac{2\pi\xi}{\lambda}\cos\beta\right) d\xi \right.$$

$$\left. - \sin\omega t \int_{\xi_s}^{\xi_b} N'_{yy} \cos\left(\frac{2\pi\xi}{\lambda}\cos\beta\right) d\xi \right\} , \qquad \text{(F-13)}$$

$$M_w^{(2)} = C_z a w e^{-\frac{2\pi\bar{h}}{\lambda}} \left\{ \cos wt \int_{\xi_s}^{\xi_b} N'_{zz}\, \xi \cos\left(\frac{2\pi\xi}{\lambda}\cos\beta\right) d\xi \right. \tag{F-14}$$

$$\left. + \sin wt \int_{\xi_s}^{\xi_b} N'_{zz}\, \xi \sin\left(\frac{2\pi\xi}{\lambda}\cos\beta\right) d\xi \right\},$$

$$N_w^{(2)} = C_y a w e^{-\frac{2\pi\bar{h}}{\lambda}} \sin\beta \left\{ \cos wt \int_{\xi_s}^{\xi_b} N_{yy}\, \xi \cos\left(\frac{2\pi\xi}{\lambda}\cos\beta\right) d\xi \right. \tag{F-15}$$

$$\left. - \sin wt \int_{\xi_s}^{\xi_b} N'_{yy}\, \xi \sin\left(\frac{2\pi\xi}{\lambda}\cos\beta\right) d\xi \right\}.$$

Another factor entering into the evaluation of the wave forces and moments is the fact that the ship is not really quite so slender and also that the relative ship dimensions are not small relative to some of the wavelengths. One particular dimension of importance is theship beam, which is appreciable relative to some of the wavelengths. The basic assumption of slender-body theory leading to the results given by all of the preceding formulas is that the quantity $\frac{2\pi y}{\lambda}\sin\beta$ appearing within the arguments of various sinusoidal functions is quite small. This is not true in a number of important cases, and a measure of the influence of this term should be found. Since the various integrals are really of the form

$$\int_{\xi_s}^{\xi_b} f(\xi) \begin{matrix}\cos\\ \sin\end{matrix}\left\{\left(\frac{2\pi\xi}{\lambda}\cos\beta + \frac{2\pi y}{\lambda}\sin\beta\right)\right\} d\xi, \tag{F-16}$$

a proper move would be to represent the influence of this additional term by finding the mean value across the beam. Using maximum beam as a base, since the ship is close to a full planform shape, the quantity of interest is

$$\frac{1}{B}\int_{-\frac{B}{2}}^{\frac{B}{2}} dy \int_{\xi_s}^{\xi_b} f(\xi)\begin{matrix}\cos\\ \sin\end{matrix}\left\{\left(\frac{2\pi\xi}{\lambda}\cos\beta + \frac{2\pi y}{\lambda}\sin\beta\right)\right\} d\xi$$

$$= \frac{\sin\left(\frac{\pi B}{\lambda}\sin\beta\right)}{\frac{\pi B}{\lambda}\sin\beta} \int_{\xi_s}^{\xi_b} f(\xi)\begin{matrix}\cos\\ \sin\end{matrix}\left\{\left(\frac{2\pi\xi}{\lambda}\cos\beta\right)\right\} d\xi \quad , \qquad \text{(F-17)}$$

which accounts for the influence of the beam-wavelength ratio in a more rational manner (although not the most precise method) than simply setting y = 0, The product factor

$$\frac{\sin\left(\frac{\pi B}{\lambda}\sin\beta\right)}{\frac{\pi B}{\lambda}\sin\beta} \quad , \qquad \text{(F-18)}$$

must then be used to modify all of the previous expressions for wave forces and moments.

Since the waves are short relative to the ship dimensions of beam and length, it is possible that there may be an effect due to the relative dimension of draft to wavelength in certain cases. Since the orbital velocities in deep water waves decay with depth exponentially, the net effect of this decay can be shown to result in a uniform lateral orbital velocity evaluated at the center reference condition and a vertical gradient of lateral velocity which may be interpreted as an effective "roll" angular velocity. Other effects may also occur but this appears to be most predominant and simple to handle. With the lack of any further detailed work to determine the next higher order terms in powers of wavenumber ($\frac{2\pi}{\lambda}$), this will have to suffice. The effect of this gradient term is accounted for on the basis of including the next highest inertia term to account for the hydrodynamic effect associated with the "additional" flow. In the case of side force, this leads to

$$\frac{dY_w}{d\xi} = \frac{D}{Dt}\left[(\rho S + A'_{22})v_o + A'_{42}\cdot\frac{2\pi}{\lambda}v_o\right] \quad , \qquad \text{(F-19)}$$

and for the case of roll motion

$$\frac{dK_{0_W}}{d\xi} = \frac{D}{Dt}\left[A'_{42}V_0 + A'_{44}\cdot\frac{2\pi}{\lambda}V_0\right], \qquad \text{(F-20)}$$

where A'_{44} is the local added moment of inertia of the section in roll.

The additional side force due to the lateral orbital velocity gradient is then

$$Y_W^{(3)} = -\rho g\frac{2\pi a}{\lambda}e^{-\frac{2\pi\bar{h}}{\lambda}}\sin\beta\cdot\frac{2\pi}{\lambda}\left\{\cos\omega t\int_{\xi_s}^{\xi_b}\frac{A'_{42}}{\rho}\cos\left(\frac{2\pi\xi}{\lambda}\cos\beta\right)d\xi + \sin\omega t\int_{\xi_s}^{\xi_b}\frac{A'_{42}}{\rho}\sin\left(\frac{2\pi\xi}{\lambda}\cos\beta\right)d\xi\right\}, \qquad \text{(F-21)}$$

and the additional yawing moment is

$$N_W^{(3)} = -\rho g\frac{2\pi a}{\lambda}e^{-\frac{2\pi\bar{h}}{\lambda}}\sin\beta\cdot\frac{2\pi}{\lambda}\left\{\cos\omega t\int_{\xi_s}^{\xi_b}\frac{A'_{42}}{\rho}\xi\cos\left(\frac{2\pi\xi}{\lambda}\cos\beta\right)d\xi + \sin\omega t\int_{\xi_s}^{\xi_b}\frac{A'_{42}}{\rho}\xi\sin\left(\frac{2\pi\xi}{\lambda}\cos\beta\right)d\xi\right\}. \qquad \text{(F-22)}$$

Since the sectional added moment of inertia is quite difficult to compute, and with little faith in the validity of such a result for motions of this type, an approximation was made to assist in the evaluation of the additional roll moment. The added moment of inertia is actually that of the submerged part of the ship hull due to rolling about a point either at the free surface or at the mean half-depth (depending upon the significance given to the inclusion of the exponential term combined with the use of the results of Reference 9, which were originally derived relative to the free surface). An effective total added roll inertia is chosen, leading to the form

$$K_0^{(3)} = -\frac{A_{44}}{L}\omega^2\cdot\frac{2\pi a}{\lambda}e^{-\frac{2\pi\bar{h}}{\lambda}}\sin\beta\left\{\cos\omega t\int_{\xi_s}^{\xi_b}\cos\left(\frac{2\pi\xi}{\lambda}\cos\beta\right)d\xi + \sin\omega t\int_{\xi_s}^{\xi_b}\sin\left(\frac{2\pi\xi}{\lambda}\cos\beta\right)d\xi\right\}, \qquad \text{(F-23)}$$

and this can be further simplified by assuming only a small error if ξ_s and ξ_b are replaced by $-\frac{L}{2}$ and $\frac{L}{2}$, respectively, leading to

$$K_o^{(3)} \approx -A_{44}\omega^2 \cdot \frac{2\pi a}{\lambda} e^{-\frac{2\pi\bar{h}}{\lambda}} \sin\beta \cdot \frac{\sin\left(\frac{\pi L}{\lambda}\cos\beta\right)}{\frac{\pi L}{\lambda}\cos\beta} \cdot \cos\omega t \quad , \tag{F-24}$$

The value of A_{44} in Equation (F-24) was chosen to be the same as the added moment of inertia of the ship due to rotation about the C.G., for lack of a more precise figure. Comparing the net result with available theory indicates that it is of the proper order, and hence a value of $A_{44} = 3 \times 10^7$ slug-ft^2 was used in the calculations. The corrective factor in Equation (F-18) must also be used for the additional terms due to vertical gradients, such as the results in Equations (F-21), (F-22) and (F-24).

Referring the total roll moment from the free surface level to the center of gravity results in

$$\begin{aligned} K_W &= K_{o_W} + (\overline{OG})\, Y_W \\ &= K_{o_W}^{(1)} + K_{o_W}^{(3)} + (\overline{OG})\left[Y_W^{(1)} + Y_W^{(2)} + Y_W^{(3)}\right] \quad , \end{aligned} \tag{F-25}$$

where the factor of Equation (F-18) multiplies all of the component terms. In the case of beam seas, the representation of the roll moment assumes an interacting form, especially for the components denoted as $K_{o_W}^{(1)}$ and $(\overline{OG})\, Y_W^{(1)}$. Since there is no sinusoidal weighting function affecting the ξ-integrations, the various terms in the integral result in the following:

$$-\int_{\xi_s}^{\xi_b} S_{z_{c_b}}\, d\xi = \nabla(\overline{OB}) \tag{F-26}$$

and

$$\frac{1}{12}\int_{\xi_s}^{\xi_b} B^{*3}\, d\xi = \frac{2}{3}\int_{\xi_s}^{\xi_b}\left(\frac{B^*}{2}\right)^3 d\xi = \nabla|BM| \quad , \tag{F-27}$$

where ∇ is the displaced volume, $\overline{(OB)}$ is the vertical distance from the free surface to the CB, and $|BM|$ is the metacentric radius (the integral in Equation (F-27) defines the moment of inertia of the waterplane area). On this basis, for beam seas, the result for the sum of $K_{o_W}^{(1)}$ and $(\overline{OG})\, Y_W^{(1)}$ is

$$K_{o_W}^{(1)} + (\bar{OG})\, Y_W^{(1)} = \frac{2\pi a}{\lambda} e^{-\frac{2\pi \bar{h}}{\lambda}} \cos \omega t \left[W |GM| - g\left(A_{42} + (\bar{OG}) A_{22}\right)\right], \tag{F-28}$$

which contains the elements of the usual naval architectural representation of the exciting roll moment in terms of the displacement, metacentric height, and the effective wave slope. Other terms are certainly present, as well, but the influence of coupling with the sway degree of freedom will alter the final form of the wave roll-moment excitation representation.

G. Solution of Equations of Motion

The equations of motion resulting from all of the constituent terms derived in the preceding sections are given by the following:

$$m\ddot{x} = -N_x \dot{x} - k_x x + m|BG|\ddot{\theta} + X_w , \tag{G-1}$$

$$m\ddot{y} = -\int_{\xi_s}^{\xi_b} A'_{22}\, d\xi \cdot \ddot{y} - \int_{\xi_s}^{\xi_b} A'_{22}\, \xi\, d\xi \cdot \ddot{\psi} - \int_{\xi_s}^{\xi_b} \left(A'_{42} + (\bar{OG}) A'_{22}\right) d\xi \cdot \ddot{\phi} \tag{G-2}$$

$$- C_y N_{y\dot{y}} \dot{y} - N_{y\dot{\psi}} \dot{\psi} - C_y N_y |BG| \phi - k_y y + Y_w ,$$

$$m\ddot{z} = -\int_{\xi_s}^{\xi_b} A'_{33}\, d\xi \cdot \ddot{z} + \int_{\xi_s}^{\xi_b} A'_{33}\, \xi\, d\xi \cdot \ddot{\theta} - C_z N_{\dot{z}} \dot{z} + N_{z\theta} \dot{\theta} - \rho g \int_{\xi_s}^{\xi_b} B^*\, d\xi \cdot z \tag{G-3}$$

$$+ \rho g \int_{\xi_s}^{\xi_b} B^* \xi\, d\xi \cdot \theta + Z_w ,$$

$$I_{x_T}\ddot{\phi} = -\int_{\xi_s}^{\xi_b}\left(A'_{42} + (\bar{OG})A'_{22}\right)d\xi\cdot\ddot{y} - \int_{\xi_s}^{\xi_b}\left(A'_{42} + (\bar{OG})A'_{22}\right)\xi\, d\xi\cdot\ddot{\psi} - N_\phi\phi$$

$$- C_y N_y |BG|\dot{y} - N_{y\psi}|BG|\dot{\psi} - W|GM|\phi + K_{o_w} + (\bar{OG})Y_w \quad , \qquad \text{(G-4)}$$

$$I_y\ddot{\theta} = \int_{\xi_s}^{\xi_b} A'_{33}\xi\, d\xi\cdot\ddot{z} - \int_{\xi_s}^{\xi_b} A'_{33}\xi^2 d\xi\cdot\ddot{\theta} + N_{z\theta}\dot{z} - C_\theta N_\theta\dot{\theta} + \rho g\int_{\xi_s}^{\xi_b} B^*\xi\, d\xi\cdot z$$

$$- \rho g\int_{\xi_s}^{\xi_b} B^*\xi^2 d\xi\cdot\theta + m|BG|\ddot{x} + M_w \quad , \qquad \text{(G-5)}$$

$$I_z\ddot{\psi} = -\int_{\xi_s}^{\xi_b} A'_{22}\xi\, d\xi\cdot\ddot{y} - \int_{\xi_s}^{\xi_b} A'_{22}\xi\, d\xi\cdot\ddot{\psi} - \int_{\xi_k}^{\xi_b}\left(A'_{42} + (\bar{OG})A'_{22}\right)\xi\, d\xi\cdot\ddot{\phi} \qquad \text{(G-6)}$$

$$- N_{y\dot{\psi}}\dot{y} - C_\psi N_\psi\dot{\psi} - N_{y\psi}|BG|\dot{\phi} - K_\psi\psi + N_W$$

where I_{x_T} in Equation G-4 represents the total roll moment of inertia, made up of the barge inertia and the added roll moment of inertia due to the fluid.

Since the exciting forces and moments are sinusoidal functions, the motions will also be sinusoidal with the same frequency. Defining

$$x = \bar{x}e^{i\omega t},\ y = \bar{y}e^{i\omega t},\ z = \bar{z}e^{i\omega t},\ \phi = \bar{\phi}e^{i\omega t},\ \theta = \bar{\theta}e^{i\omega t},$$
$$\psi = \bar{\psi}e^{i\omega t},\ X_w = \bar{X}e^{i\omega t},\ Y_w = \bar{Y}e^{i\omega t},$$

the equations of motion are then converted to (complex) algebraic linear equations. The longitudinal motions of surge, heave and pitch are coupled to each other (Equations (G-1), (G-3) and (G-5)), while the lateral motions of sway, yaw and roll are similarly coupled (Equations (G-2), (G-4) and (G-6)). In matrix form the equations may be represented by

$$\begin{bmatrix} a_{11} & 0 & a_{13} \\ 0 & a_{22} & a_{23} \\ a_{31} & a_{32} & a_{33} \end{bmatrix} \begin{bmatrix} \bar{x} \\ \bar{z} \\ \bar{\theta} \end{bmatrix} = \begin{bmatrix} \bar{X} \\ \bar{Z} \\ \bar{M} \end{bmatrix} \tag{G-7}$$

for the longitudinal motions, where the coefficient matrix is symmetric, i.e. $a_{13} = a_{31}$, $a_{23} = a_{32}$. The matrix elements are defined by:

$$a_{11} = (-m\omega^2 + i\omega N_x + K_x) \tag{G-8}$$

$$a_{13} = a_{31} = m|BG|\omega^2 \tag{G-9}$$

$$a_{22} = -\left(m + \int_{\xi_s}^{\xi_b} A'_{33}\, d\xi\right)\omega^2 + i\omega C_z N_z + \rho g \int_{\xi_s}^{\xi_b} B^* d\xi \tag{G-10}$$

$$a_{23} = a_{32} = \omega^2 \int_{\xi_s}^{\xi_b} A'_{33}\, \xi\, d\xi - i\omega N_{z\theta} - \rho g \int_{\xi_s}^{\xi_b} B^* \xi\, d\xi \tag{G-11}$$

$$a_{33} = -\left(I_y + \int_{\xi_s}^{\xi_b} A'_{33}\, \xi^2 d\xi\right)\omega^2 + i\omega C_\theta N_\theta + \rho g \int_{\xi_s}^{\xi_b} B^* \xi^2 d\xi \tag{G-12}$$

The lateral equations are represented by

$$\begin{bmatrix} b_{11} & b_{12} & b_{13} \\ b_{21} & b_{22} & b_{23} \\ b_{31} & b_{32} & b_{33} \end{bmatrix} \begin{bmatrix} \bar{y} \\ \bar{\psi} \\ \bar{\phi} \end{bmatrix} = \begin{bmatrix} \bar{Y} \\ N \\ \bar{K}_0 + (\bar{OG})\bar{Y} \end{bmatrix}, \tag{G-13}$$

where the matrix here is also symmetric, i.e.:

$b_{12} = b_{21}$, $b_{13} = b_{31}$, $b_{23} = b_{32}$. The elements are defined by

$$b_{11} = -\left(m + \int_{\xi_s}^{\xi_b} A'_{22}\, d\xi\right)\omega^2 + i\omega C_y N_y + K_y \tag{G-14}$$

$$b_{12} = b_{21} = -\omega^2 \int_{\xi_s}^{\xi_b} A'_{22}\, \xi\, d\xi + i\omega N_{y\psi} \tag{G-15}$$

$$b_{13} = b_{31} = -\omega^2 \int_{\xi_s}^{\xi_b} \left(A'_{42} + (\bar{OG})A'_{22}\right) d\xi + i\omega C_y N_y |BG| \tag{G-16}$$

$$b_{22} = -\left(I_z + \int_{\xi_s}^{\xi_b} A'_{22}\, \xi^2 d\xi\right)\omega^2 + i\omega C_\psi N_\psi + K_\psi \tag{G-17}$$

$$b_{23} = b_{32} = -\omega^2 \int_{\xi_s}^{\xi_b} \left(A'_{42} + (\overline{OG}) A'_{22} \right) \xi d\xi + i\omega N_{y\psi} |BG| \qquad \text{(G-18)}$$

$$b_{33} = -\omega^2 I_{x_T} + i\omega N_{\phi} + W |GM| \qquad \text{(G-19)}$$

The presence of symmetric matrices helps in effecting an easier solution of the equations, obtained by matrix inversion on a large digital computer. The solutions are then available for each degree of freedom and also for any linear combination of degrees of freedom. The real form of the final solutions is obtained by taking the real part of the complex function, which was the original definition implied in the complex representation of the solution variables.

H. Response Amplitude Operator and Spectral-Energy Analysis

Each motion of the barge in response to a regular sinusoidal wave having a given frequency and propagating in a given direction will be sinusoidal also, and of the same frequency, but will, in general, possess a different phase. In addition, the amplitude of each motion will, in general, differ from that of the wave, the ratio of the former to the latter being a function of the wave frequency and the heading of the wave relative to the heading of the barge. Direct application of this amplitude-ratio function, known as the response amplitude operator for the particular motion of interest, yields the energy-spectrum analysis of the corresponding barge-motion time history occurring for a given barge heading in an irregular random sea of known energy spectrum. The response amplitude operator for a certain motion variable, say, heave, is a function of frequency and relative heading, is thus a continuous functional representation of the amplitude of the responses to various unit sinusoidal waves (wave amplitude = 1 ft.) of different frequencies and directions. It is obtained directly from the solutions of the equations of motion.

In order to arrive at an effective characterization of the barge motions individually in a random sea, in which case these motions themselves have a random nature, the quantity (function) known as the spectra-energy density, or the energy spectrum, of each motion must be found. This spectrum is a measure of the variation of the squares of the amplitudes of the sinusoidal components of the motion, as a function of frequency and wave direction. The total area under the spectral-energy density curve contains much of the statistical information on average amplitudes, near-maximum amplitudes, etc., for the particular motion considered. For an arbitrary motion, represented by the i-subscript, the energy spectrum of that motion, due to the effects of irregular waves, is given by

$$\Phi^{(i,i)}(\omega) = |T_{i\eta}(\omega)|^2 A^2(\omega) \quad , \tag{H-1}$$

for a particular fixed barge heading in a unidirectional, irregular sea, where $A^2(\omega)$ is the spectral density of the surface elevation time history, or wave spectrum, and $|T_{i\eta}|$ is the response amplitude operator for that heading. The Neumann wave spectrum for a unidirectional fully-developed sea is represented by

$$A^2(\omega) = C\,\omega^{-6} e^{-2g^2/(\omega v_w)^2} \tag{H-2}$$

where C is an empirical constant having the value, 51.5 ft.^{2}/sec.^{5}, v_w is the wind speed in units of ft./sec., and $A^2(\omega)$ has the units ft.^{2}-sec. The wave spectrum for a non-unidirectional sea, allowing for angular variation (a two-dimensional spectrum), is represented by

$$A^2(\omega, \beta_w) = \begin{cases} \frac{2}{\pi} C\,\omega^{-6} e^{-2g^2/(\omega v_w)^2} \cos^2 \beta_w, & \text{for } -\frac{\pi}{2} < \beta_w < +\frac{\pi}{2}, \quad 0 < \omega < +\infty \\ 0, & \text{otherwise} \end{cases} \tag{H-3}$$

where β_w is an angle measured from the direction toward which the wind is blowing

(the predominant wave direction). In this case, the motion spectrum occurring for a particular barge heading, β_B, measured relative to the wind direction is

$$\Phi^{(i,i)}(\omega) = A^2(\omega) \frac{2}{\pi} \int_{-\pi/2}^{+\pi/2} d\beta_W \cos^2\beta_W \left| T_{i\eta}(\omega,\beta) \right|^2 , \qquad \text{(H-4)}$$

where $\beta = \beta_W - \beta_B$, and this energy spectrum will depend upon the angle β_B.

The spectral technique for analyzing random irregular time histories of motion, as embodied in the formulas given above, is applicable to linear systems only, since in that case a unique response amplitude operator is obtained. The spectral techniques used herein follow from linear superposition of the responses to individual frequency components contained in the excitation, and the final synthesis of the effects (in a mean-square sense) is represented by the motion spectrum.

From the spectral density function, $\Phi^{(i,i)}(\omega)$, for a particular motion, there may be obtained, in principle, all the statistical, or probabilistic, properties possessed by the random, or stochastic, process, corresponding to the various possible realizations of the time histories of that motion, induced by the assumed stochastic surface-elevation process. The manner of obtaining certain of these properties is quite direct. For example, the total area, E_i, under the spectral-density function curve, as defined above,

$$E_i = \int_0^\infty d\omega \, \Phi^{(i,i)}(\omega)$$

is equal to $2\sigma_i^2$, i.e. twice the variance of the ordinates on the corresponding time-history curve. Here the ordinate dispersion, or standard deviation, has been denoted by σ_i, which is the root-mean-square value of the deviations of the ordinates from the mean, or average, ordinate. In other words, by analogy, given a time history recorded under temporally-homogeneous conditions, over a long-time interval of length, T, if one sets

$$\mu_i = \frac{1}{T} \int_{-T/2}^{+T/2} dt \, f(t) ,$$

and

$$\sigma_i^2 = \frac{1}{T} \int_{-T/2}^{+T/2} dt \, (f(t) - \mu_i)^2$$

then μ_i and σ_i^2 will correspond to the mean and variance of the ordinates on the time-history curve, $f_i(t)$. The square root, σ_i of the variance is the r.m.s. value of the ordinates, measured from their mean value.

Under the assumption that the seaway is representable by a two-parameter Gaussian, or normal stochastic process which is exciting a linear system (in this case, the barge), the set of responses of the system will in turn constitute a family of time histories representable as a one-parameter vector stochastic process.

In particular, if all measurements are made from mean values, the ordinate on each such time-history curve has a probability density function of the form $p(x) = (\sigma\sqrt{2\pi})^{-1} \exp\left\{-\frac{x^2}{2\sigma^2}\right\}$. The probability of the ordinate lying between the values x_1 and x_2 is given by the definite integral $\int_{x_1}^{x_2} dx (\sigma\sqrt{2\pi})^{-1} \exp\left\{-\frac{x^2}{2\sigma^2}\right\}$. Since $E_i = 2\sigma^2$, it is seen that the area under the spectra-density curve determines the probability distribution completely. Thus, E_i or σ_i may be used to estimate the probability of the occurrence of instantaneous values in any range of interest, for any given barge motion, including infrequently-occurring large or near-maximum values.

In addition, the probability distributions of certain quantities associated with the real-valued envelope of the time-history curve are determined solely by the quantity, E_i. If, for any particular time history, the assumption is justified that the bandwidth of its energy spectrum is small compared to the mean spectral frequency, the probability distribution of the ordinates on this envelope curve may be used to approximate the probability distribution of the amplitudes of the oscillations appearing on the particular time-history curve itself. When a precise meaning for the term "envelope" is supplied, it will be found natural to consider it as corresponding to the instantaneous amplitude of the time-history curve. In the "narrow-band" case, one may employ certain often-used formulas for the mean amplitude of oscillation (one-half the distance measured from the trough to the crest of an oscillation) and for the mean of the highest one-third of such amplitudes (corresponding to one-half of the significant wave height), to estimate such parameters for any particular barge motion. In the case of the motion of sway, for example, these formulas are, respectively,

$$(Y)_{av.} = 0.88\sqrt{E_Y}$$

and

$$(Y)_{sig.} = 1.41\sqrt{E_Y}$$

While a single parameter, such as E_i, serves to specify the probability distribution of instantaneous ordinates or instantaneous amplitudes for an individual time-history curve from a Gaussian stochastic process, the complete description of the distributions of various other quantities of interest, requires a knowledge of certain other parameters. These are also obtainable from the energy spectrum for the time history in question. In particular, the low-order moments of the energy spectrum are known to determine, in addition to the r.m.s. ordinate value, the complete probability distributions of the heights of the actual peaks and troughs on the time-history curve. The mean number of zero-crossings per unit time, for the curve as well as for its slope, are determined by the moments of the energy spectrum as well. By a simple extension of the analysis and computations carried out in the present report, such parameters and probability distributions may be determined. Such additional material serves as an aid in the intuitive interpretation of nature of the time histories of the individual barge motions.

I. General Complex Response Operators and Cross-Spectral Analysis

The difference between the phase of the sinusoidal motion of the barge in response to a regular simusoidal surface-elevation wave and the phase of the wave itself is a function of the wave frequency and the heading of the wave relative to the barge. The complex response operator is formed by combining this phase difference function with the response amplitude operator (amplitude-ratio function). The response amplitude for the i-th barge motion is a complex-valued function, $T_{i\eta}(\omega,\beta)$ of frequency, ω, and the heading, β, of the wave relative to the barge; its modulus, $|T_{i\eta}(\omega,\beta)|$ is the amplitude response operator, and its argument, $Arg\{T_{i\eta}(\omega,\beta)\}$ is the result of subtracting the phase of the wave from that of the barge motion. It is convenient formally to extend the range of definition of each $T_{i\eta}(\omega,\beta)$ to negative frequencies by adopting the formal definition $T_{i\eta}(-\omega,\beta)=T_{i\eta}^{*}(\omega,\beta)$ where the asterisk denotes the complex conjugate.

In order to characterize a set of n barge motions in a random sea, the function which must be found is the $n\times n$ -matrix-valued function of frequency known as the cross-spectral density matrix for the set of motions. For each pair of motions, the corresponding element in this matrix provides complete information concerning the joint probability distributions of the pairs of values taken on by the motions at arbitrarily specified pairs of times. In addition, the cross-spectral matrix function contains information concerning the relative instantaneous amplitudes and phases of the barge motions. For a given barge heading angle, β_B, and a given pair of motions, indexed by the superscripts, r and s, the corresponding element in the cross-spectral matrix, known as the cross-spectral density function for the two motions is given by

$$\Phi^{(r,s)}_{(\beta_B,S)}(\omega)=\int_{-\pi}^{\pi}d\beta_W\,|S(\omega,\beta_W)|^2\,T^{*}_{r\eta}(\omega,\beta)\,T_{s\eta}(\omega,\beta),$$

where $|S(\omega,\beta_W)|^2=|S(-\omega,\beta_W|^2$ denotes the directional energy spectrum of the seaway. Here the symbol "β" designates, as before, the heading of the wave relative to the barge, i.e. $\beta_W-\beta_B$.

The bilateral complex Fourier transform of $\Phi^{(r,s)}_{(\beta_B,S)}(\omega)$ given for any time lag τ, by

$$\varphi^{(r,s)}_{(\beta_B,S)}(\tau)=\int_{-\infty}^{+\infty}d\omega\,e^{i\omega\tau}\,\Phi^{(r,s)}_{(\beta_B,S)}(\omega)$$

$$=\int_{-\infty}^{+\infty}d\omega\,e^{i\omega\tau}\int_{-\pi}^{+\pi}d\beta_W\,|S(\omega,\beta_W)|^2\,T^{*}_{r\eta}(\omega,\beta)\,T_{s\eta}(\omega,\beta),$$

is known as the cross-covariance function for the motion-pair. Its value for $\tau=0$, namely, $\varphi^{(r,s)}_{(\beta_B,S)}(0)=\int_{-\infty}^{\infty}d\omega\int_{-\pi}^{+\pi}d\beta_W\,|S(\omega,\beta_W)|^2\,T^{*}_{r\eta}(\omega,\beta)\,T_{s\eta}(\omega,\beta)$, reduces, in the case of an auto-covariance (i.e., r=s) to the variance

$$\varphi^{(r,r)}_{(\beta_B,S)}(0)=\int_{-\infty}^{+\infty}d\omega\int_{-\pi}^{+\pi}d\beta_W\,|S(\omega,\beta_W)|^2\,|T_{r\eta}(\omega,\beta)|^2=\int_{-\infty}^{+\infty}d\omega\,\Phi^{(r,r)}_{(\beta_B,S)}(\omega),$$

which is the total spectral energy for the r-th barge motion.

Similarly, the cross-spectral density function for the surface elevation time history, η , and the s-th barge motion is given by

$$\Phi^{(n,s)}_{(\beta_B,S)}(\omega) = \int_{-\pi}^{+\pi} d\beta_w |S(\omega,\beta_w)|^2 T^{*}_{\eta\eta}(\omega,\beta) T_{s\eta}(\omega,\beta) = \int_{-\pi}^{+\pi} d\beta_w |S(\omega,\beta_w)|^2 T_{s\eta}(\omega,\beta),$$

since the complex response operator, $T_{\eta\eta}(\omega,\beta)$, is unity for all ω and β . Further, we have for the cross-spectral density for the surface elevation and itself, i.e., the spectral energy density for η ,

$$\Phi^{(n,n)}_{(\beta_B,S)}(\omega) = \Phi^{(n,n)}_{(S)}(\omega) = \int_{-\pi}^{+\pi} d\beta_w |S(\omega,\beta_w)|^2,$$

which is independent of the barge heading angle, β_B .

Finally, we see that the variance of the surface elevation becomes

$$\sigma^2_{\eta(S)} = \varphi^{(n,n)}_{(S)}(0) = \int_{-\infty}^{+\infty} d\omega\, \Phi^{(n,n)}_{(S)}(\omega) = \int_{-\infty}^{+\infty} d\omega \int_{-\pi}^{+\pi} d\beta_w |S(\omega,\beta)|^2,$$

the total spectral energy for the surface elevation.

The particular choice of $A^2(\omega,\beta)/4$ for the directional spectrum, $|S(\omega,\beta)|^2$, for the seaway leads to

$$\sigma^2_{\eta}(A/4) = \int_0^{+\infty} d(\omega)\, A^2(\omega,\beta)/2$$

$$\Phi^{(n,n)}_{(A/4}(\omega) = \int_{-\pi/2}^{+\pi/2} d\beta\, A^2(\omega,\beta)/4 = A^2(\omega)/4$$

and

$$\sigma^2_{\eta(A/4)} = \varphi^{(n,n)}_{(A/4)}(0) = \int_{-\infty}^{+\infty} d\omega\, A^2(\omega)/4 = \tfrac{1}{2}\int_0^{\infty} d\omega\, A^2(\omega) = \tfrac{1}{2} E_{\eta}.$$

Consequently, the use of $A^2(\omega,\beta)/2$ in place of $A^2(\omega,\beta)/4$ is appropriate if one wishes to obtain the variance of the surface-elevation time history as the result of integrating a density function over the interval $(-\infty, +\infty)$.

REFERENCES (in Appendix)

1. St. Denis, M. and Craven, J. P.: "Recent Contributions under the Bureau of Ships Fundamental Hydromechanics Research Program: Part 3-Control", Journal of Ship Research, Vol. 2, No. 3, December 1958.

2. St. Denis, M. and Pierson, W. J.: "On the Motions of Ships in Confused Seas", Trans. SNAME, Vol. 61, 1953.

3. Kaplan, Paul: "Application of Slender-Body Theory to the Forces Acting on Submerged Bodies and Surface Ships in Regular Waves", Journal of Ship Research, Vol. 1, No. 3, November 1957.

4. Grim, O.: "Die Schwingungen von schwimmenden, zweidimensionalen Korpern", Hamburgische Schiffbau-Versuchsanstalt Gesellschaft Rpt No. 1172, September 1959.

5. Lewis, F. M.: "The Inertia of the Water Surrounding a Vibrating Ship", Trans. SNAME, Vo. 37, 1929.

6. Kaplan, Paul and Hawley, John K.: "Theoretical Analysis of the Motions of a Submerged Submarine Hovering Under Waves", Technical Research Group, Inc. Rpt TRG-137-Fr-1, March 1961. CONFIDENTIAL.

7. Prohaska, C. W.: "The Vertical Vibration of Ships", The Shipbuilder and Marine Engine-Builder, Oct. -Nov. 1947.

8. Kaplan, Paul and Ule, Stanley: "A Dimensional Method for Calculating Lateral Bending Moments on Ships in Oblique Waves", Technical Research Group Inc., Rpt TRG-147-SR-1, November 1961.

9. Hu, Pung Nien: "Lateral Forces and Moments on Ships in Oblique Waves", Stevens Institute of Technology, Davidson Laboratory Report 831, June 1961.

10. Holstein, H.: "Untersuchungen an einem Tauchschwingungen Ausführenden Quader", Werft-Reederei-Hafen, Dec. 1, 1936, pp. 385-389.

11. Grim, O.: "Berechnung der durch schwingungen eines Schiffskorper erzeugten hydrodynamischen Krafte", Jahrbuch der Schiffbautechnischen Gesellschaft 47, Band 1953, pp. 277-299.

12. Grim, O.: "The Hydrodynamic Forces in Roll Research", originally Schiffstechnik, Feb. 1956: translated Stevens Institute of Technology, Davidson Laboratory Note 533, May 7, 1959.

13. Vossers, G.: "Fundamentals of the Behavior of Ships in Waves", International Shipbuilding Progress, Vol. 7, No. 65, Jan. 1960.

14. Havelock, T.H.: "The Damping of Heave and Pitch: A Comparison of Two-Dimensional and Three-Dimensional Calculations", Trans. INA, Vol. 98, No. 4, October 1956.

15. Hu, Pung Nien and Kaplan, Paul: "On the Lateral Damping Coefficients of Submerged Slender Bodies of Revolution", Stevens Institute of Technology, Davidson Laboratory Report 830, Feb. 1962.

16. Technical Memorandum containing information concerning "CUSS I", supplied by U. S. Naval Civil Engineering Laboratory, Pt. Hueneme, California, August, 1961.

17. Newman, J.N.: "The Damping of an Oscillating Ellipsoid Near a Free Surface", Journal of Ship Research, Vol. 5, No. 3, Dec. 1961.

18. Deep sea mooring plan and typical mooring legs, and deep sea mooring details, U. S. Navy, Bureau of Yards & Docks, Dwgs. Nos. 896131, 896132, June 1961.

19. Wiegel, R. L., Beebe, K., and Dilley, R. A.: "Model Studies of an LSM Moored in Waves", Proc. of the Sixth Coastal Engineering Conference, Univ. of California, Berkeley, California, 1958.

20. Kaplan, Paul and Hu, Pung Nien: "Virtual Mass and Slender Body Theory for Bodies in Waves", Proc. of the Sixth Midwest Conference on Fluid and Solid Mechanics, Univ. of Texas, February 1959.

21. Korvin-Kroukovsky, B.V. and Jacobs, W.R.: "Pitching and Heaving Motions of a Ship in Regular Waves", Trans. SNAME, Vol 65, 1957.

22. Vossers, G.: "Some Applications of the Slender Body Theory in Ship Hydrodynamics", Doctoral Dissertation, Delft University, Delft The Netherlands, Published by H. Veenman & Zonen, N.V., 1962.

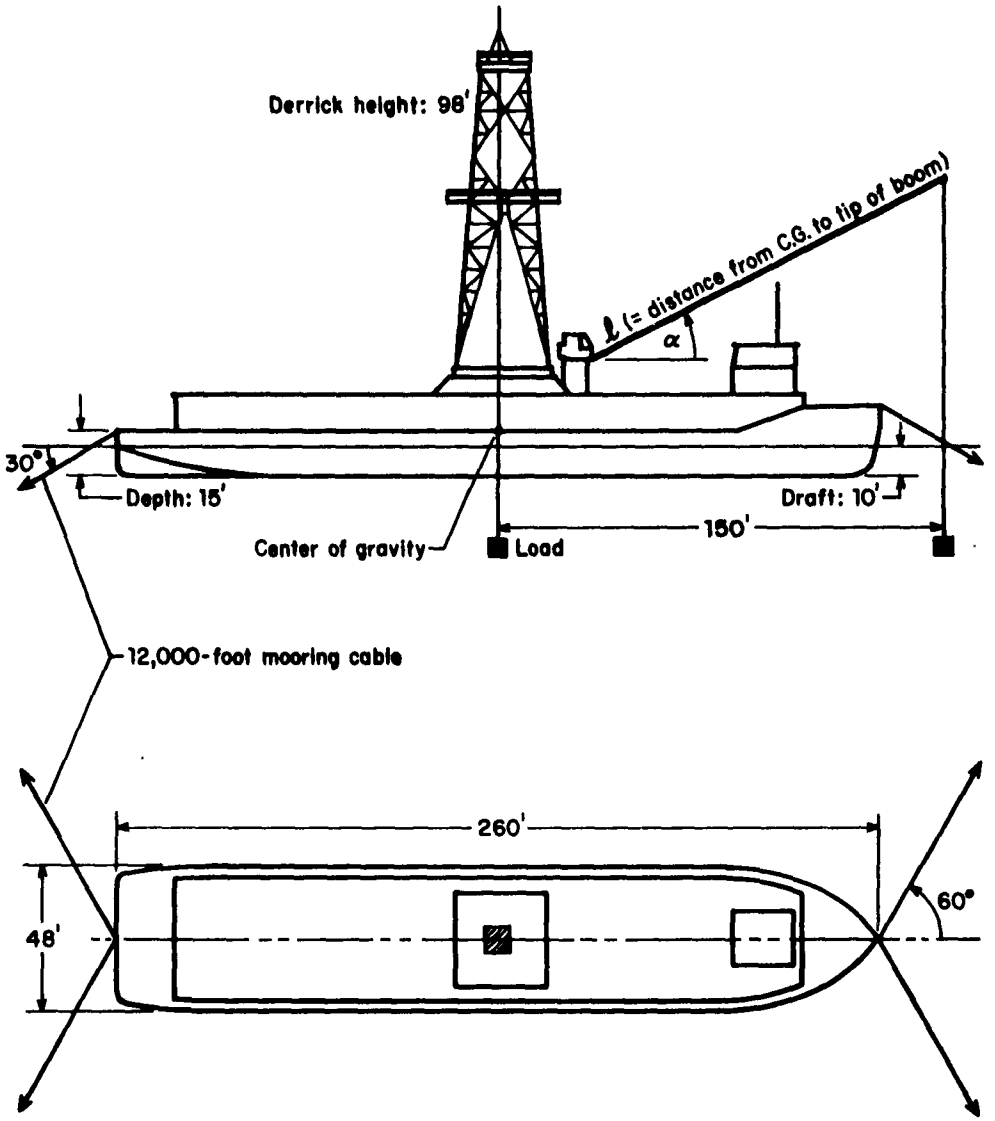

Fig. 1.1
Schematic diagram of moored barge
(Profile and plan views)

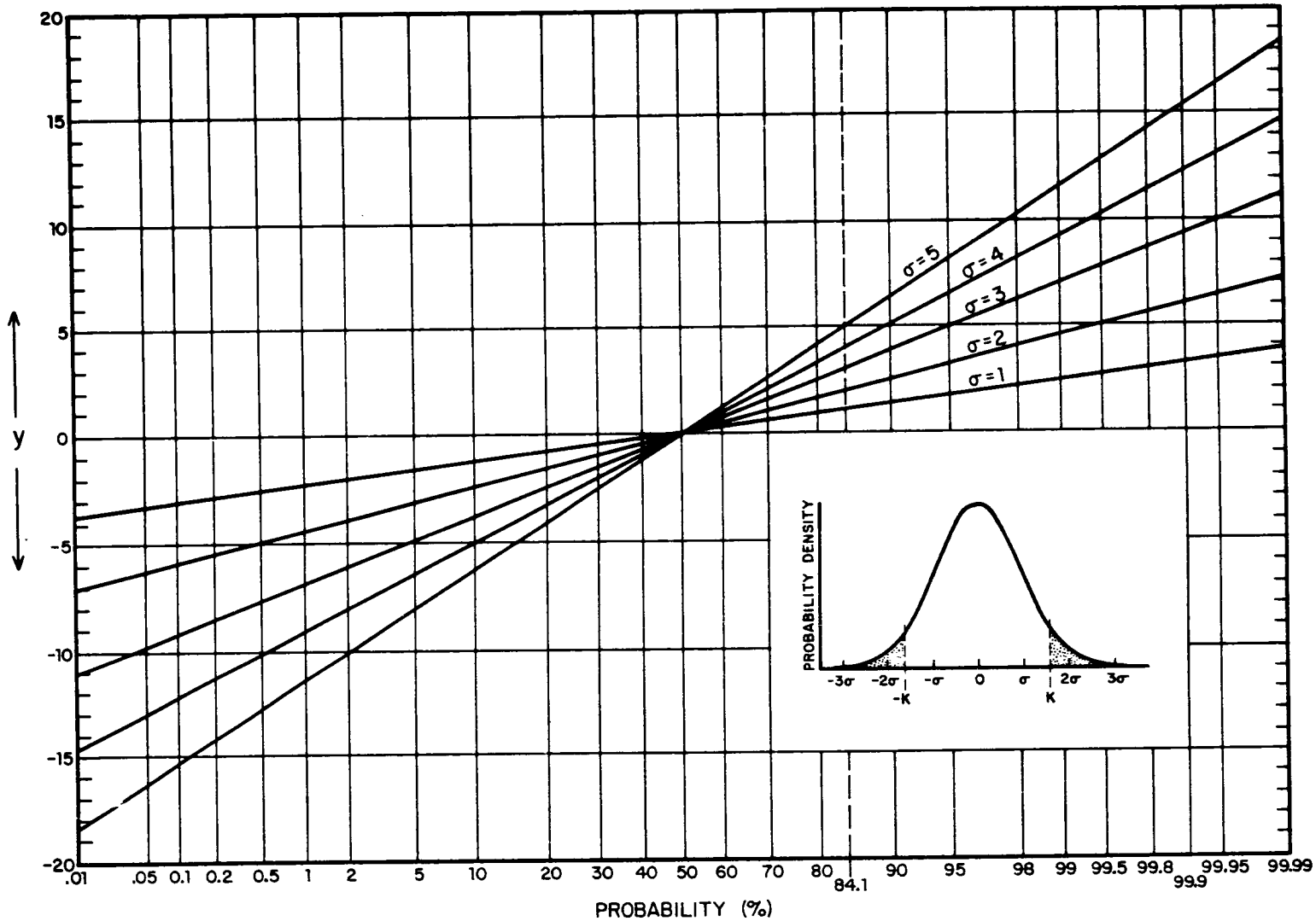

Fig. 2.1
Cumulative normal (Gaussian) probability distribution with zero mean for various RMS values

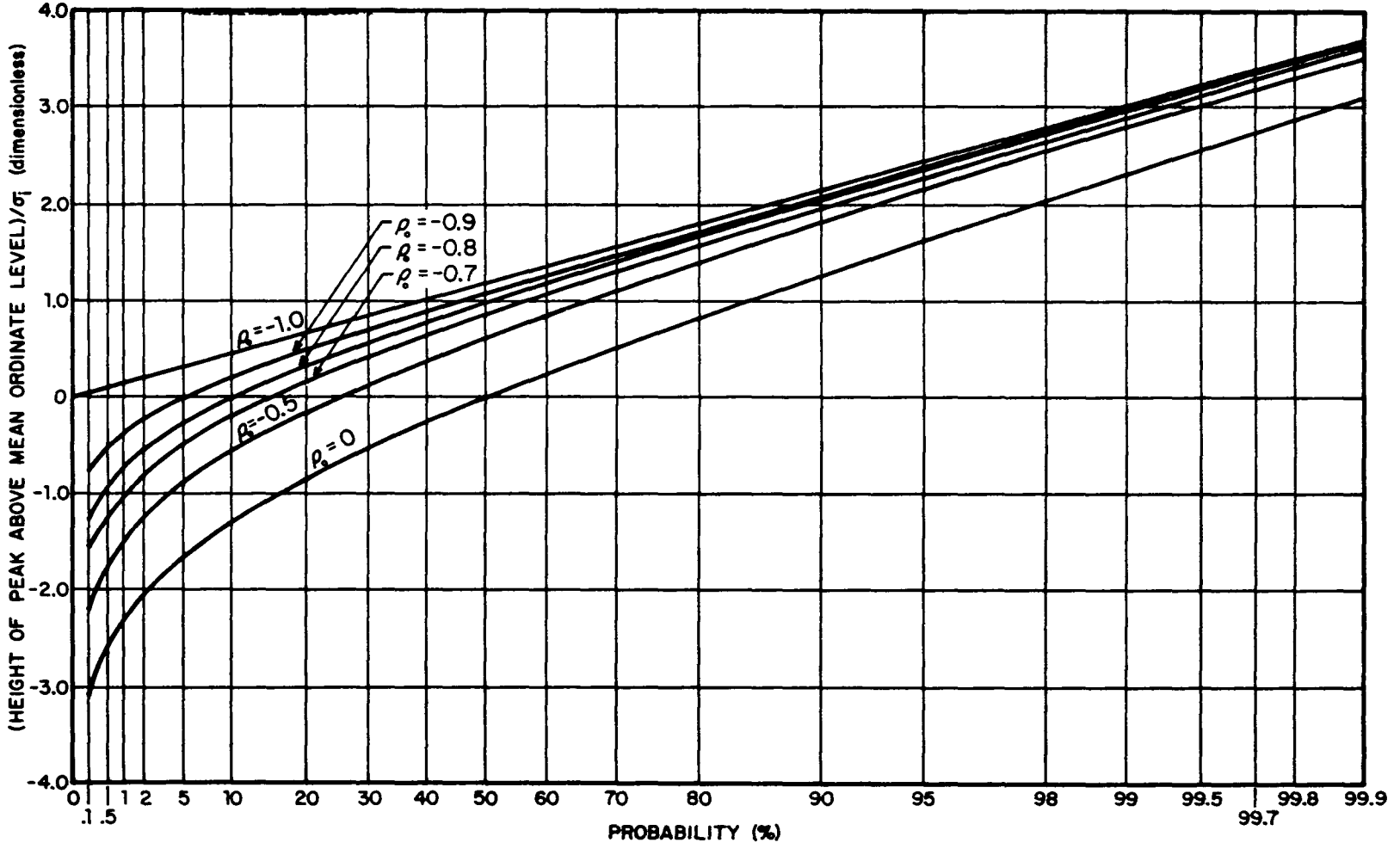

Fig. 2.2
Cumulative probability distribution of peak heights of oscillation for various values of ρ .

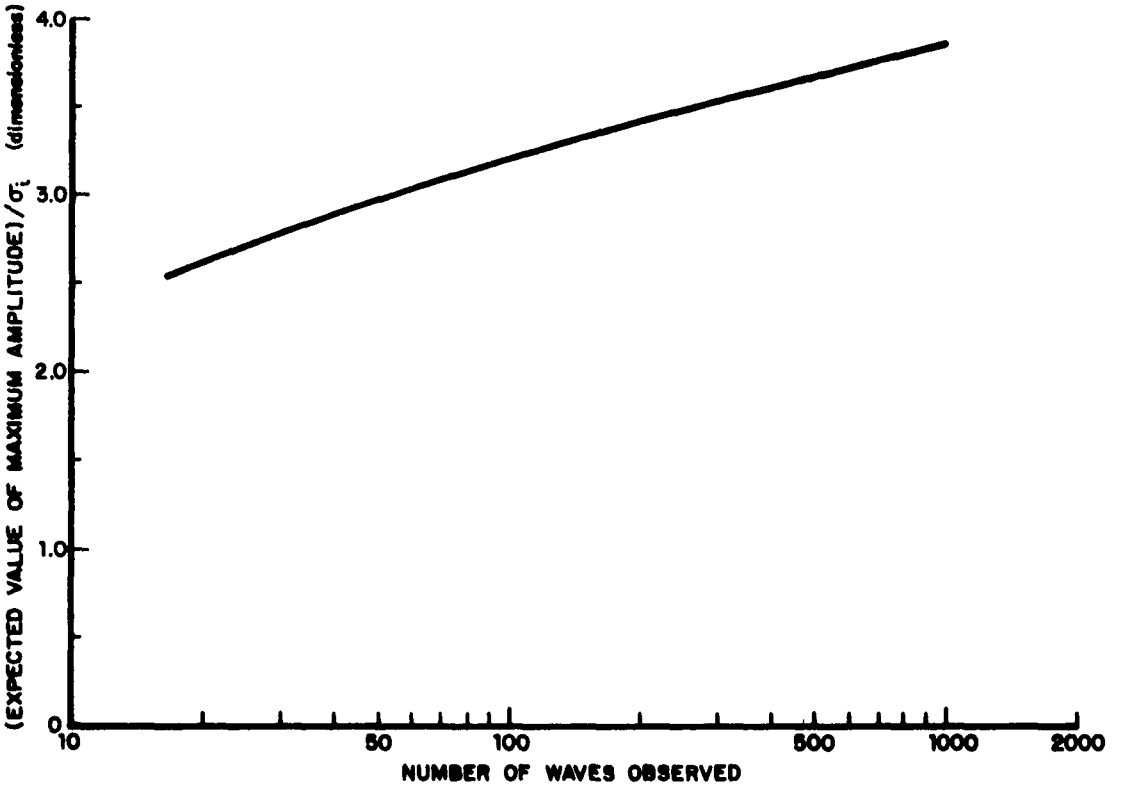

Fig. 2.3
Expected relative value of maximum wave height for various numbers of waves

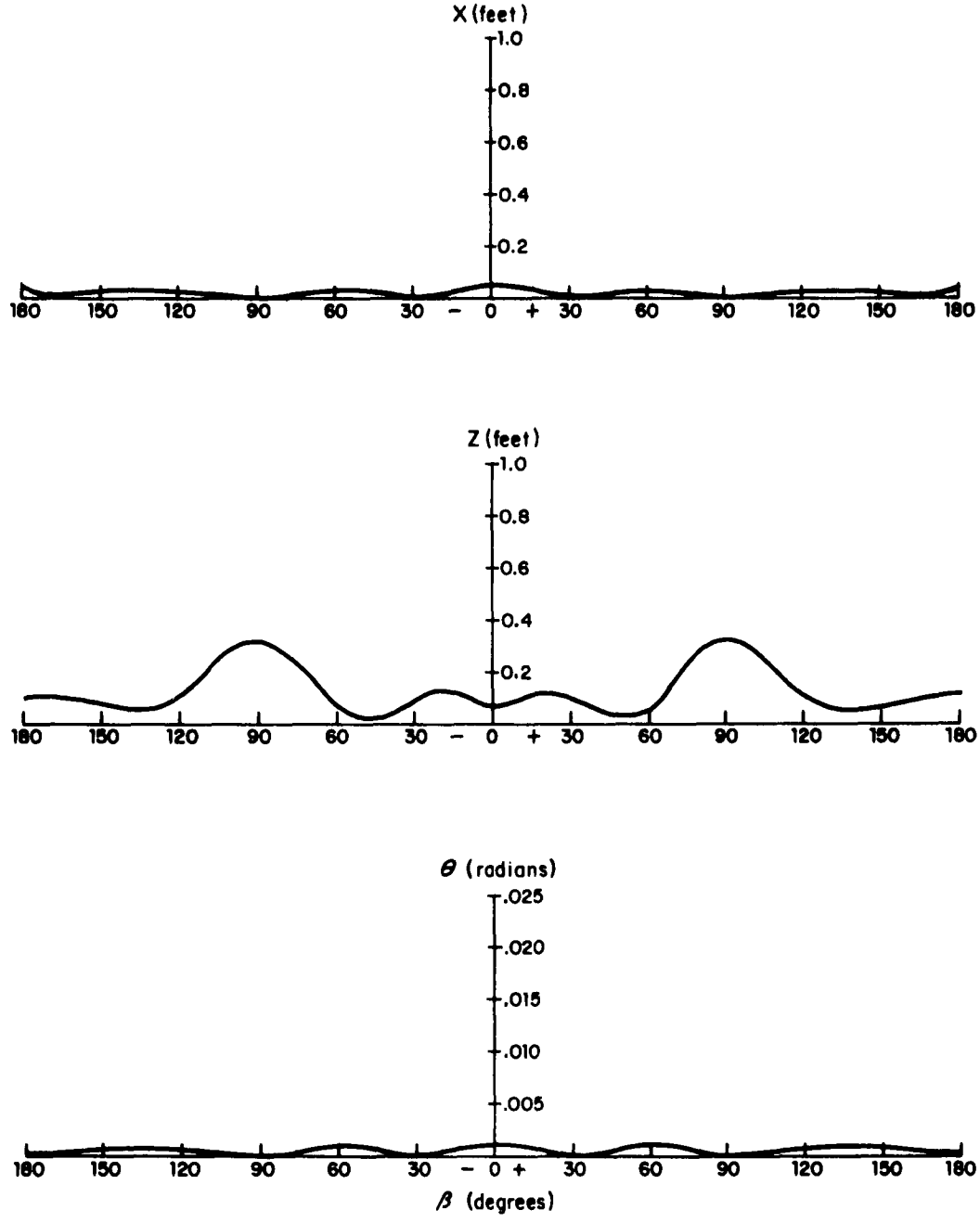

Figure 3.1
Amplitude of response for unit-amplitude wave as a function of direction of wave relative to barge
Longitudinal motion; $\lambda = 100'$

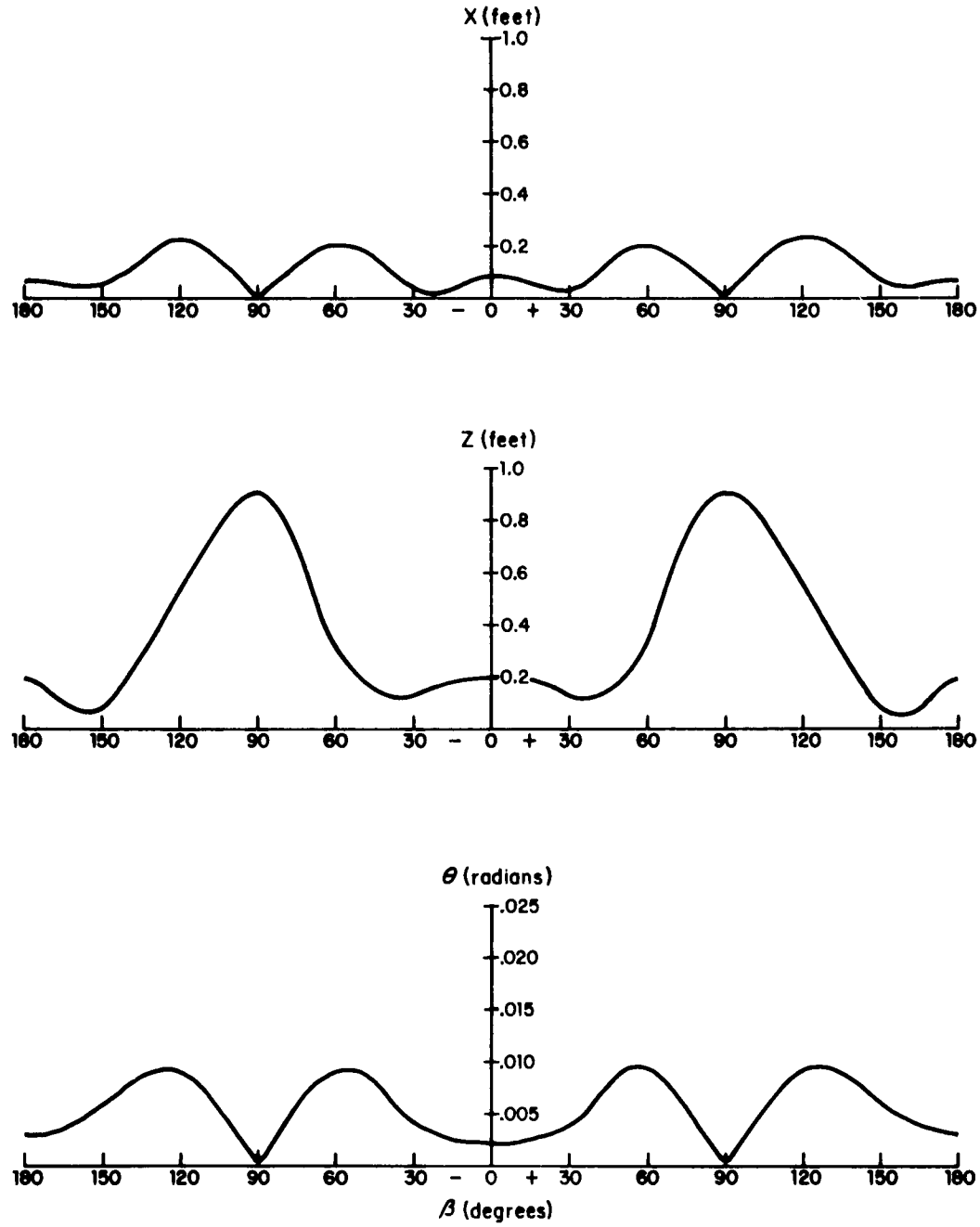

Figure 3.2
Amplitude of response for unit-amplitude wave as a function of direction of wave relative to barge
Longitudinal motion; $\lambda = 200'$

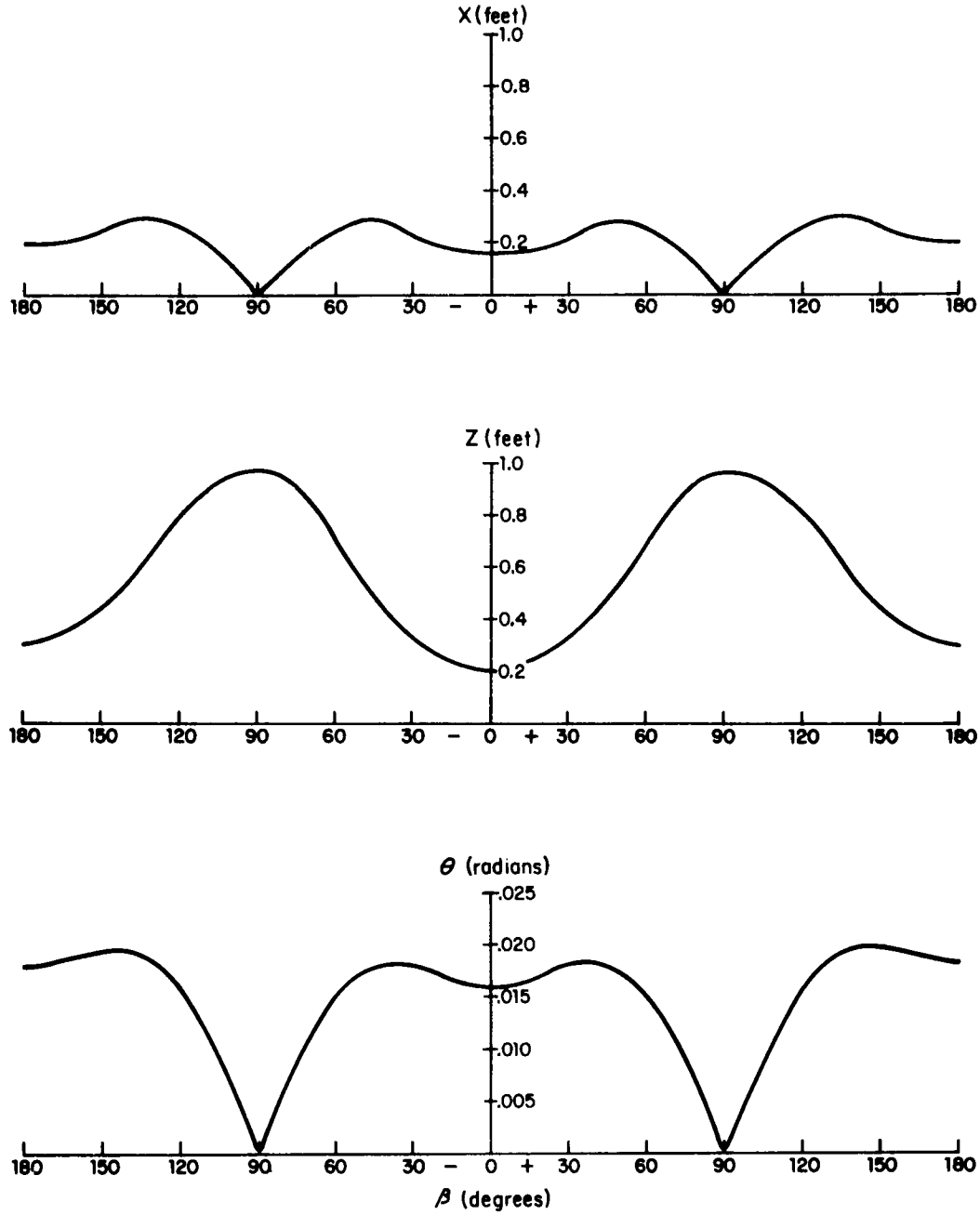

Figure 3.3
Amplitude of response for unit-amplitude wave as a function of direction of wave relative to barge
Longitudinal motion; $\lambda = 300'$

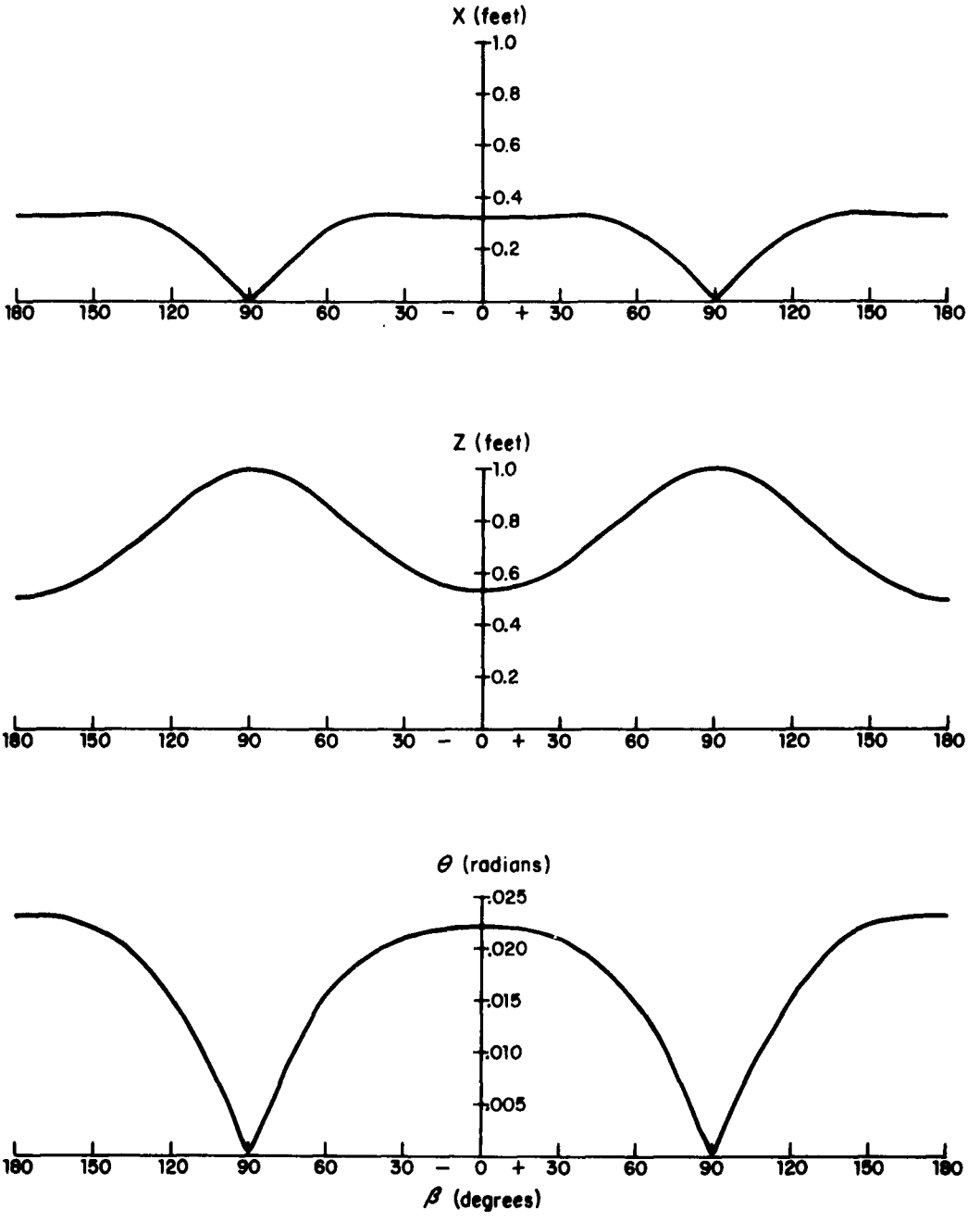

Figure 3.4
Amplitude of response for unit-amplitude wave as a function of direction of wave relative to barge
Longitudinal motion; $\lambda = 400'$

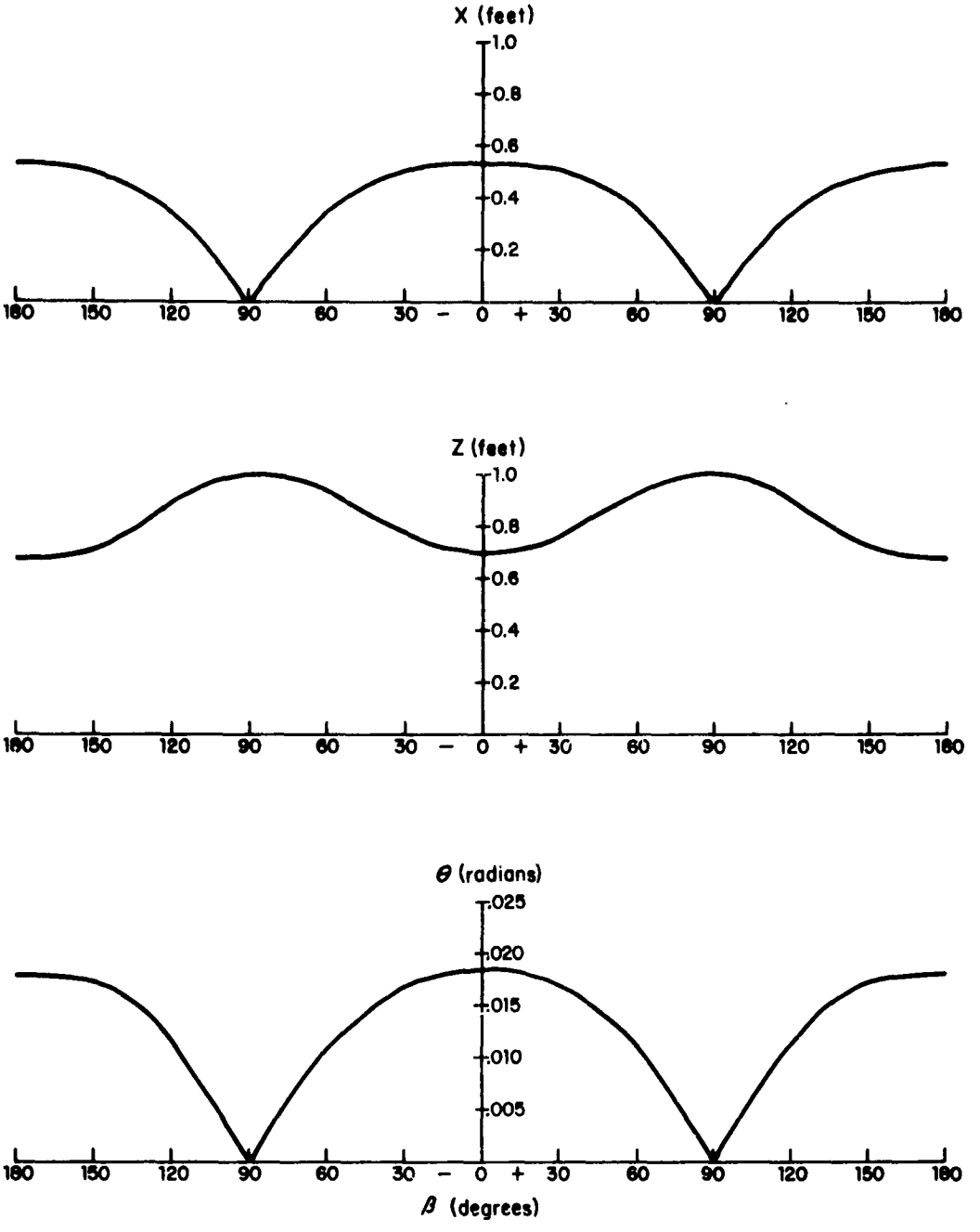

Figure 3.5
Amplitude of response for unit-amplitude wave as a function of direction of wave relative to barge
Longitudinal motion; $\lambda = 500'$

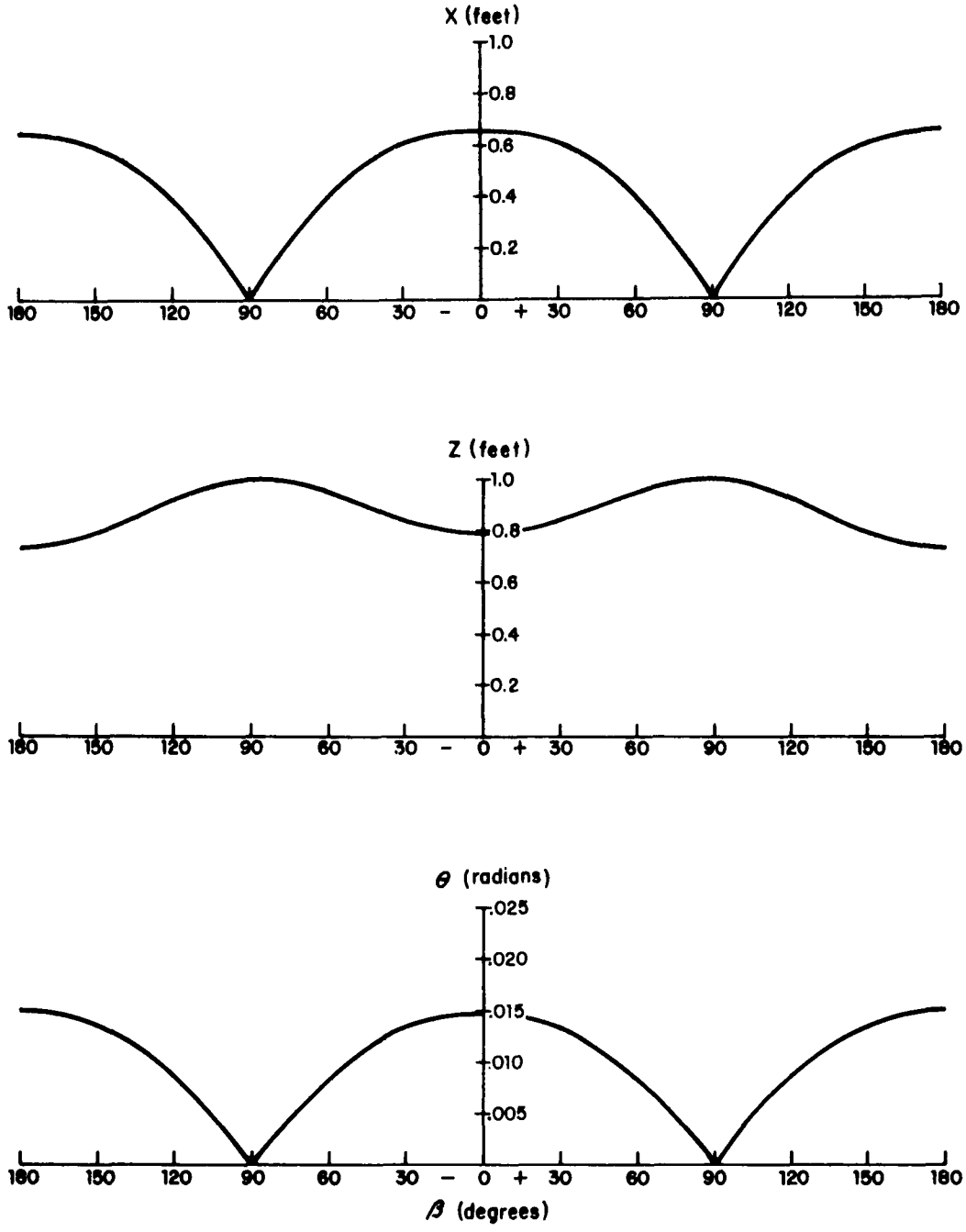

Figure 3.6
Amplitude of response for unit-amplitude wave as a function of direction of wave relative to barge
Longitudinal motion; $\lambda = 600'$

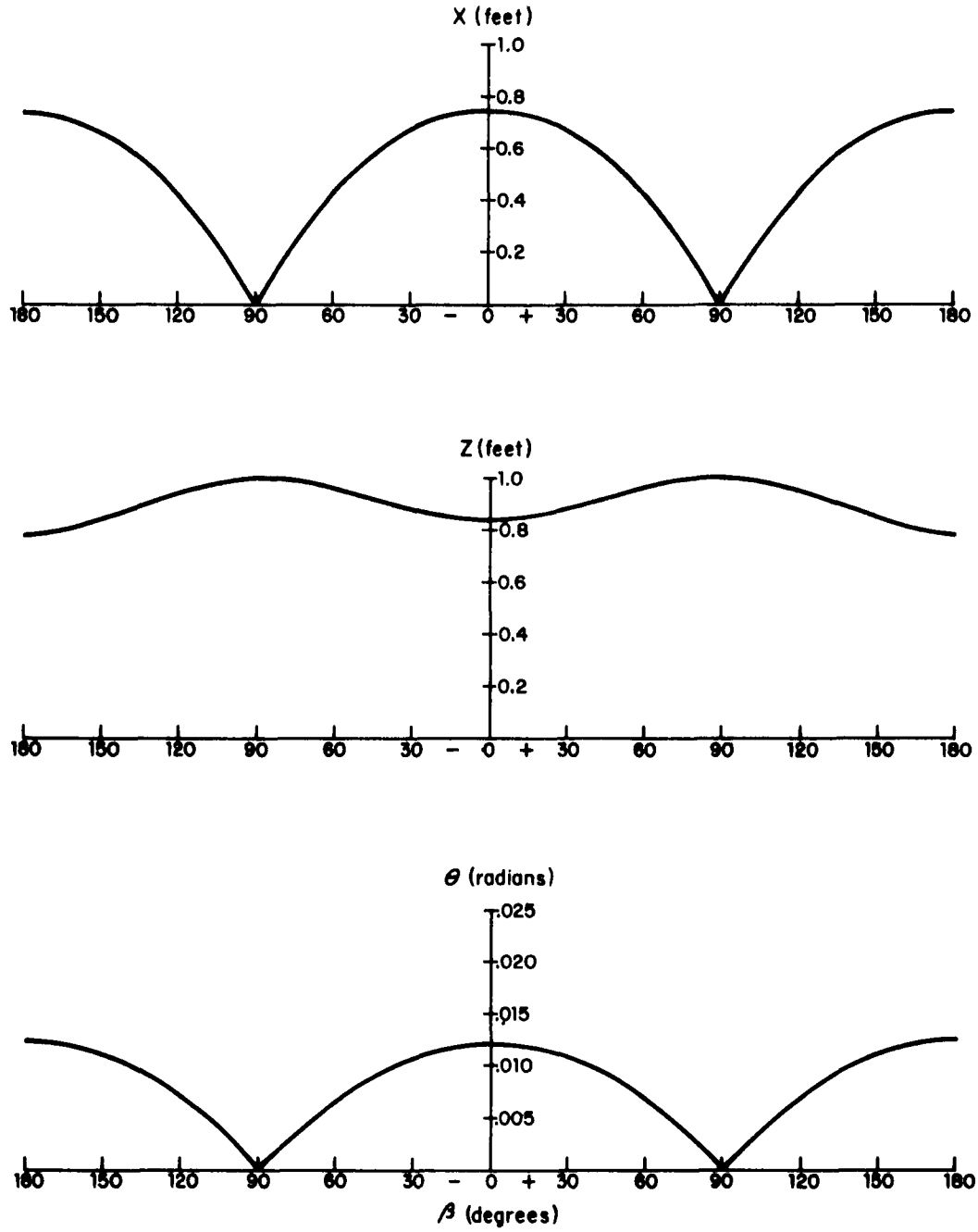

Figure 3.7
Amplitude of response for unit-amplitude wave as a function of direction of wave relative to barge
Longitudinal motion; $\lambda = 700'$

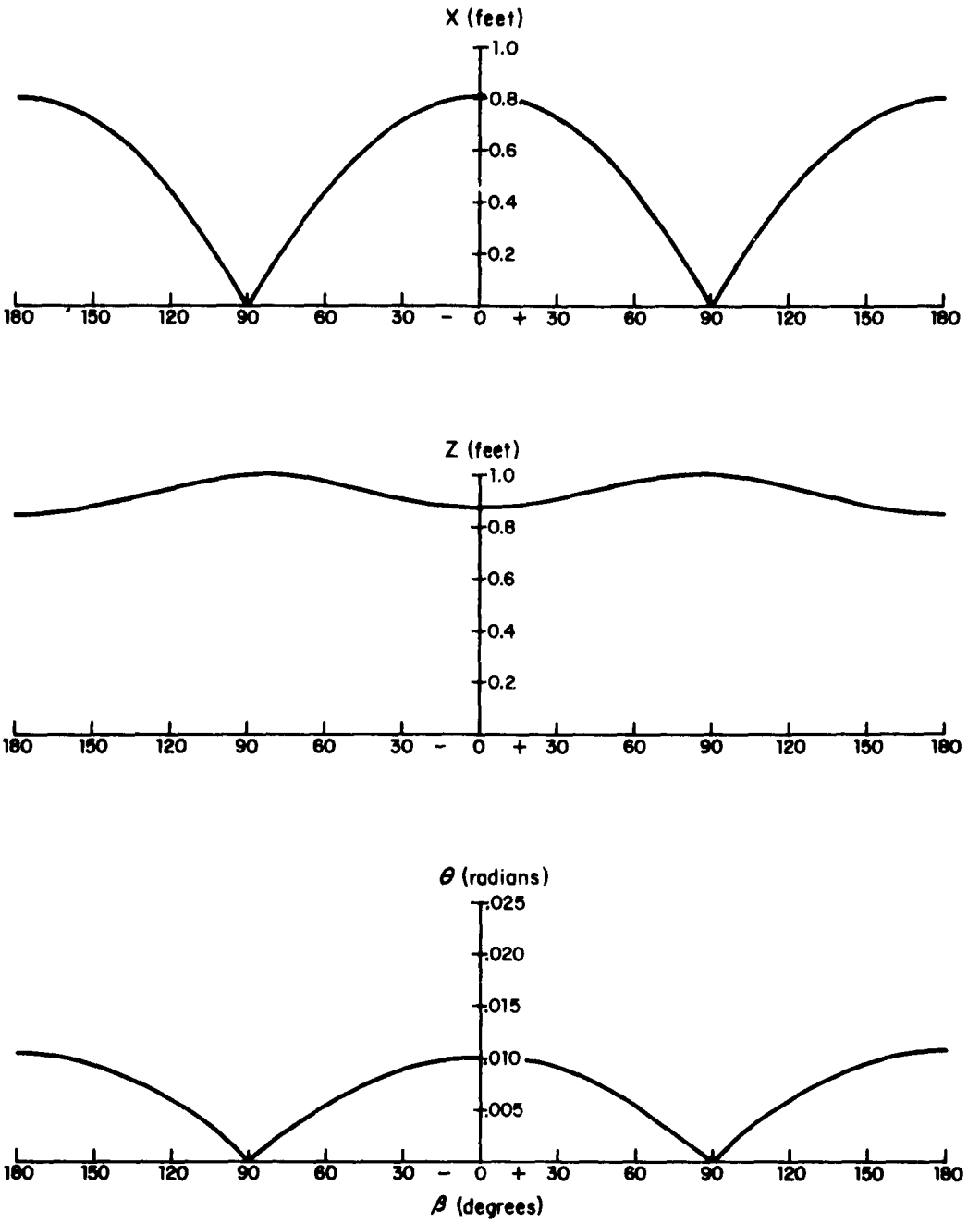

Figure 3.8
Amplitude of response for unit-amplitude wave as a function of direction of wave relative to barge
Longitudinal motion; $\lambda = 800'$

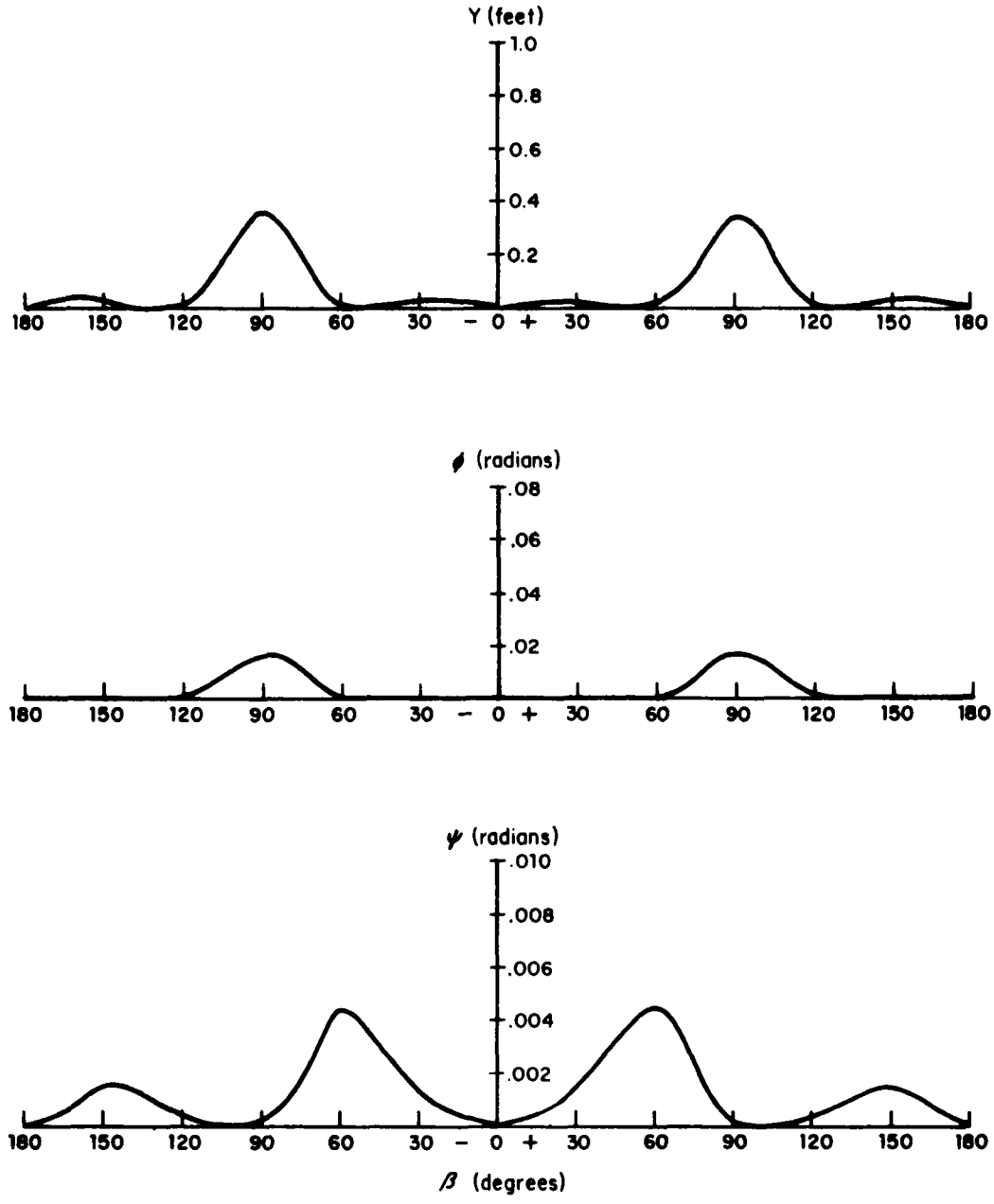

Figure 3.9
Amplitude of response for unit-amplitude wave as a function of direction of wave relative to barge
Lateral motion; $\lambda = 100'$

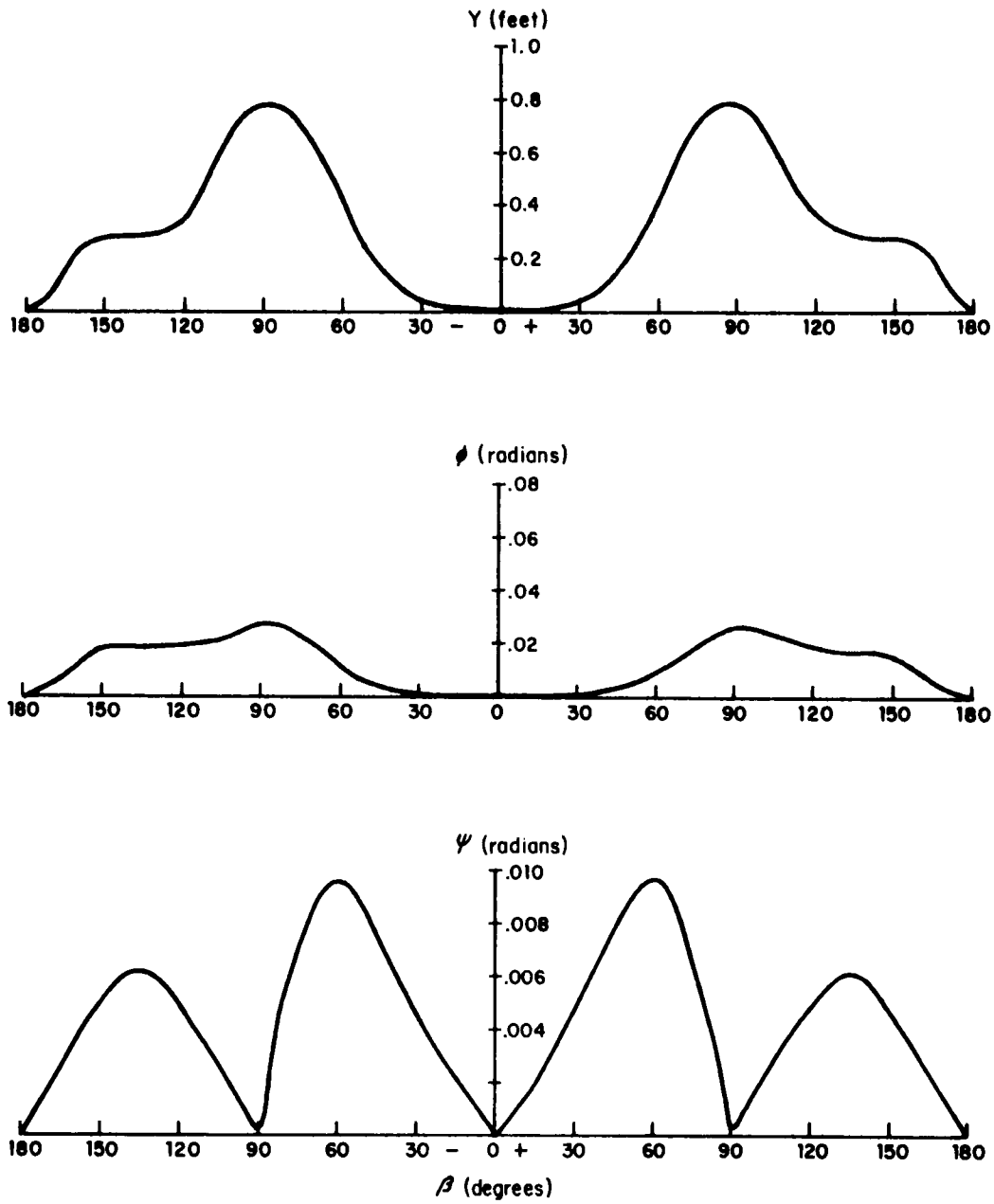

Figure 3.10
Amplitude of response for unit-amplitude wave as a function of direction of wave relative to barge
Lateral motion; $\lambda = 200'$

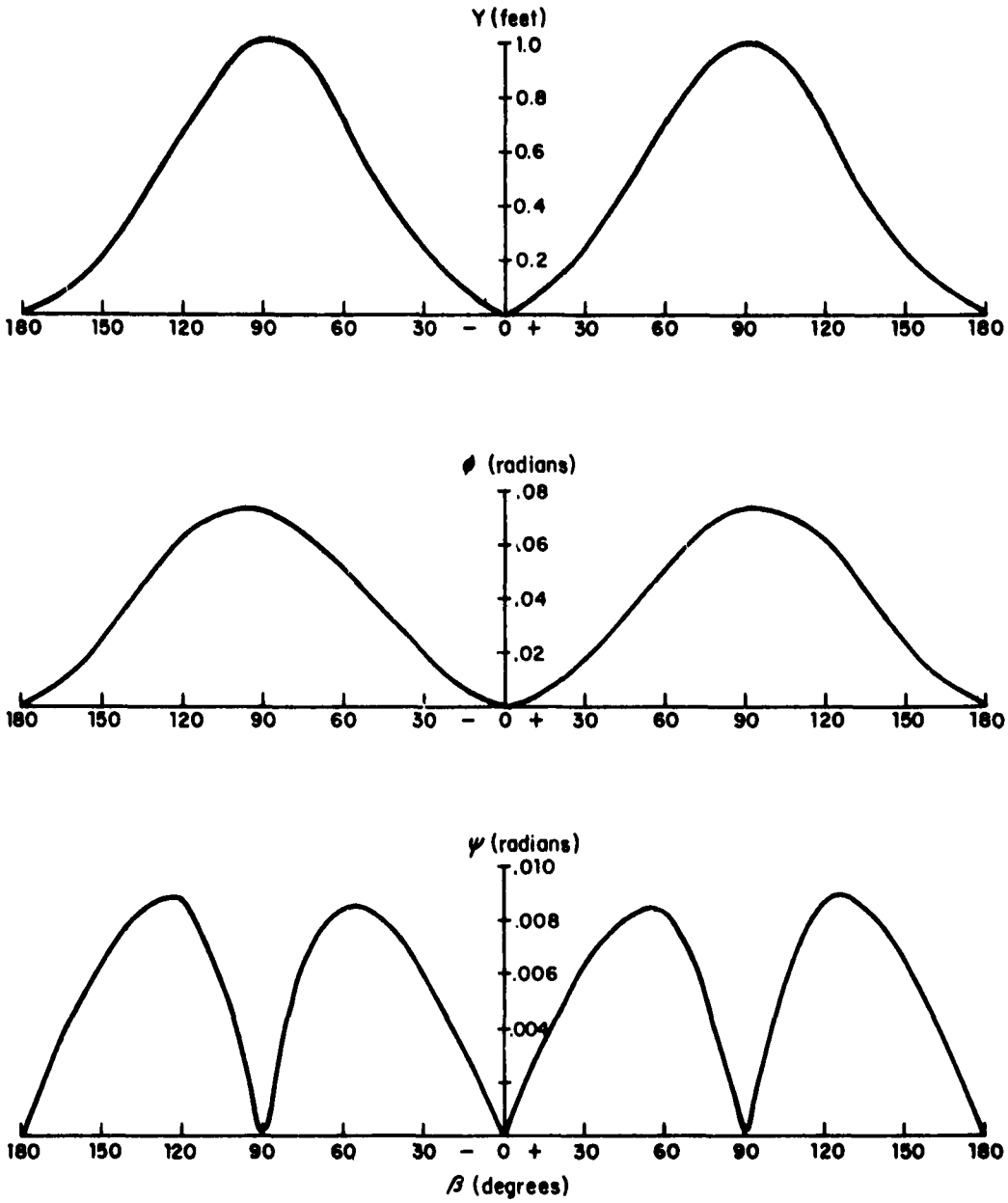

Figure 3.11
Amplitude of response for unit-amplitude wave as a function of direction of wave relative to barge
Lateral motion; $\lambda = 300'$

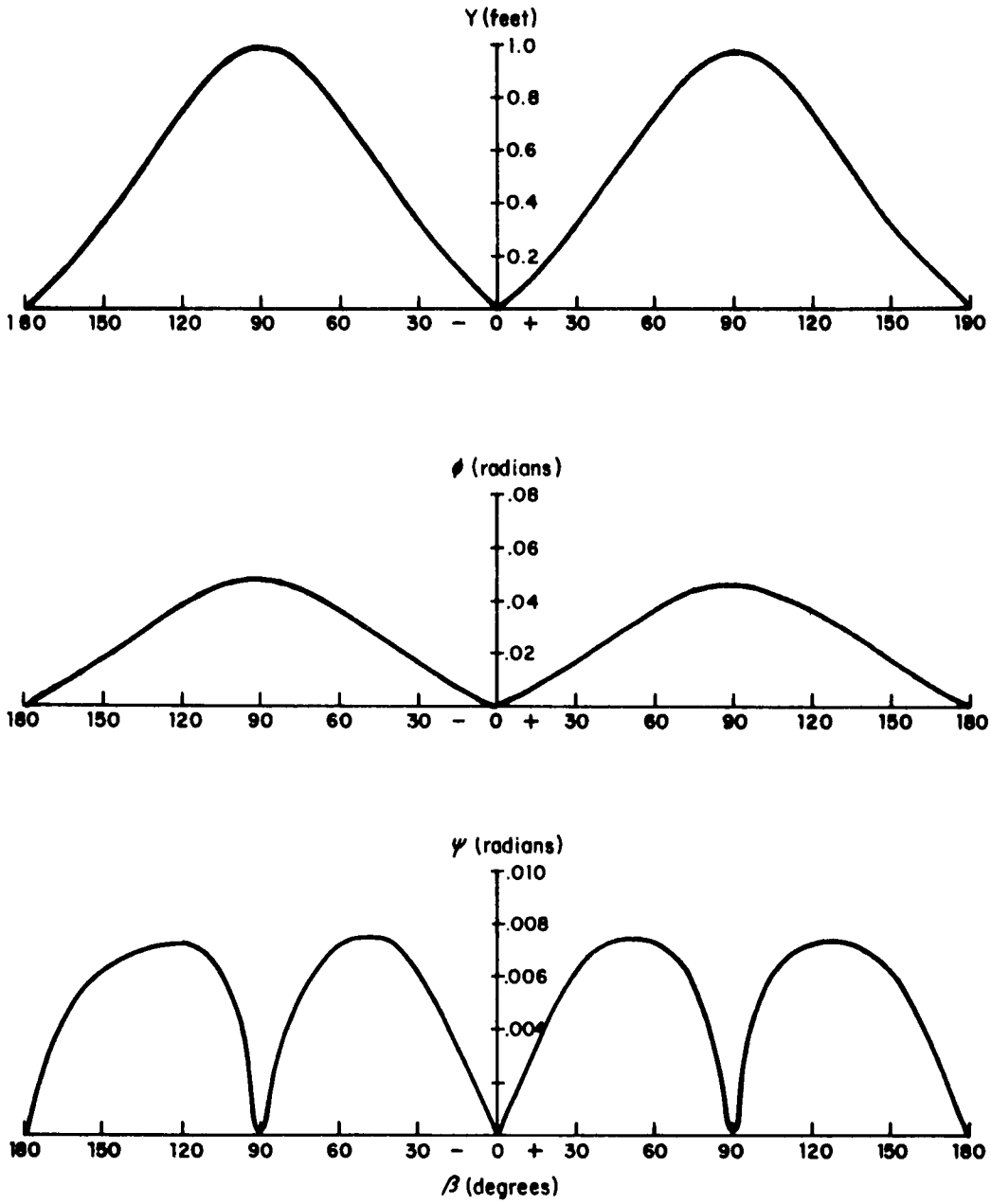

Figure 3.12
Amplitude of response for unit-amplitude wave as a function of direction of wave relative to barge
Lateral motion; $\lambda = 400'$

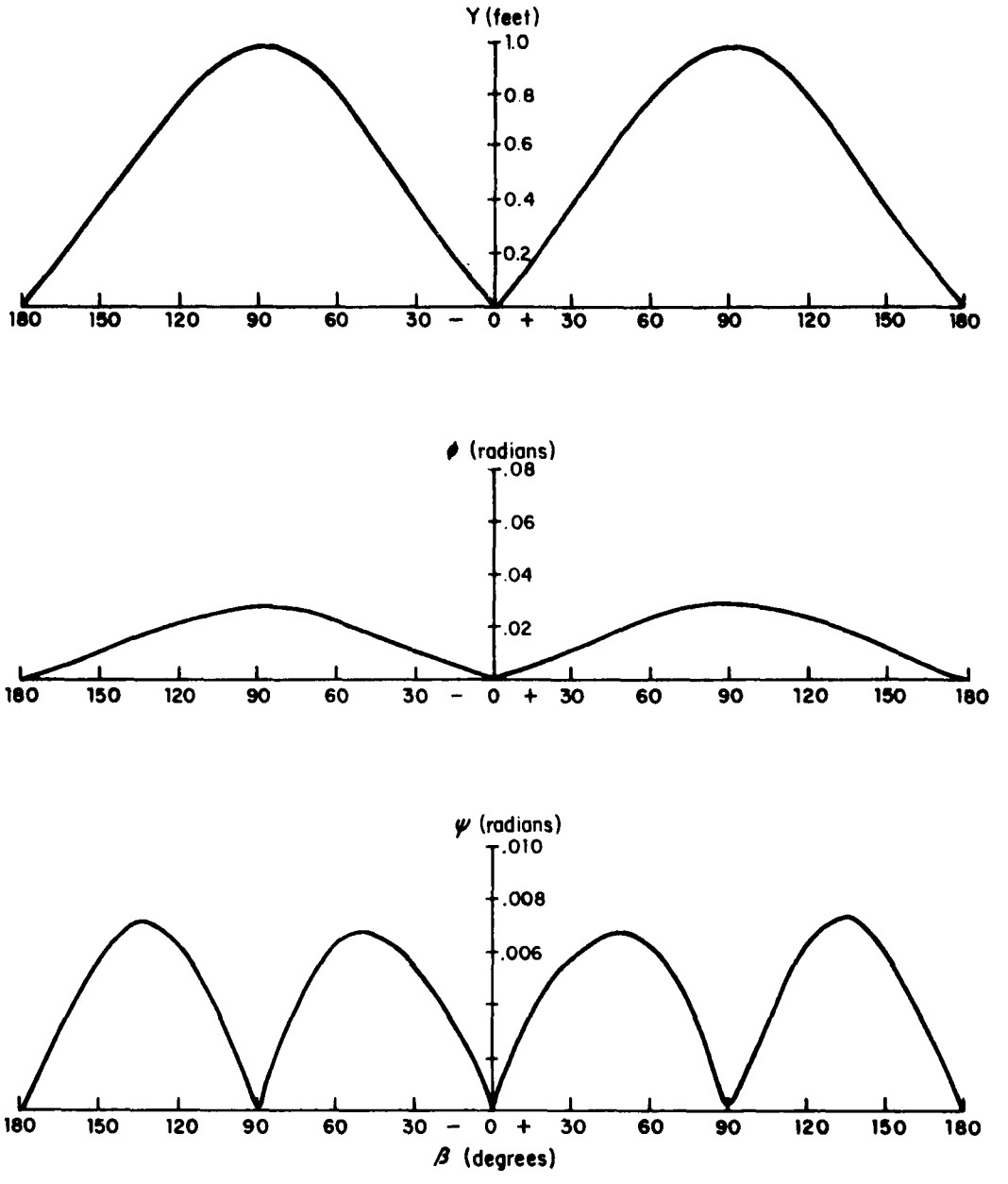

Figure 3.13
Amplitude of response for unit-amplitude wave as a function of direction of wave relative to barge
Lateral motion; $\lambda = 500'$

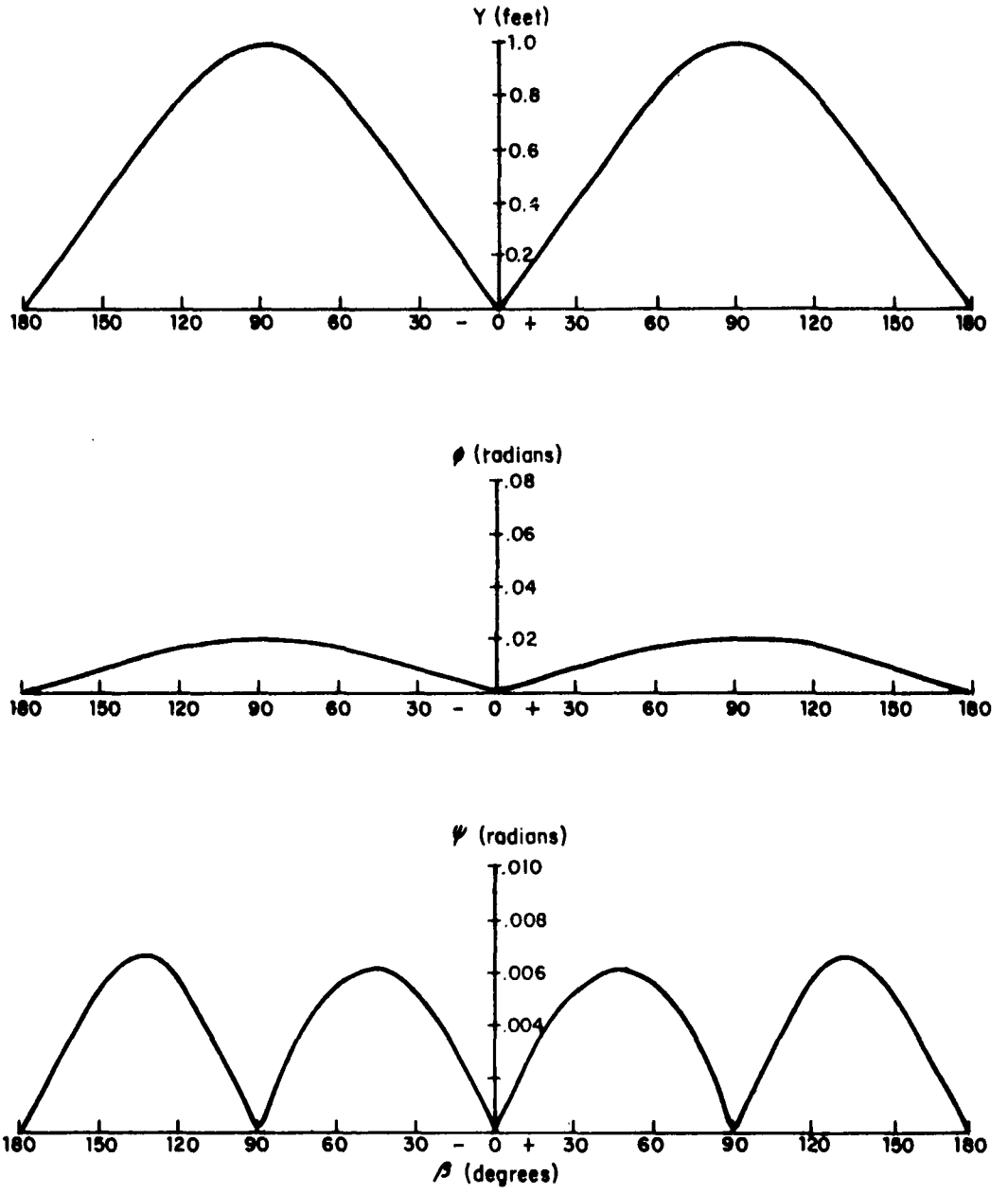

Figure 3.14
Amplitude of response for unit-amplitude wave as a function of direction of wave relative to barge
Lateral motion; $\lambda = 600'$

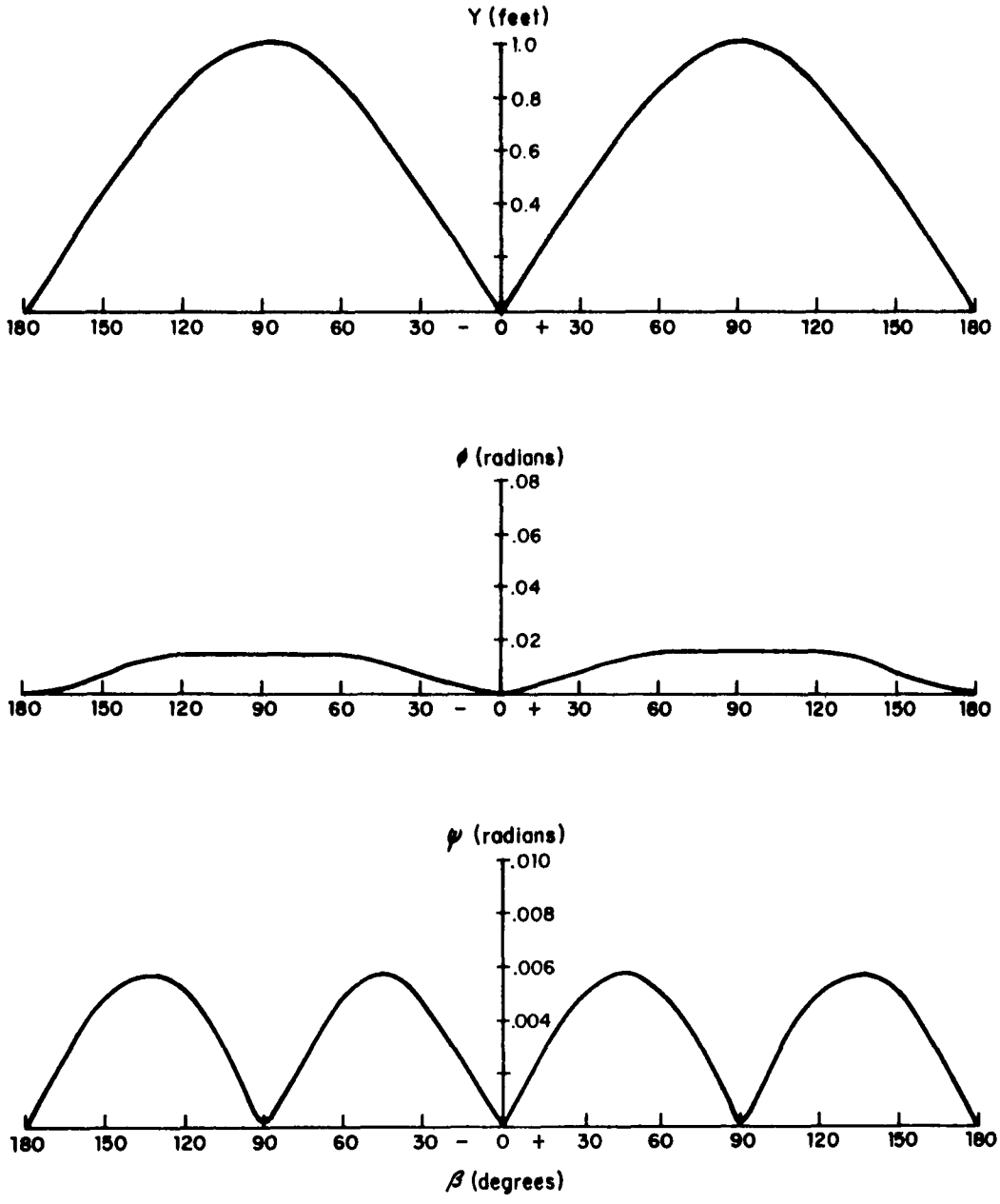

Figure 3.15
Amplitude of response for unit-amplitude wave as a function of direction of wave relative to barge
Lateral motion; $\lambda = 700'$

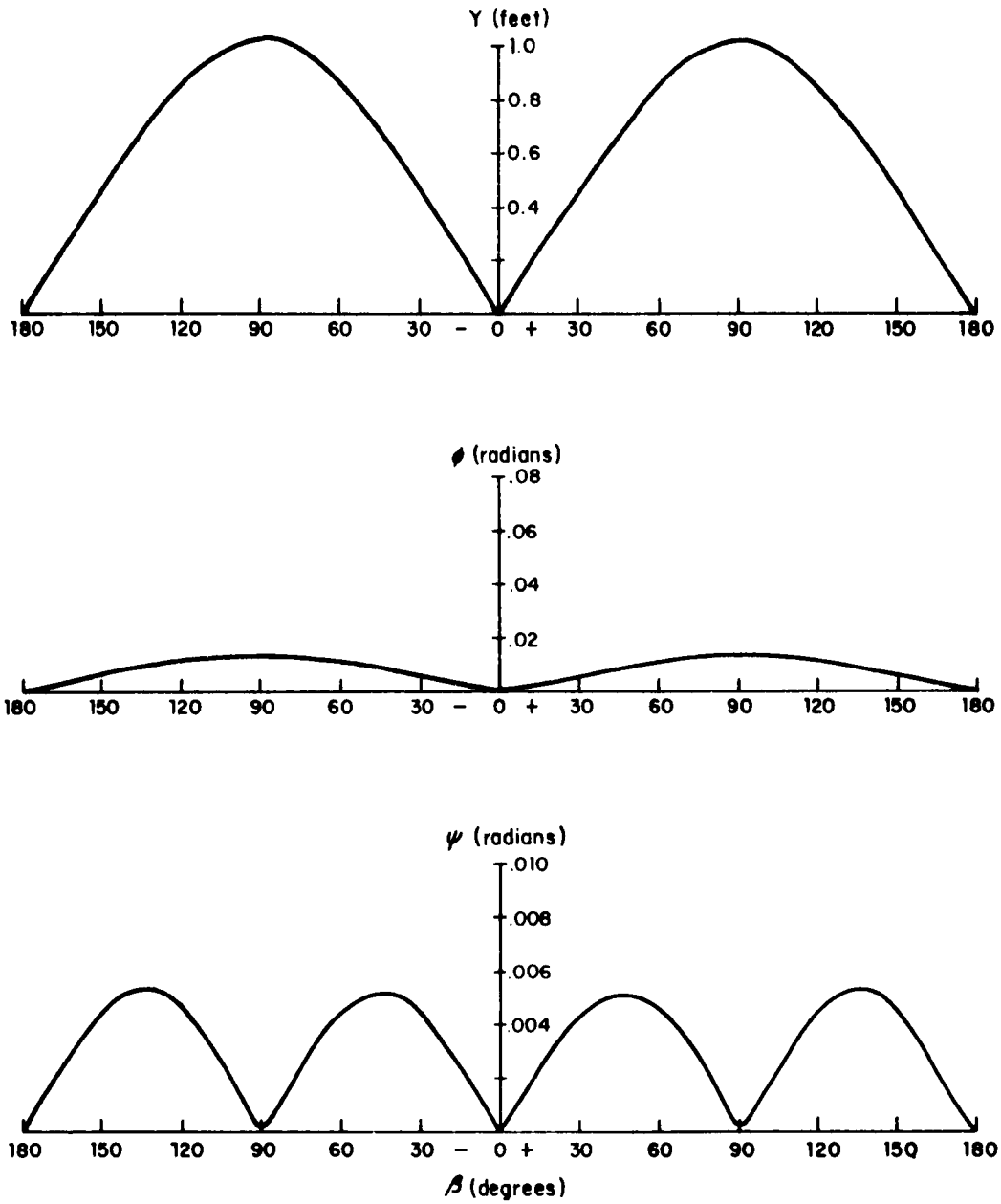

Figure 3.16
Amplitude of response for unit-amplitude wave as a function of direction of wave relative to barge
Lateral motion; $\lambda = 800'$

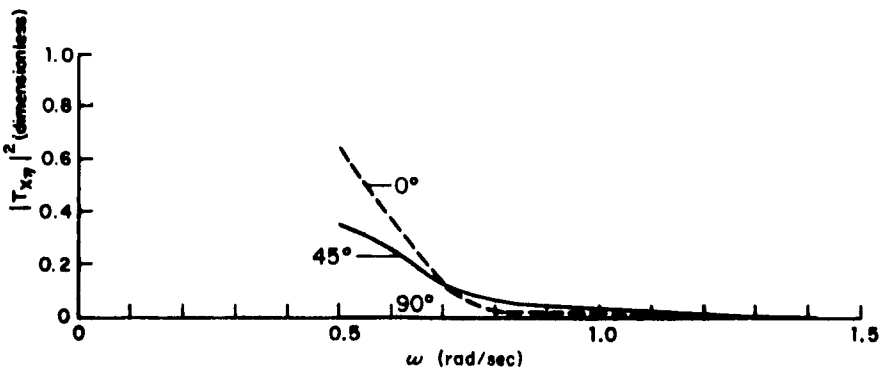

Figure 3. 17

(Response amplitude operator)^2 for surge, $|T_{X\eta}|^2$

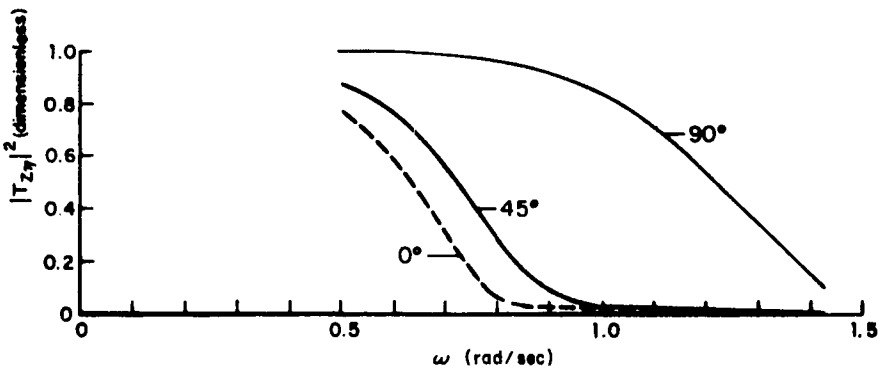

Figure 3. 18

(Response amplitude operator)^2 for heave, $|T_{Z\eta}|^2$

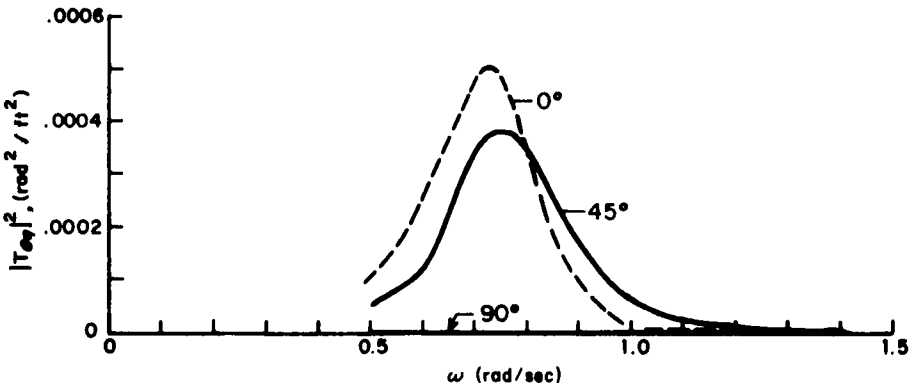

Figure 3. 19

(Response amplitude operator)^2 for pitch, $|T_{\theta\eta}|^2$

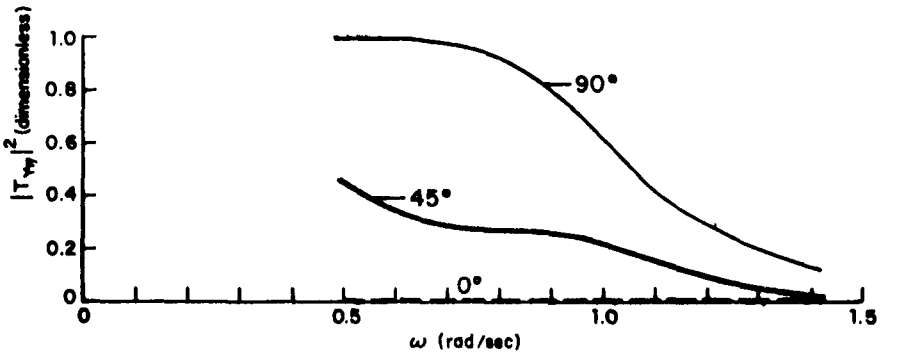

Figure 3.20

(Response amplitude operator)^2 for sway, $|T_{Y\eta}|^2$

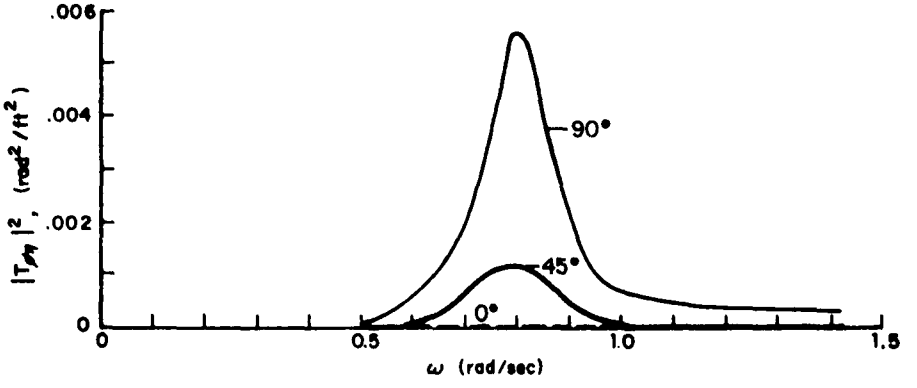

Figure 3.21

(Response amplitude operator)^2 for roll, $|T_{\phi\eta}|^2$

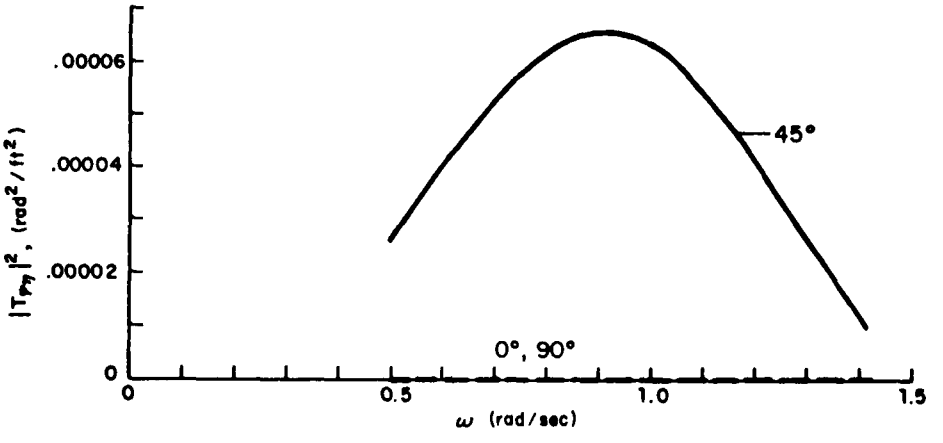

Figure 3.22

(Response amplitude operator)^2 for yaw, $|T_{\psi\eta}|^2$

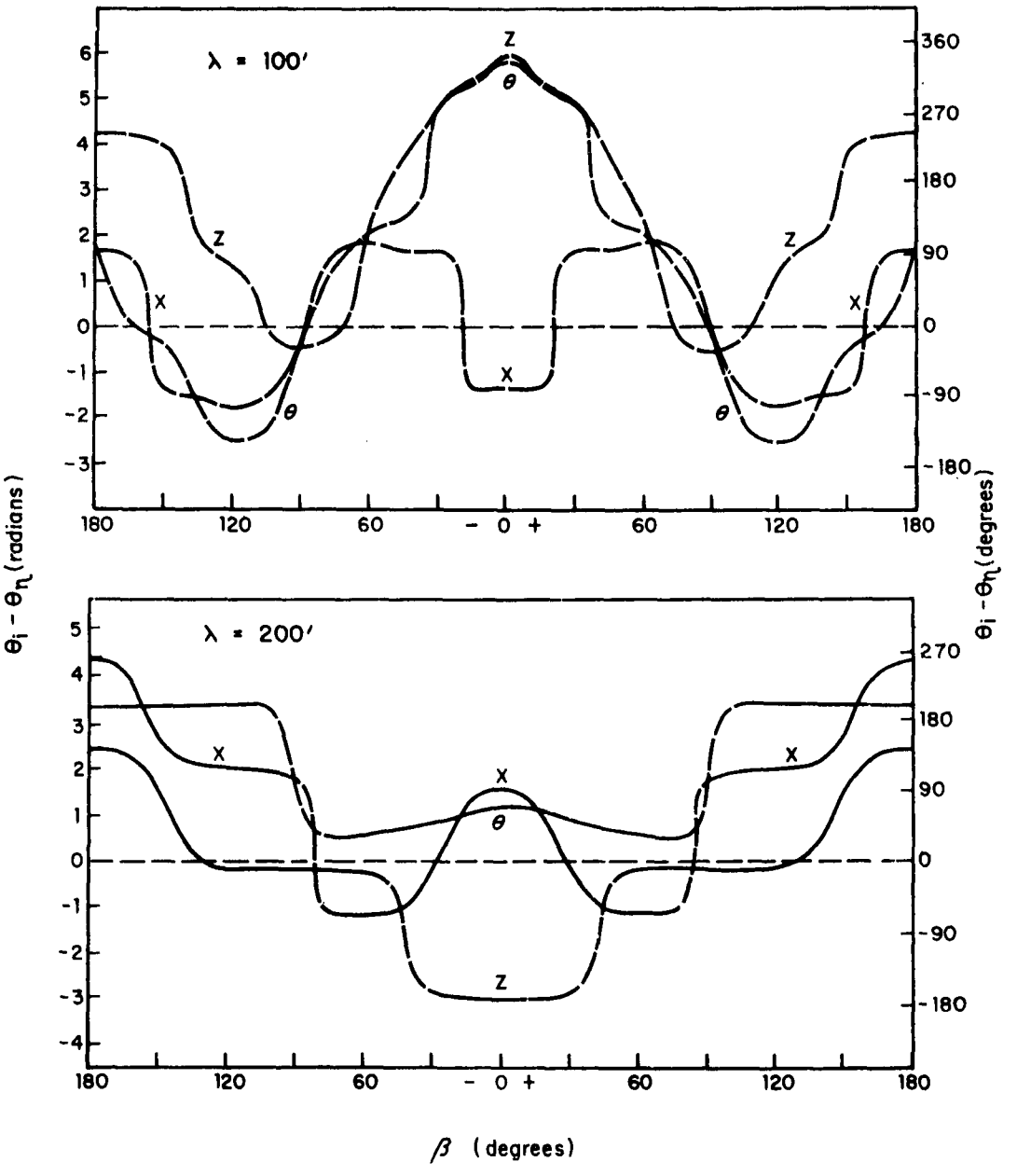

Figure 3.23

Phase shift characteristics for longitudinal ship motions in regular seas, as a function of wave heading; λ = 100' and 200'
$\theta_i - \theta_\eta$ = difference of phase of ship motion, i, and phase of sinusoidal surface elevation

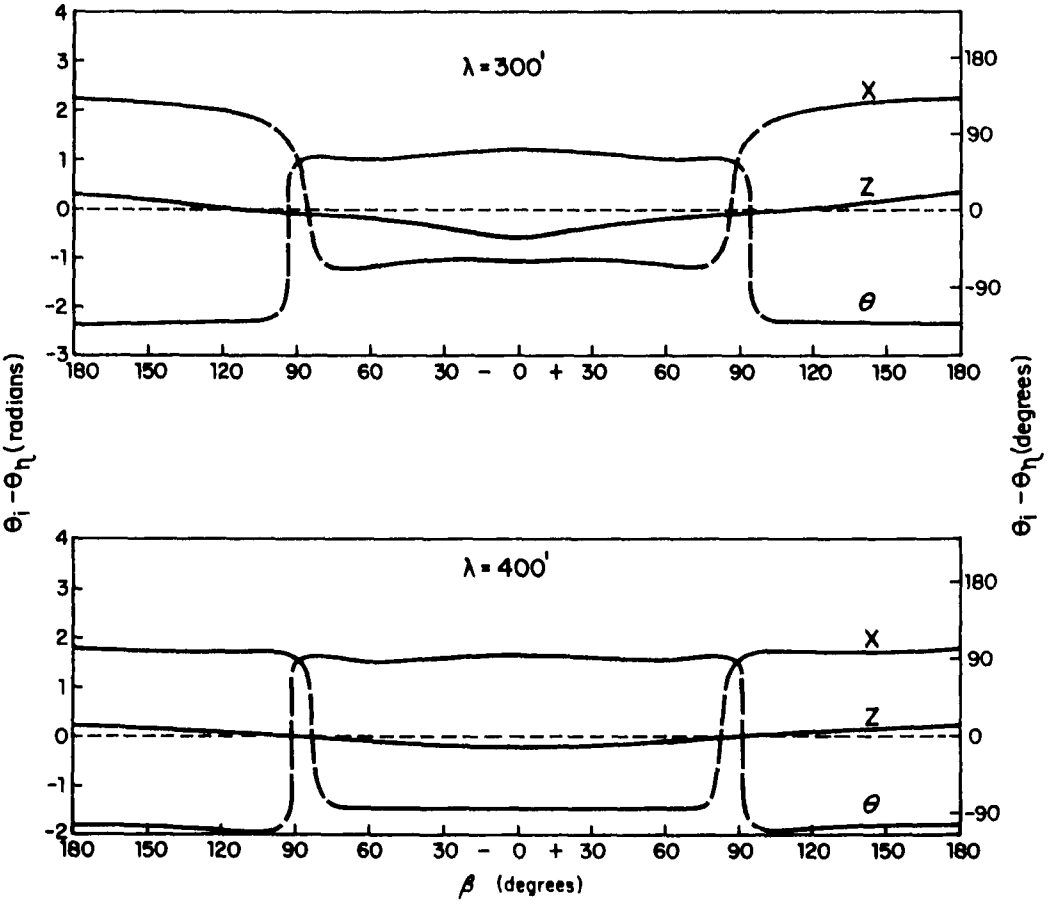

Figure 3.24

Phase shift characteristics for longitudinal ship motions in regular seas, as a function of wave heading; λ = 300' and 200'
$\theta_i - \theta_\eta$ = difference of phase of ship motion, i, and phase of sinusoidal surface elevation

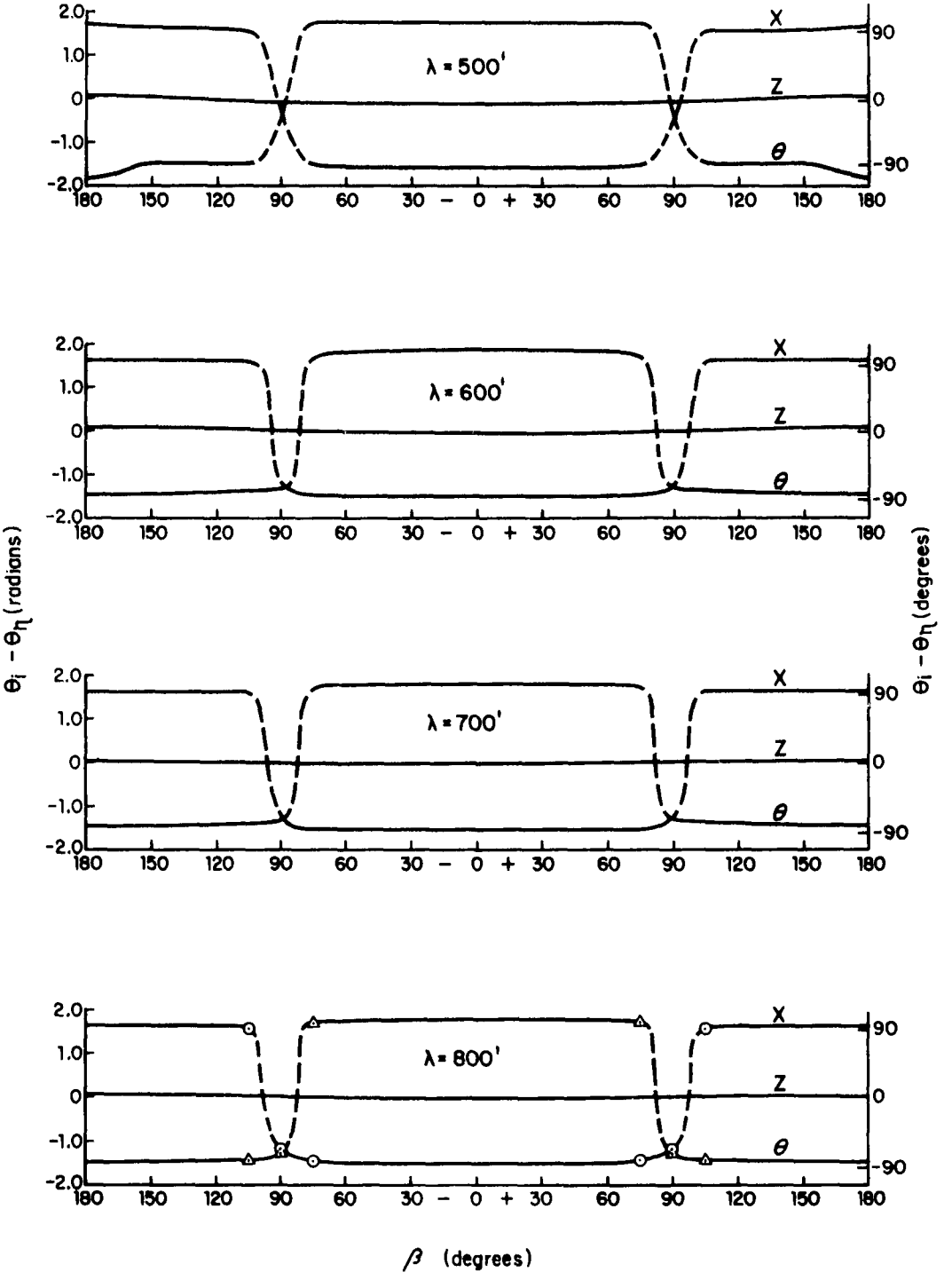

Figure 3.25

Phase shift characteristics for longitudinal ship motions in regular seas, as a function of wave heading; λ = 500', 600', 700' and 800'

$\theta_i - \theta_\eta$ = difference of phase of ship motion, i, and phase of sinusoidal surface elevation

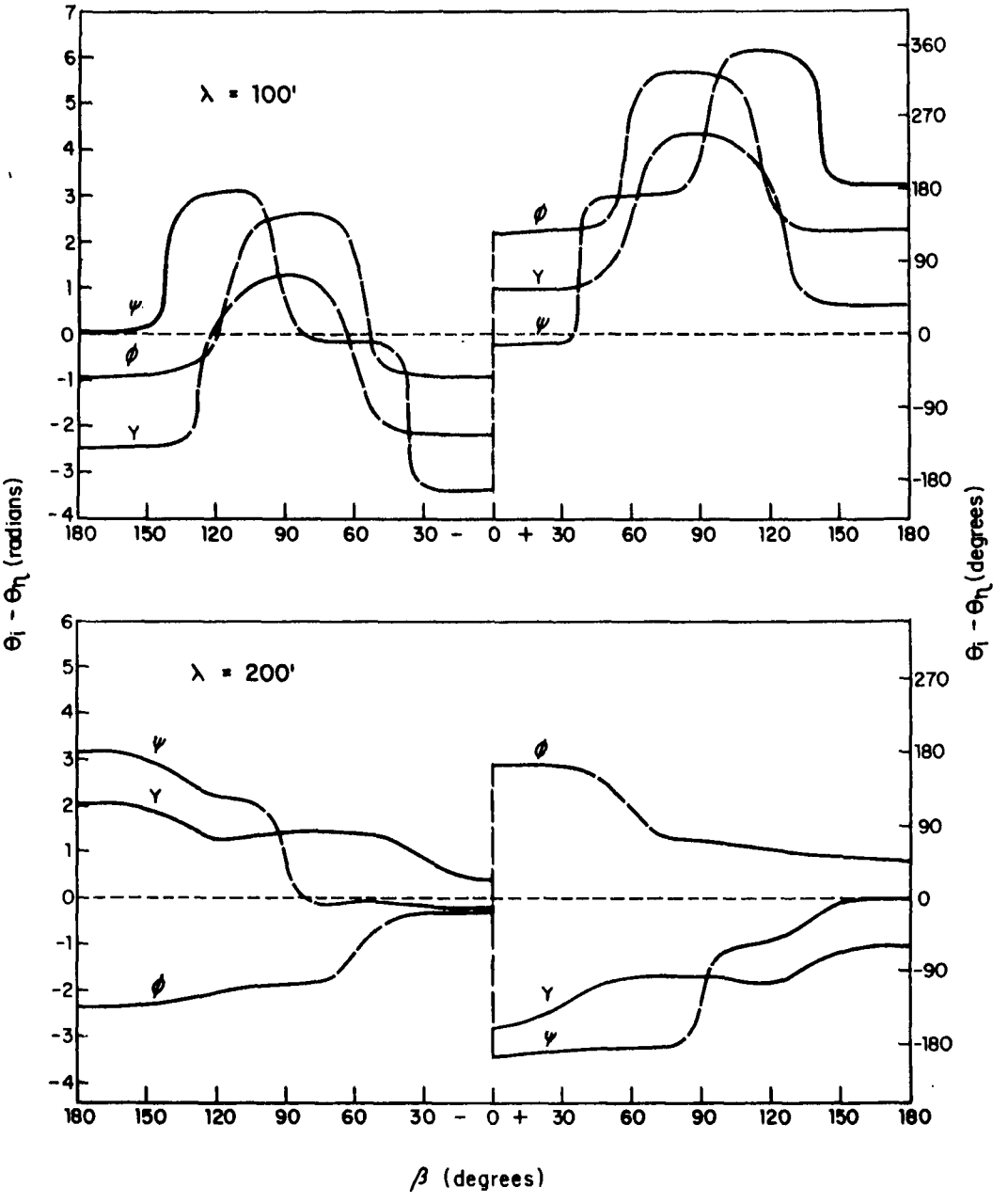

Figure 3.26

Phase shift characteristics for lateral ship motions in regular seas, as a function of wave heading; λ = 100' and 200' $\theta_i - \theta_h$ = difference of phase of ship motion, i, and phase of sinusoidal surface elevation

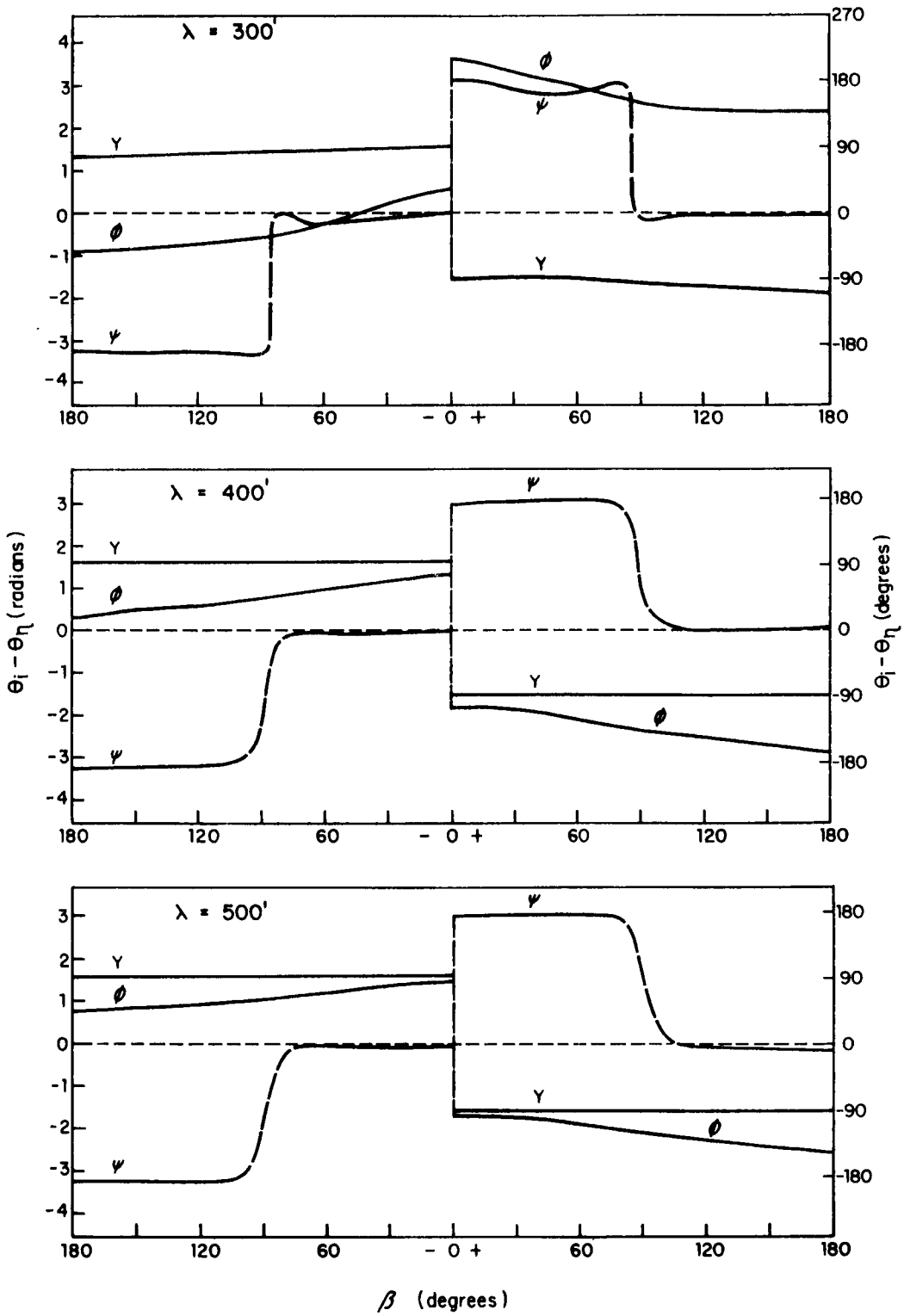

Figure 3.27

Phase shift characteristics for lateral ship motions in regular seas, as a function of wave heading; λ = 300', 400' and 500'
$\theta_i - \theta_\eta$ = difference of phase of ship motion, i, and phase of sinusoidal surface elevation

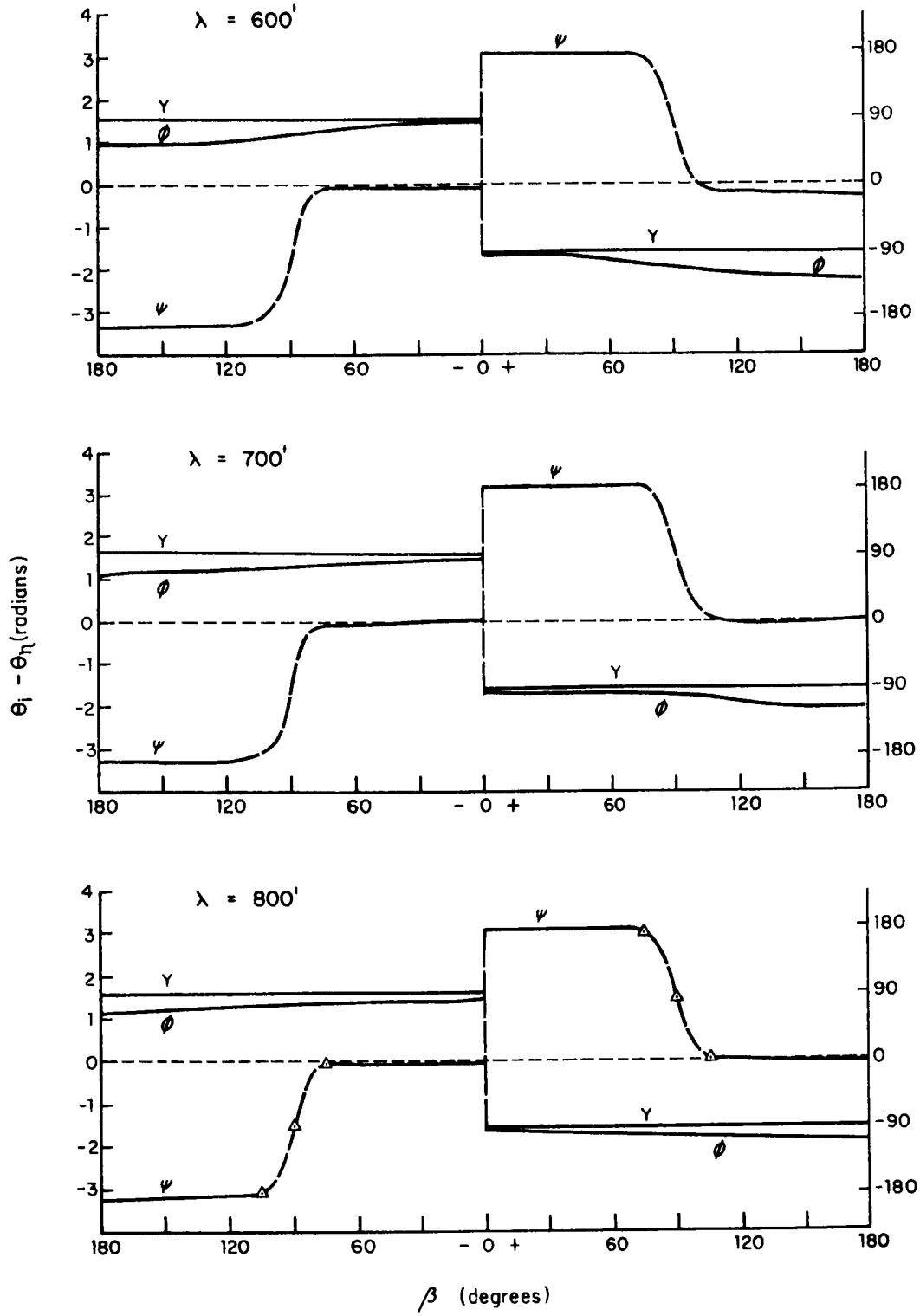

Figure 3.28

Phase shift characteristics for lateral ship motions in regular seas, as a function of wave heading; λ = 600', 700' and 800'
$\theta_i - \theta_\eta$ = difference of phase of ship motion, i, and phase of sinusoidal surface elevation.

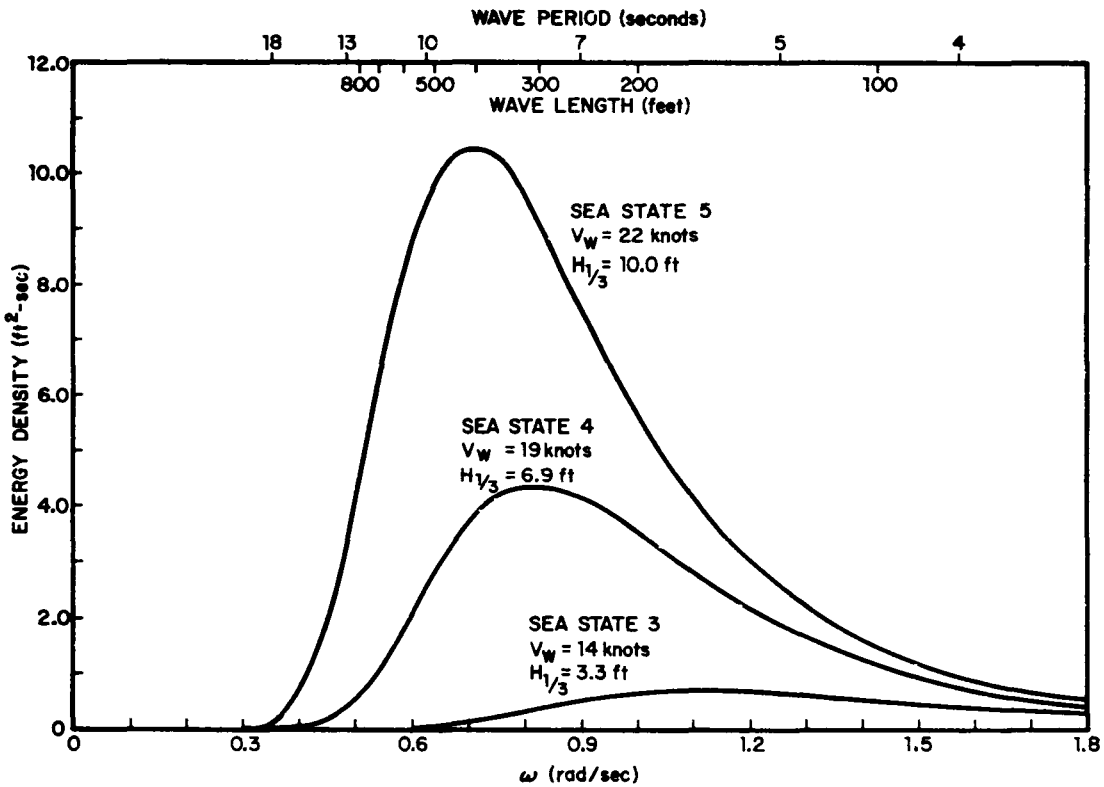

Figure 3.29

Spectral energy density for surface elevations, as used in computations
(Neumann model for wind velocities indicated)

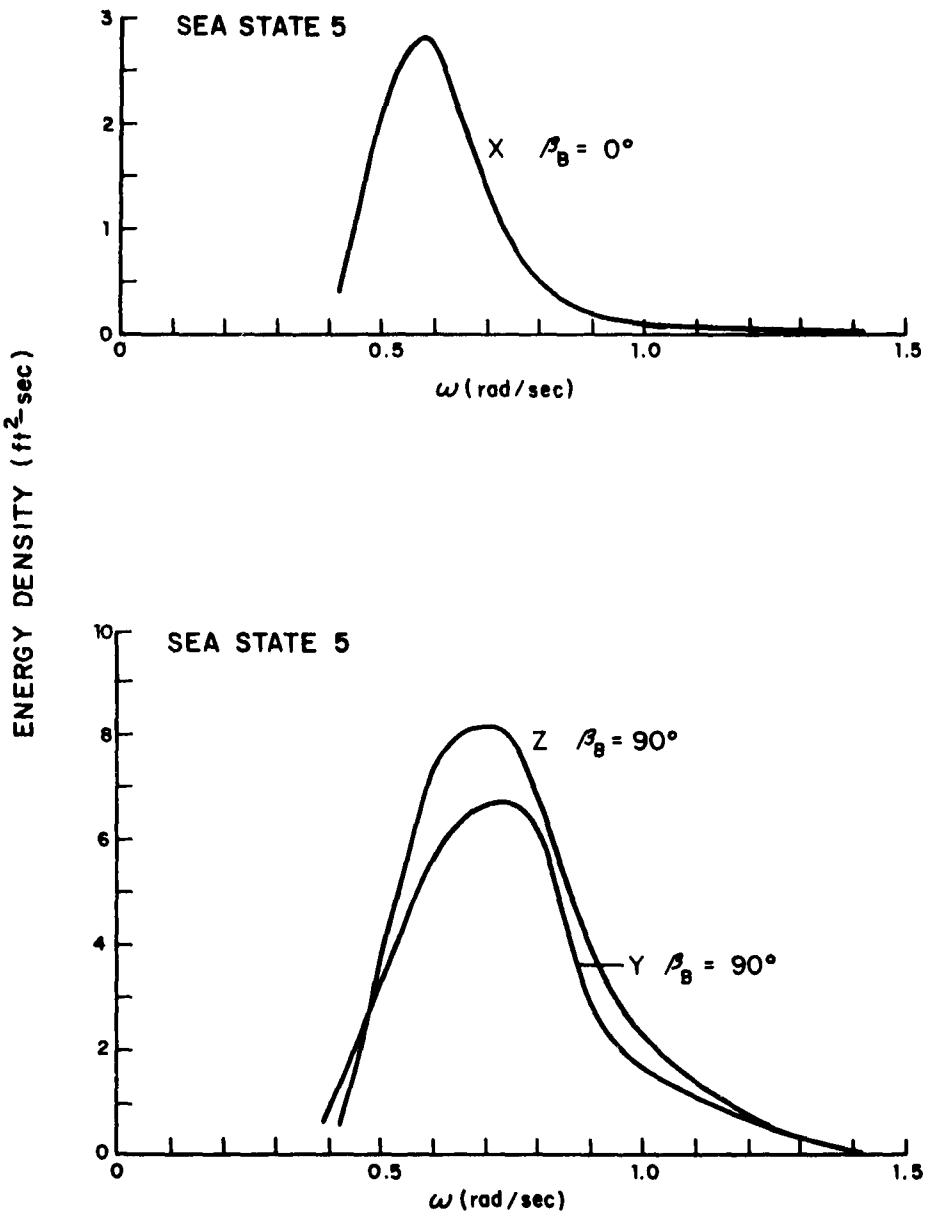

Figure 3.30

Spectral energy density for translational barge motions for indicated barge heading β_B

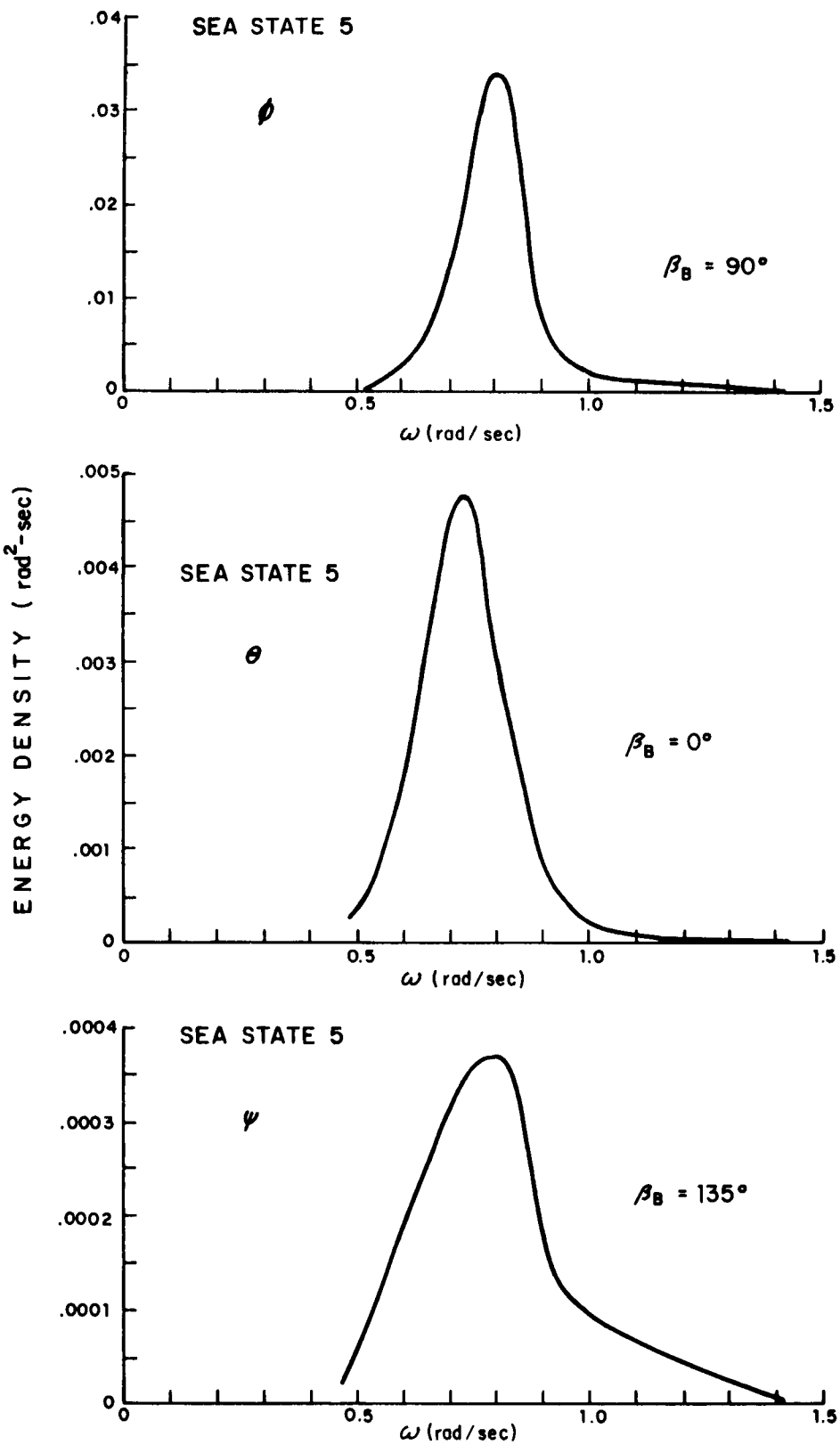

Figure 3.31

Spectral energy density for rotational barge motions for indicated barge heading β_B

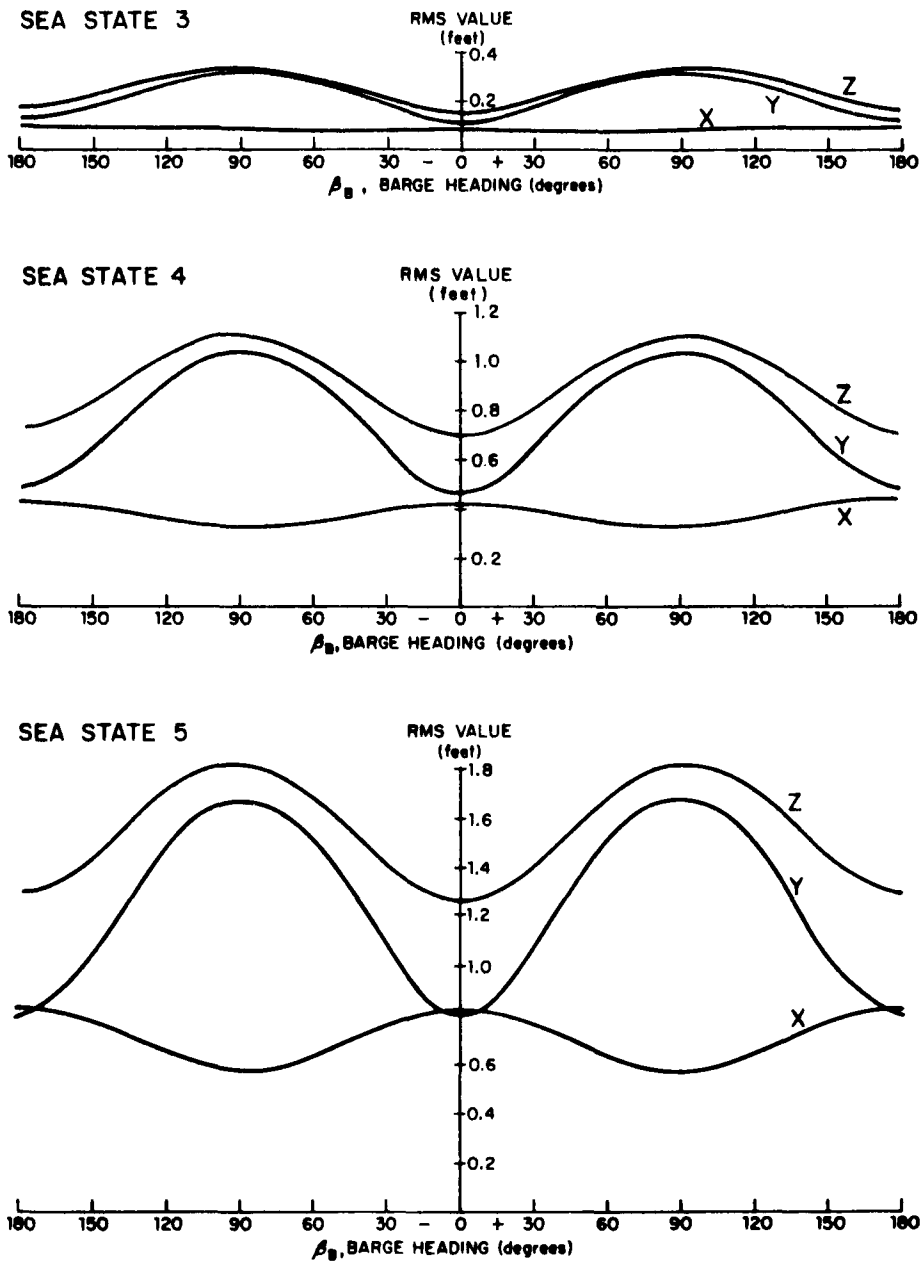

Figure 3.32

RMS values of the translational barge motions as a function of barge heading at indicated sea state

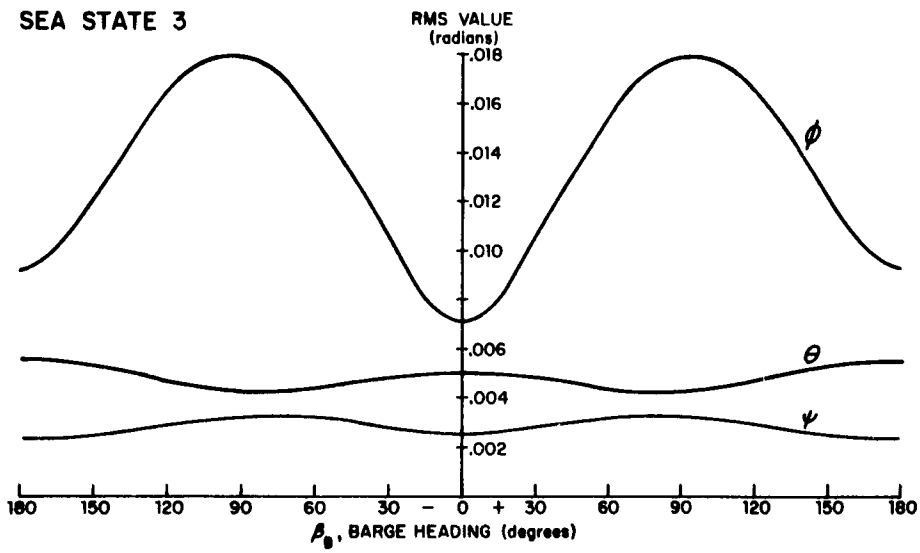

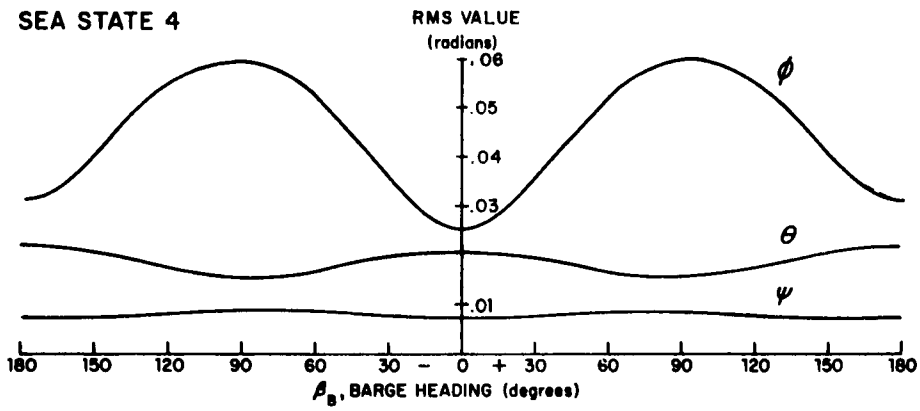

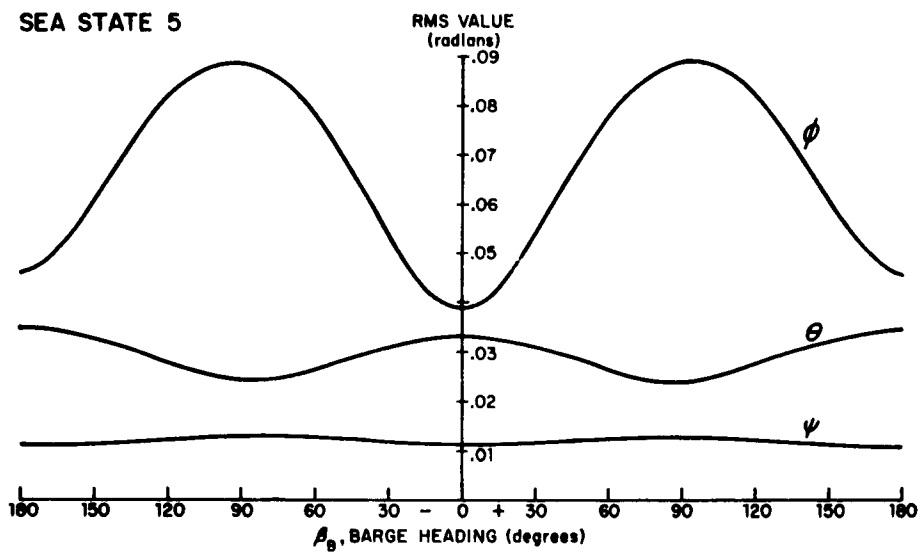

Figure 3.33

RMS values of the rotational barge motions as a function of barge heading at indicated sea state

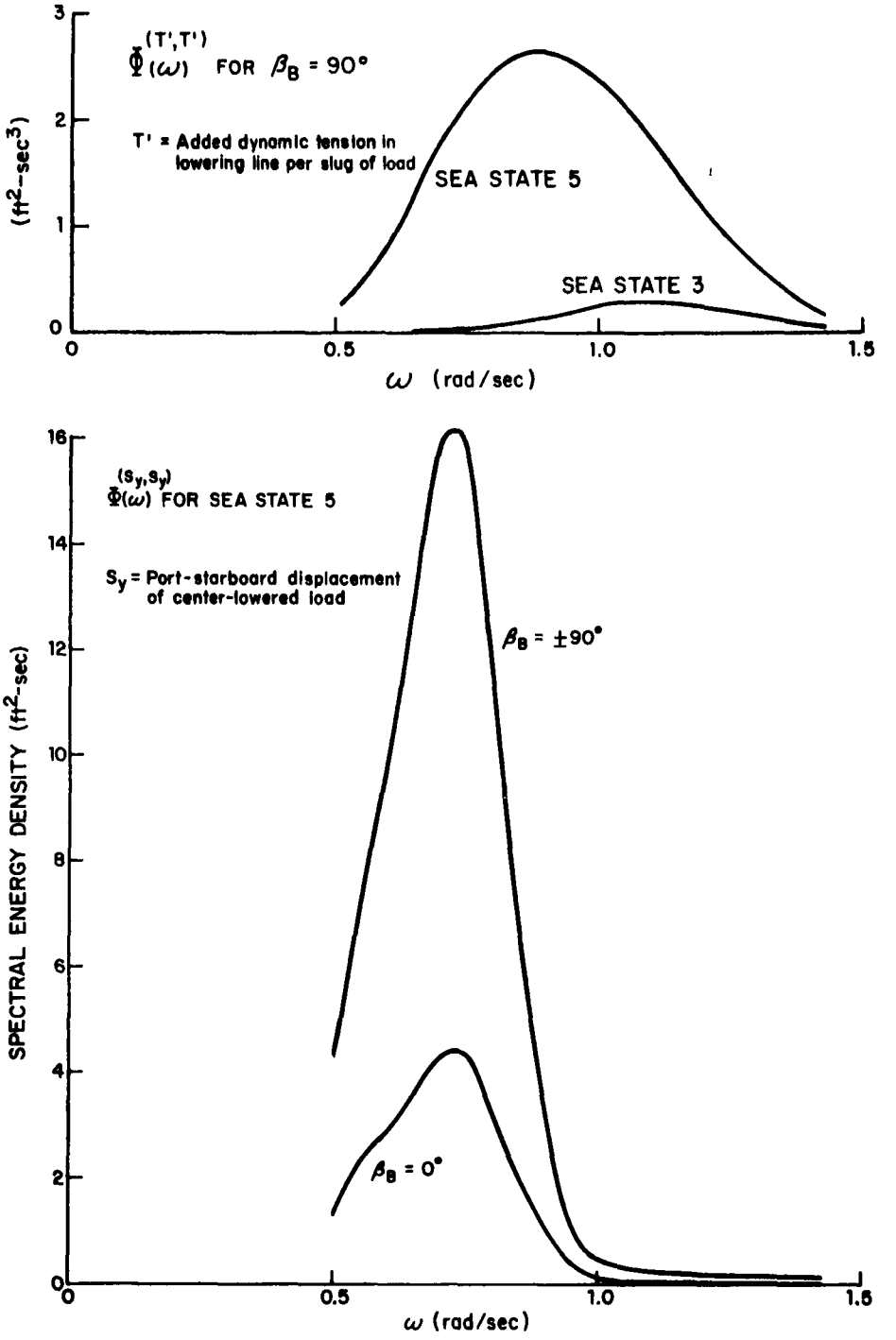

Figure 4.1

Spectral energy density functions for added dynamic tension in lowering line and lateral displacement for center-lowered load, for indicated barge heading and sea state

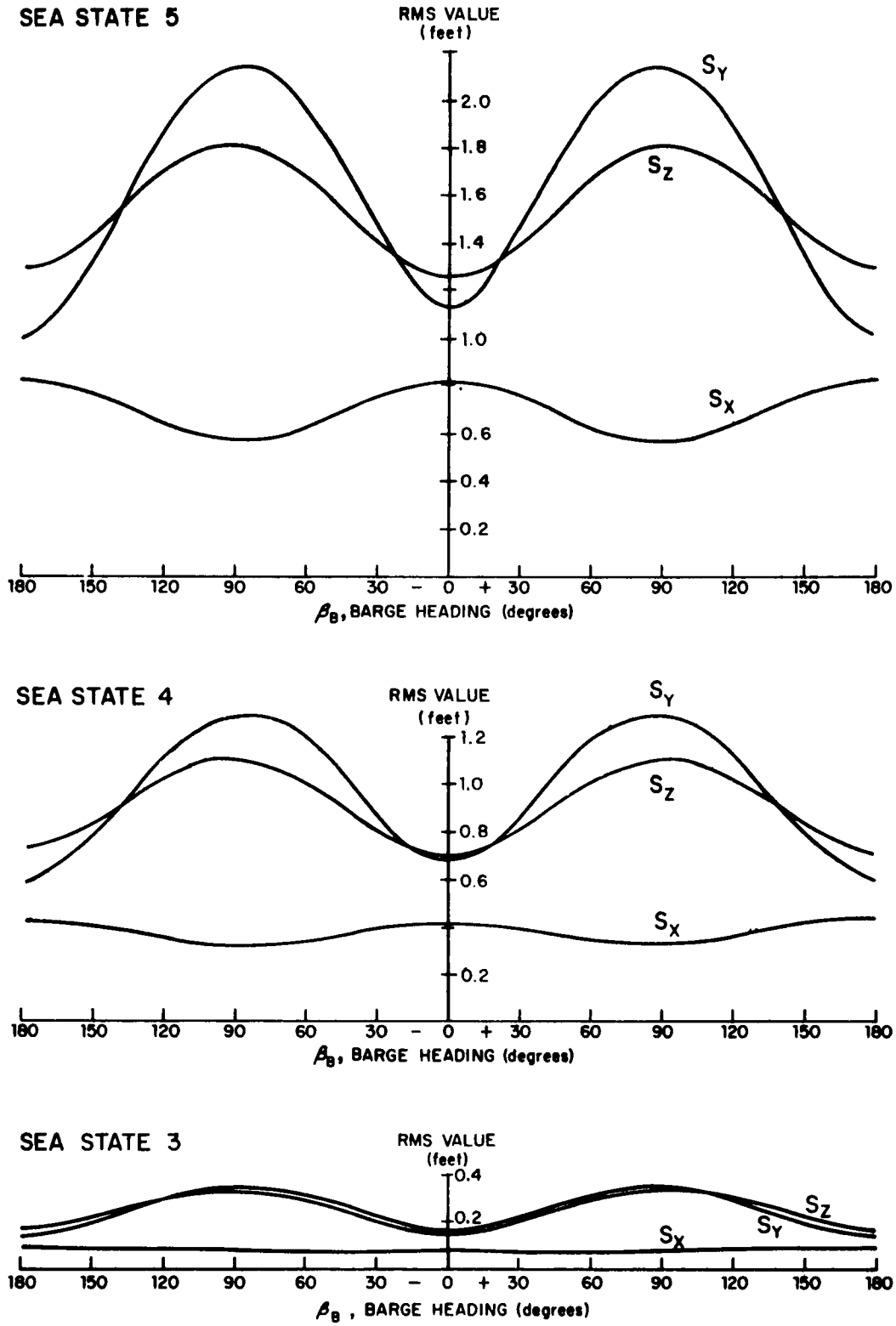

Figure 4.2

RMS values of load displacements for center-lowered load, as a function of barge heading at indicated sea state

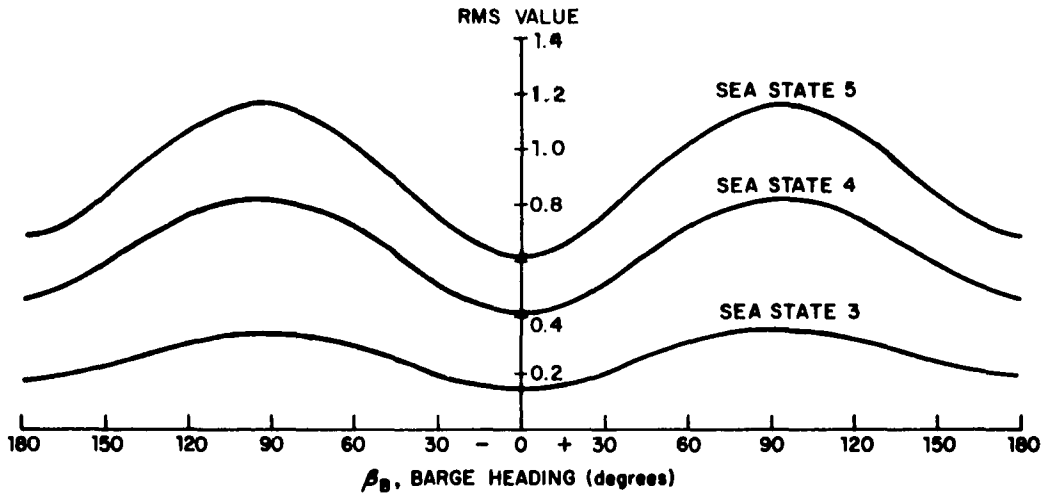

Figure 4.3

RMS values of added-dynamic line tension (pounds/slug) and vertical load acceleration (feet/second^2) for center-lowered load, as a function of barge heading at indicated sea state

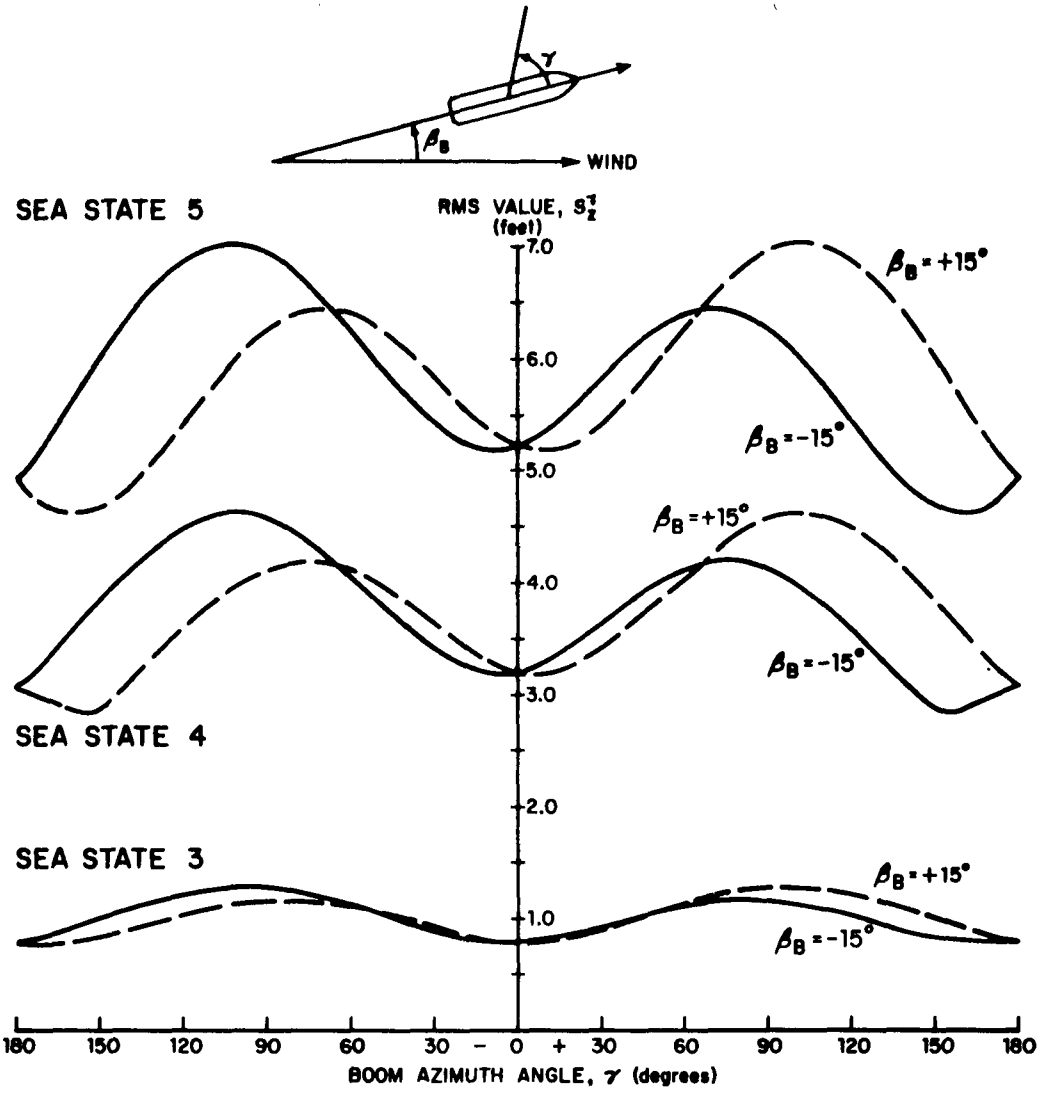

Figure 4.4

RMS values of vertical component of load displacement for boom-lowered load as a function of boom azimuth angle, for indicated barge heading and sea state

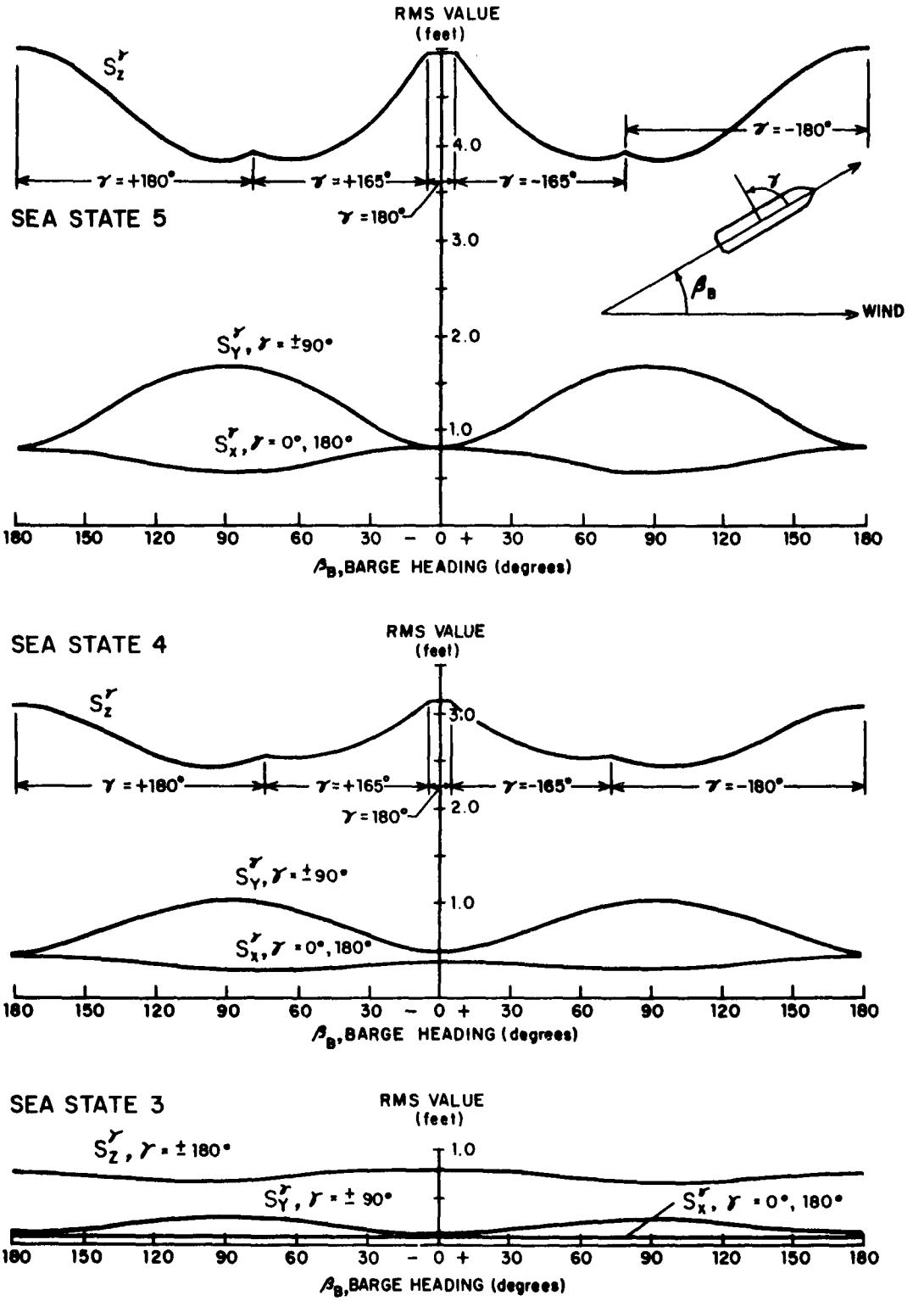

Figure 4.5

Minimum RMS values of load displacements for boom-lowered load as a function of barge heading at indicated sea state

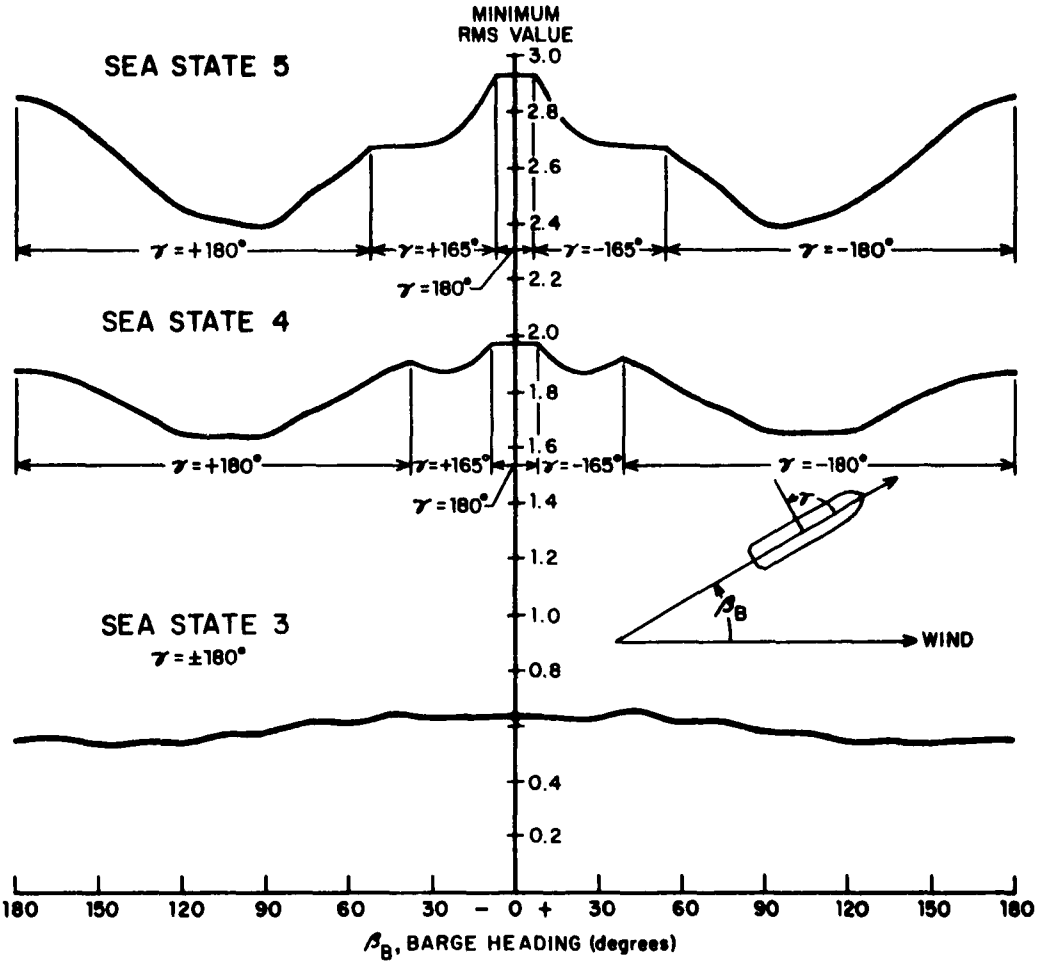

Figure 4.6

Minimum RMS values of added-dynamic line tension (pounds/slug) and vertical load acceleration (feet/second^2) for boom-lowered load, as a function of barge heading at indicated sea state

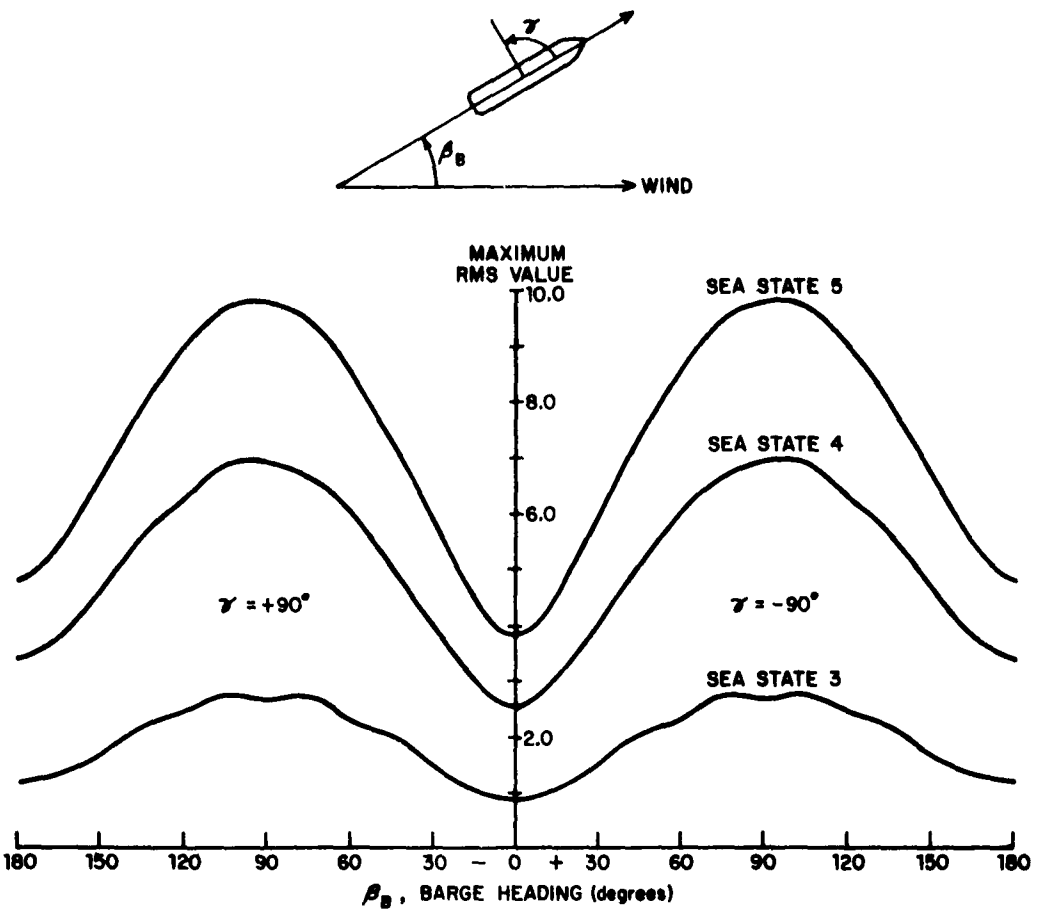

Figure 4.7

Maximum RMS values of added-dynamic line tension (pounds/slug) and vertical load acceleration (feet/second^2), for boom-lowered load, as a function of barge heading at indicated sea state

(Maximizing boom azimuth angles, γ = +90° and -90°)

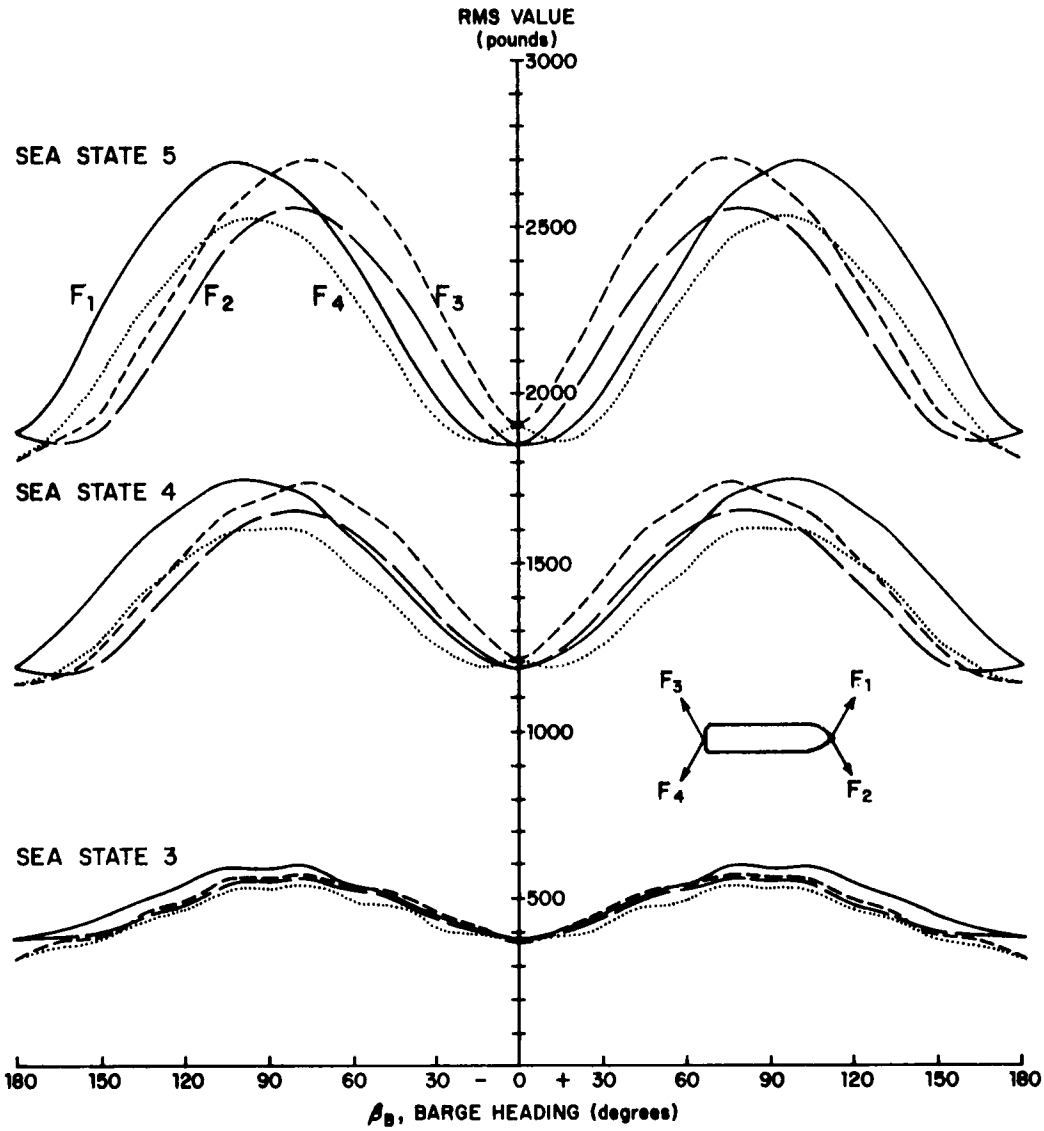

Figure 4.8

RMS values of mooring cable forces as a function of barge heading at indicated sea state

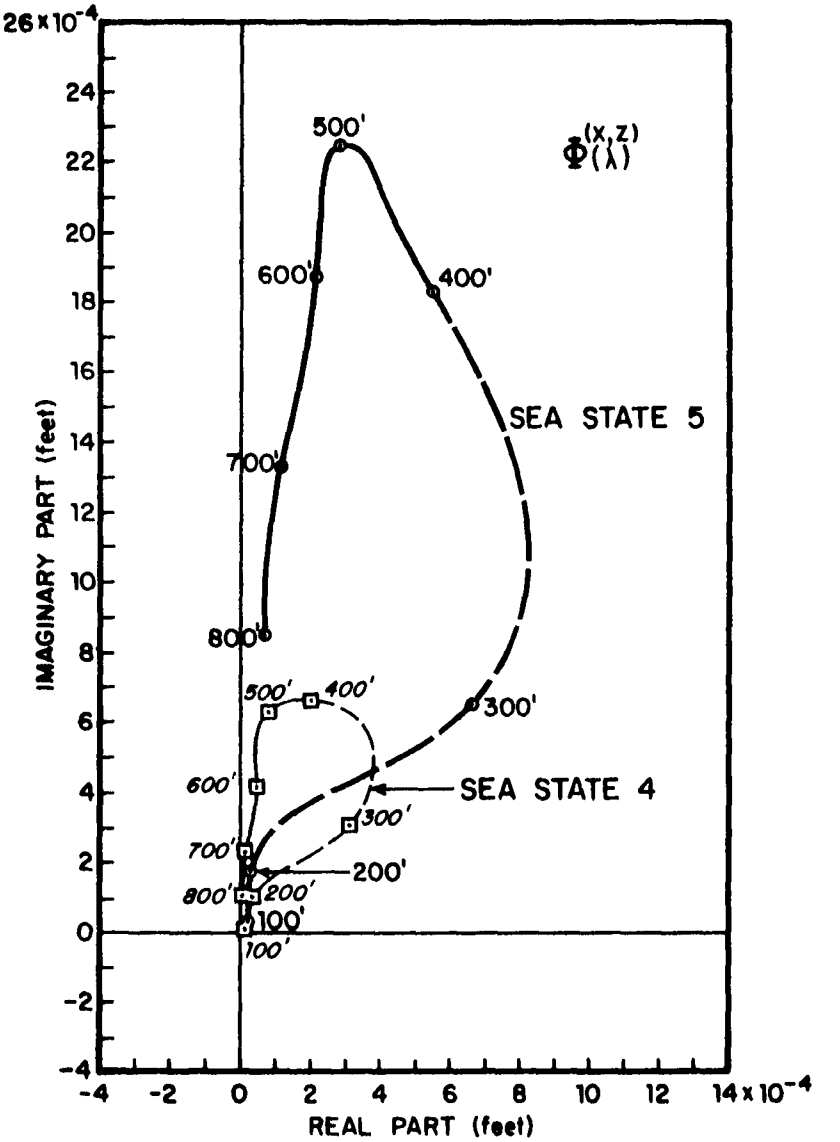

Figure 5.1

Complex cross-spectral energy-density function (absolute) for surge and heave (x, z) for barge heading 0° and indicated sea state. NOTE: On this scale, points for sea state 3 are indistinguishable from the origin (0, 0)

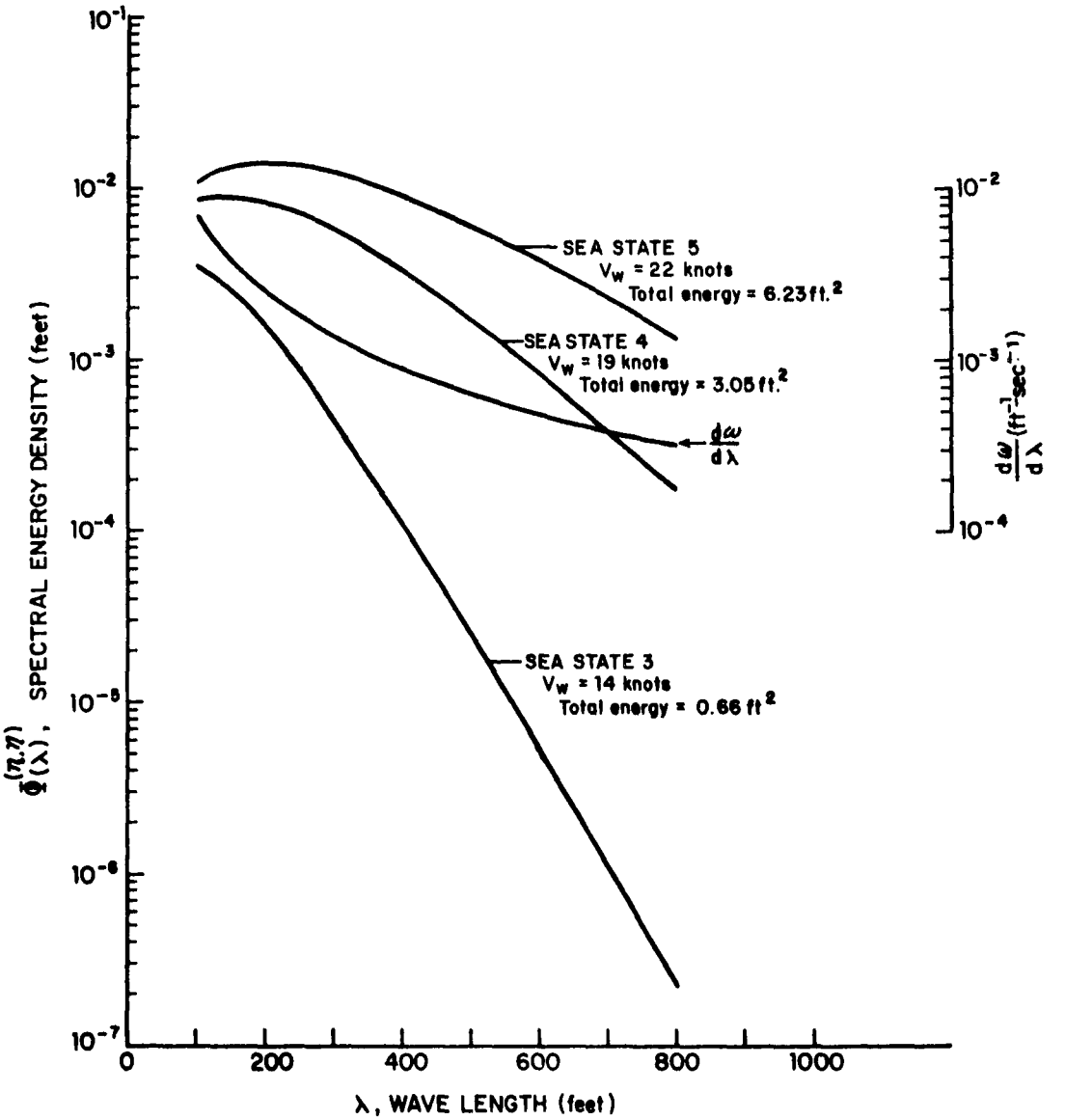

Figure 5.2

Neumann surface-elevation spectral-density functions, $\Phi^{(\eta\eta)}(\lambda)$, with respect to wave length, for indicated sea states, together with the derivative $d\omega/d\lambda$.

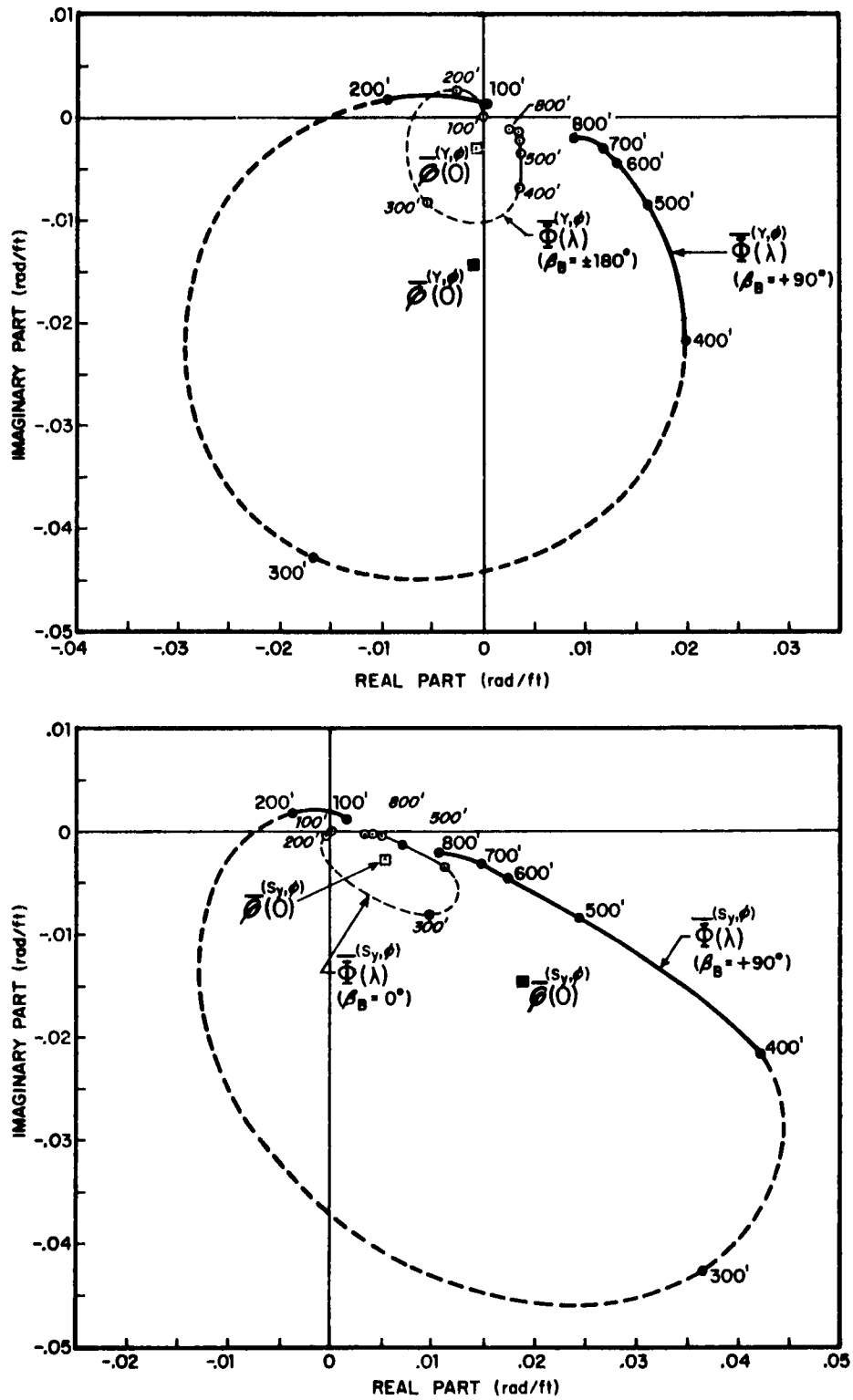

Figure 5.3

Complex cross-spectral energy-density functions and values of corresponding complex cross-covariance functions, both relative to surface elevation, for sway, roll, and lateral displacement of center-lowered load, indicated at barge headings

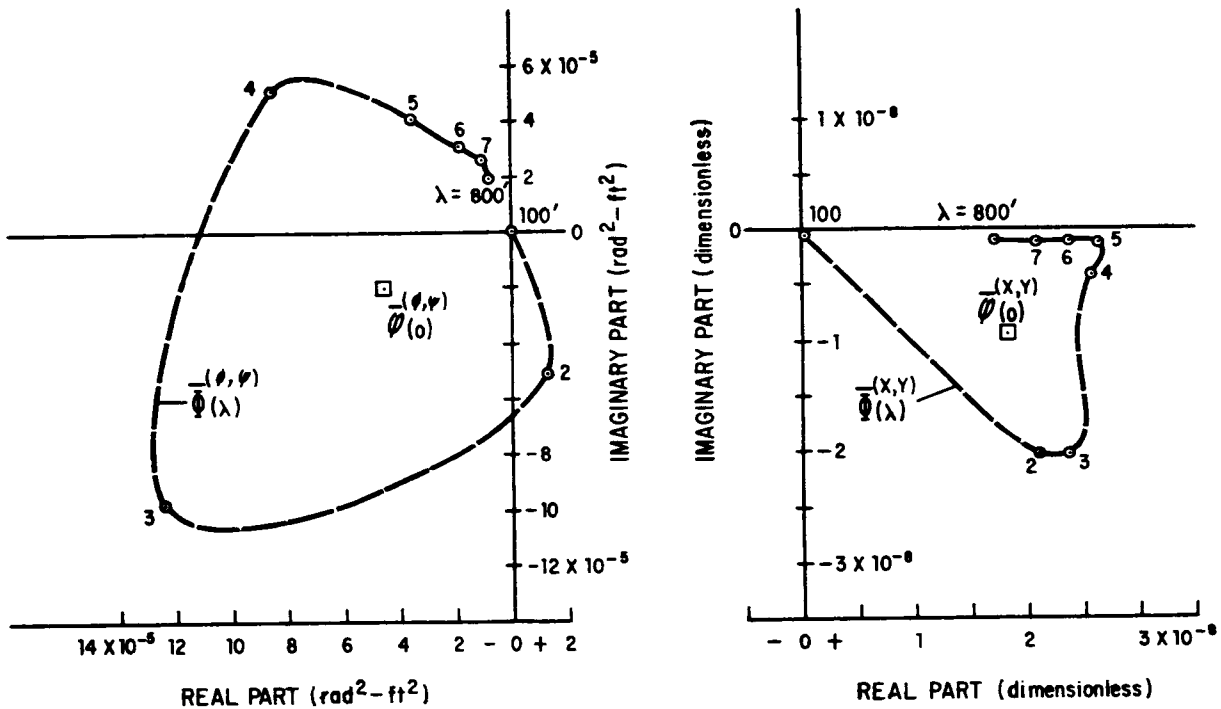

Figure 5.4

Complex cross-spectral energy-density functions and values of corresponding complex cross-covariance functions, both relative to surface elevation, for surge, sway, roll, and yaw, at barge heading $\beta_B = \pm 180°$

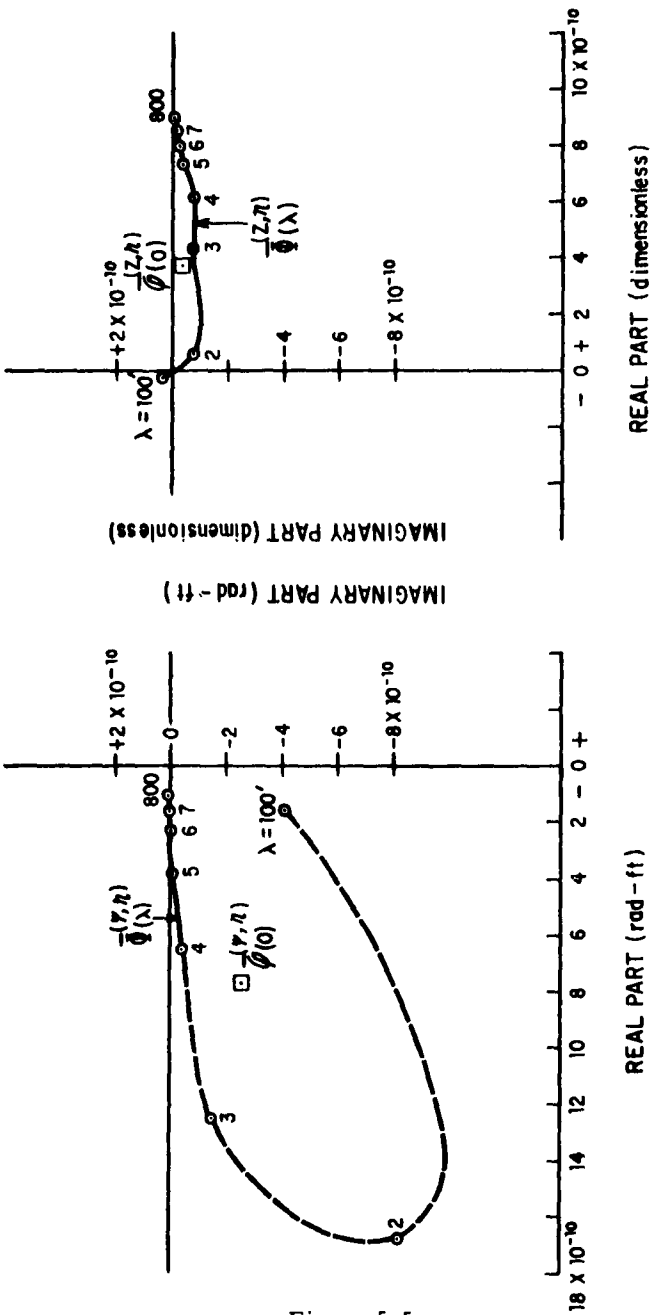

Figure 5.5

Complex cross-spectral energy-density functions and values of corresponding complex cross-covariance functions, both relative to surface elevation, for heave, yaw, and surface elevation, at barge heading $\beta_B = \pm 180°$

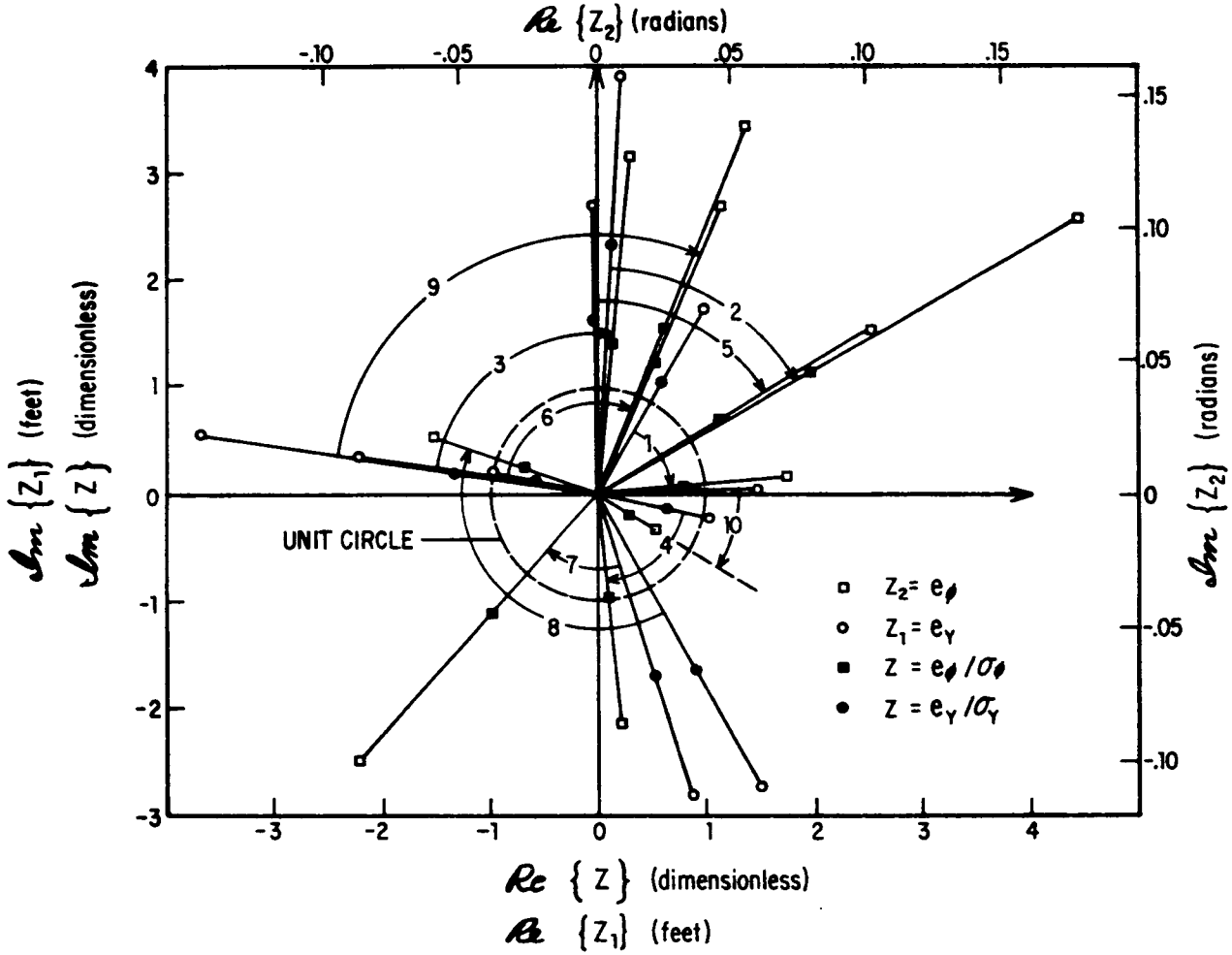

Fig. 5.6
Randomly-generated sample values of simultaneous instantaneous roll and sway phase and amplitude

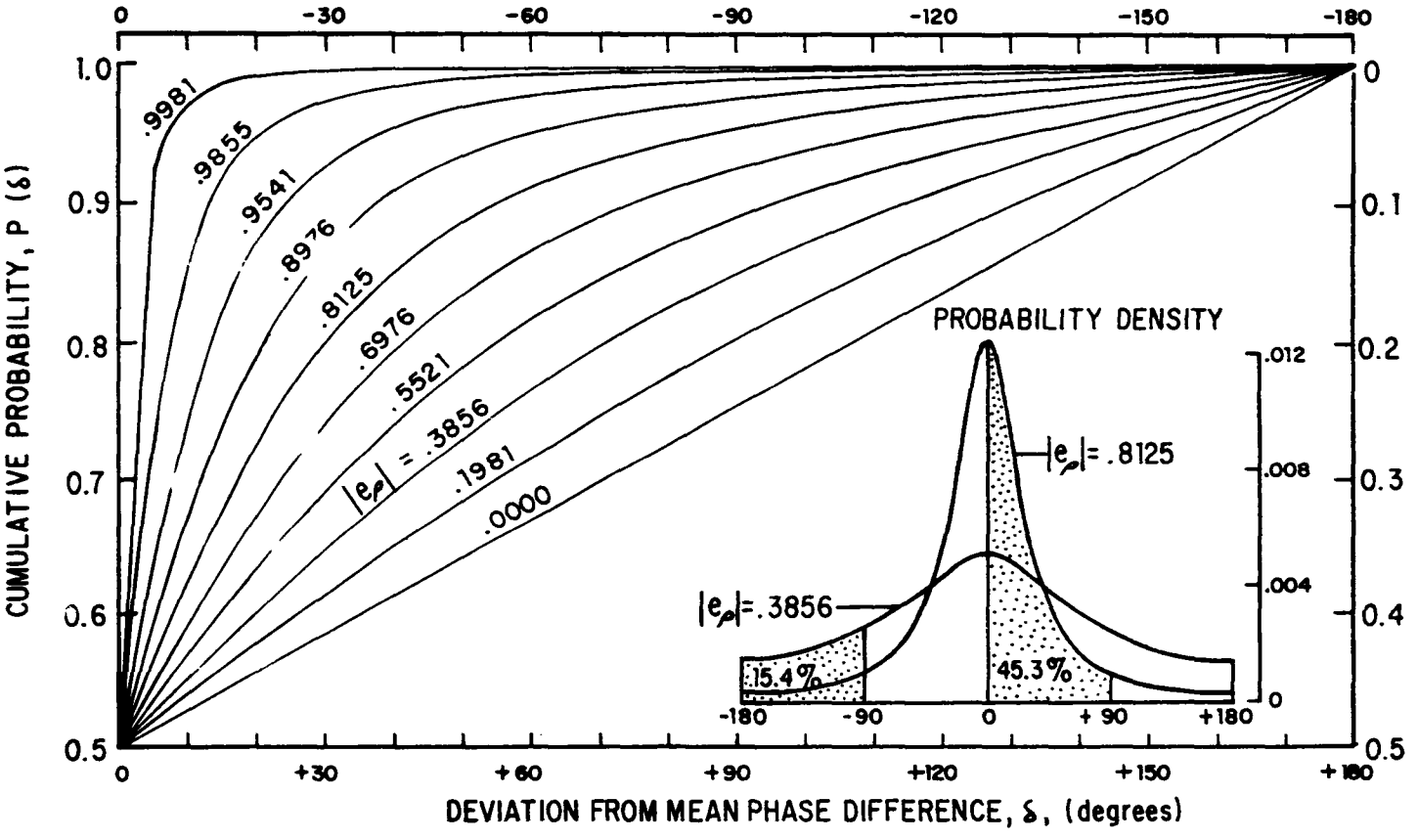

Fig. 5.7
Cumulative probability distribution of instantaneous phase difference for various values of $|e_\rho|$

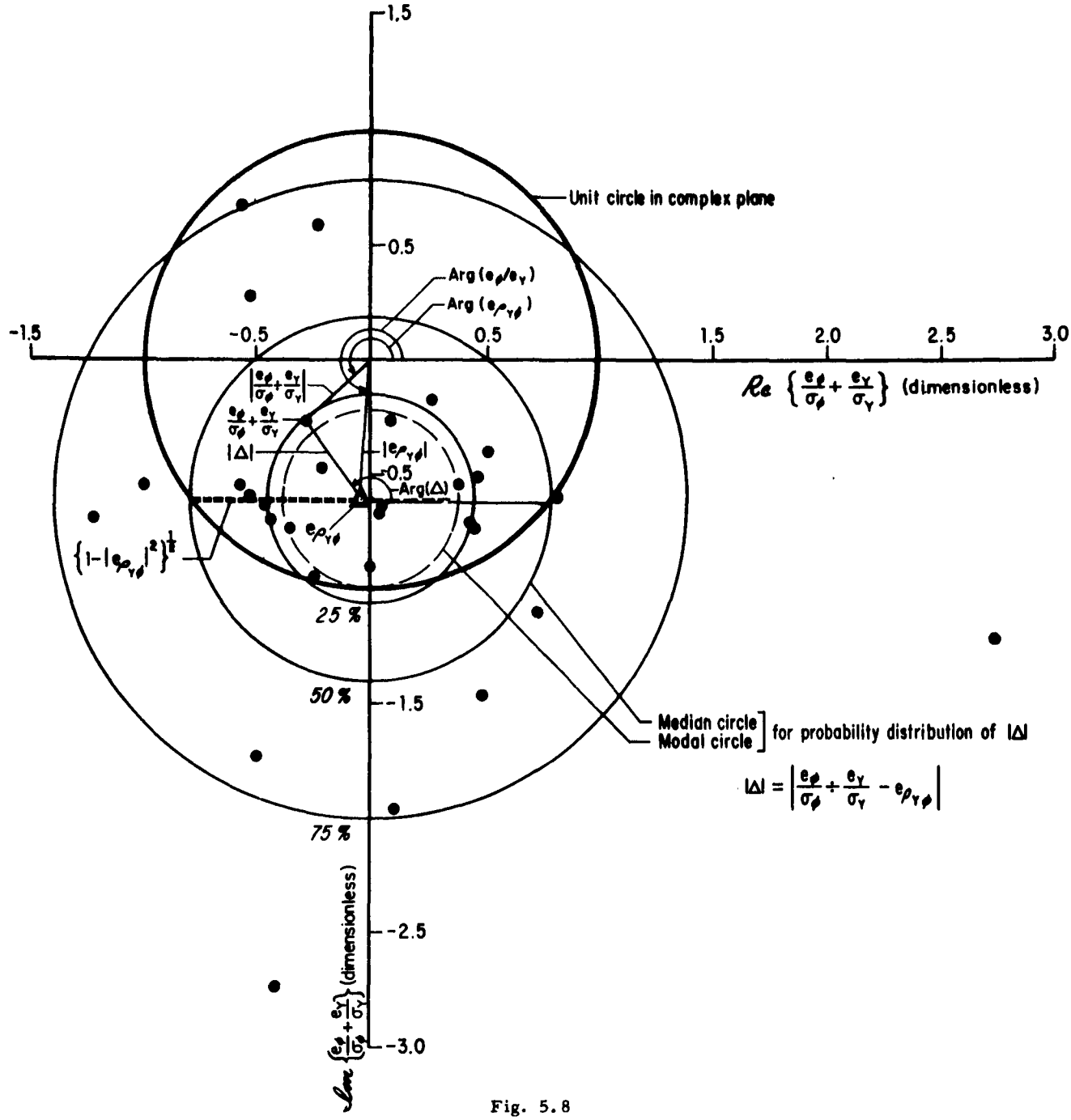

Fig. 5.8

Complex-plane plot of points corresponding to random sample (of size 30) of values of normalized instantaneous complex envelope ratio, e_ϕ/e_γ, for sway and roll showing instantaneous phase difference, $\theta_\phi - \theta_\gamma$, and normalized instantaneous amplitude ratio, $(r_\phi/\sigma_\phi)\div(r_\gamma/\sigma_\gamma)$

(Sea State 5 - Barge Heading +90°)

(Quartile circles centered at complex-envelope correlation coefficient, $e_{\rho_{\gamma\phi}}$, contain indicated theoretical percentage of points)

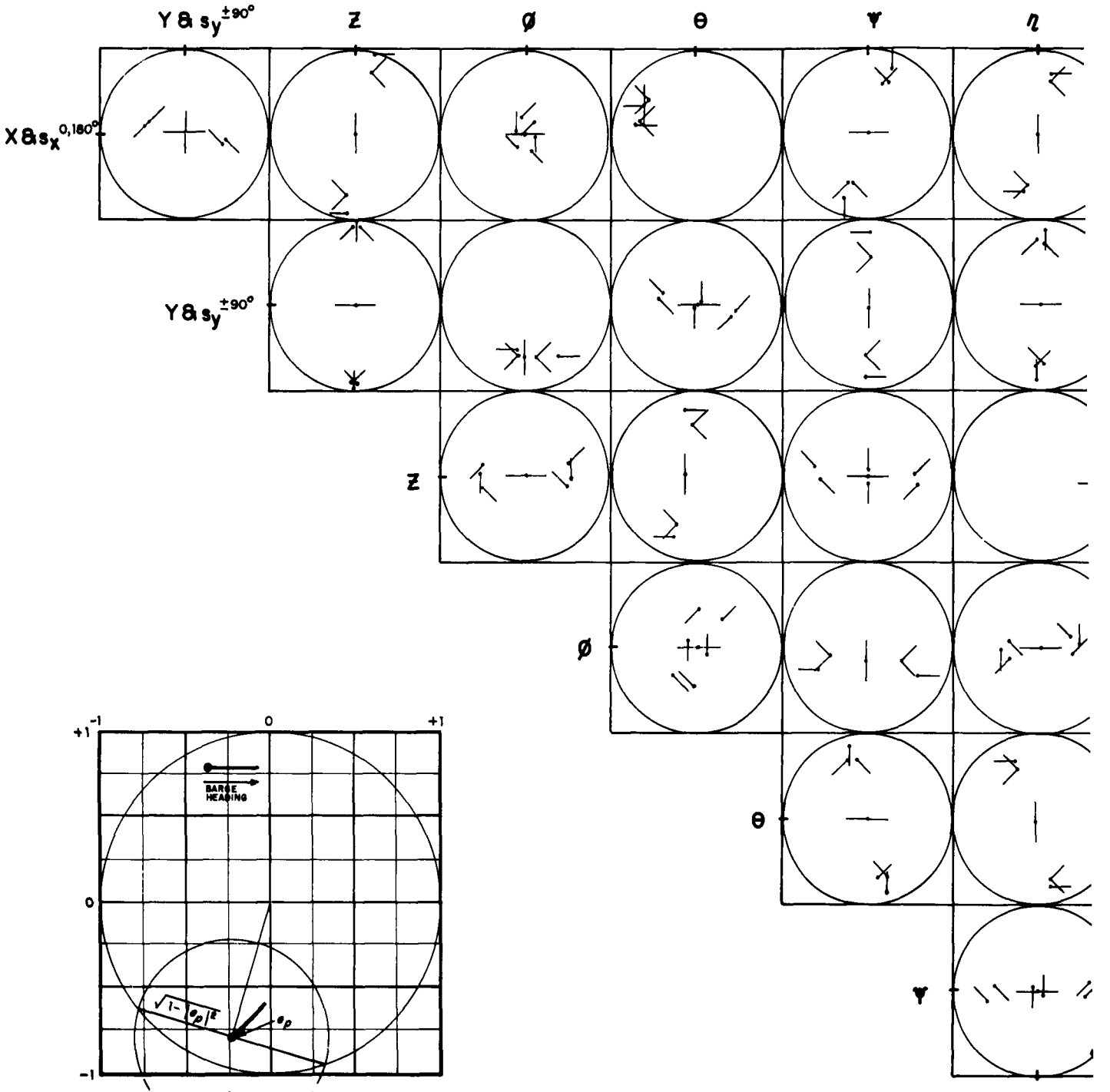
Y & $s_y^{\pm 90°}$
Z
ø
θ
ψ
η
X & $s_x^{0,180°}$
Y & $s_y^{\pm 90°}$
Z
ø
θ
ψ

-1
0
+1
+1
BARGE HEADING
0
$\sqrt{1-|\sigma_\rho|^2}$
σ_ρ
-1
50%

1

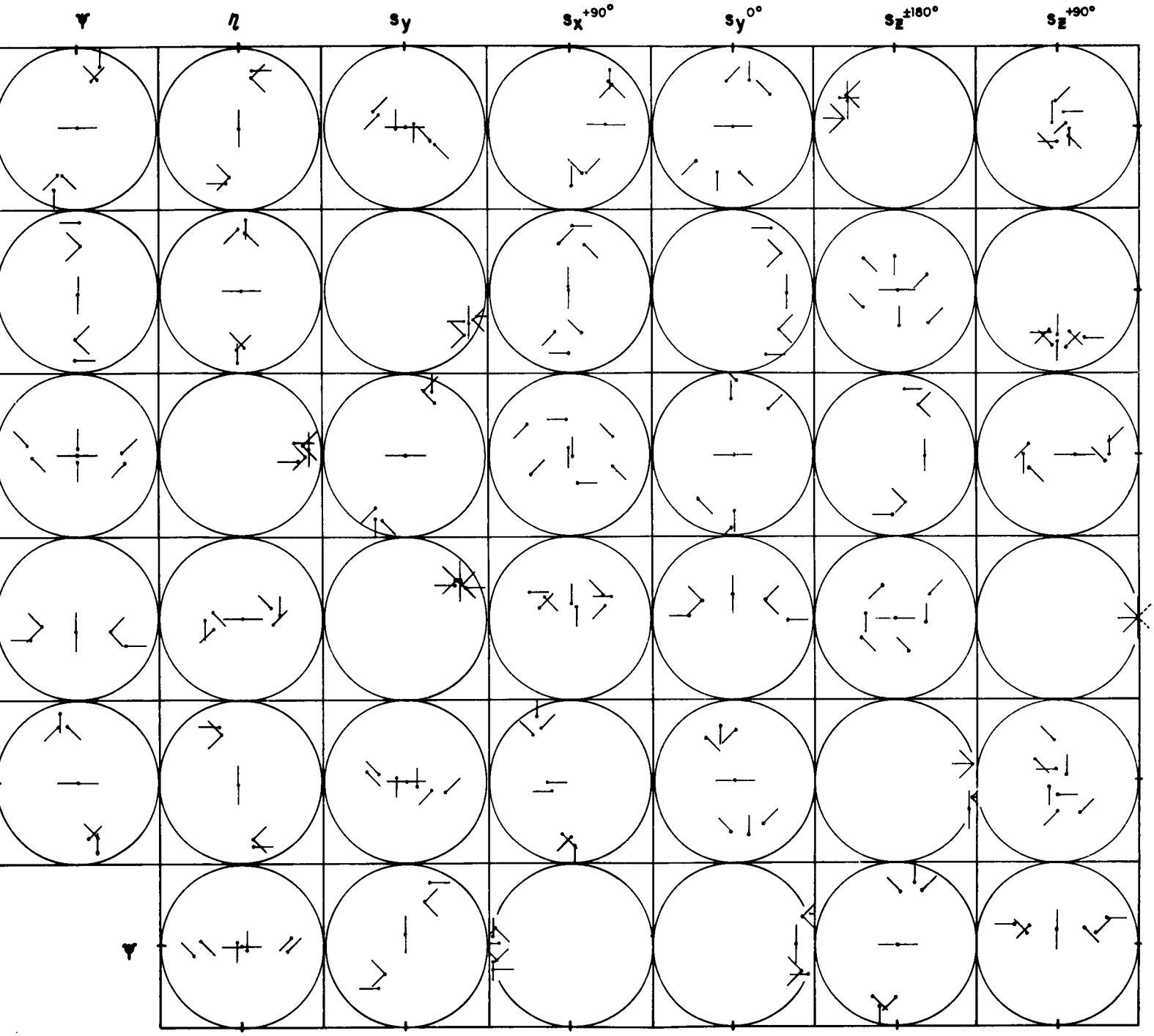

2

Fig. 5.9.1 Values of the complex envelope of the correlation coefficient between motions indicated at 45° barge heading increments

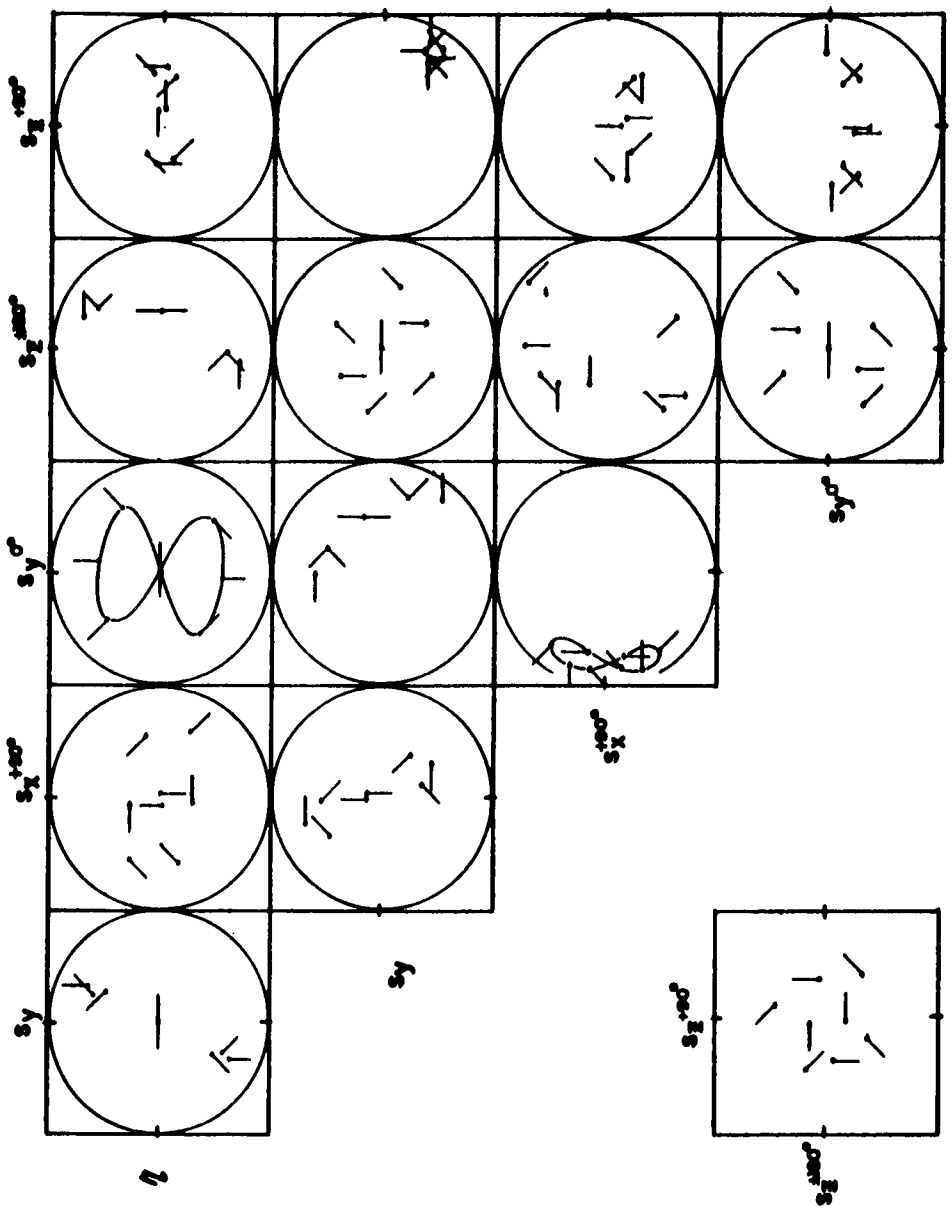

Fig. 5.9.2 Values of the complex envelope of the correlation coefficient between motions indicated at 45° barge heading increments

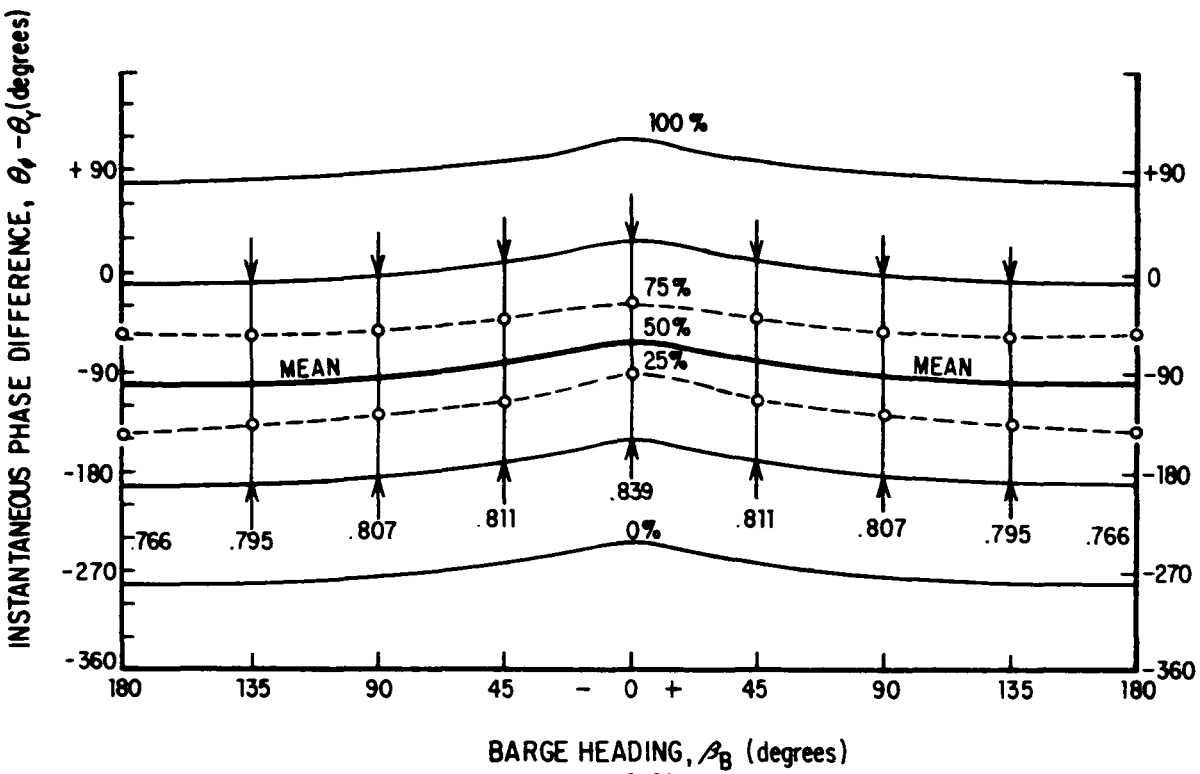

Fig. 5.10

Mean and percentile points of distribution of instantaneous phase difference between sway and roll as a function of barge heading in State 5 Sea

(Probability of phase difference lying in shown band is given at the barge heading indicated)

DISTRIBUTION LIST FOR CONTRACT NBy-32206

No. of Copies	
1	Commander, U. S. Army Transportation Research and Development Command, Fort Eustis, Virginia
1	The Director, Waterways Experiment Station, Vicksburg, Mississippi
1	President, Beach Erosion Board, Washington, D. C.
1	Chief, Bureau of Ships (Code 638), Department of the Navy, Washington 25, D. C.
1	Department of Civil Engineering, Princeton University, Princeton, New Jersey
1	Department of Civil Engineering, University of Washington, Seattle, Washington
1	Department of Meteorology and Oceanography, Texas A&M College, College Station, Texas
1	Department of Engineering, University of California, Berkeley, California
1	Department of Civil Engineering, California Institute of Technology, Pasadena, California
1	Department of Civil and Sanitary Engineering, Massachusetts Institute of Technology, Cambridge, Massachusetts
1	Department of Meteorology and Oceanography, New York University, New York, New York
1	Institute of Technology, University of Minnesota, Minneapolis, Minnesota
1	Department of Civil Engineering, Carnegie Institute of Technology, Pittsburgh, Pennsylvania
10	Chief, Bureau of Yards and Docks (Code 70), Navy Department, Washington 25, D. C.
1	Chief of Naval Research, Navy Department, Washington 25, D. C.
1	Chief of Naval Operations (OP-07), Navy Department, Washington 25, D. C.
1	Chief of Naval Operations (OP-04), Navy Department, Washington 25, D. C.

No. of Copies	
1	Director, U. S. Naval Research Laboratory, Washington 25, D. C.
1	Superintendent, U. S. Naval Academy, Annapolis, Maryland
1	Officer in Charge, U. S. Naval School, Civil Engineer Corps Officers, U. S. Naval Construction Battalion Center, Port Hueneme, California
1	Superintendent, U. S. Naval Postgraduate School, Monterey, California
1	Commanding Officer and Director, U. S. Naval Underwater Sound Laboratory, Fort Trumbull, New London, Connecticut Attn: Public Works Officer
1	Commanding Officer and Director, U. S. Navy Mine Defense Laboratory, Panama City, Florida Attn: Public Works Officer
1	Commanding Officer and Director, David W. Taylor Model Basin, Washington 7, D. C. Attn: Public Works Officer
1	Commanding Officer and Director, U. S. Naval Engineering Experiment Station, Annapolis, Maryland
1	Commandant, Marine Corps Schools, Quantico, Virginia Attn: Public Works Officer
1	Deputy Chief of Staff, Research and Development, Headquarters, U. S. Marine Corps, Washington, D. C.
1	President, Marine Corps Equipment Board, Marine Corps School, Quantico, Virginia
2	Library of Congress, Washington, D. C.
1	Chief of Staff, U. S. Army, Chief of Research and Development, Department of the Army, Washington, D. C.
1	Office of the Chief of Engineers, Assistant Chief of Engineering for Civil Works, Department of the Army, Washington, D. C.
1	Chief of Engineers, Department of the Army, Attn: Engineering R&D Division, Washington, D. C.
1	Chief of Engineers, Department of the Army, Attn: ENGCW-OE, Washington, D. C.
1	Director, U. S. Army Engineer Research and Development Laboratories, Attn: Information Resources Branch, Fort Belvoir, Virginia

No. of Copies	
1	Headquarters, U. S. Air Force, Directorate of Civil Engineering, Attn: AFOCE-ES, Washington, D. C.
1	Deputy Chief of Staff, Development, Director of Research and Development, Department of the Air Force, Washington, D. C.
1	Director, National Bureau of Standards, Department of Commerce, Connecticut Avenue, Washington, D. C.
2	Office of the Director, U. S. Coast and Geodetic Survey, Washington, D. C.
2	Director of Defense Research and Engineering, Department of Defense, Washington, D. C.
2	Director, Division of Plans and Policies, Headquarters, U. S. Marine Corps, Washington, D. C.
1	Librarian, Arthur D. Little, Inc., Acorn Park, Cambridge 40, Massachusetts
1	Librarian, Scripps Institute of Oceanography, La Jolla, California, Attn: Dr. W. C. Van Dorn
1	Librarian, Global Marine Exploration Company, 650 South Grand, Los Angeles 17, California
10	Armed Services Technical Information Agency, Arlington Hall Station, Arlington 12, Virginia
1	Director, Atlantic Division (Code A100A) Bureau of Yards and Docks/Area Public Works Officer 90 Church Street, New York 7, New York